DOE/MC/21181-1950, Vol. 12
(DE90000431)

Geological Evolution and Analysis of Confirmed or Suspected Gas Hydrate Localities

Volume 12. Basin Analysis Formation and Stability of Gas Hydrates of the Beaufort Sea

Topical Report

P.D. Finley
J. Krason

Work Performed Under Contract No.: DE-AC21-84MC21181

For
U.S. Department of Energy
Office of Fossil Energy
Morgantown Energy Technology Center
P.O. Box 880
Morgantown, West Virginia 26507-0880

By
Geoexplorers International, Inc.
5701 East Evans Avenue
Denver, Colorado 80222

October 1988

PREFACE

This document is Volume XII of a series of reports entitled *Geological Evolution and Analysis of Confirmed or Suspected Gas Hydrate Localities.* Volume XII is a study titled *Basin Analysis, Formation and Stability of Gas Hydrates of the Beaufort Sea.* This report presents a geological description of the Arctic margin of northern Alaska and northwestern Canada, including regional and local structural settings, geomorphology, geological history, stratigraphy, and physical properties. It provides the necessary regional geological background for more in-depth research of the area. Detailed discussion of bottom simulating acoustic reflectors, sediment acoustic properties, and distribution of hydrates within the sediments are also included in this report. The formation and stabilization of gas hydrates in sediments are considered in terms of phase relations, nucleation, and crystallization constraints, gas solubility, pore fluid chemistry, inorganic diagenesis, and sediment organic content. Together with a depositional analysis of the area, this report is a better understanding of the thermal evolution of the locality. It should lead to an assessment of the potential for both biogenic and thermogenic hydrocarbon generation.

Project Manager
Gas Hydrates

CONTENTS

Page

Page

ILLUSTRATIONS

Page

Page

Page

Page

Page

TABLES

PLATES

BASIN ANALYSIS, FORMATION AND STABILITY OF GAS HYDRATES OF THE BEAUFORT SEA

By Patrick Finley and Jan Krason

EXECUTIVE SUMMARY

Geological factors controlling the formation, stability, and distribution of gas hydrates of the Beaufort Sea region were investigated by basin analysis. Geological, geophysical, and geochemical data from the region were assembled and evaluated to determine the relationships of geological environments and gas hydrates.

This study was performed for the U.S. Department of Energy Morgantown Energy Technology Center by Geoexplorers International, Inc. as part of a evaluation of 24 offshore sites worldwide where the presence of gas hydrates has been confirmed or inferred.

The Beaufort Sea is the southern part of the Arctic Ocean offshore of the North Slope of Alaska and the Yukon and Mackenzie districts of Canada. The Beaufort Sea study region extends northward from the Arctic coasts of Alaska and Canada between Point Barrow on the west to Cape Beaufort on the east. The northern boundary of the Beaufort Sea study region is 72.5°N. The study region comprises broad continental shelves, slopes, rises, and the Arctic abyssal plain.

The sediments of northern Alaska and northwest Canada can be grouped into three distinctive sequences deposited in different tectonic settings. The oldest identified sedimentary rocks of the region are the pre-Mississippian Franklinian sequence. Rocks of the Franklinian sequence were deposited in a geosyncline between Cambrian and Devonian time. The Franklinian sediments were lithified, deformed and uplifted between Late Devonian and Early Mississippian time. The resulting erosion surface has been recognized throughout the Arctic region and is termed the Arctic platform. The platform subsided slightly and remained stable from Early Mississippian time to the late Jurassic. Upon this surface, thick accumulations of shelf clastics and carbonates comprising the Ellesmerian sequence were deposited. Uplift of the northern source of the Ellesmerian sediments in Jurassic time created an extensive regional angular unconformity. The Ellesmerian sequence was eroded to a thin edge and removed from the northernmost parts of the Arctic platform underlying the present Beaufort continental shelf. Rifting and

sea-floor spreading to the north throughout Late Jurassic and Early Cretaceous time produced the present passive margin north of Alaska. The subsequent uplift of the Brooks Range to the south and post-rifting subsidence to the north resulted in a reversal in the direction of sediment transport. Orogenic sediments of the Brookian sequence filled the foreland Colville Trough, overtopped the northern limit of the Arctic platform, and produced a northward prograding sedimentary wedge which underlies the present outer continental shelf and slope.

The composition and thermal history of the strata beneath the outer continental shelf and slope of the Beaufort Sea study region is not known directly due to limited drilling. Proximity to the huge hydrocarbon accumulation at Prudhoe Bay and the Canadian Beaufort shelf indicate that rich, mature source rocks exist in the study region. Thermal maturity and hydrocarbon generation potential estimates are obtained by extrapolation of onshore and nearshore trends and by thermal modeling. The source rocks for the Prudhoe Bay accumulation are not present over much of the study region. Tertiary sediments equivalent to the sources for the gas and condensate fields of the Mackenzie delta require burial to 4,000 m to attain maturity. Thus, gas hydrate formation from thermogenic gas requires large scale vertical migration from mature source beds to the gas hydrate stability zone. Adequate organic carbon content and rapid sedimentation of the tertiary shelf and slope sediments of the Beaufort Sea indicate good potential for microbial methanogenesis.

Bottom simulating reflectors (BSRs) which are interpreted to indicate the base of the gas hydrate stability zone occur in seismic profiles from offshore of northern Alaska. Single channel and multichannel seismic lines display abundant BSRs within sediments of the outer continental shelf, slope, and rise. Seismic evidence of gas seeps were also noted in some areas of the continental shelf.

Bottom simulating reflectors are common on the continental slope northwest of Prudhoe Bay which is dominated by normal faulting and mass wasting. Bottom simulating reflectors are also common on the continental slope northwest of Prudhoe Bay to the Canadian border which is characterized by widespread shale diapirism. A 50 km stretch of the continental slope north of Prudhoe Bay is devoid of definite BSRs.

Seismic lines from offshore of Alaska suggest that the base of the gas hydrate stability zone is a principal locus of slope failure. Single channel and multichannel seismic lines indicate that incompetent gassy sediments beneath the gas hydrate stability zone fail and the overlying sediment slides downslope.

Bottom simulating reflectors overlying shale diapirs in the Beaufort Sea study region are found at lesser subbottom depths than BSRs distant from diapirs at similar water depths. Modeling indicates geothermal gradients over the diapirs averages 5.5 to 6°C/100 m compared to typical slope gradients of 4.2°C/100 m. The heat flow over shale diapirs increases regularly to the east.

Geothermal gradients derived from BSRs away from diapirs show a distinct relationship to water depth. Mean geothermal gradients increase regularly from about 3.2°C/100 m at a water depth 300 m to about 4.5°C/100 m at 1,150 m water depth. Mean geothermal gradients vary randomly from 4.2 to 4.7°C/100 m between 1,200 m and 2300 m water depth. Mean geothermal gradients decrease beneath the lower continental slope and continental rise, decreasing to 3.3°C/100 m at 3,000 m water depth.

Geothermal gradients of the Beaufort continental slope decrease from west to east reaching a minimum north of Camden Bay, Alaska. Gradients appear to then increase regularly to the east.

Modeling gas hydrate stability conditions indicate that biogenic gas hydrates should be stable in sediments beneath water deeper than about 200 m at prevailing temperature and pressure conditions of the Beaufort Sea study region. Gas hydrates composed of thermogenic gas of 91% methane and 9% heavier hydrocarbons should be stable in sediments beneath water less than 10 m deep. Variation of the thickness and location of the gas hydrate stability zone to be expected in the Beaufort Sea study region is modeled using different geologic parameters.

Subsea permafrost at subbottom depths of as little as 150 m can stabilize underlying biogenic gas hydrates at water depths as shallow as 1 m. Lower sea levels in the Pleistocene exposed large areas of the present Beaufort shelf to permafrost-forming conditions. Despite subsequent inundation, relict subsea permafrost exists in the Beaufort Sea study region. The lateral extent of subsea permafrost is uncertain. Evidence from well logs obtained during exploratory drilling offshore of Canada indicates that gas hydrates exist beneath the permafrost zones and that subsea permafrost is widespread beneath parts of the Beaufort shelf.

Estimates of potential gas resources associated with hydrates were derived from the available seismic and drilling evidence of gas hydrates in the Beaufort Sea study region. The estimates have a wide range due to uncertainties on the vertical extent of hydrates indicated on sieismic lines. We determined a most-probable in-place estimate for gas in hydrate form in the continental slope and rise offshore of Alaska of 1.2×10^{13} m^3 or 400 trillion cubic feet (tcf). The continental slope and rise offshore of Canada is estimated to contain 1.4×10^{12} m^3 (50 tcf) of gas in hydrate form; the lower figure due principally to the lack of demonstrated evidence of hydrate presence in the area. The continental shelf offshore of Canada is estimated to contain 4×10^{12} m^3 (140 tcf) of gas in hydrate form. The continental shelf offshore of Alaska is estimated to contain 1×10^{12} m^3 of gas in hydrates. We estimate that sub-hydrate traps exist in the study region with sufficient closed volume to contain 2×10^{13} m^3 (700 tcf) of free gas. We estimate that approximately 4.4×10^{12} m^3 (150 tcf) of free gas is present in these sub-hydrate traps.

INTRODUCTION

Gas hydrates are solid substances composed of small gas molecules enclosed in a crystal lattice of water molecules. Gas hydrates can be formed from various gases and water at high pressures and low temperatures when a sufficiently high concentration of dissolved gas exists. Conditions favorable for natural gas hydrate formation and preservation occur in some continental margin and deep sea sediments where adequate amounts of hydrocarbon gases are available. Large quantities of natural gas with possible resource potential may be present in offshore gas hydrates or trapped beneath impermeable gas hydrate layers.

This report presents the results of a study on the geological factors which control the formation and stability of gas hydrates in the sediments beneath the Beaufort Sea. The Beaufort Sea study region comprises the southern Arctic Ocean north of Alaska and the Mackenzie District of Canada. This study is part of a project performed for the U.S. Department of Energy's Morgantown Energy Technology Center by Geoexplorers International, Inc. The main purpose of the project is to evaluate the geological controls of gas hydrate formation and stability and to make preliminary assessments of gas resources associated with gas hydrates.

The presence of gas hydrates in the Beaufort Sea study region has been indicated by seismic data and exploratory drilling. Single channel seismic lines from the continental margin north of Alaska exhibit distinct bottom simulating reflectors (BSRs) which are inferred to mark the base of the gas hydrate stability zone in sediments. Multichannel seismic lines from the eastern part of the Alaskan continental margin demonstrated that BSRs occur over large areas of the Beaufort Sea study region. Exploratory drilling on the Beaufort continental shelf offshore of Canada detected evidence of gas hydrates beneath a subsea permafrost layer. Extensive onshore drilling on the North Slope of Alaska and the Mackenzie Delta south of the Beaufort Sea study region has shown that gas hydrates exist in environments analogous to those found on the Beaufort continental shelf.

In this study we have assembled and analyzed all available information of gas hydrates of the Beaufort Sea study region. We document the seismic evidence of gas hydrate presence in the region and assess its relationship to geological factors. We apply a gas hydrate stability model to the seismic data from the study region. We discuss and assess data which suggest that gas hydrates exist in Beaufort continental shelf sediments.

This report is presented in two sections:

Part I - Basin Analysis examines the structural geology and sedimentary environments of the Beaufort Sea study region. Based on this information, the regional hydrocarbon generation potential is discussed.

Part II - Formation and Stability of Gas Hydrates describes the seismic and drilling evidence of gas hydrate presence in the study region. The evidence is analyzed in detail in view of the information presented in Part I to indicate which factors may control the formation and stability of gas hydrates in the Beaufort Sea study region.

Acknowledgements

Geoexplorers International, Inc. and the authors are grateful to the U.S. Department of Energy, Morgantown Energy Technology Center for the opportunity to participate in the gas hydrate research program. Rodney Malone of METC reviewed the report for technical content and style. Charles Komar expedited printing of this report.

PART I

BASIN ANALYSIS

The Beaufort Sea study region is underlain mainly by sediments derived from the uplift of the Brooks Mountains in Alaska and smaller associated structures to the east. The Late Cretaceous to Tertiary uplifts introduced large volumes of terrigenous sediments to the basin as a northward prograding sedimentary wedge. resulted in Great thickness of syn- and post-orogenic sediments were deposited in the Mackenzie Delta offshore of Canada.

The reservoir and source rock lithologies of the supergiant Prudhoe Bay oil field are absent by nondeposition or erosion over the vast majority of the study region. However, recent gas and condensate discoveries in the Tertiary sediments of the Canadian Beaufort shelf indicate good hydrocarbon generation potential in correlative lithologies throughout the study region. Probable thermal history of the potential Tertiary source rocks suggests that large scale vertical migration would be necessary for thermogenic gas to be incorporated in gas hydrates in the Beaufort Sea study region.

Location

The Beaufort Sea is the southern part of the Arctic Ocean offshore of the north coast of Alaska and the Yukon and Northwest Territories of Canada. The northern boundary of the Beaufort Sea is not well defined, but generally coincides with the northernmost withdrawal of the polar ice pack in summer. In this study, 72.5°N constitutes the northern boundary of the region discussed. The western boundary of the study region is Point Barrow, Alaska at about 156.5°W (Plate 1). The Beaufort Sea study region extends eastward to Cape Beaufort, Canada at about 128°W longitude (Plate 2).

Geomorphology

The study region comprises the continental shelf, continental slope, continental rise, and abyssal plain beneath the Beaufort Sea. The western Beaufort shelf from Point Barrow to the Mackenzie Trough near the international boundary averages 60 km wide (Plates 1 and 2). The eastern Beaufort shelf extending to the eastern limit of the study region is wider than offshore of Alaska, averaging 100 km from the shore to the 200 m isobath (Plate 2). The continental slope offshore of Alaska

and Canada is characterized by irregular topography; mass wasting and diapirism have altered sediment transport and created numerous canyons and intraslope basins. The continental rise is dominated by mass wasting deposits and a broad apron of sediments from the Mackenzie River. The northern part of the Beaufort Sea study region consists of a featureless abyssal plain seaward of the continental rise.

Western Beaufort Shelf

The western Beaufort shelf stretches some 700 km from Barrow Canyon north of Point Barrow to the Mackenzie Trough (Plates 1 and 2). The inner portion of the shelf typically slopes from the shoreline to the 60 m isobath at 1 m/km (0.06°). The shelf is steeper seaward to the shelf break (16 m/km, 0.9°). Grantz et al. (1981) defined the shelf slope break using structural as well as bathymetric criteria. The shelf extends seaward to a zone of active slumping which constitutes the shelf edge and ranges in depth from 200 m to 600 m. Between the Barrow Canyon and the Colville River delta, the shelf is a wave-cut surface with a thin veneer of Holocene sediments (Grantz et al., 1981). The shelf between the Colville River and the Mackenzie Sea Valley is a product of more abundant clastic input which has filled local structural depressions with thick sediment accumulations resulting in the present surface. The floor of the western Beaufort shelf is marked by ice gouges in the Holocene sediments caused by seasonal breakup and movement of grounded ice.

Eastern Beaufort Shelf

The Beaufort shelf widens to more than 100 km and exhibits more local sea-floor relief between the Mackenzie Trough and Cape Beaufort (Plate 2). Valleys 10 to 20 m deep have been cut into the shelf offshore of the Kugmallit Bay where a distributary channel of the Mackenzie River delivers sediment to the shelf.

Based on geomorphology the Beaufort continental shelf is best divided at the Mackenzie Trough (Grantz et al., 1981). However, many of the published research results upon which this report was based deal with either the portion of the study region which is offshore of Alaska or that which is offshore of Canada. To simplify discussion of the previous work on the Beaufort Sea study region we use the terms "Alaskan Beaufort shelf" and "Canadian Beaufort shelf" to refer to the Beaufort continental shelf offshore of the United States and Canada respectively.

Continental Slope

The topography of the continental slope beneath the Beaufort Sea has resulted from mass wasting processes and active diapirism. Grantz et al. (1981) defined the continental slope to begin at the sharp change in sea-floor gradient from less than 1° on the shelf to 4° to 16° on the slope. This shelf-slope break occurs at about 220 m water depth north of Barrow, but steadily increases in depth eastward, reaching 600 m depth near the U.S.-Canada border (Plates 1 and 2). This plunge of

the shelf-slope break toward the Mackenzie Trough has been attributed to isostatic subsidence due to sediment loading of the continental slope and rise by the Mackenzie Delta (Grantz et al., 1981).

The Beaufort continental slope includes submarine canyons, sediment ponds, and slump and glide deposits. Since the poorly consolidated sediments of the outer continental shelf dip seaward, bedding plane slip, block slides, and slumps are common (Grantz et al., 1981). Continued mass wasting preserves the steep dip of the slope and builds up the continental rise at the expense of the shelf-edge material. Slump and slide deposits on the continental slope range from featureless mounds of debris to very large discrete slide blocks which retain their internal stratification after downslope dislocation of 20 to 30 km.

Slump and slide deposits on the continental slope have acted as barriers to downslope sediment transport. Sediment ponds have formed due to the damming effect of slope and slump deposits. Mass wasting deposits on the upper slope are eventually remobilized downslope; sediment ponding is most pronounced on the lower continental slope.

Diapirs underlying the Beaufort continental margins of Canada and northeastern Alaska have accelerated mass wasting and sediment ponding processes on the continental slope (Grantz et al., 1980). The arching of strata over a rising diapir increases the rate of mass wasting on the seaward flank of the uplifts. The increased slope on the diapir flanks and the probable minor seismic activity associated with diapirism accelerates slumping, block glides, and debris flows. The landward limbs of the diapirs and diapiric ridges of the continental slope principally function as dams, blocking downslope transport from slumps higher on the continental shelf and slope forming sediment accumulations termed "intraslope basins" in the terminology of Buffler (1983). The sediment ponds landward of the diapirs and enhanced wasting have resulted in the steep and irregular topography of the continental slope offshore of northeastern Alaska.

The continental slope beneath the Beaufort Sea offshore of Canada is dominated by sediment accumulation from the Mackenzie River. The Mackenzie Delta has prograded steadily seaward throughout the Tertiary (Willumsen and Cote, 1982). The shelf edge has migrated northward from approximately the location of the present shoreline starting in the late Cretaceous to the present shelf-slope break. The slope offshore of the Mackenzie Delta is thus composed of rapidly deposited delta-front sediments and turbidite deposits. Although the continental slope offshore of the Mackenzie Delta is not thoroughly surveyed due to nearly continuous pack ice cover, the few available seismic lines suggest a geomorphological parallel with the well studied Mississippi Fan of the Gulf of Mexico and the Magdalena Fan of the Colombia Basin.

Submarine Canyons

Two large submarine canyons dominate the continental margin of the Beaufort Sea. The Mackenzie Trough offshore of the Mackenzie River and the Barrow Canyon, north and west of Point Barrow convey large amounts of sediment from littoral depths to the continental rise and abyssal plain of the southern Arctic Ocean.

The Mackenzie Trough extends northwestward from Mackenzie Bay (Plate 2). The trough is about 50 km wide and 300 to 500 m deep. Its U-shaped profile and continuation beneath water depths of less that 50 m suggests a possible glacial origin. A lobe of the Buckland continental ice sheet extended down the Mackenzie valley and onto what is now the Eastern Beaufort shelf in the middle Wisconsin stage, about 100,000 yr. ago (Hill et al., 1985). The lobe projected 150 m offshore in a northeasterly direction, with the maximum extent of ice coincident with the 250 m isobath at the floor of the Mackenzie Trough. Hill et al. (1985) determined a relative sea level lowering of at least 140 m occurred during the Buckland glaciation. Formation of the trough by ice scouring during this and earlier Pleistocene glacial maxima is likely. The trough landward of the 30 m isobath appears to have been partially filled in by clastic detritus deposited during the retreat of the ice in late Pleistocene time.

The Barrow Canyon cuts northwestward into the Chukchi shelf and the western Beaufort shelf and slope. Grantz et al. (1981) subdivided this submarine canyon into the Barrow Sea Valley, which cuts into the continental shelf, and the Barrow Sea Canyon, which is incised into the continental slope (Plate 1). The valley is about 200 km long and 10 km wide. Grantz et al. (1981) attributed the valley to stream cutting during subaerial exposure of the continental shelf during Pleistocene lowstands in sea level. The canyon, with a maximum depth of 900 m, continues northward from near the shelf-slope break. Two smaller abandoned canyons are found on the continental slope east of the Barrow Sea Canyon. Grantz et al. (1981) proposed that all of these canyons were cut by turbidity flows from the Barrow Sea Valley. The smaller canyons to the east were sequentially pirated due to the more direct route offered by the present Barrow Sea Canyon. In this report the Barrow Sea Valley and the Barrow Sea Canyon are collectively referred to as the Barrow Canyon.

Continental Rise and Abyssal Plain

The continental rise offshore of Alaska narrows from 120 km wide on the west to 60 km wide near the Canadian border. The sediments as much as 200 km eastward from the Barrow Canyon were delivered to the rise principally by the canyon system (Grantz et al., 1981). The remainder of the continental rise offshore of Alaska is composed of sediment derived from turbidity currents and slumps of nearby shelf material.

The continental rise offshore of Canada as defined by Grantz et al. (1981) extends over 400 km seaward from the mouth of the Mackenzie Trough. The expansive sediment apron gently slopes northwesterly from about 1,500 m to 3,200 m water depth. The rise overlaps the lower extensions of the Alaska continental rise.

The Canada Abyssal Plain occurs northwest of the lower reaches of the continental rise. Its flat topography suggests a thick sediment accumulation. Distal turbidites cover the few areas of the abyssal plain which have been seismically surveyed. The abyssal plain is here defined as occurring between 3,200 m and 4,000 m depth.

Regional Tectonics

Early Cretaceous rifting and subsequent uplift of the Brooks range controlled the present structure and stratigraphy of the Beaufort Sea study region. Rifting and sea floor spreading in Neocomian time created the present Canada Basin and the passive continental margin of the Beaufort Sea. Uplift of the Brooks range by thrusting in the Cretaceous and early Tertiary provided vast quantities of sediments which were deposited over the ancestral rifts and prograded seaward to construct the sedimentary prism underlying the present continental shelf, slope, and rise in the study region.

The Alaskan sector of the study region is dominated by the Brooks Range, the adjacent foreland basin, and the passive Beaufort continental margin (Grantz et al., 1980). The Brooks Range is composed of northerly thrusted nappes (Bird, 1985). The mountain front strikes west to east across north central Alaska 200 to 300 km south of the Beaufort Sea coast for a distance of about 500 km. At about 150°W, the trend of the range shifts to the northeast and converges on the coastline; the northern limit of the range is located a mere 60 km south of the coastline at the Canadian border.

Sediments from the nascent Brooks Range were deposited in a foreland basin to the north (Bird, 1985). The Colville Trough, also called the Colville Foredeep, contains 6,000 to 8,000 m of synorogenic sediments along its axis 100 km from the mountain front. The shallow dipping north flank of the Colville Trough contains less than 2,000 m of syn- and post-orogenic sediment near the Beaufort Sea shoreline.

The Barrow Arch is a broad anticlinal structure beneath the coastal plain of northern Alaska and the continental shelf of the Beaufort Sea (Grantz et al., 1981) (Figure 1). The Barrow Arch defines the northern limit of the Colville Trough. The crest of the arch trends east-southeast from Point Barrow beneath the inner continental shelf to near the Colville River delta, where it verges shoreward, intersecting the shoreline near the Canning River delta. The Barrow Arch plunges and loses its identity as a discrete structure near the Canning River delta. The super giant Prudhoe Bay oil field is located near the crest of the Barrow Arch.

Seaward of the Barrow Arch, the Cretaceous and Tertiary sedimentary prism which forms the continental shelf and slope has been downwarped by subsidence and growth faulting. The hinge line of the subsidence closely parallels the Barrow Arch from point Barrow to offshore of the Colville River delta (Figure 1). From the Colville River delta eastward, the hinge line swings to the northeast while the Barrow Arch continues to the southeast. Thus, a broad shelf underlain by Cretaceous and Tertiary sediments which have not undergone tensional growth faulting or subsidence is found between the hinge line and the arch in the eastern portion of the continental margin offshore of Alaska. Tensional stresses in the eastern part of the Alaska continental shelf have been partially accommodated by formation of the Dinkum Graben, in which 8,000 m of sediments have accumulated since the Early Cretaceous (Grantz et al., 1981) (Figure 1).

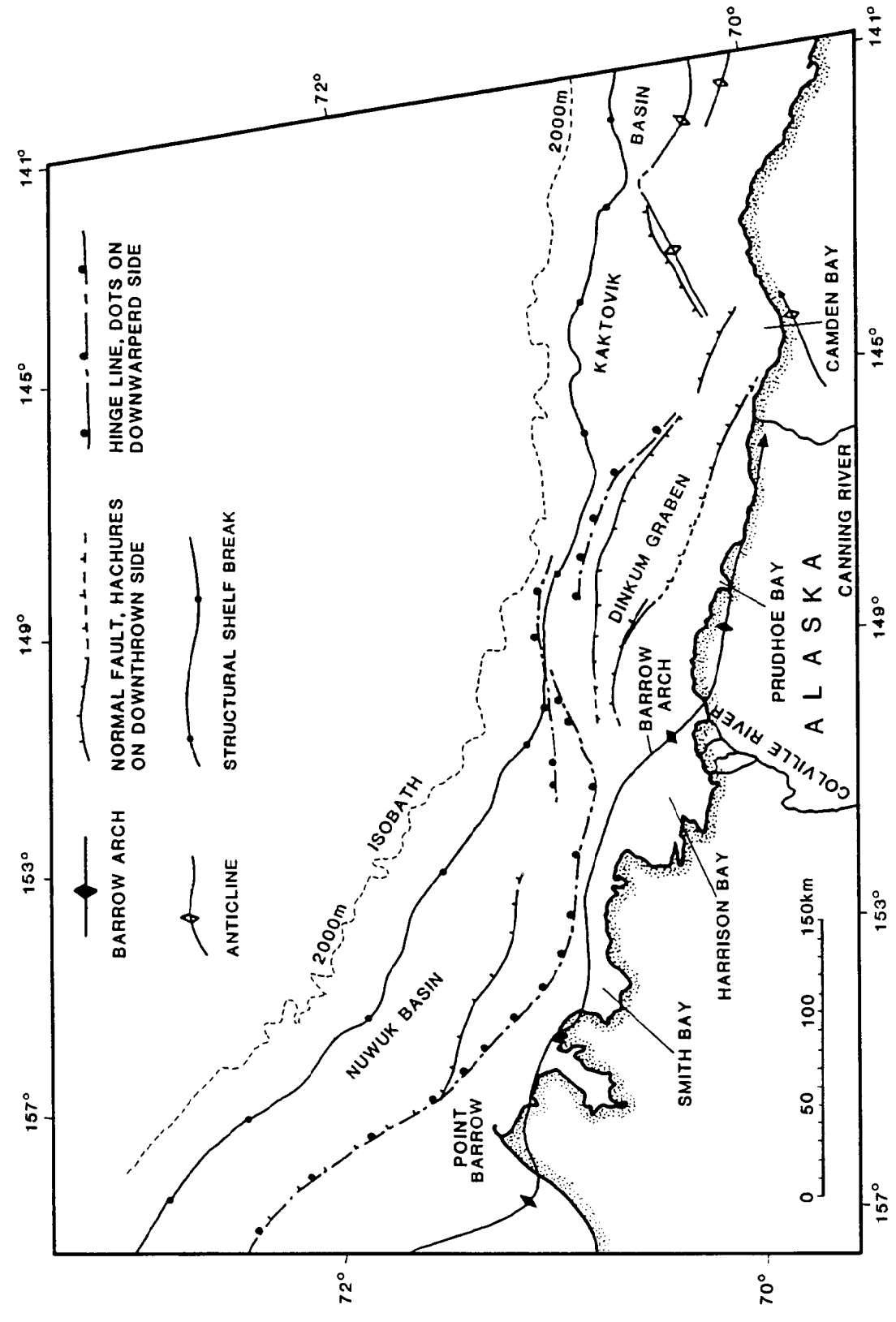

Figure 1. TECTONIC MAP OF THE BEAUFORT SEA STUDY REGION OFFSHORE OF ALASKA
After Grantz and May, 1982

The eastward culmination of the Brooks Range uplift in northwestern Canada is expressed by a series of right-lateral and thrust faults (Jones et al., 1980) (Figure 2). The Brooks Range thrusting produced a series of smaller en echelon ranges east of the Canada-Alaska border, among them the British, Barn, and Richardson mountains. Landward of the eastern boundary of the Beaufort Sea study region, the relatively undeformed Northern Interior Platform was unaffected by the tectonism of the Brooks Range uplift. These two structural provinces are separated by a series of right-lateral faults, among them the Kaltag and Trevor Faults. Drainage of large portions of the Canadian interior during the Tertiary and Quaternary by the Mackenzie River deposited huge volumes of sediments, forming the Mackenzie delta. The load of this sedimentary prism produced a large normal fault system, the Eskimo Lakes Fault Zone which separates the Mackenzie delta from the Northern Interior Platform (Jones et al., 1980). Further sedimentation produced growth faults in the delta sediments and mobilized underlying shale beds producing shale diapirs beneath the continental shelf, slope and rise of the Beaufort Sea offshore of Canada.

Stratigraphy Offshore of Alaska

Most of the sediments underlying the Beaufort Sea study region are terrigenous clastic detritus derived from the uplift of the Brooks Range and associated structures (Figure 3). Older sedimentary rocks are limited to the nearshore areas of the continental shelf where water depths are very shallow. Although gas hydrate presence is typically restricted to offshore sediments of the continental slope and rise, the cold temperatures of the Beaufort Sea study region suggest that gas hydrates may be found in the sediments of the near shore parts of the continental shelf underlain by older sediments. This, and the presence of hydrocarbons in these older rocks beneath the adjacent coastal plain of the Alaskan North Slope, dictates discussion of rocks deposited prior to the Brooks Range uplift, although their areal extent beneath the study region is limited.

Tectonic Controls on Sediment Deposition

The sediments of arctic Alaska and northwest Canada can be grouped into three distinctive sequences deposited in different tectonic settings (Lerand, 1973). The oldest identified sedimentary rocks of the region are the pre-Mississippian Franklinian sequence (Figure 4). Rocks of the Franklinian sequence were deposited in a geosynclinal environment between Cambrian and Devonian time (Grantz and May, 1982). The Franklinian sediments were lithified, deformed, and uplifted between Late Devonian and Early Mississippian time. The resulting erosion surface has been recognized throughout the Arctic region and is termed the Arctic platform. The platform subsided slightly and remained stable from Early Mississippian time to Late Jurassic-Early Cretaceous time. Upon this surface, thick accumulations of shelf clastics and carbonates comprising the Ellesmerian sequence were deposited (Figure 4). Northern source for Ellesmerian sediments is assumed based on depositional features of the rocks. Regional uplift of the northern source

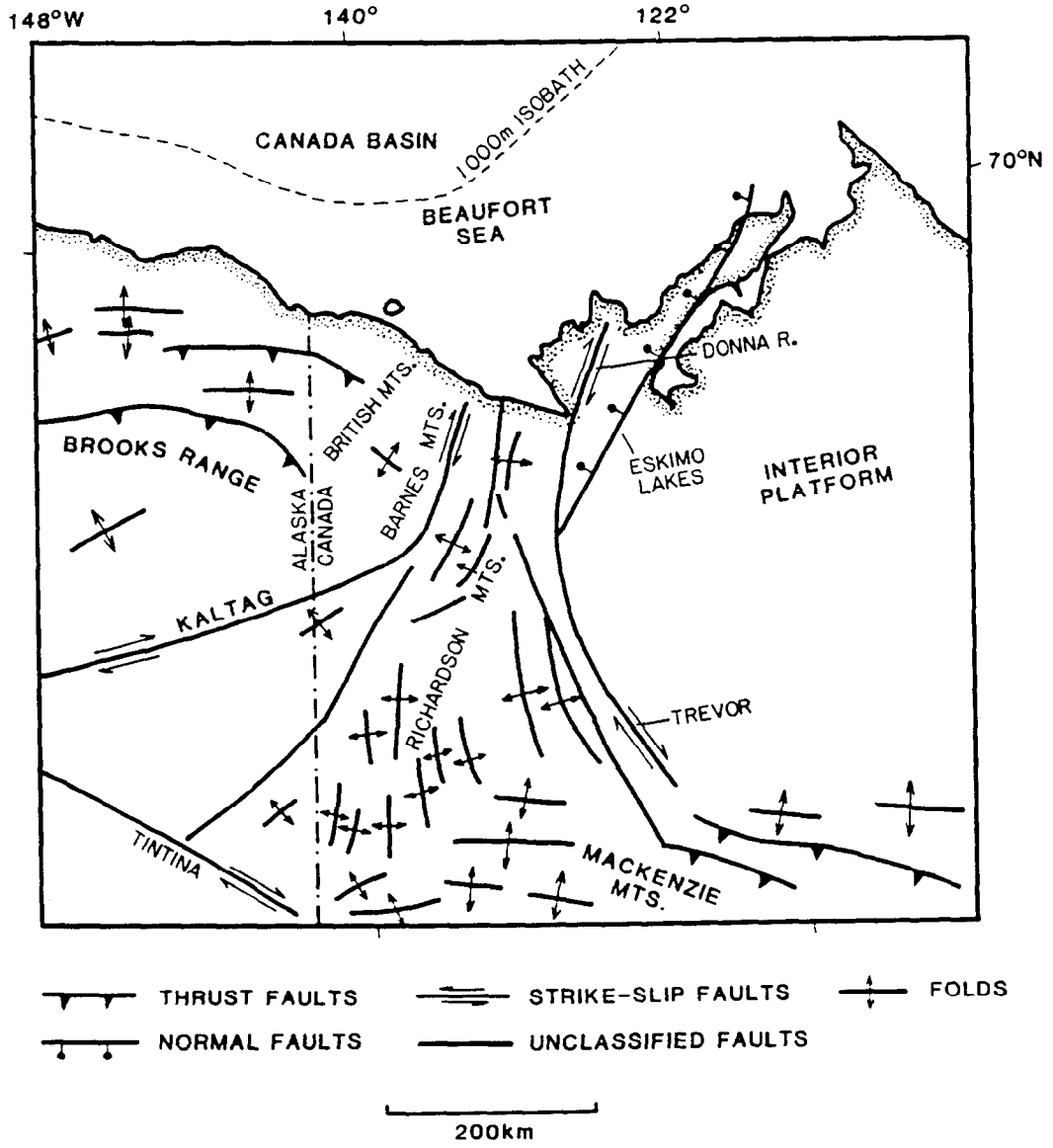

Figure 2. TECTONIC MAP OF NORTHEAST ALASKA, NORTHERN YUKON AND NORTHWEST TERRITORIES

After Jones et al., 1979

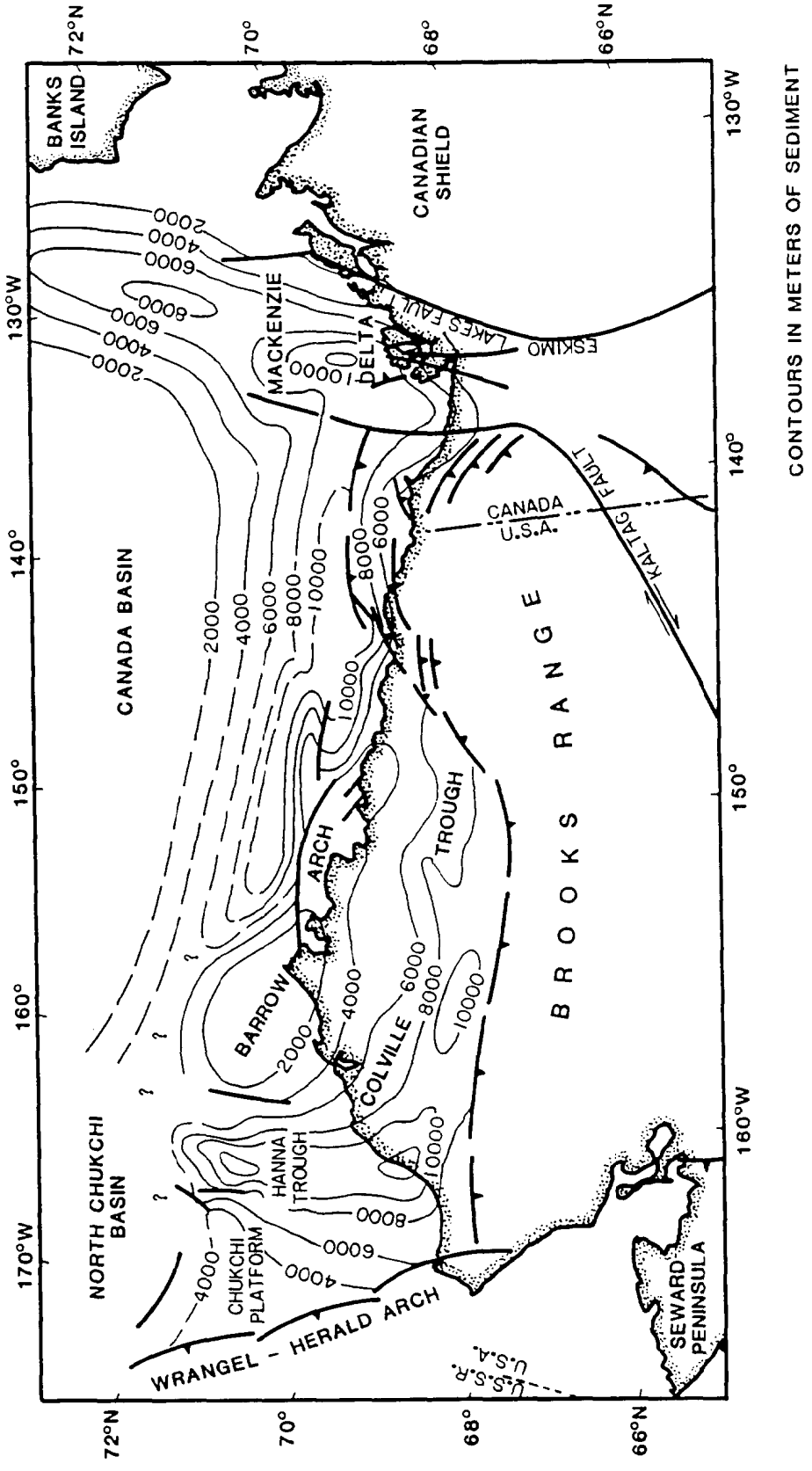

Figure 3. TOTAL SEDIMENT THICKNESS, BEAUFORT SEA STUDY REGION

After Hubbard et al., 1987

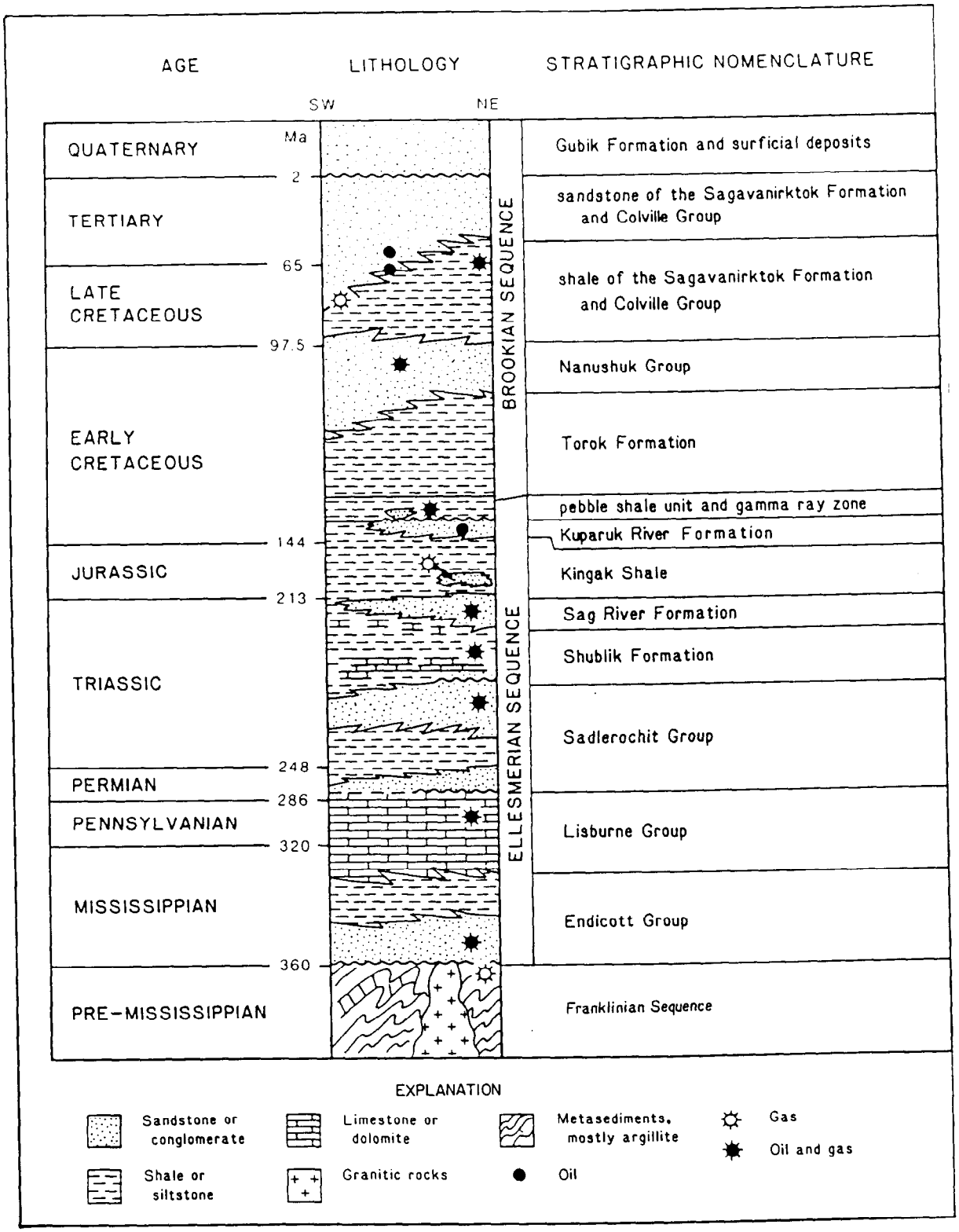

Figure 4. **SCHEMATIC STRATIGRAPHIC COLUMN OF THE NORTH SLOPE OF ALASKA**

After Bird, 1985

of the Ellesmerian sediments in Jurassic time created an extensive regional angular unconformity in the sediments with the Ellesmerian sequence thinned to a wedge edge and stripped from the northernmost parts of the Arctic platform which underlie the present outer continental shelf. Rifting and seafloor spreading of the source terrain to the north throughout Late Jurassic and Early Cretaceous time produced the passive margin. The uplift of the Brooks Range to the south and post-rifting subsidence to the north resulted in a reversal in the direction of sediment transport. Orogenic sediments of the Brookian sequence (Figure 4) filled the foreland Colville Trough, overtopped the bordering Barrow Arch, and produced a northward prograding sedimentary wedge which underlies the present outer continental shelf and slope.

Franklinian Sequence

The Franklinian sequence is typically metamorphosed and deformed argillites and carbonates (Grantz and May, 1982). These rocks generally mark the acoustic basement of the region due to their alteration. Due to the heat and pressure that these rocks experienced in Cambrian to Mississippian time they are generally considered overmature with respect to hydrocarbon generation, and thus also constitute the economic basement of the region (Grantz et al., 1980; Grantz et al., 1982a).

Ellesmerian Sequence

The Ellesmerian sequence was deposited in Devonian to Early Cretaceous time over the Franklinian Sequence on a regionally extensive erosional surface, the Arctic Platform. Uplift of metamorphosed Franklinian sequence to the north of the present coast of Alaska lead to deposition of a southward prograding prism of sediments. Ellesmerian sediments generally thicken and become more fine grained to the south (Craig et al., 1985). The top of the Ellesmerian sequence is defined by a regionally extensive unconformity which truncates progressively older beds northward. The Ellesmerian sequence wedges out beneath the Beaufort continental shelf due to northward erosion of the thinner units. Ellesmerian rocks underlie only 2% of the study region, but the prodigious oil production from these rocks at Prudhoe Bay oil field warrants their examination.

The age of the basal Ellesmerian strata is disputed. Bird (1985) placed the basal Ellesmerian beds beneath the North Slope oil fields in the Early Mississippian series. Grantz et al. (1979, 1980, 1982) and Grantz and May (1982) concurred with an Early Mississippian age for initiation of Ellesmerian sedimentation beneath the present Beaufort shelf. Craig et al. (1985), however, stated that sedimentation on the Arctic Platform began in Middle Devonian time.

The basal Ellesmerian unit is the Endicott Group (Figure 4). This unit contains orogenic conglomerates from the uplift of the source terrane to the north overlain by marine sandstones, mudstones and shales (Grantz and May, 1982). Older, thicker units tend to have been deposited to the south, beneath the present Alaska coastal plain with thinner, younger sediments to the north beneath the present Beaufort shelf (Craig et al., 1985).

The Lisburne Group is composed of marine platform carbonates deposited in Late Mississippian to Pennsylvanian time (Figure 4). The Lisburne group records a slow marine transgression. Lisburne group sediments progressively onlapped exposed basement north of the depositional limit of the Endicott Group (Craig et al., 1985). In addition to limestone and dolomite, marine sandstone, shale, and chert have been recognized in the Lisburne Group (Grantz et al., 1982a). Sea level drop and epeiric uplift in Late Pennsylvanian to Early Permian time eroded the Lisburne Group and produced yet another recognized unconformity (Craig et al., 1985).

The Sadlerochit Group (Figure 4) records a Late Permian to Early Triassic transgression of the sea followed by an Early to Late Triassic regression due to increased sediment supply from the north (Craig et al., 1985). The basal Sadlerochit unit, Echooka Formation, consists of a transgressive sandstone of Late Permian age. The marine shales of the Kavik formation of Early Triassic age overlie the Echooka Formation. Coarser sediments of the overlying Ivishak Formation (Early to Middle Triassic) reflect renewed uplift of clastic sediment sources to the north or northeast.

The Shublik Formation was deposited in a moderate marine environment resulting from a Middle to Late Triassic transgression (Craig et al., 1985) (Figure 4). The Shublik Formation is composed of mudstone, limestone, dolomite, siltstone and sandstone (Bird, 1985).

Glauconitic sandstone and shales of the Upper Triassic to Lower Jurassic Sag River Formation overlie the Shublik Formation (Figure 4). The Sag River and the overlying Karen Creek Sandstone record a minor regression of the sea (Bird, 1985).

Deeper marine conditions in Jurassic time led to deposition of the Kingak Shale (Figure 4). The Kingak Shale consists of dark gray to black noncalcareous pyritic shale with minor siltstone interbeds (Bird, 1985). The Kingak shale records deep water deposition to the southeast, while to the northwest, siltier facies were deposited. Deepening water in the Jurassic resulted in a retreat of the coarser-grained units to the northwest as evidenced by the more organic-rich fine shales overlying silts in the Kingak section near Barrow (Craig et al., 1985). Increasing sand content in the uppermost beds of the Kingak Formation record increased sediment supply from the northern source terrane which preceded the Cretaceous rifting episode. Craig et al. (1985) suggested that this shoaling was gradual and the result of thermal uplift of the crust prior to rifting.

Continued uplift of the Arctic Platform prior to and coincident with rifting exposed the entire Ellesmerian Sequence of northern Alaska to subaerial erosion (Figures 5 and 6) . The resulting surface is variously called the Pebble Shale unconformity (Bird, 1985) or the Lower Cretaceous unconformity (Jamison et al., 1980). The Pebble Shale unconformity progressively truncates the Ellesmerian sequence northward (Craig et al., 1985). However, the unconformity between the Lisburne and Sadlerochit Groups had previously beveled the lower Ellesmerian units northward; most of the missing section represented by the Pebble Shale unconformity is from within the thick Kingak Formation.

The Pebble Shale overlies the Pebble Shale unconformity (Figures 4, 5, and 6). The thin, widespread unit is composed of distinctive matrix-supported pebbles and sand grains. The shale component of this formation is dark gray to black with occasional pyrite, glauconite, and green shale beds. The coarser material is well

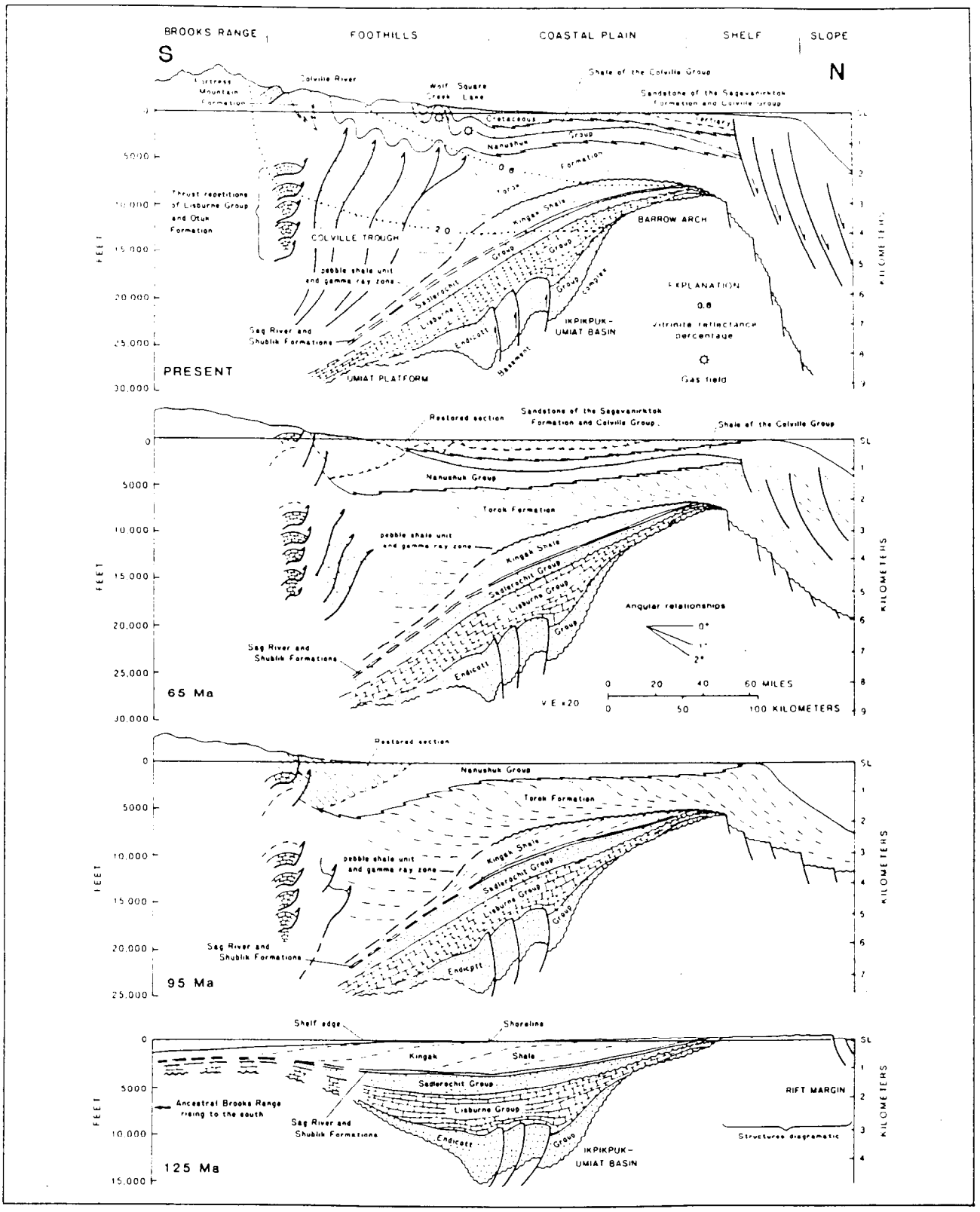

Figure 5. **RECONSTRUCTED STRUCTURAL AND STRATIGRAPHIC CROSS SECTIONS OF THE NORTH SLOPE OF ALASKA AT 153°W**

From Bird, 1985

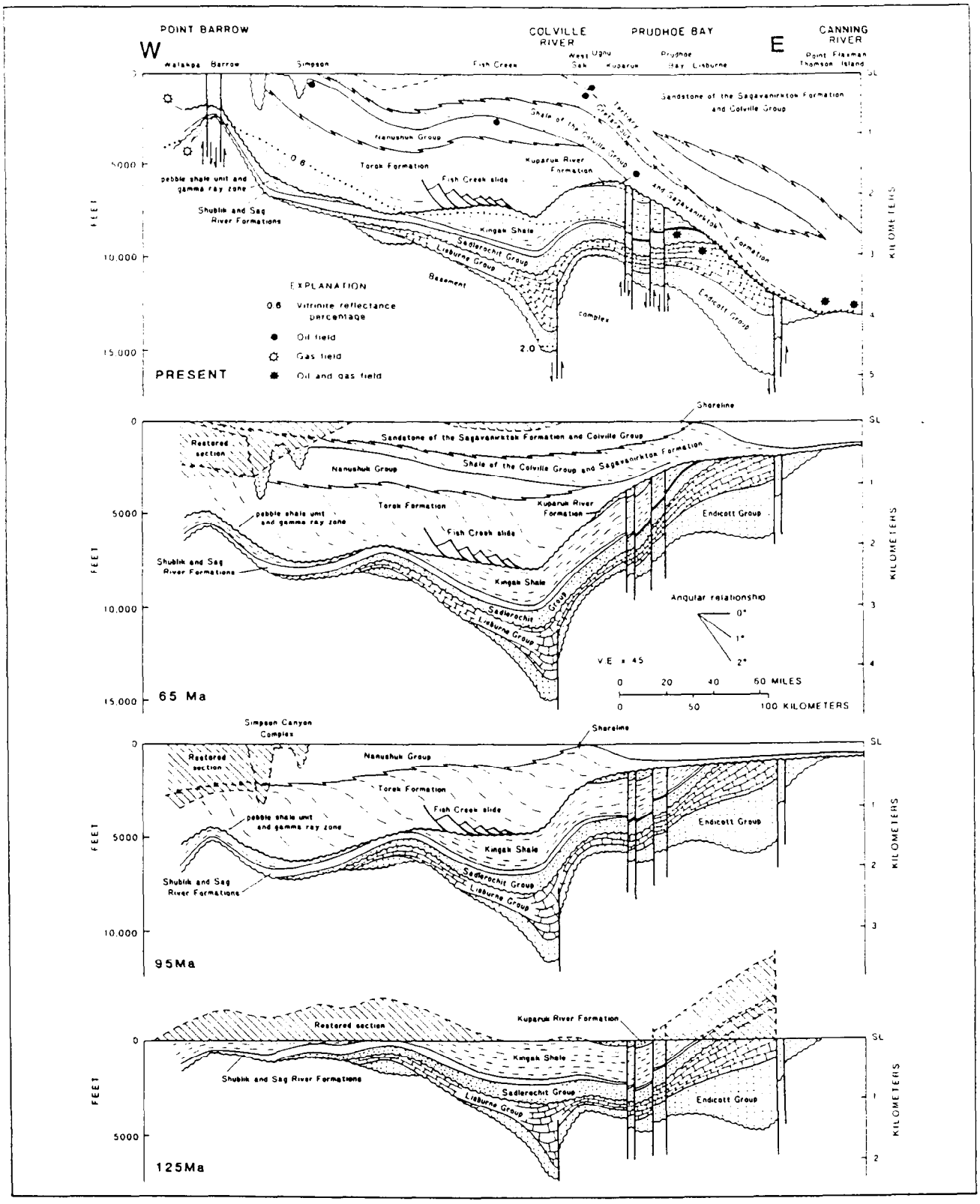

Figure 6. RECONSTRUCTED STRUCTURAL AND STRATIGRAPHIC CROSS SECTIONS OF THE NORTH SLOPE OF ALASKA BETWEEN POINT BARROW AND CANNING RIVER

From Bird, 1985

rounded. Pebbles average less than 2 cm in diameter, but cobbles as large as 25 cm have been reported (Bird, 1985). The sand component of the Pebble Shale ranges from fine grained to coarse grained and is frosted. Sandstone units in the Pebble Shale are localized to the north, near the presumed sediment source. The top of the Pebble Shale is variously defined by a regional unconformity (Craig et al., 1985) or by the Gamma Ray Zone, a radioactive bed with a distinctive well log signature (Bird, 1985).

The Pebble Shale is conventionally considered the uppermost unit of the Ellesmerian sequence of the North Slope of Alaska (e.g. Bird, 1985; Grantz et al., 1980, 1982a). In a geological report on the Beaufort shelf, Craig et al. (1985) proposed that the Pebble Shale defines the "rift sequence". They noted that both contacts of the Pebble Shale are regionally widespread unconformities. The upper surface of the Pebble Shale beneath the Beaufort Shelf is well defined seismically and was termed the Breakup unconformity by Grantz et al. (1974, 1980, 1982a). The rifting processes occurring during the deposition and/or erosion of the Pebble Shale generated numerous grabens beneath the Beaufort Shelf which are filled with strata deposited contemporaneously with the Pebble Shale. The unique depositional setting of these Neocomian age rift deposits and their possible importance as prospective petroleum source rocks or reservoirs indicated their elevation to sequence rank (Craig et al., 1985). In this report, the more traditional terminology of including the Pebble Shale with the Ellesmerian sequence is adopted.

Brookian Sequence

The Brookian sequence was deposited on the present North Slope and beneath the present Beaufort Sea offshore of Alaska between early Cretaceous and Pliocene time (Figure 4). The Brookian sequence is composed of clastic sediments derived from the uplift of the Brooks Range. The sediments prograded northward in contrast to the southerly sediment transport during deposition of the Ellesmerian sequence (Figure 5). The Brookian sediments are by far the most voluminous strata in the offshore Alaska part of the study region. The Brookian sequence varies in thickness from less than 1,000 m over the Barrow Arch to 12,000 m beneath the outer Beaufort Shelf (Craig et al., 1985) (Figure 7).

The Torok Formation (Albian to Aptian) is the basal unit of the Brookian sequence in the western part of the study region (Figure 4). The Torok is composed of fluvial synorogenic detritus near the Brooks Range front, but becomes increasingly marine to the north. In the Beaufort Sea study region, the Torok Formation consists of abyssal plain and continental slope deposits dominated by pelagic clays, turbidites, and thin sand lenses (Craig et. al, 1985). The upward change of the Torok Formation from shale to coarser grained material records the northeastward progradation of a sedimentary wedge of clastic material from the Brooks uplift coupled with the thermal subsidence of the rifted continental margin.

The Nanushuk Group overlies the Torok Formation beneath the study region west of the Colville River and east of Point Barrow (Bird, 1985) (Figures 4 and 6). Outside of this area, the Nanushuk Group comprises marine and nonmarine shale, siltstone, sandstone, coal and conglomerate (Grantz et al., 1980). The Aptian

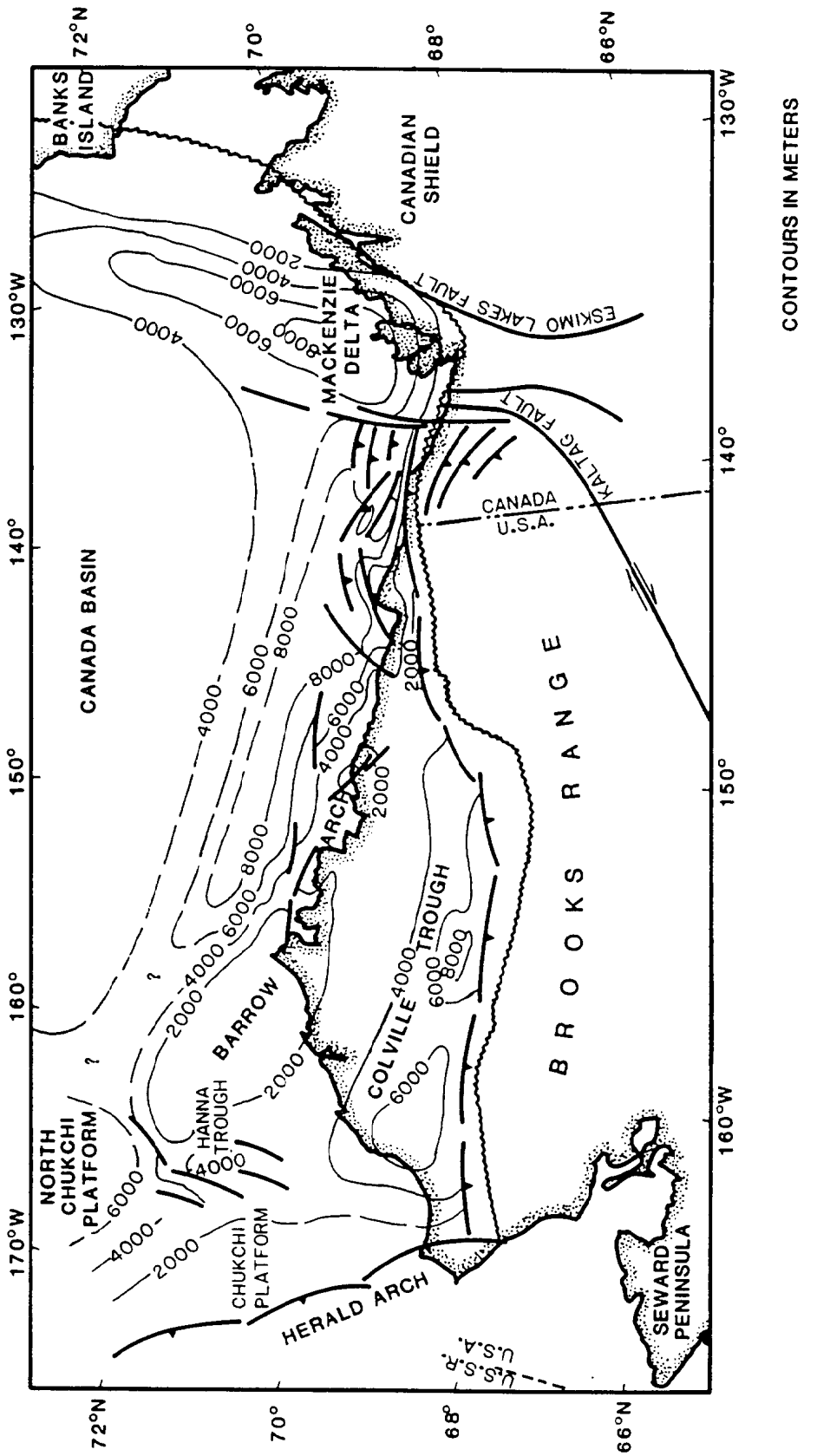

Figure 7. TOTAL THICKNESS OF BROOKIAN SEDIMENTS, BEAUFORT SEA STUDY REGION

After Hubbard et al., 1987

to Cenomanian Nanushuk Group represents fluvial and deltaic facies deposited as the continental margin prograded steadily northeastward (Figures 5 and 6).

To the east of the Colville River the Brookian progradational wedge sediments are younger (Cenomanian to Tertiary) and thicker (Craig et al., 1985) (Figure 6). An eastward shift of the principal depocenter with concurrent basinal subsidence resulted in deposition of the Colville Group, composed of marine shales and minor sandstones. The dominantly sandy Sagavaniriktok Formation contains both marine and nonmarine facies.

The Brookian sediments, beginning with the upper members of the Torok Formation, overtopped the Barrow Arch and the buried tectonic hinge line and were deposited in great quantities seaward of these basement highs (Figure 5). The exact subdivision of the Brookian sediments which prograded seaward of the Barrow Arch and the tectonic hinge line building the present outer shelf and slope is not known due to a lack of drilling control and an abundance of growth faults and slumps which disrupt seismic reflectors. The thickest accumulations were named the Nuwuk Basin and the Kaktovik Basin by Grantz and May (1982). The Nuwuk Basin (Figure 1) is the term used for the prograding Tertiary wedge seaward of the hinge line offshore of the western part of the North Slope of Alaska. The Kaktovik Basin (Figure 1)refers to the thick sediment accumulations offshore of the eastern part of the North Slope. The distribution of Brookian sediments onshore and beneath the inner continental shelf suggests that the bulk of the sediments in the Nuwuk Basin are older than those of the Kaktovik Basin. The preponderance of Torok Formation and Nanushuk Group onshore of the Nuwuk Basin and the younger rocks of the Colville Group and Sagavaniriktok Formation onshore of the Kaktovik Basin is likely to be duplicated in the undrilled distal offshore basins.

Quaternary Deposits

The eustatic drop in sea level during Pleistocene glaciations exposed Brookian sediments on the continental shelf north of Alaska and terminated deposition of Brookian progradational deposits (Craig et al., 1985). The Pleistocene sediments range from outwash silt and gravel to peat. The Pleistocene deposits are considered to be correlative with the Gubik Formation onshore. Holocene sediments are generally unconsolidated muds which increase in thickness near the shelf edge (Dinter, 1982).

Stratigraphy Offshore of Canada

The continental margin of the Canadian sector of the study region is dominated by the Mackenzie delta. The delta and associated cone and deep sea fan have deposited vast quantities of sediment during the Tertiary and Quaternary. Sediment loading from deltaic deposition caused subsidence of underlying rocks. The resulting downwarp offshore of Canada also affected deposition offshore of Alaska as demonstrated by the eastward shift of the depocenter offshore of Alaska during the Brookian sequence sedimentation. Because of the thickness of the delta sediments offshore of Canada, earlier strata are not well known or described.

The Beaufort Sea offshore of Canada has been extensively explored for hydrocarbons since the 1960s. Geological models and terminology vary greatly across the international border. Exploration in and north of Alaska has applied the rifting model to explain the formation of prospective structures. Since commercial deposits of the North Slope are reservoired in Ellesmerian sequence a tectonic controlled sedimentation model to determine pre-rift sediment distribution and post-rift deformation has been the most widely used. The Canadian petroleum and gas discoveries in the Beaufort Sea study region have been reservoired in the Tertiary delta sediments. Exploration has thus stressed traps in these thick clastic wedges; older rocks are so deeply buried as to be nonprospective. Available data pertain to the deltaic cycles and patterns of progradation of the Tertiary delta sediments. Tectonic control of sediment distribution is often not stressed in the Canadian literature (e.g. Dixon, 1986). The names given the lithological units and the tectonically derived sequences are therefore not exactly correlative from offshore Alaska to Canada; most Canadian workers have concentrated on strata equivalent in age to the Brookian strata, but use different formational subdivisions.

Cretaceous Rocks

Dixon (1986) reconstructed the Cretaceous paleography of northwestern Canada. The principal sediment source for Cretaceous deposits in the study region was thought to be from the southeast through Barremian time. Uplift to the northeast in Aptian time redirected transport, with coarse sediments being deposited on present land areas, and silts and deep water clastics being deposited on the present offshore areas. By Albian time deep water turbidites were being deposited in the study region. During the late Cretaceous, the Brookian orogeny for the southwest reoriented the sediment supply. A continental margin elevated to the southwest formed, and shelf and slope facies successively developed toward the northeast. The study region received outer shelf, slope, and abyssal sediments during Late Cretaceous time.

Tertiary Deltaic Sequences

By Paleogene time an identifiable delta was being built by the ancestral Mackenzie River into the Beaufort Sea. The delta prograded northward during the Tertiary as the outlet slowly swung to the east and northeast. The two principal literature sources for Tertiary delta stratigraphy (Willumsen and Cote, 1982; Dixon. 1986) differ somewhat in the locations given to the shoreline and shelf edge during the Tertiary progradation, but their conclusions are compatible.

Willumsen and Cote (1982) divided the Cenozoic sediments of the continental margin of the Canadian Beaufort Sea into five deltaic cycles (Figure 8). The sediments deposited during these progradational cycles range up to 10,000 m in total thickness.

The Paleocene Moose Channel Formation prograded in a northeasterly direction. During deposition of the Moose Channel Formation, the shelf edge was built out about 60 km (Figure 9). The Moose Channel Formation displays a tradi

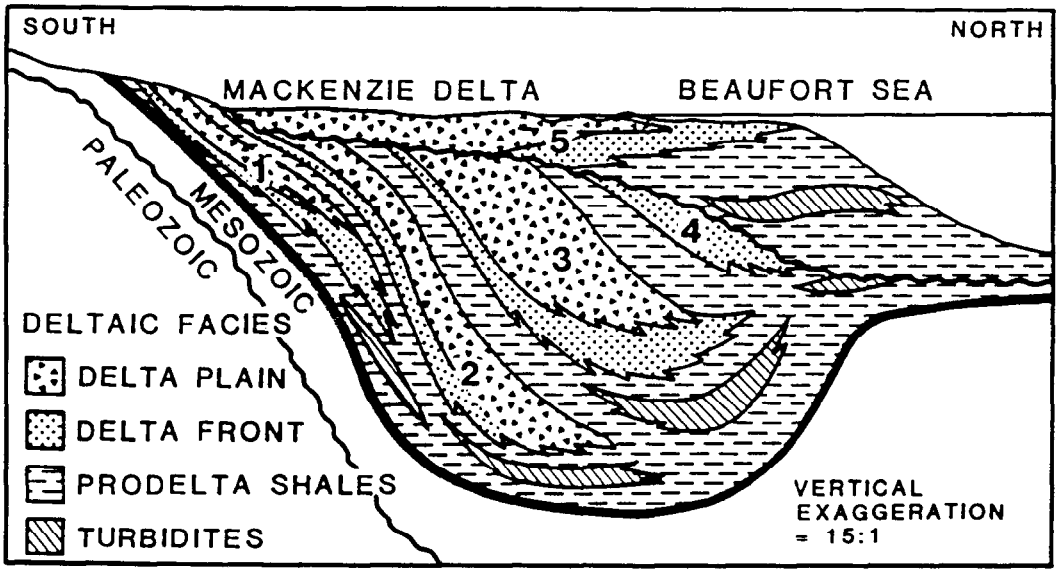

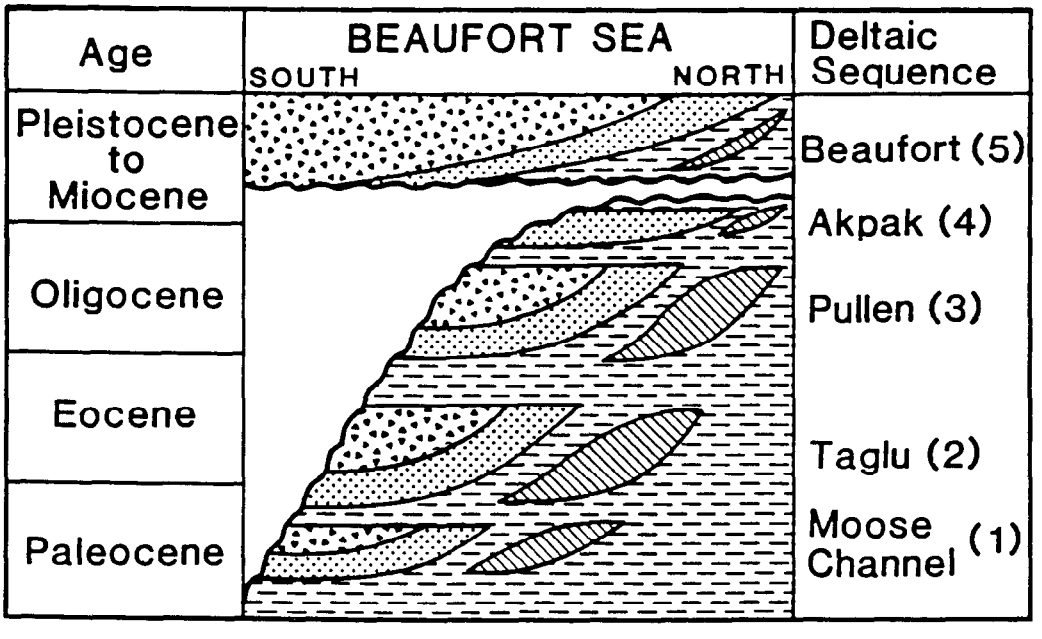

Figure 8. CROSS SECTION OF TERTIARY DELTA SEQUENCES, BEAUFORT SEA, OFFSHORE CANADA

After Willumsen and Cote, 1982

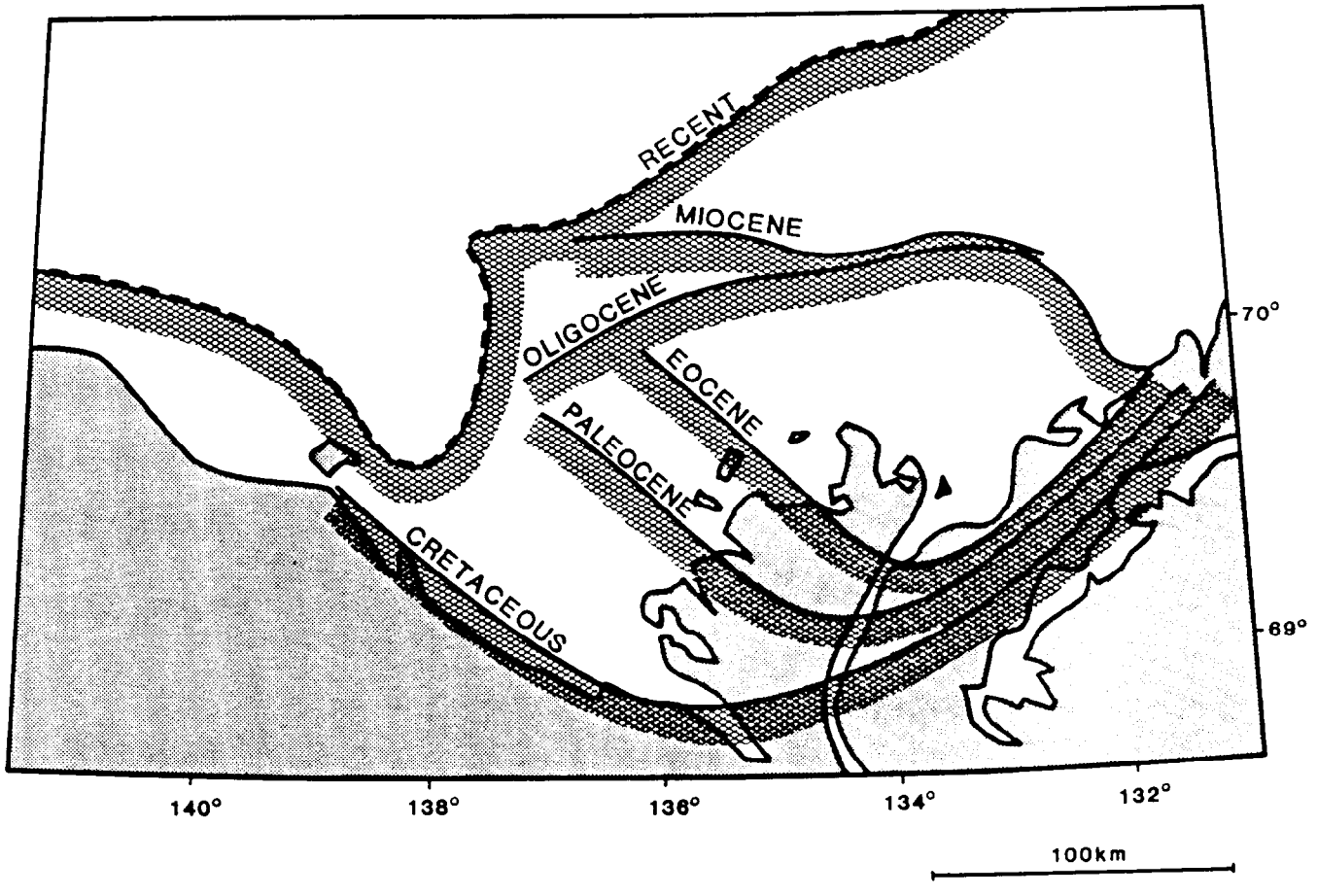

Figure 9. DEVELOPMENT OF THE BEAUFORT CONTINENTAL SHELF OFFSHORE CANADA

After Willumsen and Cote, 1982

tional sequence of deltaic facies with sandy delta-plain and delta-front sediments grading seaward to prodelta shales and eventually turbidites. Cessation of sediment influx or rapid subsidence ended the Moose Channel progradation near the end of the Paleocene. The coarser grained materials were rapidly buried in prodelta shales.

Starting in late Paleocene, another delta prograded seaward. The Taglu delta sequence reached its maximum extent near the end of the Eocene (Figure 8), and extended the continental shelf seaward an additional 40 km (Figure 9). A thick sequence of shales of late Eocene and early Oligocene age capped the Taglu delta sequence.

In the Oligocene a third deltaic sequence began to be constructed on the Beaufort continental margin (Figure 8). The Pullen deltaic sequence advanced the shelf edge by an average of 70 km (Figure 9). The Pullen delta was deposited by fluvial systems which had shifted 80 km to the east compared to the location of the river mouth during Taglu deposition. The shift of the depocenter to near the location of the present mouth of the Mackenzie River allowed direct sediment access to the eastern part of the present shelf during the outbuilding. Thus, very thick accumulations of relatively coarse grained sediments were deposited in the Pullen delta sequence during Oligocene time. The eastern part of the shelf was thus prograded up to 120 km seaward before subsidence and/or transgression stopped the deposition of the Pullen delta sediments.

In the early Miocene another delta, informally termed the Akpak sequence, was deposited on the shales covering the Pullen sequence (Figure 8). The Akpak delta prograded only a short distance beyond the extent of the Pullen delta. Regional uplift in the early Miocene stopped deposition and a wide spread erosional surface removed most of the Akpak deposits and some underlying sequences as well.

The unconformity was submerged and covered by a fifth Cenozoic delta in the middle Miocene. This sedimentary wedge, termed the Beaufort sequence, continued to prograde through the Pliocene and Pleistocene (Figure 8). The shelf was extended to near its present position during deposition of the Beaufort sequence (Figure 9).

Hydrocarbon Generation Potential

The hydrocarbon generation potential of the rocks of the Beaufort Sea study region was discussed by Craig et. al (1985), Grantz et al. (1982a), and Magoon and Claypool (1985). Geochemical work on the onland portion of the Mackenzie delta by Snowdon (1982) can be extended to similar sediments in the offshore Canada portion of the study region.

North Slope of Alaska

An extensive geochemical program to determine the source rocks for the prodigious oil accumulations of the North Slope of Alaska was undertaken by the U.S. Geological Survey (USGS). Early studies indicated that oils from the North Slope could be grouped into two groups: those similar to oils produced from

Ellesmerian reservoirs, principally the Triassic Ivishak sandstone, at the Prudhoe Bay field, and those similar to oils produced from the Cretaceous Nanushuk Group of the Brookian sequence at the Umiat field (Magoon and Claypool, 1981). Subsequently, a program to refine oil/source rock correlation for the North Slope was established by the USGS (Magoon and Claypool, 1985). Splits from 9 oil samples and 15 rock samples were analyzed by 30 commercial, government, and academic geochemical labs. Although the analytical results and geological interpretations varied markedly among the participants of the study, some general relationships emerged.

Oils. The majority of the labs which analyzed the 9 oil samples concurred with Magoon and Claypool (1981) that oils from the Umiat and Prudhoe Bay fields are geochemically distinct (Claypool and Magoon, 1985). All participants recognized a class of oils defined by the Prudhoe Bay sample. All but two of the labs in the study identified another type of oil, that from the Umiat field. Although the Umiat oils were markedly different, three of the labs determined that the differences were not statistically significant. The researchers varied greatly in their interpretations of the possible groupings for oils from North Slope fields other than Prudhoe Bay and Umiat. Some interpreted oils from other fields to comprise their own unique groups, while other investigators concluded that these oils represented mixtures of the two principal types. Overall, little agreement existed as to the exact relationship among North Slope oils except for a general dissimilarity between oils from Ellesmerian reservoirs (e.g. Prudhoe Bay oils) and oils from Brookian reservoirs (e.g. Umiat oils).

Potential source rocks. Sixteen samples of rocks from the North Slope were also analyzed. The samples were taken from five lithological units which had been shown to have source rock potential in previous studies (Magoon and Bird, 1985). Four Ellesmerian sequence units were sampled: the Permian Echooka Formation, the Triassic Shublik Formation, the Jurassic Kingak Shale, and the lower Cretaceous Pebble Shale. Samples from the basal Brookian unit, the lower Cretaceous Torok Formation, were also included in the analyses. A wide variety of geochemical parameters were analyzed for including total organic carbon content (TOC). Pyrolysis yield, bitumen content and composition, kerogen composition and origin, and isotopic signatures.

The research groups varied in their interpretation of the hydrocarbon source potential of the north slope rocks examined. Generally, the samples of the Echooka and Shublik Formations, the Kingak Shale, and Pebble Shale were judged to be dominantly oil-prone sources, whereas the Brookian Torok Formation rocks were interpreted to be gas-prone hydrocarbon sources.

Correlation of North slope oils with potential source rocks by geochemical means was accomplished by most of the research groups in the study summarized by Claypool and Magoon (1985). Although as much inconsistency among labs was noted in oil-rock correlation as with rock and oil geochemical parameters, the majority of research groups agreed in general terms. Rocks of the Shublik Formation and Kingak Shale were the most likely sources of the Prudhoe Bay crude oil.

Pebble Shale and Torok Formation were interpreted by most workers as the most likely source of the oil in Brookian sequence reservoirs in the Umiat Field.

Alaskan Beaufort Shelf

Studies on the source rock potential of the North Slope of Alaska are directly applicable to only the most nearshore portion of the Beaufort Sea study region. The Ellesmerian source rocks identified as the most probable sources of the Prudhoe bay crude oil and associated natural gas pinch out to the north beneath the Beaufort shelf (Figure 6). The vast majority of the Beaufort Sea study region is underlain by Brookian strata equivalent to the Torok Formation and younger units. However, the geochemical characterization of North Slope hydrocarbon sources (Magoon and Claypool, 1985) contribute to the assessment of gas hydrate potential of the Beaufort Sea study region. Samples of the Torok Formation from beneath the North Slope were judged by the 67% of the participating researchers to have source rock potential. Of the workers who considered the tested samples of the Torok Formation to be a potential source, 39% determined that the rocks were predominantly gas prone, 17% interpreted the rocks as oil prone, while 44% did not report the most likely product from the Torok. Thus, the only Brookian sediments for which analytical data are available have source rock potential. If the Brookian sediments beneath the Beaufort Sea study region are similar, they would be expected to also display source potential.

The Brookian rocks of the Beaufort Sea study region differ from the well-studied examples from the North Slope. To the north beneath the Beaufort Sea study region, Brookian strata thicken and change in character from shelf to slope and abyssal plain depositional units. Additionally from west to east, the brookian sediments of the Beaufort Sea study region become younger and more deltaic. Thus while the prospects for organic-rich Brookian sediments in the Beaufort Sea study region are good, the data from onland studies must be extrapolated with care.

Analytical data from a few exploratory wells drilled on the Beaufort shelf support the onland studies and indicate that the Brookian sediments of the study region have sufficient organic carbon to generate sizable amounts of natural gas. Craig et al. (1985) summarized the geochemistry of three wells offshore wells drilled beneath Camden Bay about 150 km east of Prudhoe Bay. The Brookian strata from these wells are generally younger than those beneath Prudhoe Bay, and thus may be more representative of the sediments of the bulk of the study region. The Brookian sediments at these three wells have moderate source potential based on organic carbon content. The kerogen of the Brookian section of these wells is almost exclusively terrigenous (Type III) as evidenced by the low hydrogen index obtained from pyrolysis (Figure 10). Type III kerogen is generally considered to have low potential as a oil source, but to be a good source of gas. At the Exxon Point Thompson #2 well a few of the samples analyzed plot well outside the trend denoting terrigenous kerogen on the Van Krevelen diagram in Figure 10. The elevated hydrogen index of these isolated samples indicate the possible presence of rock units containing kerogen of a more marine nature which would be expected to generate liquid hydrocarbons in addition to gas. Craig et al. (1985) noted that the rocks with marine

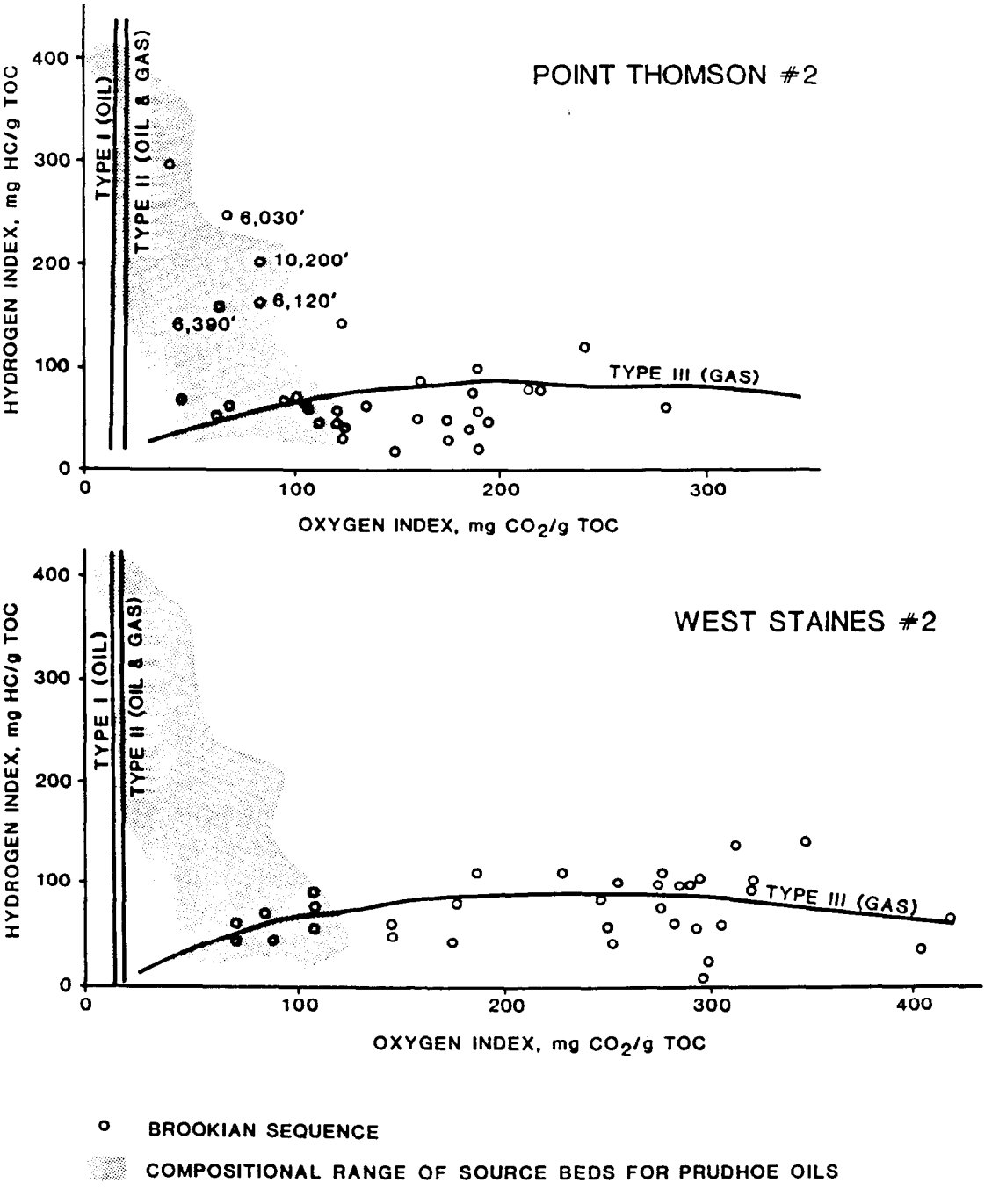

Figure 10. VAN KREVELEN DIAGRAMS OF POTENTIAL BROOKIAN SOURCE ROCKS FROM THE BEAUFORT CONTINENTAL SHELF, CAMDEN BAY, ALASKA

After Craig et al., 1985

organic components are localized in beds at the transition from foreset prodelta facies to topset deltaic facies. They suggested that the marine organic matter may have been preserved beneath quiet water of interdelatic bays or estuaries. Thus the layers of sediments rich in marine organic matter may have prograded seaward along with the advancing delta complex in the Tertiary. Alternatively, Craig et al. (1985) proposed that these prospective source beds may have formed during an Oligocene anoxic event and thus may continue seaward parallel to time lines, in contrast to the diachronous nature of the source beds deposited in quiet water settings in an advancing delta.

Craig et al. (1985) organized the data, including those upon which Figure 10 is based, into a log formats for the three drill holes to illustrate the change of geochemical parameters with depth. The geochemical logs from Craig et al. (1985) are reproduced in this report as Plates 3, 4, and 5. The data illustrated for the three wells were derived principally from pyrolysis, TOC analysis, and petrographic kerogen analysis.

Data from the Point Thomson No. 2 well (Plate 3) were collected only for subbottom depths of 1,550 - 2,030 m and 3,000 - 4,300 m. Thus, the geochemical characteristics of the Brookian sediments in the depth range typical of the gas hydrate stability zone in the Beaufort Sea study region (roughly 0 - 600 m subbottom) were not determined. The shallowest data point reported at about 1,550 m had a total organic carbon value of 4% which rapidly diminishes to 0.4% at 1,700 m. The corresponding maturity indices indicate insufficient maturity for thermogenic gas generation. However, the sporadically high TOC values suggest a very good potential for biogenic gas or early diagenetic gas (Hunt, 1979; Hunt et al., 1984). The presence of migrated oil at 1,800 to 2,000 m depth demonstrates that hydrocarbon migration to shallower depths within the gas hydrate stability zone may also occur.

A more complete data set is presented for the nearby Point Thomson No. 3 well (Plate 4). The shallow Brookian sediments have TOC values averaging about 1% with some as rich as 2%. These gas prone sediments could serve as moderately good sources for biogenic gas hydrates without necessitating substantial migration. In this well also, migrated oil at 2,000 m depth suggests that elsewhere in the area migration of thermogenic gas to the gas hydrate stability zone could occur.

The onshore West Staines No. 2 well depicts the geochemical conditions of shallow Brookian sediments which may be correlative with strata on the shelf of the Beaufort Sea study region. The TOC plot on Plate 5 shows that most of the Brookian section contains between 0.6% and 1.6% organic carbon with a typical value of 1%. Of particular interest is the section between about 650 m and 1,050 m depth which displays very high TOC values. Organic carbon values between 1.5 and 4.0% suggest a very good potential for biogenic methane production exists in some shallow Brookian sediments.

The stratigraphic interval between 650 m and 1,020 m depth is of particular interest because of the relatively high pyrolysis yield of the sediments. The column in Plate 5 labeled "$S_1 + S_2$" indicates the sum of the hydrocarbons driven off from the sample during laboratory pyrolysis including hydrocarbons simply volatilized by

the heating (S_1) and those produced by high-temperature destruction of kerogen (S_2). The $S_1 + S_2$ value for the carbon-rich section is generally greater than 2,000 ppm, the threshold selected by Craig et al. (1985) in conformance with the suggestions of Tissot and Welte (1984) to indicate moderate source potential. The hydrogen index for the West Staines No. 2 (Figure 10 and Plate 5) demonstrates that terrestrial type III organic matter abounds in the interval of interest.

The data from Plate 5 suggest that mobile bitumen is present in the organic carbon rich interval between 650 m and 1,020 m at the West Staines No. 2 well. The $S_1 + S_2$ column ("genetic potential" of Tissot and Welte, 1984) shows that the sum of mobile bitumen (S_1) and hydrocarbons generated from heating kerogen (S_2) is high for the interval. However, the hydrogen index which is the thermally liberated hydrocarbons (S_2) divided by the total organic carbon content (TOC) is low, indicating terrestrial, gas-prone organic matter (Figure 10 and Plate 5). The hydrogen index for the carbon rich interval at the West Staines No. 2 well is similar to that of Brookian sediments which are much lower in TOC at both the West Staines No. 2 well (Figure 10, Plate 5) and at the Point Thomson No. 3 well (Figure 10 and Plate 4). The transformation ratio ($S_1/(S_1 + S_2)$) of the West Staines No. 2 well (Plate 5) shows values indicating anomalously high thermal maturity for such shallow sediments. The estimated thermal maturity from vitrinite reflectance (V_{Ro}) and the temperature at which laboratory thermal degradation is at its maximum (T_{max}) are very much lower through the interval of interest than is the maturity estimate from the transformation ratio (Plate 5). The transformation ratio ($S_1/(S_1 + S_2)$) is typically interpreted as an indicator of thermal maturity (Tissot and Welte, 1984), since an abundance of bitumen (S_1) and thus a high transformation ratio would result from in situ thermal cracking of kerogen. Since the two other measures of thermal maturity, vitrinite reflectance and T_{max}, are consistent with the shallow burial depth and substantially less than that indicated from the transformation ratio, it is likely that the abundance of mobile hydrocarbons (S_1) indicated by the anomalously high transformation ratio are not from in situ thermal degradation of kerogen.

Alternatively, the abundance of bitumen present in the shallow Brookian sediments at the West Staines No. 2 may indicate the presence of migrated hydrocarbons. The ratio of bitumen to organic carbon (TOC) is an effective parameter for indication of the possible presence of migrated hydrocarbons or possible sample contamination by organic drilling fluids. The bitumen to TOC ratio requires tedious wet extraction of the rock to generate a gravimetric concentration of bitumen in the rock. The extraction procedure was reported for the Point Thomson No. 2 well (Plate 3) and the Point Thomson No. 3 (Plate 4), but apparently was not performed for the West Staines No. 2 well (Plate 5). However, Tissot and Welte (1984) cited anomalously high transformation ratio ($S_1/(S_1 + S_2)$) at shallow depths as evidence of migrated hydrocarbons.

Canadian Beaufort Shelf

The abundant hydrocarbon discoveries in the Beaufort Sea offshore of the Mackenzie delta demonstrate the presence of rich mature source rocks. Early geochemical studies of the sediments of the Canadian Beaufort shelf discovered that the deltaic siltstones contained adequate amounts of terrestrial organic matter for

gas generation, but rapid deposition had limited their thermal maturity. An unusual abundance of organic matter derived from tree resin in the immature sediments led investigators to propose that the organic matter of the Beaufort shelf may generate hydrocarbons at thermal maturity levels much lower than those generally accepted. Subsequent studies suggested that the resin rich sediments of the Beaufort shelf cannot generate thermal hydrocarbons at anomalously low levels of maturity.

Snowdon (1980, 1981) and Powell and Snowdon (1981) reported on the geochemistry of oils and rocks from the Beaufort shelf and Mackenzie delta area. Most of their samples were from the onland parts of the Mackenzie delta, but data were also reported for an offshore well, the Netserk B-44.

Only six rock samples from the Netserk well were analyzed in detail by Snowdon (1981), from depths of 330, 887, 1,637, 2,954, 3,219, and 3,475 m. The samples were analyzed for total organic carbon content (TOC), quantity and composition of extractable organic matter (bitumen), and kerogen type and maturity. In addition, TOC values for rocks recovered from other depths were presented in a graphical format along with the results of gas logging (Figure 11). Organic carbon content decreased downhole from 2.5% at 330 m to 1.0% at 3,218 m before increasing to 1.6% at 3,474 m. Values reported on the TOC log also show high TOC levels at the 300 m level diminishing with depth before increasing again to high values at 3,000 m. The organic matter was found to be overwhelmingly of terrestrial origin, consistent with the deltaic origin of the sediments. Snowdon (1981) reported that marine (amorphous) organic matter ranged from 0.5 to 5.2% of the TOC with the remainder present as terrestrial (herbaceous and coaly) types. Thermal maturity of the sediments, measured as vitrinite reflectance (Ro), increased regularly downhole from 0.27% at 330 m to 0.62% at 3,475 m. The low maturity at depth was taken to indicate rapid sediment deposition. The maturity of the deepest sediment tested is near the minimum generally considered necessary for thermal hydrocarbon generation. The gas logs (Figure 11) show that an appreciable quantity of gas is contained in the sediment, even at relatively shallow subbottom depths. The "Percent Wet Gas" curve on the log indicates that measurable amounts of thermogenic gas are not detected above about 1,500 m. Thus, it appears that the upper 4,000 m of the sedimentary section in the Beaufort continental shelf may be generating sizable quantities of biogenic gas from the adequate TOC levels measured in the sediments (0.5 to 2.5%).

Among the organic matter identified by Powell and Snowdon (1981) and Snowdon (1980, 1981) relatively large quantities of the maceral resinite was found in the Tertiary sediments of the Mackenzie Delta and Beaufort shelf. Resinite is thought to be derived from tree sap and resins which had not decomposed subsequent to deposition.

Using geochemical parameters Snowdon (1980, 1981) determined that the high gravity oils and condensates discovered in the wells studied were probably generated in sediments near the depths of the reservoirs with little vertical migration. Hydrocarbons were discovered as shallow as 2,000 m in some of the wells. However, the depth to thermal maturity in the drill holes measured was about 4,000 m for incipient oil generation. Rocks with the generally accepted level of thermal maturity required for gas and condensate generation (Ro = 1.3%) were not penetrated in the wells studied. Thus a geochemical paradox was present: oils appeared

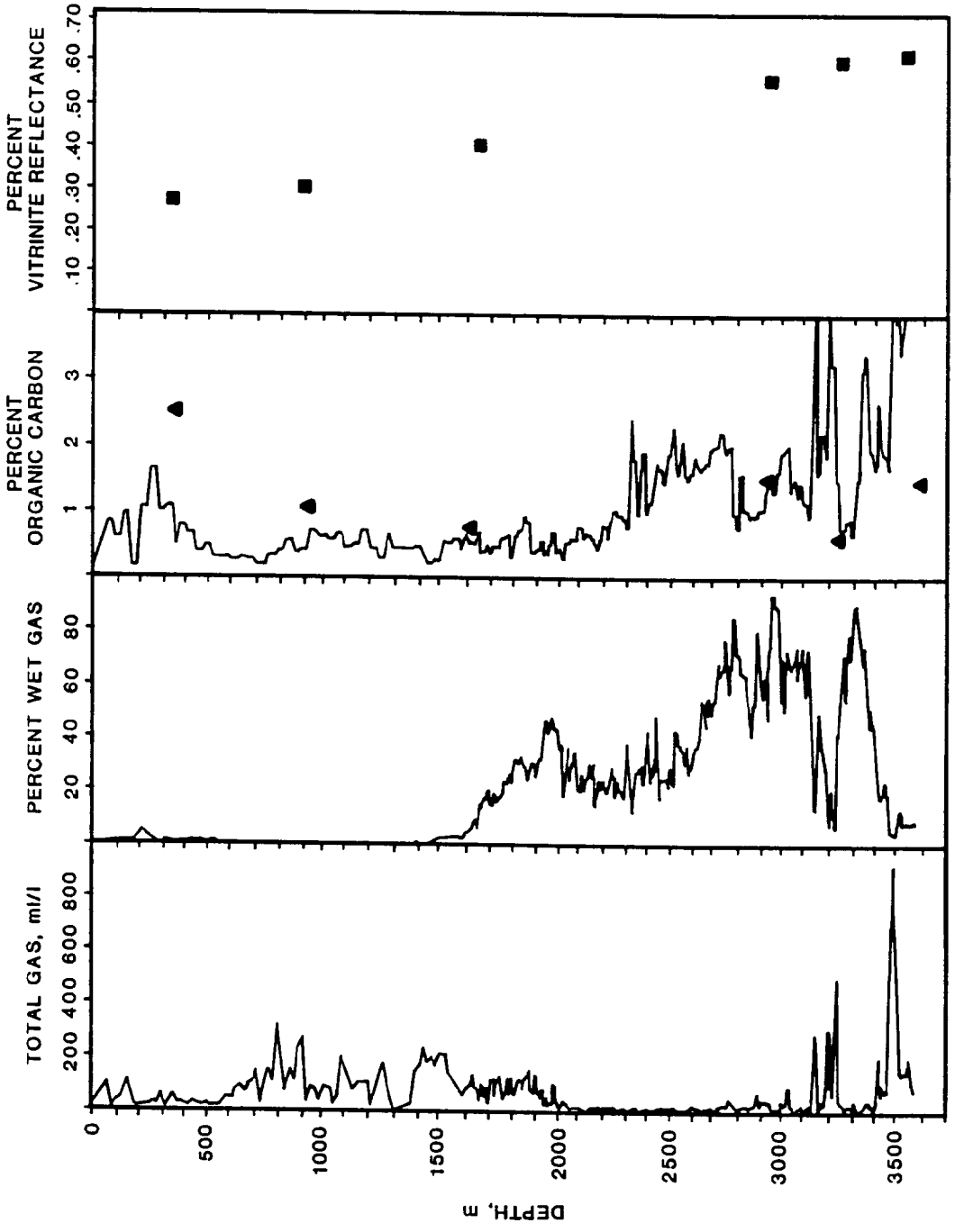

Figure 11. GEOCHEMICAL CHARACTERISTICS OF NETSERK WELL, CANADIAN BEAUFORT SHELF

Modified from Snowdon, 1981

to be generated at depths much shallower than the depth of sufficiently mature potential source rocks. Snowdon (1980, 1981) and Snowdon and Powell (1982) proposed that the generation of light oils and condensates in the Mackenzie Delta and Beaufort shelf had occurred at anomalously low levels of thermal maturity due to the very high resinite content of the sediments. They stated that resinite may begin to generate gas and liquid hydrocarbons with much less heating than required for other maceral types.

Studies were subsequently undertaken by Lewan and Williams (1987) to test the hypothesis of Snowdon (1980, 1981) and Snowdon and Powell (1982). Resinite samples from throughout the world were concentrated and subjected to simulated thermal maturation. Hydrous pyrolysis of resinite samples produced principally aromatic compounds rather than the saturated hydrocarbons attributed by Snowdon (1980, 1981) and Snowdon and Powell (1982) to resinite source material. Additionally the study by Lewan and Williams (1987) did not demonstrate generation of hydrocarbons by resinite at temperatures lower than those required by other terrestrial organic carbon types. Lewan and Williams (1987) inferred that the high resinite content of the Beaufort shelf sediments could not have produced the oil and condensate in adjacent reservoirs. Substantial vertical migration is thus required to accommodate the shallow gas and condensate accumulations in the Canadian part of the Beaufort Sea study region.

Thermal Maturity

The few available studies on the source rock potential of the Tertiary sediments of the Beaufort Sea study region suggest good potential for microbial gas generation. Studies reported by Snowdon (1981) and Craig et al. (1985) indicated that the rapid sediment accumulation in the Tertiary and low geothermal gradients resulted in slow maturation of organic matter; minimum depths to thermal maturity of 3,000 to 4,000 m were derived.

In the absence of drilling data, Grantz et al. (1982a) estimated the thermal characteristics of the Alaskan portion of the Beaufort Sea study region based on tectonic history. Grantz et al. (1982a) used the method proposed by Royden et al. (1982) to determine the thermal history of a passive continental margin. The model is based on the rate of subsidence and the change in heat flow which occurs subsequent to rifting. Using relationships developed principally on the Atlantic coast of the United States, the method of Royden et al. (1980) permits estimation of thermal maturity of margin sediments using only the present depth of the unconformity produced during the continental breakup. Thermal maturity estimates for three areas of the study region offshore of the study region are diagrammed in Figure 12. The depth to various stages of thermal maturity is plotted through time. Many interpretations exist as to the maturity at which different stages of oil generation begin (e.g. Tissot and Welte, 1984; Hunt, 1979; Snowdon, 1980; Hedberg, 1974; Dow, 1977); but Grantz et al. (1982a) did not specify which convention was used to convert numerical time and temperature values to generation stages. Each of the three diagrams in Figure 12 show rapid maturation in the Cretaceous due to the very high heat flow during and immediately after the rifting episode. According to the model used to derive the curves, biogenic methane formation is the only plausi-

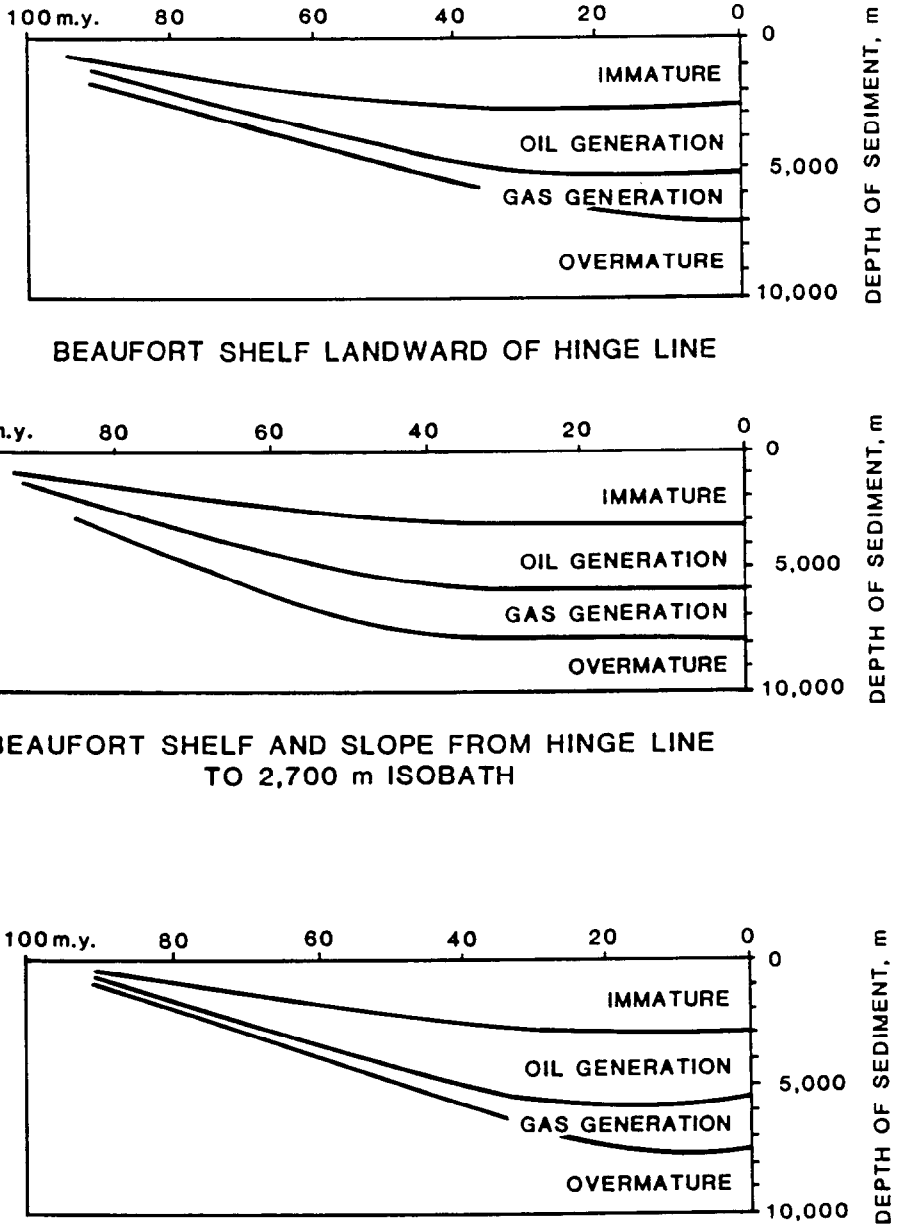

Figure 12. ESTIMATED THERMAL HISTORY OF POST-RIFT SEDIMENTS OF THE BEAUFORT SEA STUDY REGION

Modified from Grantz et al., 1982

ble hydrocarbon generation mechanism expected in sediments at depths of less than 2,800 m to 3,800 m. Significant thermal gas generation is not projected to occur at depths of less than 5,000 m to 6,000 m. Although some associated natural gas would be generated concurrently with oil generation in the 3,000 to 6,000 m depth interval, the work of Grantz et al. (1982a) indicates that vertical migration distances of at least 5,000 m would be required to introduce thermogenic natural gas to the gas hydrate stability zone in the Beaufort Sea study region.

Craig et al. (1985) estimated geothermal gradients and thermal maturity of the sediments of the study region based on a few key drill holes and extrapolation of regional trends apparent from onshore drilling. Estimates of geothermal gradients range from 2.7 to 3.6°/100 m for the study region (Table 1). By coupling these predicted geothermal gradients with sedimentation rates derived from seismic sections, Craig et al. (1985) derived probable depths to various levels of thermal maturity. Thermal maturity corresponding to a vitrinite reflectance of 0.6%, estimated by Hunt (1979) and Dow (1977) to correspond to the oil generation threshold, occurs at 2,800 m beneath the majority of the continental shelf offshore of the North Slope of Alaska (Table 1). The same level of maturity probably occurs at greater depths in other parts of the study region due to the combined effects of lower geothermal gradients (Camden and southern Nuwuk Basins) and rapid sedimentation (Nuwuk and Kaktovik Basins). The depths predicted by Craig et al. (1985) for thermal maturity corresponding to Ro=0.6% (Table 1) are generally greater than those calculated by Grantz et al. (1982a) for initiation of oil generation (Figure 12). The difference is most profound in the Nuwuk and Kaktovik basins where Grantz et al. (1982a) projected a depth of about 3,000 m, and Craig et al. (1985) estimated depths of 3,700 to 4,700 m. The somewhat arbitrary demarcation between the oil generation and gas generation windows ranges from 3,750 m beneath the continental shelf landward of the tectonic hinge line to 7,150 m beneath the Kaktovik and Nuwuk Basins (Table 1). Grantz et al. (1982a) predicted a depth range of 5,000 to 6,000 m for the top of the gas generation zone (Figure 12).

Although the estimates of the depths to various levels of thermal maturity vary among the investigators, the implication for gas hydrate distribution is consistent: vertical migration of several thousands of meters is required for accumulation of substantial quantities of thermogenic natural gas in hydrate form in the Beaufort Sea study region.

Table 1.

PREDICTED GEOTHERMAL GRADIENTS AND DEPTHS TO THERMAL MATURITY, BEAUFORT SEA OFFSHORE ALASKA

Area	Geothermal Gradient, °C/100 m	Top of Oil Generation Window (R_0 = 0.6%)	Top of Gas Generation Window (R_0 = 1.35%)
Arctic Platform (shelf shoreward of hinge line)	3.6	2,800 m (100°C)	3,750 m (136°C)
Canadian Basin (eastern part of Arctic Platform)	3.3	3,100 m (100°C)	4,200 m (136°C)
Kaktovik and Nuwak Basins	2.7	4,700 m (131°C)	7,150 m (198°C)
Southern Nuwak Basin (between hinge line and shelf break)	2.7	3,700 m (100°C)	5,050 m (165°C)

PART II

FORMATION AND STABILITY OF GAS HYDRATES

Seismic and drilling evidence of gas hydrates has been reported from the Beaufort Sea study region. Abundant bottom simulating reflections (BSRs), interpreted to mark the lower limit of the gas hydrate stability zone occur in seismic profiles from offshore Alaska. During exploratory drilling on the Beaufort continental shelf offshore of Canada, sediment intervals with high resistivity and seismic velocity and low permeability which released large quantities of mud gas were penetrated beneath permafrost. These unusual intervals were interpreted to contain gas hydrates (Weaver and Stewart, 1982).

Very low water temperatures of the Beaufort Sea suggest that gas hydrates could occur beneath relatively shallow water depths. Relict permafrost on the Beaufort continental shelf extends to depths of 400 to 800 m subbottom. The low temperatures and high pressures beneath the subsea permafrost are sufficient to stabilize gas hydrates, although water depths on the shelf are much less than the generally accepted minimum for offshore gas hydrate stability.

Grantz et al. (1976) reported strong bottom simulating reflectors on single channel seismic profiles from the continental slope and rise north of Alaska. Subsequent multichannel seismic sections also showed abundant BSRs beneath the slope and rise (Grantz et al., 1980). Additionally, enhanced- amplitude reflectors parallel with bedding planes were noted from the outer continental shelf and upper slope. These were also presumed to be caused by gas hydrates. Seismic evidence of gas seeps has been noted in a few areas of the continental shelf.

Evidence of Gas Hydrates from Single Channel Seismic Data

Bottom simulating reflectors (BSRs) on some single channel seismic records were described by Grantz et al. (1976). The seismic lines had been collected by the USGS in August and September 1973 aboard the U.S. Coast Guard Cutter *Burton Island*. Grantz et al. (1976) reported that the BSRs occurred at 100 to 300 m subbottom beneath water from a minimum depth of 400 to 600 m to the deepest water surveyed at 2,500 m. The BSRs were reported to occur beneath 60% of the lines beneath water deeper than 400 to 600 m, giving an estimated minimum areal extent of 7,500 km^2. Grantz et al. (1976) described the BSRs as strong beneath bathymetric high and weak or absent beneath local bathymetric depressions. Reflections of sediment layers beneath the BSRs were reportedly bowed downward. The polarity

of the BSRs was reported to be reversed relative to the sea floor reflection. Grantz et al. (1976) concluded that the BSRs indicated pools of free gas trapped beneath a gas hydrate cap.

The seismic lines upon which these interpretations were based have been released as an open-file report (Grantz et al., 1974). The available seismic records are single channel analog profiles. A 160 kJ sparker (arc) was the principal seismic source used. Lines were collected from Point Barrow to Mackenzie Bay (Plate 6). Most of the lines were shot over the Beaufort continental shelf. Pack ice prevented surveying substantial areas of the continental slope except offshore between Point Barrow and Harrison Bay where sediments beneath water as deep as 2,500 m were surveyed.

Figure 13 shows a short segment of Line 363 with a BSR typical of those noted by Grantz et al. (1976). The section was shot while traversing the continental slope from southeast to northwest about 100 km north of the Colville River delta. The course of the ship was oblique to the strike of the slope; the seismic Line records neither a pure dip section nor a strike section. Two distinct BSRs are evident in Figure 13. A reflector parallels the sea floor about 0.45 sec subbottom beginning at the left border of the section and continuing for about 5 km. Although the single channel section has poor resolution of deeper sedimentary layers, the BSR at the left part of the figure clearly cuts across the sediment layers which appear to be dipping steeply to the northwest. Farther to the southeast, the BSR becomes diffuse and cannot be resolved from the sedimentary reflectors and noise. The BSR reappears beneath the bathymetric high at the right-center of the figure. The BSR mimics the sea floor topography but is more subdued. This is consistent with the form of gas hydrate reflectors which have been documented in other regions of the world. Since the BSR represents a pressure and temperature dependent boundary, the general topography of the seafloor is mimicked by the isothermal surface coincident with the hydrate phase boundary. At the subbottom depths at which the hydrate phase boundary occurs, the small perturbations in local heat flow patterns caused by minor sea floor irregularities are minimal. Thus, only the large scale changes in sea floor relief are reflected in the morphology of the isotherms at 200 to 800 m depths. The BSR in Figure 13 is very well defined beneath the high. The poor quality analog records do not permit a direct estimation of the reflection coefficient of the BSR as described from multichannel data by Shipley et al. (1979), but the BSR beneath the high appears to be at least as reflective as the most reflective sediment layer. The amplitude of the BSR is greater than that of the return from the sea floor over the high, and is of a similar magnitude to the seafloor reflector on the left portion of the figure.

The high reflectivity of the BSRs in the bathymetric highs of this set of seismic lines indicates that the impedance contrast between the layers causing the BSR is greater than beneath adjacent intervals away from the bathymetric high. Grantz et al. (1976) stated that the BSRs displayed reverse polarity which would indicate that they represent a transition from high velocity and/or density material above to low velocity and/or density material below. From the poor quality copies of the available seismic lines we are not able to confirm or refute the reverse polarity reported by Grantz et al. (1976), but given the appearance and subbottom depths

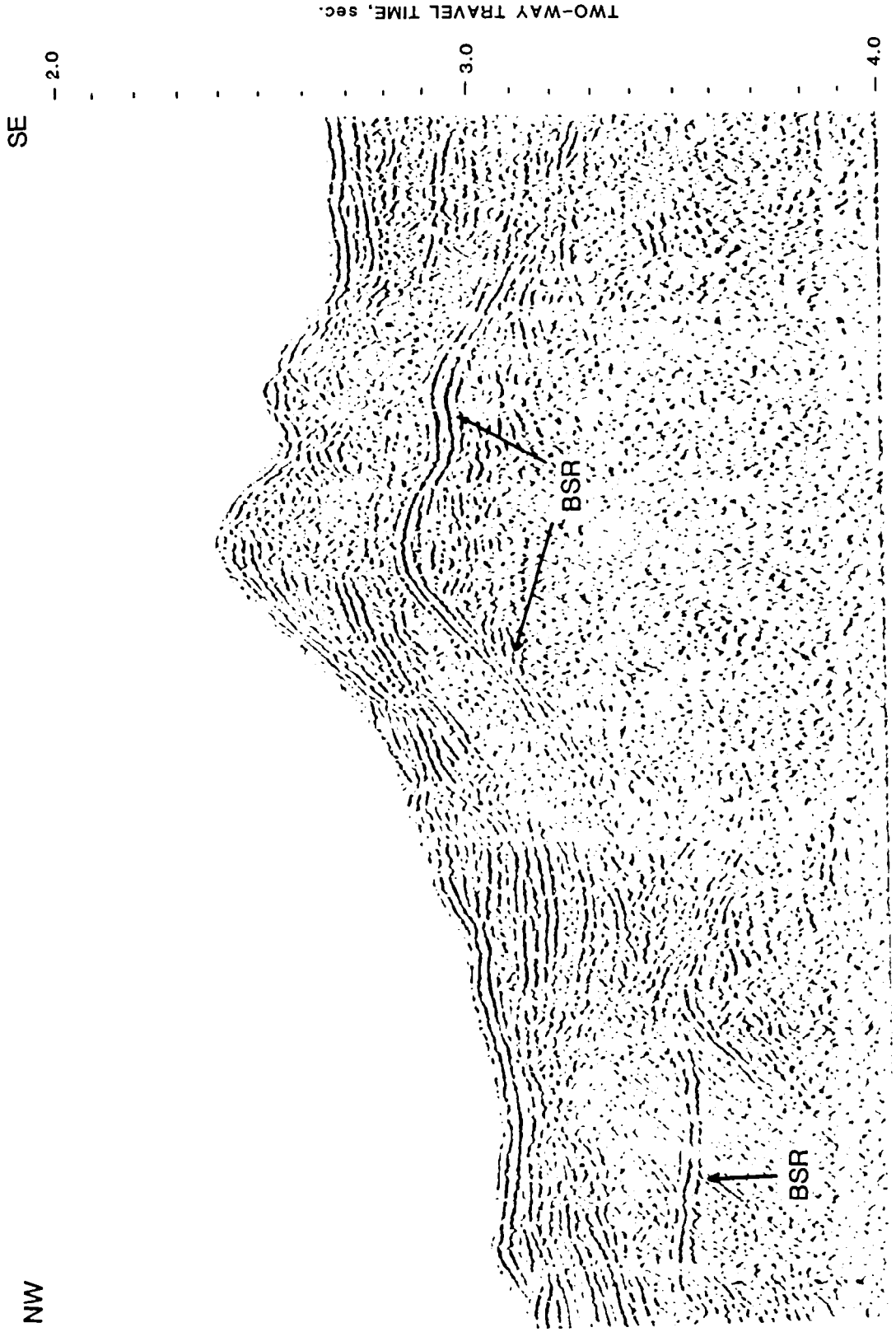

Figure 13. SEGMENT OF SINGLE CHANNEL SEISMIC LINE 363, ALASKAN CONTINENTAL SLOPE OFFSHORE OF THE COLVILLE RIVER DELTA

of the reflectors, their gas-hydrate origin, and thus their reverse polarity, seem very likely.

A high impedance contrast at a hydrate boundary can be obtained by either extensive hydrate formation in the gas hydrate stability zone, or by underlying low density or velocity sediment. Gas hydrates in the interstices of sediment greatly increases their seismic velocity (Stoll and Bryan, 1979; Pearson et al., 1982). The same impedance contrast exhibited by a thick layer sediments containing hydrates overlying non-hydrated sediment could also be attained by a relatively thin hydrate-bound sediment layer capping an interval of sediment with interstices filled with free gas. The gas in the pore spaces both decreases the effective density of the sediment and greatly slows seismic impulses resulting in very low impedance. De Boers et al., (1985) estimated that a layer of gas hydrate impregnated sediment as thin as one meter could trap a gas column underneath and thereby produce a density/velocity decrease decessary to produce a BSR

Our research on BSRs from other regions has not conclusively shown whether BSRs are due to free gas presence beneath the hydrate layer. The calculated impedance changes on seismic lines displaying distinct BSRs neither require nor preclude trapped free gas; the range of seismic velocity and density measured in offshore sediments makes can accommodate either model of BSR formation. The most extensive data base of impedance change at BSRs was presented by Shipley et al. (1979). Using digital seismic data collected by the University of Texas, Shipley et al. (1979) calculated the impedance change represented by BSRs on lines from Blake Outer Ridge, Colombia Basin, and Panama Basin. Shipley and Didyk (1982) calculated the impedance change at BSRs from University of Texas lines from the Middle America Trench offshore of Oaxaca, Mexico. Shipley and Didyk (1982) demonstrated that the impedance change observed offshore of Mexico was best explained by gas hydrate filled sediments overlying unconsolidated sediments without free gas. Finley and Krason (1986b) calculated reflection coefficients and impedance contrasts at a BSR from a seismic line of the Middle America Trench offshore of Guatemala based on an expanded trace presented by Ladd et al. (1982). Finley and Krason (1986b) determined that the BSR was best explained by assuming that free gas was contained in the pore space of the sediments underlying the BSR. However, by invoking densities and seismic velocities within the range of those measured in Deep Sea Drilling Project (DSDP) cores from the area, the impedance change represented by the BSR offshore of Guatemala could have conceivably resulted from underlying sediments without significant free gas in the interstices.

Presence of Free Gas

Grantz et al. (1976) proposed that the BSRs offshore of Alaska were caused by free gas trapped underneath a gas hydrate cap. Grantz et al. (1976) stated that the association of BSRs and local bathymetric highs indicated pooling of free gas beneath the BSR. Since BSRs coincide with isothermal surfaces which generally mimic the sea floor topography, any local bathymetric high defines a corresponding structural high in the base of the gas hydrate stability zone. If sufficient methane exists to form enough hydrate at the base of the gas hydrate stability zone to plug the sediment pores to upward gas migration, a bathymetric high defines an antifor-

mal trap for subsequently generated or migrated gas. Free gas at the base of the gas hydrate stability zone, by analogy with conventional anticlinal hydrocarbon traps, would be expected to migrate up the dip of an inclined segment of the impermeable surface by buoyant forces and to pool in the structural highs beneath corresponding bathymetric highs. Accumulation of free gas in the interstices of the sediment beneath such traps would decrease both the density and seismic velocity of the sediment. Decrease of both of these properties due to gas accumulation would increase the impedance contrast of the gas-filled sediment and the overlying gas hydrate-filled sediment with its higher density and seismic velocity. Since the amplitude of the BSR is dependent on the impedance contrast at the base of the hydrate stability zone, gas pooled in anticlinal traps beneath bathymetric highs should increase the intensity of the BSRs observed on seismic sections of bathymetric highs. Indeed, the BSR illustrated in Figure 13 is most visible beneath the bathymetric high and becomes much less distinct away from the high.

The reappearance of the BSR beneath the small bathymetric trough at the left quarter of the seismic section in Figure 13 would appear to contradict the assumption of a relationship of BSR impedance with trapped free gas. The BSR, while not as distinct as in the adjacent anticlinal trap is substantially more visible than in the intervening sediments. However, the enhanced definition of the BSR along the left border of Figure 13 could also be ascribed to trapped free gas if a stratigraphic rather than structural trapping mechanism is invoked. Gas could migrate up dip along more permeable layers of the steeply inclined sediments which coincide with the more distinct portion of the BSR. The permeability decrease at the base of the gas hydrate stability zone could then trap the migrating gas bringing about a greater impedance contrast and therefore a more visible BSR. Such a trap would require that the steeply northwest dipping beds in which the BSR is developed be composed of discrete strata of highly permeable sediment alternating with less permeable layers. If the dipping sequence did not contain relatively impermeable interbeds, the gas would rapidly migrate up dip to the adjacent anticline, and the BSR would not be distinct.

Although the presence of a strong BSR beneath both a bathymetric low and an adjacent bathymetric high can be explained by assuming different trapping mechanisms, some inconsistencies remain. The stratigraphic trapping model described above requires permeable migration pathways to deliver gas to the base of the gas hydrate stability zone and relatively impermeable layers to retain the free gas at the structural low and prevent its rapid migration up the dip of the gas hydrate stability zone to the adjacent structural trap. However, if such impermeable interbeds exist in the sediment section, they would be expected to impede migration along the base of the gas hydrate stability zone elsewhere in the section. The existence of strata sufficiently impermeable to permit the formation of a free gas pool beneath the gas hydrate stability zone at the left of Figure 13 would seem to preclude migration along the base of the zone to the extent necessary to form the gas pool in the adjacent anticlinal trap.

Another criterion used by Grantz et al. (1976) to infer the presence of free gas trapped beneath the gas hydrate stability zone in the Beaufort Sea study region is the distortion of sediment reflectors beneath the BSRs. Since gas trapped in sediment pores diminishes seismic velocity, a reflector within or beneath a gas-charged zone would have a longer seismic return time than if no free gas were pre-

sent. On a seismic time section an anomalously long return time due to free gas presence would be manifested by reflections displaced toward the bottom of the display. The reflections from within or beneath the free gas zone would thus appear on the section to be deeper than equivalent reflections from an adjacent area without trapped free gas. The reflections from sediment layers beneath many of the particularly strong BSRs from the Beaufort Sea study region are bowed downward as would be expected if low velocity material such as gas-charged sediment were present beneath the BSRs. The effect can be seen beneath the antiformal section of BSR shown in Figure 13. Whereas the sediment reflectors above the BSR appear to be arched in an anticlinal manner generally conformable with the seafloor topography and the BSR itself, the reflectors beneath the BSR appear to define a synclinal orientation. The bowed reflectors in Figure 13 could certainly be an accurate representation of the true sediment orientations rather than an expression of a velocity anomaly due to trapped gas (velocity push down). However, such reflection orientations are common beneath bathymetric highs in the seismic lines published by Grantz et al. (1974). The effect is particularly noticeable on a pair of highs on Line 331 (Figure 14). The segment of Line 331 shown in Figure 14 is located about 40 km east-southeast of the portion of the slope illustrated in Figure 13 (Plate 6). The BSR beneath the bathymetric highs in Figure 14 is very distinct. The hydrate reflector appears to be similar in amplitude to the seafloor return, and perhaps even greater. The localization of the BSR beneath bathymetric highs is also well expressed in Figure 14; the BSR quickly dies out in the troughs on either side of the pair of highs. The apparent velocity push down beneath the BSRs is most evident beneath the smaller of the highs. The reflectors on each flank of the BSR-defined anticline are consistently bent downward upon crossing the BSR toward the interior of the anticline. The amplitude of the BSR appears to be undiminished in the small trough separating the two bathymetric highs. This suggests that if underlying free gas is responsible for the impedance contrast at the BSR, free gas must also be present beneath the small trough. The sediment reflectors beneath the trough are bowed downward suggesting that the greater thickness of low velocity material underlies the two highs. However, even in this section with such a well defined BSR, the interpretation of velocity features is not unambiguous; the resolution of the sediment layers above and below the BSR is insufficient to rule out the possibility that the downward bowed reflectors in Figure 14 are not in fact accurate depictions of the true sediment orientations.

Another example of possible velocity push down of reflectors beneath BSRs is seen in Figure 15. Seismic Line 333 was shot approximately parallel to strike of the continental slope. The section of Line 333 presented in Figure 15 is located approximately 40 km east of the segment of Line 363 shown in Figure 13. The general form of the BSR in Line 333 (Figure 15) resembles that of the previous examples in that it is most visible beneath bathymetric highs. Beneath adjacent bathymetric lows, the BSR in Figure 15 either becomes more diffuse or becomes entirely unresolvable. The orientations of sedimentary layers within the gas hydrate stability zone are much better depicted in Figure 15 than in the previous examples. The sedimentary reflectors along the west flank of the broad bathymetric high near the center of the figure are subparallel to both the sea floor and the BSR, but dip more steeply to the west. Likewise, the sediments above the BSR on the east flank of the

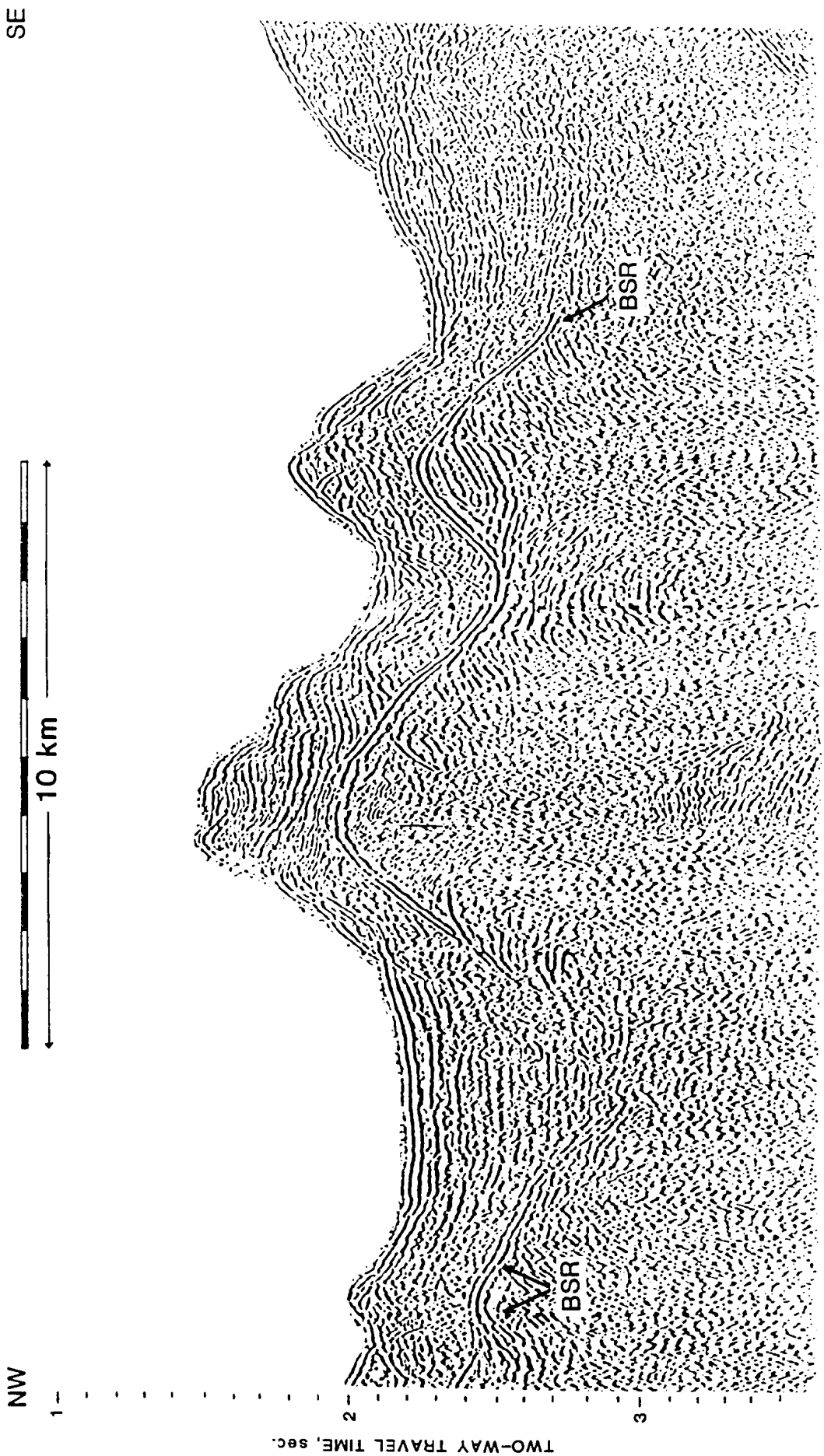

Figure 14. SECTION OF SINGLE CHANNEL SEISMIC LINE 331 OFFSHORE ALASKA SHOWING POSSIBLE VELOCITY PULLDOWN BENEATH BSR

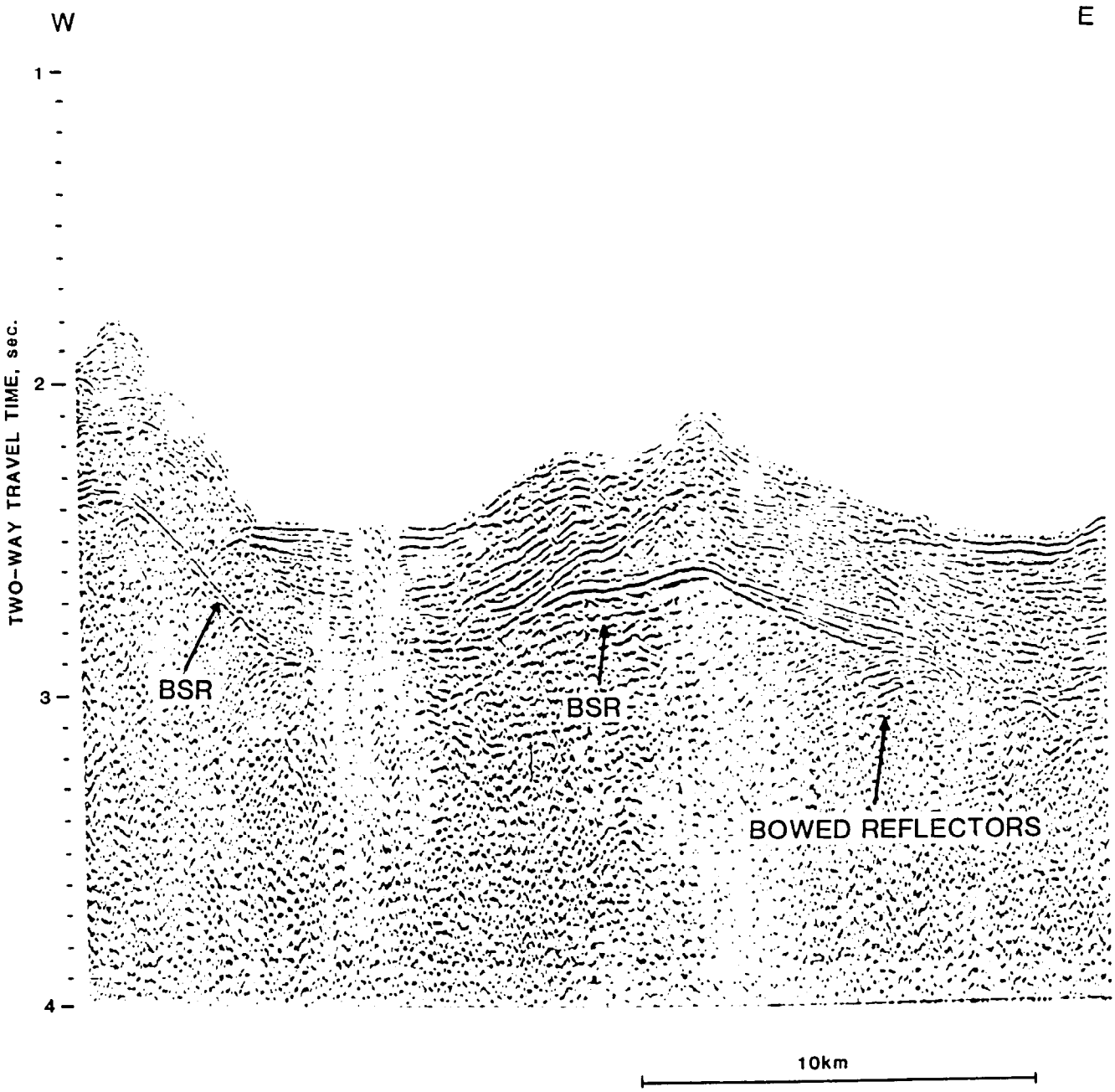

Figure 15. SEGMENT OF SINGLE CHANNEL SEISMIC LINE 333, OFFSHORE ALASKA

bathymetric high dip to the east. Thus the sedimentary reflectors within the gas hydrate stability zone define a true anticline coincident with the seafloor high and the antiformal BSR. However, the sediment layers below the BSRs appear to define a syncline with the strata on the east flank dipping west and those on the west flank dipping east. Alternative explanations of the contrasting stratal orientations above and below the BSR illustrated in Figure 15 are certainly possible. However, the most obvious alternative hypotheses require invoking an improbable sequence of geological events to produce a syncline immediately capped by an anticline. For example, separating the structures by an unconformity which was later deformed by compressional forces implies a less likely sequence of events than simple distortion of seismic returns by low velocity sediments beneath a gas hydrate boundary.

The broad anticlinal structure near the center of Figure 15 is crossed by a northeast-southwest seismic line. Seismic Line 361 (Figure 16) was shot approximately normal to the strike of the continental margin. The BSR evident on Line 333 (Figure 15) is also clearly visible on Line 361 (Figure 16). The BSR on Line 361 (Figure 16) continues from near the seaward limit of the line at about 2170 m (2.9 sec) water depth landward for 35 km. The BSR becomes indistinguishable beneath the upper slope at about 970 m (1.3 sec) water depth. Along its length the BSR decreases in subbottom depth from about 0.51 sec (about 460 m) at 2,100 m water depth to 0.31 sec (280 m) beneath 1,600 m of water (2.1 sec).

Gas Hydrates and Mass Wasting Processes

Line 361 (Figure 16) also depicts the results of mass wasting of the continental slope. We interpret the mass of sediment located about halfway up the continental slope which protrudes above the general slope profile on Figure 16 to be a slide deposit. Grantz et al. (1979, 1980, 1982) noted that slides, slumps, and block glides are dominant features of the geomorphological development of the continental margin offshore of the North Slope. The jumbled mass of sediment on the slope in Figure 16 appears to have been deposited from the continental slope immediately above. The contorted sediment reflections from within the slide deposit contrast with the generally parallel reflectors which comprise the continental slope above and below the mass. The apparent failure surface above the deposit is smoothly concave. This surface is less reflective than the other sea floor reflections. The relative youthfulness of this surface may be a cause of its relatively diffuse character in the seismic profile. Whereas the seafloor of the lower continental slope and the continental shelf is probably composed of conformably bedded sediments which would give a coherent reflection, the surface of the failure plane and the slide debris would be expected to be composed of material which was agitated during the failure event. This surficial sediment would represent only one depositional cycle rather than the thinner alternating sediment layers which give the stronger returns.

The configuration of the BSR and the possible slide surface on Line 361 (Figure 16) suggests that the slope failure may have occurred along a gas hydrate phase boundary. If the trend of the BSR is projected upslope from the left border of Figure 16, it corresponds with the concave failure surface constituting the seafloor above the slide deposit. Although the correspondence in the shape and trend of the slide surface and the lower slope BSR is possibly coincidental, the presence of free

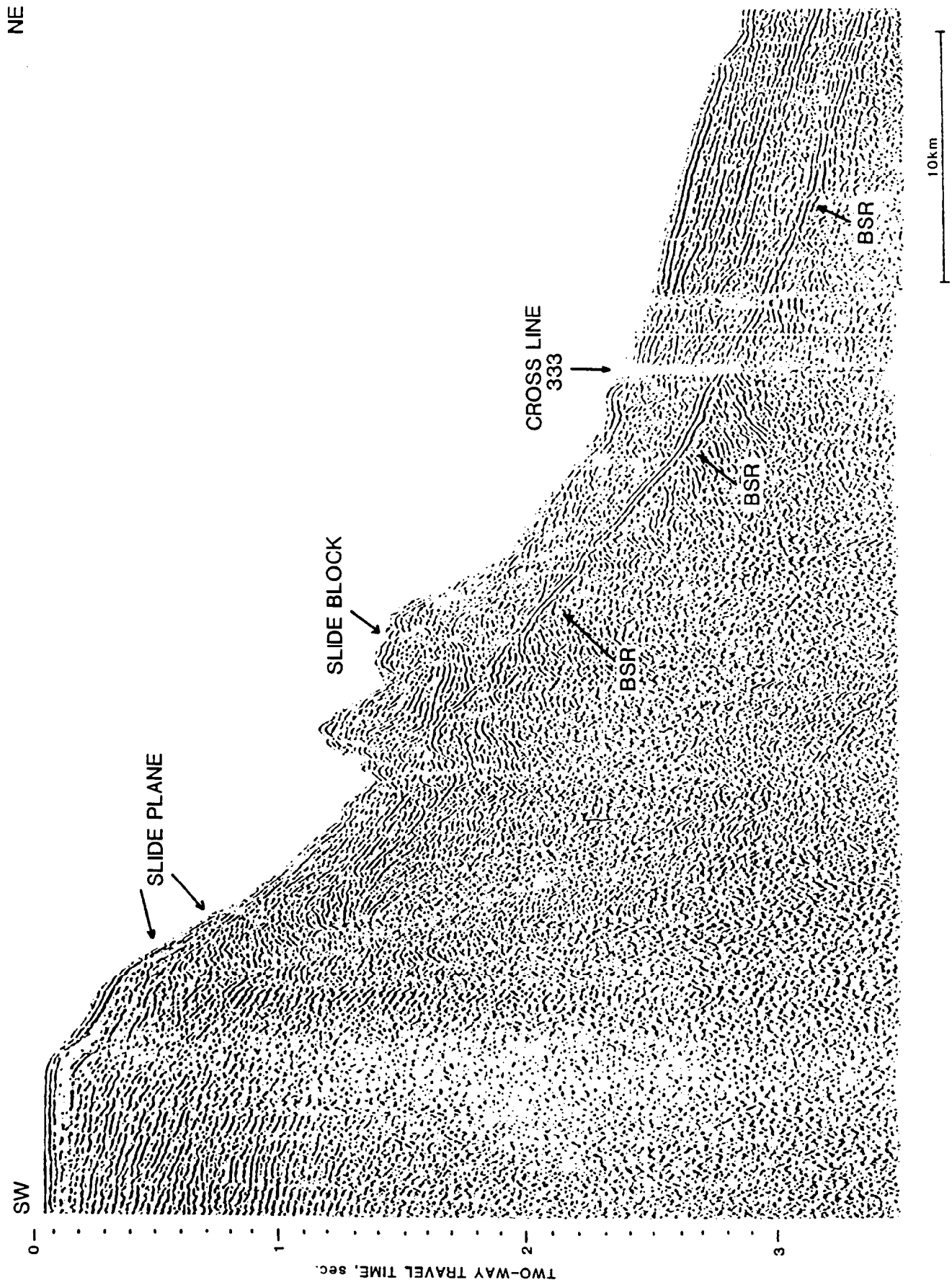

Figure 16. SECTION OF SINGLE CHANNEL SEISMIC LINE 361 SHOWING RELATIONSHIP OF BSR TO SLIDE SURFACE

gas beneath an impermeable hydrate cap could enhance the failure potential of a submarine slope.

McIver (1977, 1982) proposed that gas hydrate phase boundaries may be principal loci of submarine sliding and slope failure. McIver (1977, 1982) stated that the permeability reduction caused by gas hydrate formation interferes with normal dewatering, cementation, and compaction processes. As a result, sediments which are currently within the gas hydrate stability zone would be less consolidated than expected for sediments of the same age and depth of burial which were not hydrated. With continued sedimentation, the base of the gas hydrate stability zone moves upward relative to the sediments. Thus, in a typical scenario proposed by McIver (1977, 1982), the sediments immediately beneath the base of the gas hydrate stability zone tend to be incompetent because of retardation of lithification processes while the sediment was in the gas hydrate stability zone. Additionally the sediment would be even more water rich than the hydrated sediment because water expelled from compaction of deeper sediments would collect beneath the base of the gas hydrate stability zone due to the lack of an escape route through the impermeable gas hydrate. The presence of free gas beneath the base of the gas hydrate stability zone, as has been suspected in this and other gas hydrate locations, was claimed by McIver (1977, 1982) to decrease the competence of the unhydrated sediments even more. McIver (1982) proposed that a sudden release of gas at the base of the gas hydrate stability zone due to sediment heating or sea level lowering would produce a layer of sediment that is " ...underconsolidated, anomalously water-rich and gas-cut". McIver (1982) further proposed that this sediment layer "...could form a glide plane along which massive wedges of hydrated sediment might slide".

The interpretations of McIver (1977, 1982) stressed the role of rapid hydrate dissociation in triggering slides, but do allow for the slides along the base of the gas hydrate stability zone due to normal sedimentary processes. McIver (1977, 1982) limited the areas most likely to be affected by gas hydrate induced slides to upper slope sediments overlain by water depths near the minimum necessary to stabilize hydrates (400 to 800 m). He projected that as the ocean depth approaches the minimum necessary to stabilize gas hydrates, the gas hydrate stability zone tapers to a "feather edge" (Figure 17). Instability at this contact of the base of the gas hydrate stability zone and the sea floor at the minimum water depth for gas hydrate stabilization was proposed by McIver (1977, 1982) to initiate sliding, gas blowouts, and mud volcanos. We have modeled the morphology of the gas hydrate stability zone near the minimum depth for hydrate stability using a computer program which calculates the pressure and temperature at 1 m intervals throughout the sediment column. The results of this modeling (Krason et al., 1986) contradict some of the details of the published findings of McIver (1977, 1982); the gas hydrate stability zone does not taper to a feather edge. Instead, it diminishes rapidly in thickness from both the top and the bottom as water depth decreases. The model suggests that the shoreward limit of gas hydrate stability is a blunt, curved surface in cross section, rather than a sharp wedge shown in Figure 17.

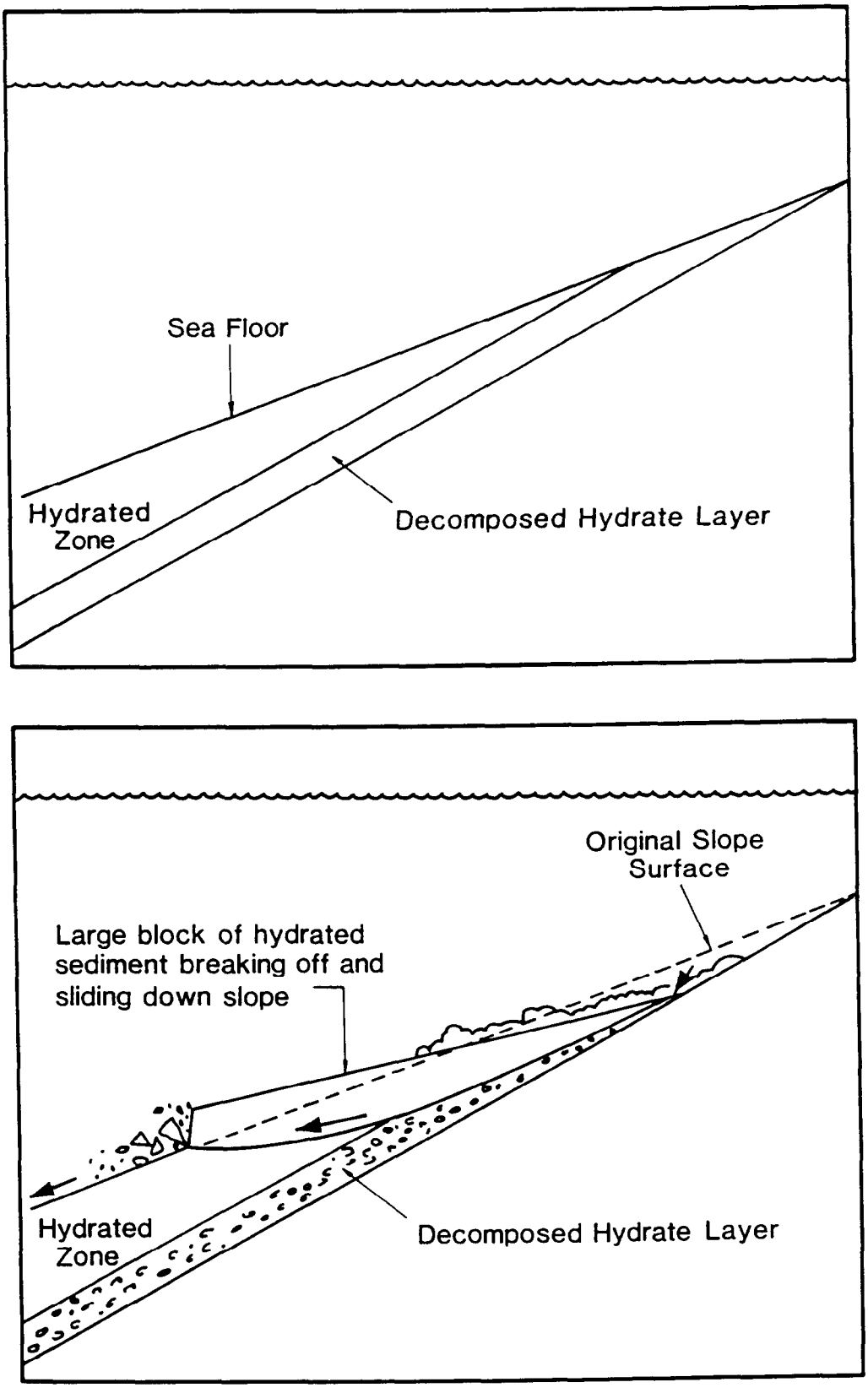

Figure 17. SCHEMATIC DIAGRAM OF INITIATION OF SUBMARINE SLIDE AT THE BASE OF THE GAS HYDRATE STABILITY ZONE

After McIver, 1982

Acoustic Transparency

Many of the single channel seismic lines from the 1973 survey aboard the *Burton Island* (Grantz et al., 1974) display a change in amplitude of sediment reflections across the BSRs. Shipley et al. (1979) noted that bedding surface reflectors above BSRs on multichannel seismic lines from Blake Outer Ridge and the Panama Basin have lower amplitudes than reflectors beneath the BSRs. This contrast in acoustic transparency across the base of the gas hydrate stability zone has also been documented on seismic lines from the Colombia Basin (Finley and Krason, 1986a) and the Middle America Trench (Ladd et al., 1982; Finley and Krason, 1986b). The exact cause of the amplitude change is unclear. It presumably indicates that partial cementation of sediments within the gas hydrate stability zone decreases the impedance contrast between sediment layers. The anomalously transparent sediments continue from the BSR to the sea floor at the Blake Outer Ridge, implying continuous distribution of hydrates throughout the interval (Shipley et al., 1979). However, drilling recovered hydrates only in thin, widely separated bands in contrast to the distribution predicted by seismic data (Shipley et al., 1979; Krason and Ridley, 1985). Stefanon (1980) has shown that free gas in sediments of the Aegean Sea can amplify seismic returns by causing "double reverberation", suggesting that the amplitude contrast across gas hydrate boundaries may be due to enhanced reflectivity of underlying gas-rich sediments in addition to diminished reflectivity within the gas hydrate stability zone.

The most pronounced examples of amplitude changes across the base of the gas hydrate stability zone from the Beaufort Sea study region come from the continental slope near the Barrow Canyon at the western edge of the study region (Plate 6). Seismic Line 303 (Figure 18) from just east of the Barrow Canyon shows a distinct difference in the strength of the returns from above and below the BSR. The difference in reflector definition across the BSR varies along the line of section being most pronounced in stretches where the BSR is most distinct.

Velocity Effects of Gas Hydrates on Sediment Reflectors

The apparent contrast of sediment reflector amplitude across BSRs on single channel seismic lines is enhanced by velocity push down of sediments beneath the base of the gas hydrate stability zone. At water depths greater than 2.7 sec (2,000 m) the reflectors beneath the BSR are not only better defined, but also appear to be much thicker.

The marked contrast in the apparent thickness of each stratal unit coupled with the apparent difference in dip angles of strata beneath and above the BSR raise the possibility that the BSR may be an angular unconformity rather than a gas hydrate phase boundary. Several lines of evidence indicate that the BSR on Line 303 (Figure 18) is not an unconformity. The BSR mimics the seafloor topography, is located at the proper depth for a gas hydrate phase boundary, and attains a progressively greater subbottom depth with increasing water depth. Although an unconformity could certainly exhibit the same properties, it is exceedingly unlikely that an unconformity would exhibit all simultaneously over the entire length of the section.

This Page Intentionally Left Blank

Figure 18 is in a pocket located inside the back cover.

This Page Intentionally Left Blank

Moreover, upon close examination it is apparent that although the sedimentary reflectors on either side of the BSR do meet at an angle, a consistent relationship exists between the angles of incidence. Beds beneath the BSR consistently dip in the same direction as those above, but at a much greater angle. The consistent relationship is perhaps analogous to the refraction of light upon passing from a high velocity to a low velocity material. The parallel would seem reasonable, for the existence of a hydrate BSR depends on the higher acoustical impedance of the hydrated layer relative to underlaying sediments.

If the assumption of the base that the gas hydrate stability zone as a refraction interface is valid, the magnitude of the refraction may give an indication of the physical properties of the sediments above and below the BSR. The angles at which the sediment reflectors intercept the BSR should be related to the difference in acoustical impedance across the BSR. By invoking certain limiting assumption, Snell's law may be applicable to the refraction of acoustic energy at the BSR. Snell's law states that the ratio of the sines of the angles of incidence of refracting waves is proportional to the ratio of the velocity of the wave in the two media:

$$\sin \theta_1 / \sin \theta_2 = v_1 / v_2$$

Assumptions of constant seismic velocity through each the sediment sections above and below the BSR permits the conversion of angles of incidence of the reflectors to relative velocities. In practice, a thickness of at least 0.10 to 0.20 sec of sediment (roughly 100 to 300 m depending on actual velocities) is necessary to obtain a confident measurement of the two angles of incidence.

Angles at which the sediment reflectors intercept the base of the gas hydrate stability zone were measured at four points on Line 303 (Figure 18) where the reflectors and BSR are particularly distinct. Application of Snell's law to the measured angles is summarized in Table 2. The ratio of seismic velocities above and below the BSR ranges from 1.7 to 2.4. The velocities of sediments beneath the hydrate layer (v_2) which produce these velocity ratios are presented for various possible values of the velocity of hydrated sediments (v_1). The values selected for the velocity of hydrated sediments (v_1) range from those suggested by Shipley and Didyk (1982) for hydrated sediments of the Middle America Trench to the values obtained experimentally by Stoll and Bryan (1979) and Pearson et al. (1982).

The values calculated for the velocity of sediments beneath the BSR (v_2) strongly suggest the presence of free gas beneath portions of the BSR (Table 2, Figure 18). The v_2 values in Table 2 are much lower than the values reported by Grantz et al. (1982a) for the seismic velocity of non-hydrated sediments beneath the Beaufort shelf based on seismic stacking velocity measurements from later multichannel surveys. At 500 m subbottom depth, Grantz et al. (1982a) reported a velocity value of about 1.8 km/sec. Even if the highest velocity value for the hydrated section (v_1) of 2.4 km/sec is assumed, the value calculated for unhydrated section (v_2) is still substantially less than the probable sediment velocity value reported by Grantz et al. (1982a). The v_2 values in Table 2 range from 0.75 km/sec to 1.3 km/sec; all are below the seismic velocity of water (1.5 km/sec). Free gas in interstices of the sediment attenuates and slows seismic pulses due to the compressibility of the gas. Free gas in pore spaces is the most reasonable explanation

for seismic velocities of sediments beneath the gas hydrate stability zone which are lower than the velocity expected for either water or sediment.

Table 2.

REFRACTION OF SEDIMENT REFLECTORS, SEISMIC LINE 303

Angle of Incidence		v_1/v_2	v_2 (km/sec)		
Above BSR	Beneath BSR		$v_1=1.8$	$v_1=2.0$	$v_1=2.2$
5°	12°	2.4	0.75	0.83	0.92
4°	9°	2.2	0.82	0.91	1.0
8°	18°	2.2	0.82	0.91	1.0
7°	12°	1.7	1.1	1.2	1.3

The seaward end of seismic Line 324 (Figure 19) intersect Line 303 at a point where a BSR is very well defined on Line 303 (Figure 18). However the seaward end of Line 324 does not display a distinct BSR. Close examination of Line 324 (Figure 19) does reveal a faint BSR near the northeast end of the line with coincides with the subbottom depth of the BSR on Line 303 (Figure 18), 0.42 sec. On Line 324 (Figure 19) no stratal reflectors are visible above or beneath the BSR, whereas the sediment layers are well defined at the corresponding point on Line 303 (Figure 18). The point of intersection of the two lines is near the location chosen for the foregoing velocity analysis based on the incidence angles of the reflectors. The section on which the BSR is easily visible (Line 303) was shot using both the 160 kJ arcer (sparker) and a 300 in^3 air gun for a seismic source. The end of Line 324, where the BSR is poorly visible was shot using only the 160 kJ arcer. Additionally the filter settings used in the two contrasting sections differed: Line 324 cut out frequencies above 60 Hz, Line 303 cut out frequencies above 76 Hz. However, other lines of the same survey were shot with the same source and filter settings as those used on Line 324 and attained very good resolution of the BSR and sediments. The lack of good resolution on Line 324 may be due to random noise and drift in the analog detection and recording equipment.

As the BSR is traced landward along Line 324 the resolution of both the stratal reflectors and the BSR improves indicating that the seismic equipment became more sensitive. However, the improvement in visibility of the stratal reflectors seems to exceed that of the BSR. The BSR on Line 303 (Figure 18) corresponding to the BSR at the end Line 324 (Figure 19) is very distinct; both acoustical transparency and apparent seismic velocity change across the BSR on Line 303. Once the resolution on Line 324 has improved sufficiently to permit stratal reflectors to be picked, the BSR appears to have become less reflective relative to the strata. In addition, no change in either acoustical transparency or apparent sedi-

Figure 19 is in a pocket located inside the back cover.

This Page Intentionally Left Blank

ment thickness, indicating velocity push down, is evident on Line 324. From the decrease in BSR amplitude relative to stratal reflector amplitude and the decrease in velocity features it would seem that either the degree of gas hydrate development and/or sub-hydrate gas trapping decreases upslope along Line 324 from the northeast end of the line toward the bathymetric high at about 2.0 sec water depth.

Anomalous Depths to Reflectors

Another apparent BSR is located on Line 324 (Figure 19) beneath the bathymetric trough landward of the isolated bathymetric high discussed above. The BSR beneath the trough is distinct and likely of hydrate origin. Sediment reflectors can be traced through the BSR. While the sediment reflectors are evident on either side of the BSR, their amplitude is clearly greater beneath the BSR. Additionally, some degree of refraction of the sediment reflectors at the BSR is evident, further supporting a hydrate origin.

The magnitude of the refraction can confidently be measured at only two points in the trough. Angles of incidence of 13° and 24°, and 15° and 27° were measured at the two locations. Applying Snell's law to the incidence angles, a value of 1.7 is obtained for the ratio of the velocity of the hydrated section (v_1) to the velocity of the underlying sediments (v_2). By extension of the analysis presented for Line 303, a range of probable seismic velocities of the sediments beneath the BSR (v_2) of 1.1 to 1.4 km/sec is calculated. Thus, the extent of refraction at the BSR indicates a seismic velocity for the underlying sediments which is compatible with the presence of free gas beneath the BSR.

The subbottom depth of the BSR on Line 324 appears to be anomalously shallow. A nominal value of 0.22 sec subbottom for the BSR in the trough is measured. The "actual" subbottom depth of a BSR is not always easily obtained. Since many BSRs are actually not a single reflector, but a series of closely spaced signals, the true depth of a BSR on a section depends on the convention used to measure the depth. Measuring from the first positive-phase return of the seafloor to the first negative-phase return from the base of the gas hydrate stability zone a consistent value of 0.22 is obtained. Measuring from the first sea floor return to the most distinct BSR return gives a depth of about 0.27 sec. Beneath the same depth of water (2.0 sec or about 1,500 m) the BSR on the adjacent line (Line 303, Figure 18) averaged 0.40 sec subbottom depth. One possible cause for the unusually shallow BSR beneath the trough on Line 324 (Figure 19) is unusually high heat flow resulting in a locally elevated geothermal gradient. Another possible explanation for the locally shallow BSR is unusually extensive hydrate formation in the sediments above the BSR. If the sediments were filled with gas hydrates to an unusually complete degree, the seismic velocity of the gas hydrate stability zone would be relatively high. An interval with an unusually high seismic velocity would appear as being anomalously thin on a seismic time section such as Line 324. Neither explanation is very convincing for the trough seen on Line 324.

The Line 324 (Figure 19) appears to display a smooth transition from the shallow BSR beneath the trough (0.22 to 0.27 sec subbottom depth) to the deeper, but less well defined BSR beneath the bathymetric high immediately down slope (0.4 to 0.43 sec subbottom depth beneath water 2.0 to 2.3 sec deep). On very high

contrast copies of Line 324 a faint trace of a possible BSR can be traced from the BSR beneath the trough to the BSR beneath the bathymetric high suggesting a gradual transition in whatever physical or geological parameters are causing the strikingly different subbottom depths of the BSRs in the closely spaced locations. A much more distinct reflection can be traced down slope from the trough in even low contrast prints of Line 324. This reflection dips at approximately the same angle as the anomalously shallow BSR in the trough and appears to be a direct continuation of the shallow BSR. The reflector which is aligned with the shallow BSR continues beneath the bathymetric high on Line 324. Beneath the bathymetric high, the strong reflector intersects another reflector in a discordant manner. The alignment with the shallow BSR in the trough and the discordant intersection with other reflector suggest that the strong reflector which is approximately 1.0 sec deep beneath the bathymetric high may be related to gas hydrate formation in some way.

Mass movements could be invoked to explain the combination of a strong but shallow BSR in the trough on Line 324 (Figure 19). A slide which removed material from the location of the present trough and deposited it to form the present bathymetric high could form the observed array of reflections. If sea floor of the trough on Line 324 (Figure 19) is a slide surface, then the shallow BSR may be a relict feature. The underlying weaker reflections may represent the base of the gas hydrate stability zone shifting downward to a new equilibrium position. The deep reflector beneath the bathymetric high could also represent a relict feature, a former gas hydrate phase boundary which was abandoned as the new geothermal gradient slowly was reestablished at higher stratigraphic levels following the slide. By this reasoning, the present weak BSR at 0.4 sec subbottom depth beneath the bathymetric high would be expected to be ill-defined due to its incipient nature; the base of the gas hydrate stability zone which was actively degrading may not have become sufficiently developed to display the seismic impedance contrast necessary for a distinct BSR. However, the well stratified nature of the sediments comprising the bathymetric high cast doubt on the slide scenario. The bedding appears to be continuous and undisturbed in this possibly allochthonous block in contrast the generally disrupted appearance of the sedimentary reflectors in the obvious slide block from Line 361 (Figure 16).

When the track of Line 324 is plotted on the bathymetric map of Greenberg et al. (1981), it becomes apparent that the trough on Line 324 (Figure 19) is not a simple slump or slide scar. Bathymetry suggests that the trough on Line 324 is an oblique section of a submarine canyon (Plate 6). The rough navigational plot supplied with the seismic sections shot aboard the USCGC *Burton Island* (Grantz et al., 1974) corresponds to a submarine canyon which may have been a branch of the Bering Canyon system. The geomorphological development of the Beaufort Sea study region proposed by Grantz et al. (1980) entailed progressive abandonment of submarine canyons as the main flow of the Bering Canyon system gradually shifted to the west. If the canyon cutting event was relatively recent, the shallow BSR in the floor of the canyon could indicate a gas hydrate zone which is still in the process of reequilibrating thermally.

The presence of a submarine canyon does not substantially clarify the enigmatic BSR depth relationships seen on Line 324 (Figure 19). The shelf-slope break landward of the canyon shows evidence of large scale slumping. The shelf edge appears to have failed along two concave surfaces about 15 km landward from the

former shelf edge. An enormous slump block rotated along the concave surface resulting in both the two down-thrown blocks which make up the present outer shelf and the unusual orientation of the sedimentary layers upslope from the present canyon. The rotated shelf-edge block is consistent with the classical form expected of a slump mass, but part of the mass is missing. Generally, down slope from the discrete slump block the "toe" of a slump is found. The toe typically consists of a jumbled mass of material which was fluidized and flowed downslope after being displaced by the movement of the slump block. One would expect a large jumbled mass of material downslope from the slump block on Line 324 where the present submarine canyon now exists. It is likely that the slump toe was deposited in the present canyon, and was subsequently removed down the canyon. If the slump toe had a sufficiently long residence time on the canyon before removal, the base of the gas hydrate stability zone may have migrated upward through the sediment. Recent removal of the slumped material from the canyon floor would have left a gas hydrate zone stranded at an anomalously shallow zone.

Although different mechanisms can be speculated to have produced the unusual configuration of BSRs on Line 324 (Figure 19), the actual cause requires a better understanding of the timing of the mass wasting processes along this part of the continental margin. With these few widely separated lines with very limited resolution of deep reflectors, it is difficult to assemble a consistent sequence of events which would have produced the stranded BSRs. The association of BSRs and these past sites of mass wasting noted on both section 324 (Figure 19) and Line 361 (Figure 16) suggests a close association of the processes of gas hydrate formation and mass wasting. Thus further studies with an expanded data base could clarify BSR formation and degradation patterns. However, the BSRs themselves may provide critical information on the timing of the mass wasting processes. It appears that adequate understanding of either mass wasting processes or BSR formation controlling factors requires a thorough examination of the simultaneous activity of both processes.

Seismic Line 305 (Figure 20) displays bottom simulating reflectors with some of the attributes found on Lines 303, 324, 331, and 363. Line 305 was shot along the far western part of the Beaufort Sea study region (Plate 6) subparallel to and about 40 km east of Lines 303 (Figure 18) and 324 (Figure 19). A very distinct BSR is located beneath the bathymetric high at the northeast end of the section. A second bathymetric high located just downslope from the shelf break is underlain by a distinct reflector which appears to intersect stratal reflectors as expected for the base of the gas hydrate stability zone, but does not mimic the sea floor topography

The BSR beneath the lower slope bathymetric high on Line 305 (Figure 20) is very similar to those seen on Line 303 (Figure 18). The BSR is located at a mean depth of 0.4 sec subbottom. It is most pronounced beneath the apex of the bathymetric high and becomes less well defined beneath the flanks. The BSR mimics the undulations of the seafloor on the northeast flank of the high; but, consistent with BSRs elsewhere in the study region, the relief of the BSR is much diminished compared with that of the seafloor. The sediments immediately above the BSR do not have strong reflections. It is not clear whether the lack of coherent reflections is a result of gas hydrate presence or a sedimentary section without distinct layers of

This Page Intentionally Left Blank

Figure 20 is in a pocket located inside the back cover.

This Page Intentionally Left Blank

alternating lithologies. The reflectors beneath the BSR are very reflective in comparison with those immediately above the BSR. Since no discrete sediment reflectors are discernible immediately above the BSR, it is not possible to determine if the reflector beneath the base of the gas hydrate stability zone show velocity push down effects. However, the sediments beneath the BSR seem to display a general downward bowing which suggests low seismic velocity possibly due to gas trapping. The BSR dies out shoreward beneath a trough which is underlain with well stratified sediments.

The upper slope of Line 305 (Figure 20) consists of a depression separating the shelf break from a bathymetric high underlain by disturbed sediments. A very strong reflector which dips downslope underlies the high on the upper slope. The amplitude of the strong reflector relative to the sea floor is similar to the amplitude of the BSR farther downslope on Line 305. The subbottom depth of the strong reflector beneath the upper slope on Line 305 ranges from 0.3 to 0.5 sec, within the range of the depths of BSRs on Lines 303, 324, 331, and 361. The reflector also appears to disconformably intersect sediment reflectors.

Several lines of evidence suggest that the strong reflector beneath the upper slope on Line 305 (Figure 20) does not represent the base of the gas hydrate stability zone. The reflector does not mimic the sea floor topography. The irregularities of the sea floor overlying the reflector are of sufficient relief to be reflected in the configuration of underlying isotherms. For comparison, note the definite flexure of the BSR beneath seafloor irregularities of similar magnitude on the lower slope portions of Line 305 (Figure 20). The topography of the seafloor is also not duplicated by the strong reflector on a larger scale; the profile of the reflector is only slightly convex upward, whereas the overlying seafloor defines a distinct bathymetric high. The subbottom depth of the reflector varies inversely with water depth, opposite of the relationship expected of a gas hydrate phase boundary. Since higher confining pressures enhance gas hydrate stability, the base of the gas hydrate stability zone is located at greater subbottom depths beneath deep water, assuming the same temperature and gas content is maintained. Exceptions to the direct relationship of gas hydrate reflector depth and water depth are known; in their landmark paper on BSRs, Shipley et al. (1979) presented a BSR from the Panama Basin which appeared the attain a shallower subbottom depth in progressively deeper water. The acoustic transparency of sediments above the reflector do not differ from that of the sediments below. Elsewhere in the Beaufort Sea study region BSRs of an amplitude similar to the strong reflector from the upper slope of Line 305 are accompanied by velocity push down of underlying sedimentary reflectors. A lack of discrete sediment reflectors above the suspect reflector precludes assessment of possible reflector distortion caused by underlying gas, but downward bowed reflectors similar to those further down the continental slope on Line 305 cannot be distinguished.

The origin of the strong reflector beneath the upper continental slope on Line 305 at 0.3 to 0.5 sec subbottom is problematic. The existence of a reflector with many of the characteristics associated with a gas hydrate BSR in a region with abundant evidence of gas hydrate presence suggests that it represents the base of the gas hydrate stability zone. However, the resolution of the sediment reflectors is insufficient to establish that the possible gas hydrate reflector is discordant with surrounding strata. Likewise, the lack of obvious reflectance and velocity effects found

on BSRs of similar amplitude from elsewhere in the Beaufort Sea study region suggests that the reflector on Line 305 does not mark a gas hydrate phase boundary. The sediments comprising the bathymetric high may have been deposited by very recent mass wasting. The anomalously deep position of the possible gas hydrate boundary could therefore be due to thermal reequilibration which is still in progress. Countering that possibility is the presence of 0.05 sec of apparently laminated sediments over the high, suggesting that the present topography has existed long enough for thermal reequilibration to have taken place. In view of the conflicting data, the possible hydrate origin of the reflector cannot be confirmed.

Areal extent

Estimating the areal extent of BSR occurrence on the single channel lines is complicated by the irregular grid used in the survey. The route of the *Burton Island* on the 1973 survey was largely determined by the position of the ice pack (Plate 6). The pack ice had apparently receded due north of Smith bay permitting acquisition of a few lines on the lower slope (e.g. Line 303, Figure 18; Line 305, Figure 20; and Line 324; Figure 19). To the east the ice apparently converged closer to shore as the lines north of Harrison, Prudhoe, and Camden bays typically terminated seaward on the upper or middle slope (e.g. Line 361, Figure 16). Without a grid of lines shot at regular intervals, estimates of BSR areal extent are largely speculative.

From the single seismic lines presented (Figure 13-16 and 18-20) it may appear that BSRs are ubiquitous on lines covering the continental slope. However, the lines previously presented exhibit particularly distinct and well defined BSRs. An areal estimate of BSR density based on the entire suite of seismic lines rather than just the most exemplary sections should be lower. Estimates of the proportion of the lines displaying BSRs is shown in Table 3. The mean value obtained for lines covering the upper slope is 28% BSR coverage. Only three lines--303, 304, and 363--had significant coverage of the lower continental slope (deeper than 2,000 m). The mean BSR extent of the lower slope lines is 44%. It is debatable whether the difference in the upper slope and lower values is significant. The upper slope lines included many which did not extend far onto the upper slope. Most of these lines with little northward extent, e.g. 328, 330, and 313, had very low levels of BSR development. However one of the lines with little northward extent, 361 (Figure 16), had 73% of the its length beneath water deeper than 300 m underlain by BSRs.

One seismic line traverses both the lower slope and the upper slope for a considerable distance and may provide insight into the distribution of BSRs in the two settings. A short portion of Line 363 was previously presented as Figure 13 to illustrate the occurrence of BSRs in anticlines and velocity push down features. The distribution of BSRs along the entire 170 km length of Line 363 is summarized in Table 3. Approximately 50% of the upper slope (300 to 2,000 m water depth) is underlain by BSRs while only about 32% percent of the lower slope (2,000 to 3,000 m water depth) is so underlain. This relationship with greater BSR development beneath the upper slope than beneath the lower slope is in apparent contradiction with the overall pattern suggested by the mean values in Table 3. Line 363 is reproduced in its entirety in Figure 21. The line traverses the lower slope north of

Figure 21 is in a pocket located inside the back cover.

Harrison bay (Plate 6) from northwest to southeast approximately along strike. At about 40 km from the southeast end (right) end of the upper section on Figure 21, the ship veered landward and approached the shelf break obliquely. The ship made its closest approach to shore at the central of the three closely spaced bathymetric highs at the left-center of the lower section of Figure 21, and paralleled the coast for about 20 km. At the bathymetric high in the right-center portion of the lower section the trackline of Line 363 heads back down slope. Using the arbitrary cutoff of 2,000 m between the upper slope and upper slope, about 42% of Line 363 (Figure 21) covers the lower slope and 58% covers the upper slope.

Table 3.

PROPORTION OF SINGLE CHANNEL SEISMIC LINES UNDERLAIN BY BOTTOM SIMULATING REFLECTORS

Line	Upper Slope (300-2,000 m)	Lower Slope (2,000-3,000 m)
303	62%	61%
304		40%
305	30%	
324	53%	
327	3%	
328	4%	
319	3%	
330	0%	
331	48%	
363	50%	32%
313	0%	
361	73%	
332	3%	
333	56%	
334	41%	
337	4%	
339	16%	
363	21%	33%
Mean	*28%*	*44%*

The significance of the greater abundance of BSRs beneath shallower water is not clear. As noted by Grantz et al. (1976), BSRs offshore of Alaska in the Beaufort Sea study region are concentrated beneath bathymetric highs. The upper slope portion of Line 363 (Figure 21) contains more bathymetric highs, each with typically greater local relief than the lower slope. Thus it may be that the BSR abundance noted in Table 3 is more a measure of the abundance of sea floor topographic features likely to localize BSRs. Although the quality of sediment resolution may vary

with depth of water penetrated, it appears that BSRs are more abundant in the upper slope sections of Line 363 (Figure 21) than on the lower slope based on the appearance of BSRs beneath bathymetric lows. On the lower slope sections (water depth greater than 2.75 sec) the BSRs beneath the bathymetric highs quickly dissipate away from the high and cannot be traced beneath the intervening troughs. However, the BSR which appears beneath the isolated bathymetric high on the upper slope on the right-center of the lower section of Figure 21 can be traced with confidence down the slope beneath minor troughs.

The available coverage of the 1973 data set (Grantz et al., 1974) is insufficient to correlate BSR presence with any one type of geomorphological feature. Although most BSRs are localized beneath bathymetric highs, the number and resolution of the available lines does not permit the differentiation of the bathymetric highs genetically into groups of for example, slide block, slump blocks, and remnants from continental slope erosion.

Grantz et al. (1976) stated that BSRs were found on 60% of the seismic lines beneath water depths of greater than 400 m. Our figures (28% to 44%) are somewhat lower. We possess only aged microform copies of the seismic lines (Grantz et al., 1974) with very low-quality images. Perhaps the original lines available to Grantz et al. (1976) permitted resolution of faint BSRs which were not visible on our sections. Our estimations of BSR coverage were based on percentages of the track length of a particular line underlain by a BSR. The statement of Grantz et al. (1976) that "...the BSR was identified beneath some 60% of our seismic lines in waters deeper than 400-600 m, an area of continental slope greater than 7,500 km^2." does not make clear whether 60% of the track length of lines beneath water deeper than 400 to 600 m was underlain by BSRs or whether 60% of the number of lines were underlain by BSRs. If Grantz et al. (1976) were referring to the number of lines then our corresponding factor would be close to 90%.

Generally the wide spacing of the single channel seismic lines limits the potential for establishing the extent of gas hydrate occurrence by correlating a single reflector between two or more lines. Two intersecting lines discussed previously, Lines 333 and 361 (Figures 15 and 16) demonstrate a continuity of 35 km down the dip of the slope and at least 10 km along strike, suggesting a minimum areal extent of 350 km^2.

The east end of Line 363 (Figure 21) is approximately 7 km downslope from and parallel to the west one-third of Line 333 (Figure 15). We suggest that the bathymetric high 3 km from the southeast end of Line 363 (Figure 21) is the downslope extension of the high on the west side of Line 333 (Figure 15). Bathymetric mapping by Greenberg et al. (1981) using these and other seismic lines indicated that they are the same feature. The BSR on Line 333 (Figure 15) can be traced from the left edge of the line into the adjoining trough before disappearing in a section of washed out reflectors. A lack of coherent reflectors such as is seen in the trough on Line 333 (Figure 15) has often been interpreted as a seismic "wipe out zone" indicative of free gas in the sediment (e.g. Brooks and Bryant, 1985). We are reluctant to interpret the seismic anomaly in the trough on Line 333 as an indicator of gas presence. Loss of coherent reflectors is relatively common on the suite of seismic lines from the 1973 cruise of the *Burton Island*. Although some of the features may indicate gas, their frequency and typical orientation suggests that they are

principally caused by recorder or source irregularities. In our previous discussion of the BSR on Line 333 we stated that the BSR appeared to dissipate in the trough between the two bathymetric highs. Comparison with the corresponding part of Line 363 (Figure 21) shows that farther downslope, the BSR continues beneath the trough. The continuation of the BSR beneath the trough on Line 363 (Figure 21) suggests that the BSR on Line 333 (Figure 15) may likewise continue beneath the trough where the stratal reflectors are not resolved. The BSR can be inferred to be continuous for the 7 km between the two lines and for 4 to 8 km on both Line 333 and Line 363. Thus a minimum area of about 50 km^2 can be assigned to the BSR which appears on both of these lines.

At the east end of Line 333, about 40 km from the section illustrated in Figure 15 a BSR appears beneath a bathymetric high. About 4 km upslope from the bathymetric high on the easternmost part of Line 333, a second crossing of the feature by Line 334 (Figure 22) also picks up the BSR. Approximately 6 km separate Lines 333 and 334 where the BSR is evident; the 4 km BSR is thus continuous over at least 25 km^2.

Good seismic coverage is available along one relatively small portion of the continental slope offshore of Harrison Bay. A stretch of about 40 km along strike of the margin is crossed by six seismic lines. Some of the lines are oriented obliquely to the strike of the slope while others are almost perpendicular to the strike. Sections of Lines 331, 332, and 363 cross the slope at approximately 25° to 30° angle to the slope; 331 is oriented NW-SE, and Lines 363 and 332 are oriented NE-SW (Plate 6). Lines 313, 361, and 334 trend NNE, approximately normal to the slope. Although the sections of the seismic lines are very closely spaced, the degree of BSR development varies greatly among them. The proportions of the line segment underlain by BSRs between the 0.5 and 2.7 sec water depth (375 to 2,000 m) from the most westward line to the most eastward line are: 0%, 10%, 80%, 0%, 72%, and 27% for sections of Lines 331, 313, 363, 332, 361, and 334 respectively (Figure 22).

The difference in BSR expression among these closely spaced lines implies that gas hydrates are very localized. Alternatively, variations in seismic collection or processing parameters may have enhanced or diminished the visibility of the BSRs on the sections. Two very closely spaced sections, 313 and 363, run parallel for about 8 km separated by a distance of only 10 km (Plate 6). In the closely aligned portions of these two sections only a faint BSR can be resolved for less than 1 km on Line 313 while a moderately strong BSR is found on Line 363 (Figure 21). After viewing the fairly obvious BSR on Line 363, a reflector at the same subbottom depth can be resolved on Line 313. However, without a priori knowledge, the potential BSR on Line 313 was not classified as a BSR. The only documented difference in methods used for collecting the two lines in question was in the source of acoustic energy used. A combination of a 160 kJ arc and a 300 in^2 air gun were used to obtain Line 313 on which the potential BSR was obscured among the sediment reflectors. Line 363 with the better defined BSR was shot with only a 160 kJ arc source. A pattern of better BSR resolution with a spark source as opposed to a mixed source is evident on the six closely spaced sections. The sections with the lowest proportion of BSRs in the 375 to 2,000 m water depth range--331, 313, and 333, with 0%, 10%, and 0% respectively-- were shot with the mixed source. Sections of Lines 363, 331, and 334--having respectively 80%, 72%, and 27% of their length

Figure 22 is in a pocket located inside the back cover.

between 375 and 2,000 m of water depth underlain by BSRs--were all shot with an arc alone.

The effect of the seismic source on BSR visibility may not depend as much on different degrees of resolution of the base of the gas hydrate stability zone as on different degrees of resolution of the surrounding sediment reflectors. It appears that the hydrate reflector itself is well imaged by either the arcer alone or a combination of the arcer and air gun. However, the combined source appears to give much stronger reflections from the sediment layers above and below the base of the gas hydrate stability zone, tending to mask the BSR. As an example the BSR on Line 313 could be picked after its depth was determined from comparison with the parallel segment from Line 363. The reflector identified on Line 313 as a potential gas hydrate reflector could be traced along the slope and appeared to mimic the sea floor topography. However its amplitude remained comparable to that of the surrounding sediments. The stratal reflectors on either side of the BSR are well resolved. In contrast, the BSR on the section of Line 363 which parallels Line 313 is of higher reflectivity (amplitude) than the adjacent stratal reflectors. Thus, the BSR is more easily resolved on Line 363.

Not only is the apparent contrast in amplitude evident on the two lines, but a difference in the character of the stratal reflectors is also seen. On Line 313 the wavelength of the sediment reflectors is comparable to that of the BSR. On Line 363 the wavelength of the stratal reflectors appears to be considerably less than that of the reflectors which constitute the BSR. The sediment reflectors on Line 363, which was shot with the arc source alone, appear to be closer together than those from Line 313. Alternatively stated, it appears that the sedimentary layers on either side of the BSR on Line 363 are more finely bedded than corresponding sediments on Line 313. It is most likely that the thickness of the sediment layers does not vary appreciably between the two very closely spaced lines. Thus the arcer source would seem to resolve the fine details of the bedding better than the combined arcer and air gun source. The spacing (wavelength) of the reflectors which constitute the BSR on Line 363 is greater than that of the nearby sedimentary reflectors. The vertical spacing of the sediment reflectors and the BSR returns is similar on Line 313.

The difference in visibility of BSRs on these two lines shot with different sources is thus due to the interaction of two factors. When the line was shot with the arc source alone, the sediment reflectors displayed both lower amplitude and a shorter wavelength than the gas hydrate reflectors. Due to the contrast in both amplitude and wavelength (spacing), the gas hydrate reflector was easily resolved from the adjacent sediment reflectors on Line 363. The combination of an arc and air gun source used on Line 313 was not as effective in distinguishing the gas hydrate reflector from nearby sediments. The sediment reflectors on Line 313 have an amplitude and a wavelength which are very similar to those of the gas hydrate reflector. Thus, the BSR on Line 313 was not picked on initial examination because it resembled the sediment reflectors in both amplitude and wavelength.

In spite of the apparent influence of seismic source on BSR resolution on single channel seismic lines, some degree of lateral variation in reflector strength is also evident. Two parallel seismic line segments separated by 16 km, Lines 361 (Figure 16) and 334 (Figure 22), were both shot with a 160 kJ arc as the source of seismic energy. However, the two sections display a noticeably different degree of BSR development. Line 334 has a moderately distinct BSR under a bathymetric

high, possibly a displaced slide mass, on the slope. Line 361 shows an unusually distinct BSR which is evident not only under a displaced slide mass, but also along a smoothly inclined section of the continental slope. Both lines were shot and recorded using identical parameters. The response of the instrument could have drifted sufficiently to account for the difference in BSR resolution during the eight days recording Line 334 and Line 361. However, it is more plausible that the lines accurately reflect a markedly different degree of gas hydrate development at the two locations.

Bottom simulating reflectors on single channel seismic lines 303 (Figure 18), 304, 305 (Figure 20), and 324 (Figure 19) suggest a very wide areal extent of gas hydrates on the upper and lower continental slope near the Barrow Canyon. These lines are among the highest in proportion of BSRs per surveyed distance of all the single channel seismic lines released by Grantz et al. (1974). Approximate lineal coverage of BSRs for Lines 303, 304, 305, and 324 from Table 3 is 61%, 40%, 30%, and 53% for a mean value of 46%. These lines cover an area of about 2,000 km^2. Thus, nearly 1,000 km^2 of the continental slope near the Barrow canyon appears to contain sufficient gas hydrate to cause a seismic response.

Evidence of Gas Hydrates from Multichannel Seismic Data

A large collection of multichannel seismic data from the Beaufort Sea study region was obtained by the USGS to evaluate the region for possible offshore hydrocarbon exploration. Seismic lines shot from the research vessel *S.P. Lee* in 1977, described by Eittreim and Grantz (1979), formed the basis for many publications dealing with the geology and resource potential of offshore Alaska (Grantz et al., 1979; Grantz and Dinter, 1980; Grantz et al., 1980; Grantz et al., 1981; Grantz and May, 1982; Grantz et al., 1982a; Grantz and Dinter, 1983). Prints of the multichannel seismic sections from the 1977 cruise of the *S.P. Lee* were released to the public as an open-file report by Grantz et al. (1982b). Additional seismic coverage of the continental shelf offshore of the North Slope was collected in 1980 (NOAA, 1981). Multichannel seismic lines from the Beaufort shelf offshore of the Mackenzie Delta have been collected by industry, and some have been released for publication (e.g. Willumsen and Cote, 1982; Dixon et al., 1985).

The seismic lines from the 1977 cruise of the *S.P. Lee* display distinct bottom simulating reflectors (BSRs) beneath much of the continental slope and outer continental shelf offshore of Alaska. Grantz et al. (1979) presented line drawings of two seismic lines from the continental slope offshore of Alaska with reflectors which they interpreted to represent the base of the gas hydrate stability zone. One of the lines, 714, was shot near the Canadian border; the other, 753, taken north of Prudhoe Bay. Grantz et al. (1980) and Grantz and Dinter (1980) reproduced the same drawings of Lines 714 and 753 and presented a map showing areas inferred to be underlain by patches of gas hydrates. Grantz and May (1982) and Grantz et al. (1982a) published annotated prints of Lines 751, 753, and 714. Each print had a reflector marked as a gas hydrate BSR, but the annotation obscured the actual reflectors on the published prints. Grantz et al. (1982a) also included a close up view of a BSR on Line 725. Figure 23 shows the section of Line 725 presented by

Grantz et al. (1982a). Grantz et al. (1982a) also presented a map of the areal extent of patches of gas hydrate as did Grantz and Dinter (1980) and Grantz et al. (1980), with the addition of contours on the base of the gas hydrate. Their map is reproduced in slightly modified form as Figure 24. The patterned area representing gas hydrate presence is delimited by the 400 m isobath landward and the 2,500 m isobath or the limit of data to the north. It should be stressed that Figure 24 represents only the "minimum area inferred to be underlain by patches of natural gas hydrate" (Grantz et al., 1982a); the map does not indicate continuous distribution of gas hydrates in the patterned areas.

We have independently mapped the distribution of probable gas hydrate derived BSRs from the multichannel seismic data released by Grantz et al. (1982b). Plate 7 shows the tracklines of the 1977 cruise of the *S.P. Lee*. The tracklines are overlain on the bathymetry of Greenberg et al. (1981). The patterned area on the tracklines indicated the locations of BSR which we have confidently identified. Bottom simulating reflectors are evident on about 60% of the seismic lines which extend beneath water deeper than 600 m.

A comparison of the tracklines of the 1973 cruise by the *Burton Island* (Plate 6) and those of the 1977 cruise of the *S.P. Lee* (Plate 7) shows that different parts of the continental slope and rise were covered in the two surveys. The seismic tracklines of the single channel survey of the *Burton Island* (Plate 6) covered most of the continental shelf north of Alaska, but the continental slope was surveyed only in the extreme western part of the Beaufort Sea study region between the Barrow Canyon to the west and Prudhoe Bay to the east. In contrast the continental slope east of Prudhoe Bay was very well covered with relatively closely spaced (20 km apart) parallel lines during the multichannel survey of the *S.P. Lee* in 1977 (Plate 7). A difference in the positions of the southern limit of the Arctic pack ice at the time of the surveys is the probable reason for the different degrees of coverage of the western and eastern portions of the Alaska continental margin.

Although the seaward extent of the survey by the *S.P. Lee* is less to the west of Prudhoe Bay, BSRs were identified on the few lines which do traverse deeper water (Plate 7). Neglecting the disparity in seismic coverage along the continental margin, the BSRs from the 1977 multichannel seismic survey can be subdivided into two general groups by location. A western group of BSR-bearing seismic lines extends from Line 771 north of Smith Bay eastward to Line 751 which is due north of Prudhoe Bay (Plate 7). Multichannel seismic Lines 745, 746, 747, 79, and 750 all cover portions of the continental slope which are sufficiently deep for gas hydrates, but display no BSRs. These lines define a stretch of the continental slope about 60 km along strike which is anomalously devoid of BSRs, and by extension, possibly devoid of hydrates. An eastern group of BSR bearing multichannel seismic lines is located east of the BSR-free interval, and extends from Line 744 north of the Canning River delta to the easternmost seismic line of the survey Line 714 (Plate 7).

Multichannel Seismic Lines West of Prudhoe Bay

Of the 13 multichannel seismic lines of the continental slope between Lines 774 and 751, ten display pronounced BSRs (Plate 7).

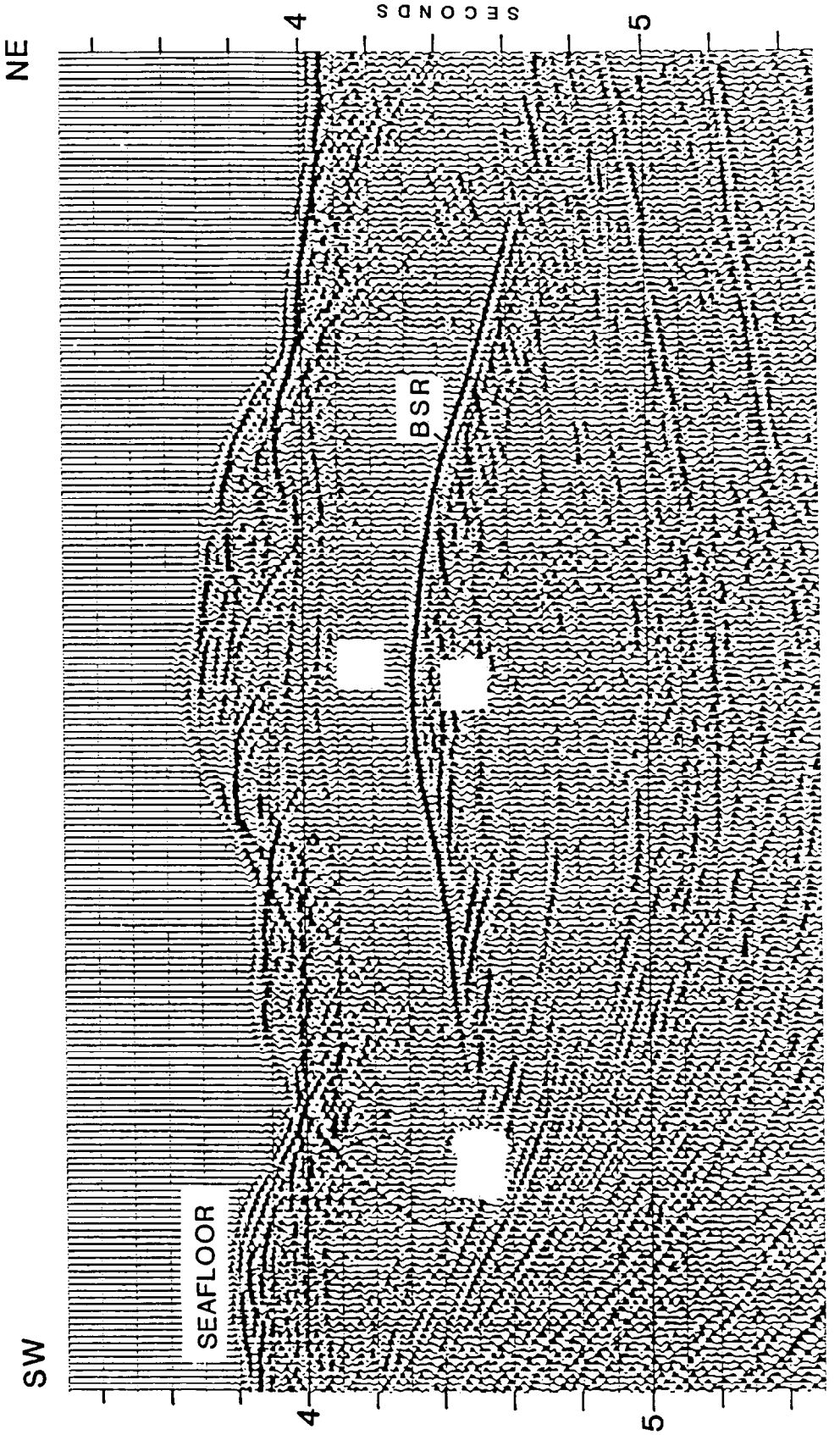

Figure 23. SEGMENT OF MULTICHANNEL SEISMIC LINE 2725 SHOWING AMPLITUDE CONTRAST ACROSS BOTTOM SIMULATING REFLECTOR

After Grantz et al., 1982

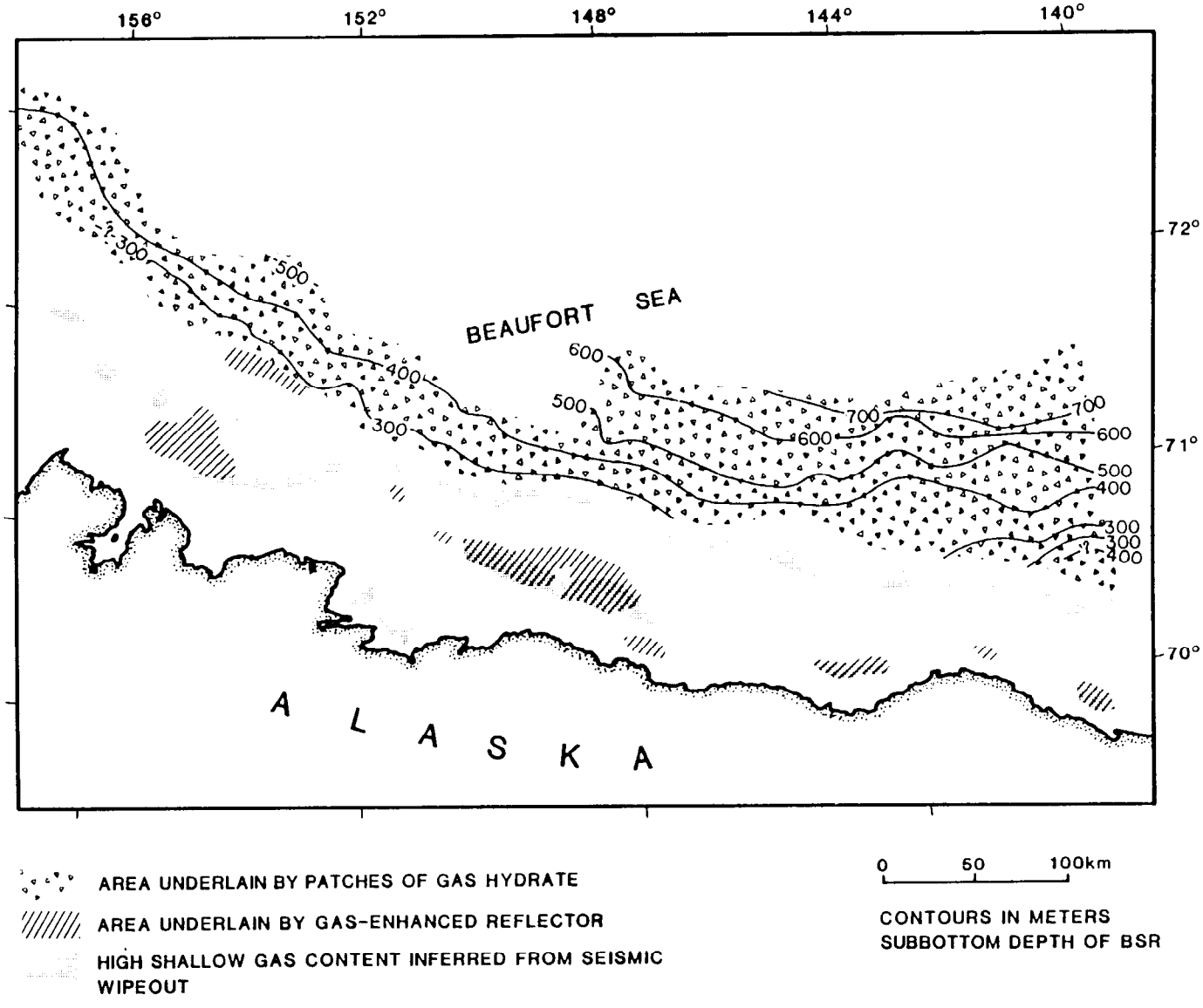

Figure 24. **DISTRIBUTION OF GAS HYDRATE AND SHALLOW GAS FROM SEISMIC DATA**

After Grantz et al., 1982 and Craig et al., 1985

Multichannel seismic line 774 crosses a 200 m deep channel in the outer continental shelf and ends at a local bathymetric high just landward of the main shelf-slope break (Figure 25). The water depth in the channel (650 m) and beneath the bathymetric high (450 m) on Line 774 is sufficient to stabilize has hydrates and form visible BSRs. A high-amplitude reflector paralleling the sea floor at 0.35 sec subbottom can be resolved beneath the canyon and beneath the bathymetric high. The sediment reflectors are insufficiently resolved to determine whether these reflectors are parallel to or discordant with the bedding planes. Without further evidence these reflectors cannot be confidently assigned to the base of the gas hydrate stability zone.

Multichannel seismic line 773 runs parallel to and 10 km to the east of Line 774 (Plate 7). Line 773 terminates on the upper continental slope beneath 1,200 m of water. A reflector parallels the seafloor at a subbottom depth of 0.3 to 0.4 sec beneath water depths of 500 to 1,000 m (Figure 25). As with Line 774, the shallow reflector on Line 773 does not demonstrably cross sediment layers, precluding assessment on its possible hydrate origin.

Multichannel seismic line 771 is the western-most of the sections shot aboard the *S.P. Lee* in 1977 that show distinct BSRs (Plate 7). A prominent scarp on the upper slope of Line 771 indicates failure of the slope by faulting and/or slumping (Figure 26). Grantz et al. (1983) have dated the faulting as late Pleistocene to Holocene age, and have estimated 420 m of total displacement on the normal fault. Beneath the scarp surface, a reflector which superficially resembles the gas hydrate BSRs described earlier on single channel seismic lines is seen at 0.2 to 0.4 sec (about 200 to 400 m) subbottom beneath water 850 to 1,000 m deep. The possible BSR mimics the seafloor topography to an extent, but does not follow the sea floor contours as do other hydrate BSRs from the study region. The possibility exists that the reflector is an ancillary fault surface rather than the base of the gas hydrate stability zone. However, a gas hydrate origin is likely based on resemblance of the feature to reflectors whose hydrate origin is less equivocal.

Another possible gas hydrate BSR is present beneath the mass of sediments displaced downslope from the fault scarp (Figure 26). A faint reflector extends for about 1.5 km at 0.45 sec subbottom beneath water 800 m to 850 m deep.

A third possible BSR on Line 771 occurs near the seaward limit of the line beneath 1600 m of water (Figure 26). The BSR extends for about 2 km at 0.40 sec subbottom. Although the nature of the sediments and the structural setting at this location are not well imaged by the seismic line, no structural disturbance similar to that upslope on Line 771 is immediately evident. The depth of the BSR is also similar to that seen on similar single channel sections from the Beaufort Sea study region overlain by 1,600 m of water.

The difference in BSR depths at the three locations where they have been tentatively identified on Line 771 suggests that they represent the base of the gas hydrate stability zone. The subbottom depth of the possible BSRs on Line 771 beneath the fault scarp and the displaced sediment mass averaged respectively 0.35 and 0.47 sec. Thermal reequilibration following faulting and displacement of sedi

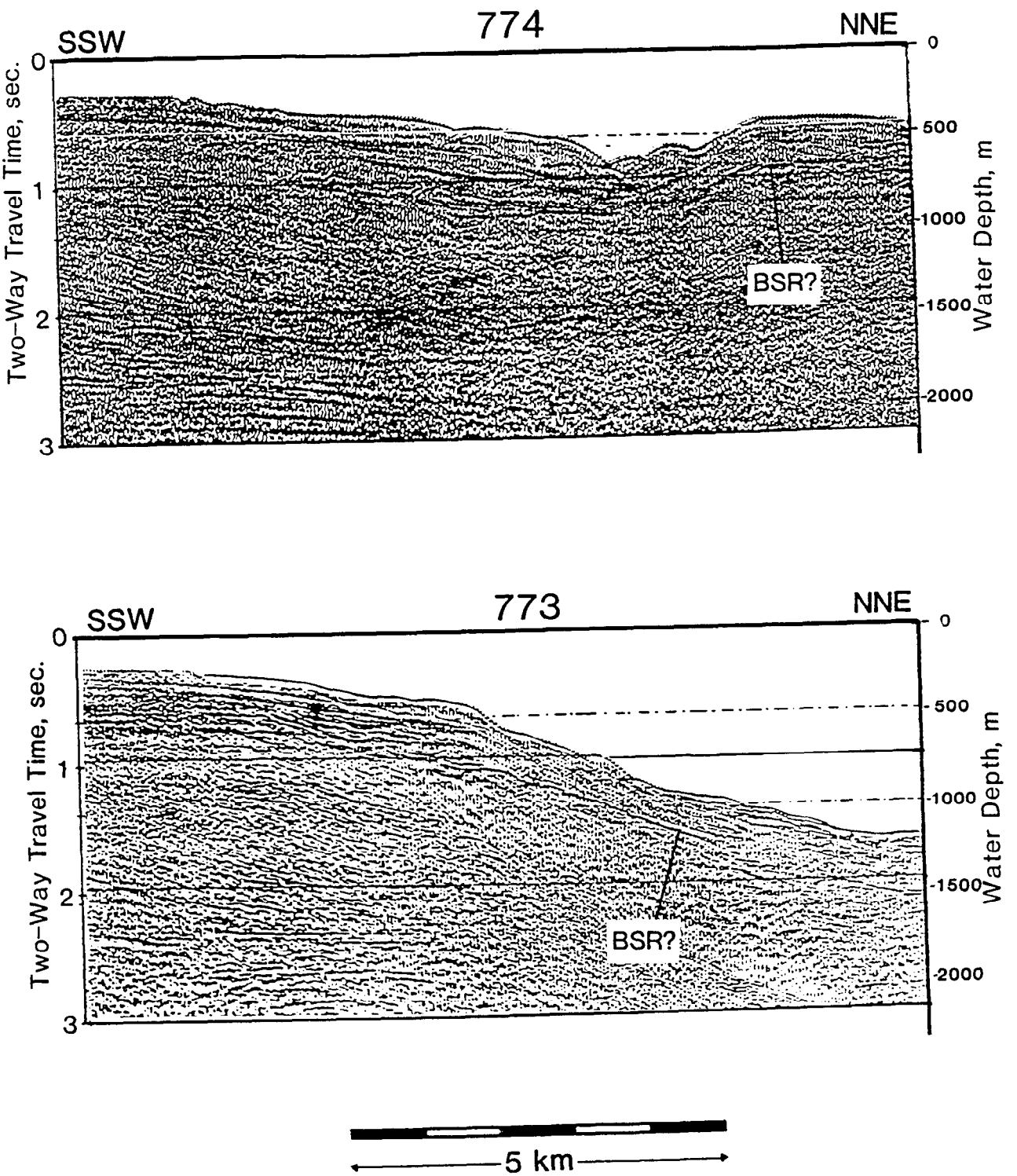

Figure 25. MULTICHANNEL SEISMIC LINES 774 AND 773

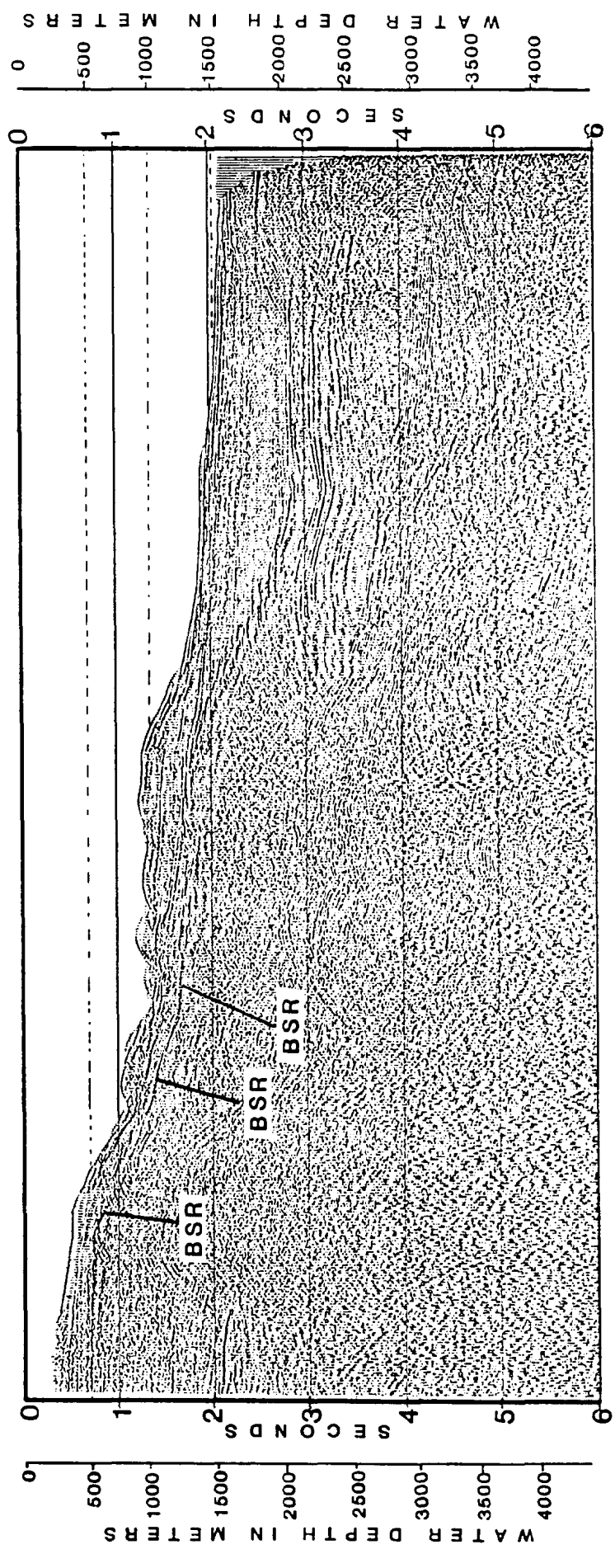

Figure 26. MULTICHANNEL SEISMIC LINE 771

ment downslope would result in a locally very high geothermal gradient in the sediments beneath the exposed fault scarp. Similarly the geothermal gradient beneath the allochthonous block would be depressed during the course of reequilibration (Krason and Ridley, 1985). The shallow BSR beneath the exposed scarp and the exceptionally deep potential BSR beneath the displaced mass are consistent with the expected configuration of isotherms beneath the area subsequent to faulting.

Multichannel seismic line 770 is oriented west to east, subparallel to the strike of the continental slope beneath water 1,700 to 2,300 m deep (Plate 7). The line crosses one bathymetric high near the center of the coverage and the flanks of two bathymetric highs at either end of the line (Figure 27, Plate 7). BSRs can be resolved on Line 770 beneath the flanks of the bathymetric highs and sporadically along the intervening troughs (Figure 27). The BSRs range in depth from 0.37 to 0.47 sec. The BSRs on three of the four surveyed flanks of the bathymetric highs are consistently 0.47 sec deep with the other being 0.40 sec. A slight difference in reflector amplitude is noted across the BSR, but to a much lesser degree than in nearby single channel lines. The central bathymetric high is of interest due to its lack of a continuous underlying BSR. the central bathymetric high has a local relief of 300 to 600 m and displays BSRs along its flanks. However, the BSRs dissipate within 1 km on either side of the anticlinal crest (Figure 27).

Multichannel seismic line 769 is oriented normal to the strike of the continental slope about 30 km east-southeast of Line 771 (Plate 7). The track of Line 769 is aligned approximately along the crest of ridge on the continental slope which is elevated about 200 m above the typical depth of the ocean floor 5 km on either side of the line. BSRs were identified on Line 769 from beneath water 1,000 m deep to the north end of the line at 2,050 m water depth (Figure 28).

Two groups of BSRs were identified on Line 769. Between 1,000 and 1,300 m depth a strong reflector exists at 0.30 to 0.32 sec subbottom depth. The possible hydrate boundary mimics the topography of the sea floor as expected of a gas hydrate reflector. The sediment reflectors immediately above and below the reflector are indistinct precluding assessment of possible discordance of the sediments and the reflector. The reflector is about 0.1 sec (about 100 m) shallower than typical Beaufort Sea BSRs in that depth range.

About 4 km downslope from the point on Line 769 at which the unusually shallow reflector dissipates, a second group of BSRs occurs with subbottom depths similar to those expected for the range of depths of overlying water (1,300 to 2,050 m) (Figure 28). The sea floor in the interval consists of a series of bathymetric highs spaced at 5 to 6 km intervals with about 100 m local relief which are probably caused by minor slumping. Beneath each of these highs distinct BSRs can be resolved. Subbottom depths range from 0.38 sec to 0.48 sec. Of the four bathymetric highs, the two deeper ones display typical reflection signatures expected of gas hydrate reflectors. The sediment reflectors above the probable base of the gas hydrate stability zone are diminished in amplitude compared with those below. On one of the bathymetric highs sediment reflectors beneath the BSR appear to display velocity push down effects manifested as a concave upward curve of the reflectors near the crest of the antiformal feature defined by the BSR. Additionally, the sedi

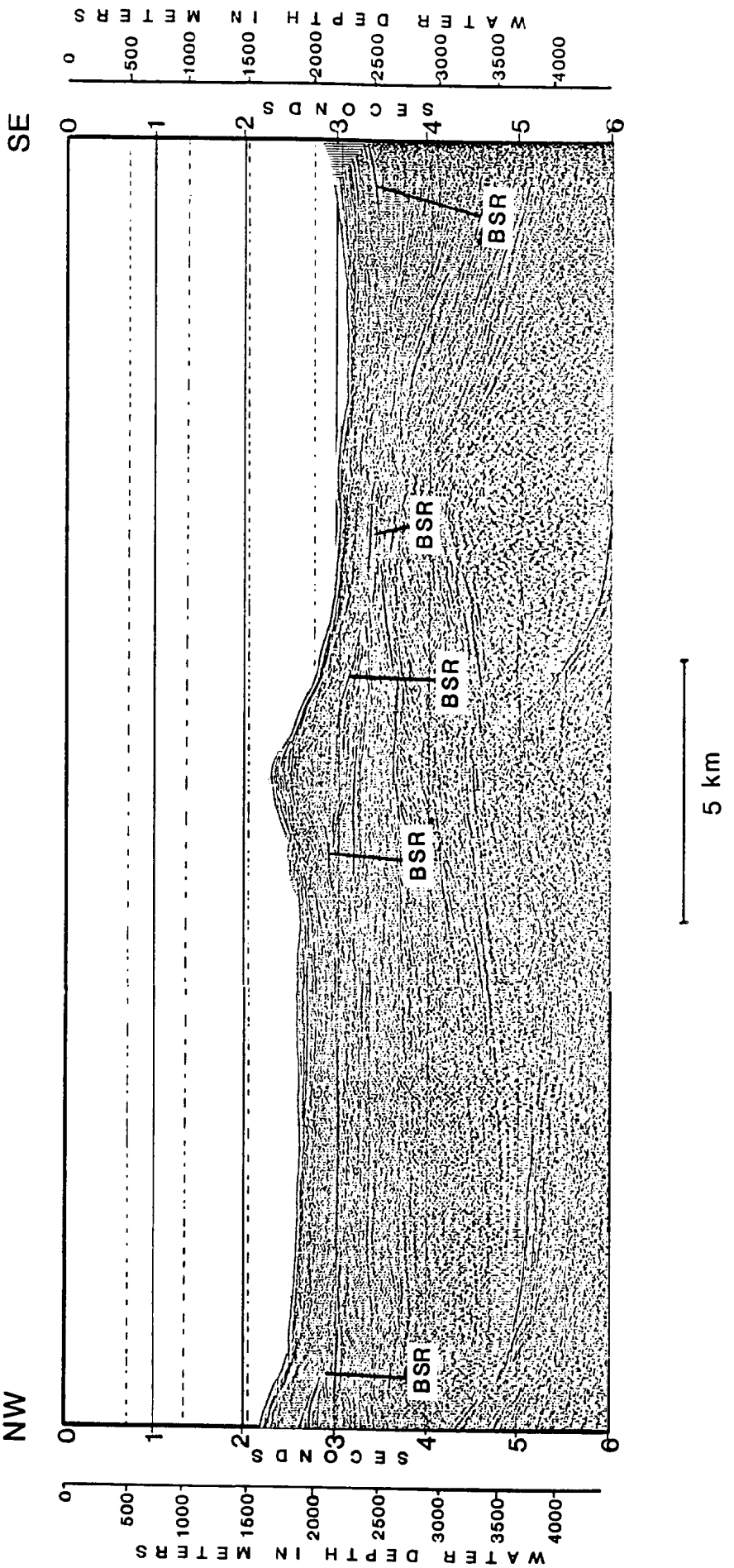

Figure 27. MULTICHANNEL SEISMIC LINE 770

Figure 28 is in a pocket located inside the back cover.

ment reflectors of the two bathymetric highs intersect the BSR at an angle of about 30° demonstrating the discordance expected of a gas hydrate phase boundary. The other two bathymetric highs do not display the characteristic reflector features of the BSRs beneath deeper water, but greatly resemble the gas hydrate BSRs in general morphology, subbottom depth, and reflector amplitude (reflectivity). The shallowest of the bathymetric highs exhibits a rather unusual combination of reflector properties above and below the BSR. The sediment reflectors, while not particularly well imaged either above or below the BSR, are of higher amplitude above the BSR. Highly reflective sediments above the BSR differs from the relationship observed in single channel seismic lines from the study region, and from the situation seen just 6 km downslope on Line 769.

Upon comparison of the closely spaced BSRs on Line 769 with such different degrees of acoustic transparency of the nearby sediments (Figure 28), it becomes clear that the amplitude of the sediment reflectors above the BSR is similar in both cases. The principal difference is in the amplitude of the reflectors beneath the BSRs. The BSR beneath shallower water shows no discrete sediment reflectors beneath the BSR, whereas the BSR downslope is underlain by very distinct sediment reflectors. The lack of discrete reflections and the generally diminished amplitude to the returns beneath the anomalous BSR resembles a seismic "bright spot" often interpreted as a sign of free gas accumulation in conventional hydrocarbon traps. While bright spots are not common beneath BSRs from the Beaufort Sea study region, they have been well documented by Buffler (1983) and Krason et al. (1985) on seismic lines from the Mexican Ridges of the western Gulf of Mexico. Perhaps gas trapped beneath the base of the gas hydrate stability zone can be manifested two types of seismic expression, bright spots and alternatively as reflectors enhanced in both amplitude and frequency.

The ridge along which Line 769 was oriented was also partially surveyed by Line 770 (Figure 27) and single channel Line 363 (Figure 21). Plate 7 shows that the seaward extent of Line 769 ended just 6 km southeast of Line 770. Comparison of Plates 6 and 7 shows that Line 769 ended just 4 km south of single channel Line 363. The bathymetry of Greenberg et al. (1981) (Plates 1, 6, and 7) indicates that the bathymetric high at the east end of Line 770 and that located 25 km from the west end of Line 363 (Figure 21) correspond to the ridge on which Line 769 was shot. Bottom simulating reflectors are evident on all three lines which surveyed the ridge. Depths to the BSRs are consistently between 0.45 and 0.48 for common water depths of 1,975 to 2,275 m. The two strike lines, 363 and 770, demonstrate that the BSR dissipates away from the ridge. BSRs are so abundant and well defined on Line 769 in large part due to the local bathymetric configuration.

Multichannel seismic line 767 is oriented down the dip of the continental slope north of Harrison Bay parallel to and about 40 km east-southeast from Line 769 (Plate 7). In contrast to Line 769, Line 767 is not located atop a ridge, but is located in a gentle trough.

A BSR is located on Line 767 beneath water 500 to 1,530 m deep, and can be traced for a distance of about 12 km (Figure 29). The subbottom depth of the BSR decreases from 0.32 sec at 500 m water depth to 0.27 sec beneath 900 m of water. The BSR remains at a consistent depth of 0.27 m from a water depth of 900 m to

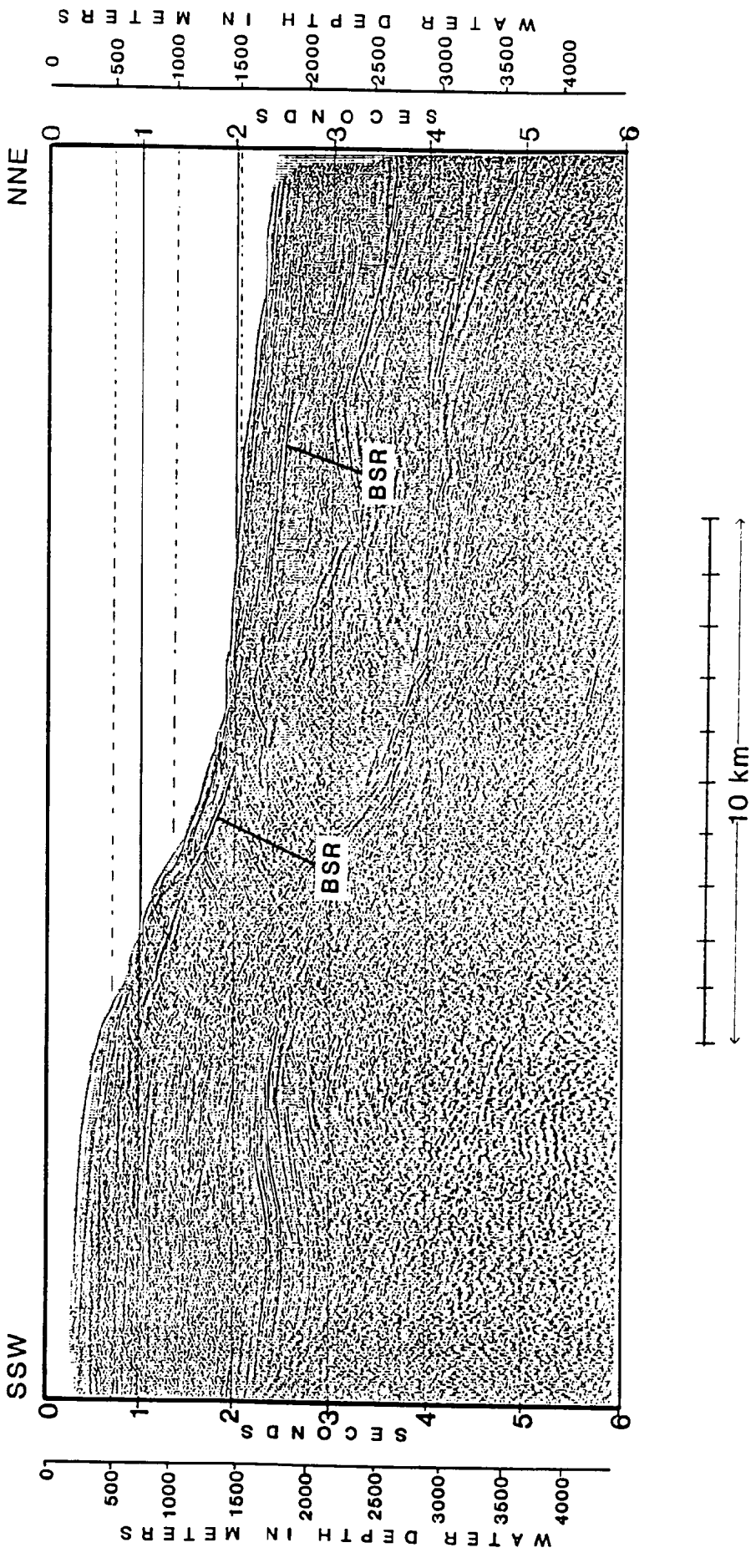

Figure 29. MULTICHANNEL SEISMIC LINE 767

1,350 m, where it deepens to 0.32 sec at 1,425 m, 0.37 sec at 1,460 m, and 0.40 sec at 1,530 m.

The water depth to hydrate depth relationship displayed on Line 767 is different than that predicted theoretically. Beneath the shallow water (500 to 800 m) the BSR averages 0.30 sec subbottom depth, while beneath water 900 to 1,350 m deep the distinct BSR maintains a depth of 0.27 sec subbottom. Since the stability of gas hydrates is enhanced by higher confining pressures, deeper water causes the base of the gas hydrate stability zone to be deeper in the sediment. The anomalous situation on Line 767 could conceivably be caused localized variation in heat flow. Higher heat flow and thus steeper geothermal gradients may prevail between 900 m and 1,350 m water depth leading to a thinner gas hydrate stability zone. Another possibility is that the gas from which the hydrate was formed beneath the more shallow water is composed of heavier hydrocarbons and/or carbon dioxide, in addition to methane, while the hydrate between 900 m and 1,350 m water depth is composed of methane without other gases. Since methane hydrate requires a lower temperature than mixed gas hydrate to be stable at a given pressure, the BSR with an unusually shallow subbottom depth may represent methane hydrate, and the BSR which is found at a greater subbottom depth but beneath shallower water could represent the base of the gas hydrate stability zone with gases other than methane present.

Yet another scenario can be postulated with a greater extent of gas hydrate formation in the sediments beneath water 900 to 1,350 m deep causing the inversion of the expected relationship between water and sediment depths of the BSRs on Line 767. The seismic velocity of sediments increases directly with the proportion of their pore space which is filled with gas hydrates (Halleck, 1982). Thus, a greater extent of gas hydrate formation in the sediments beneath water 900 to 1,350 m deep would increase the seismic velocity of the sediments above the BSR. The higher velocities of the section thoroughly cemented by gas hydrates would be manifested on a seismic time section as an apparent depth to the BSR which is shallower than that for an adjoining area with less gas hydrate present in the pore space. Halleck (1982) has calculated that increasing the degree of gas hydrate pore occupancy of ocean bottom sediments from 40% to 80% results in a 26% increase in the seismic velocity of the sediment. This indicates that increases in seismic velocity of the magnitude necessary to explain the apparent depth anomaly on Line 767 (28%) can be obtained by differential hydrate formation. However very large differences in the degree of gas hydrate formation would be required to explain the anomaly on Line 767.

Multichannel seismic line 766 is aligned along the strike of the continental slope (east-southeast) north of Harrison Bay just east of the north end of Line 767 (Plate 7). The line covers 14 km of seafloor between 1,400 and 1,900 m deep. Two bathymetric highs are crossed by Line 766 (Figure 30). A distinct BSR underlies each bathymetric high. A faint reflector, possibly a hydrate BSR, connects the bathymetric highs at the approximate subbottom depth of the BSRs on the highs. The BSR is better defined beneath the western bathymetric high. Additionally the BSR beneath the western bathymetric high is deeper subbottom (0.42 sec average) than that beneath the more gently inclined eastern bathymetric high (0.35 sec sub

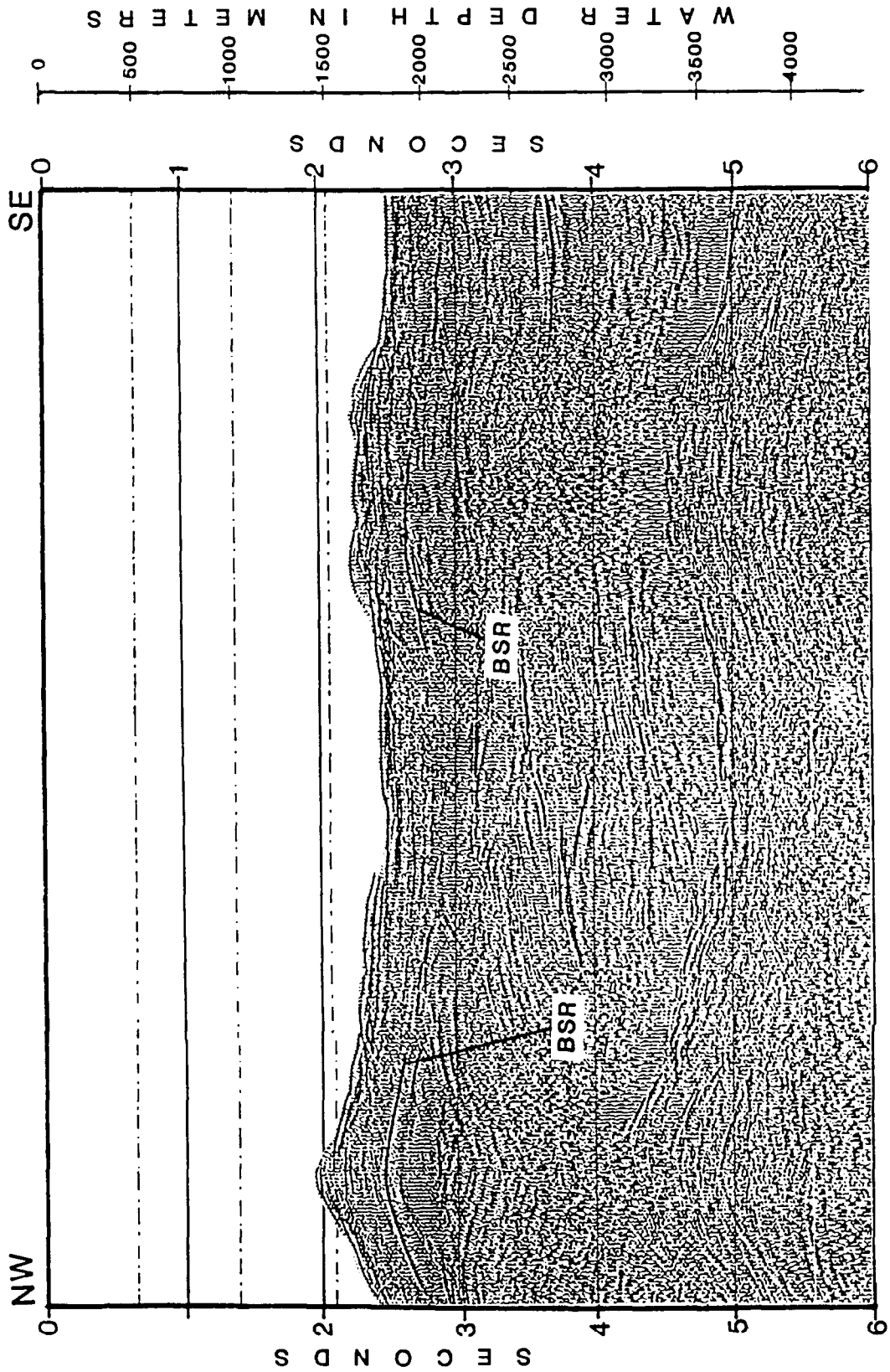

Figure 30. MULTICHANNEL SEISMIC LINE 766

bottom average). Very little difference in either the amplitude or wave length of the sediment reflectors can be distinguished immediately across the BSR on Line 766 (Figure 30). However, at 0.15 to 0.20 sec subbottom beneath the western bathymetric high a zone of very low amplitude reflections 0.3 sec thick and 1.5 km in lateral extent is evident. Beneath this seismically transparent zone, sediment reflectors are very bold and distinct. The sediment reflectors beneath the transparent zone are bowed sharply downward beneath the apex of the bathymetric high giving the appearance of a sharp syncline in the sediments. The few sediment reflectors which can be resolved above the BSR on the western bathymetric high on Line 766 appear to be generally concordant with the sea floor; thus the bathymetric high appears to be an anticline. The presence of an apparent syncline beneath the acoustically transparent zone under the BSR would require either an unconformity in the area of the BSR or a velocity decrease through the acoustically transparent zone. As previously discussed in regard to a similar feature on a single channel seismic line from the Beaufort Sea study region, a very low velocity interval beneath the BSR is the most appealing explanation for the apparent change in sediment orientation across the BSR; alternative interpretations require a series of geologically improbable events to duplicate an effect which can be obtained by assuming a low velocity layer of gas-charged sediments underlies the BSR.

Multichannel seismic line 765 crosses the continental slope subparallel to and 20 km east of Line 767 (Plate 7). The upper slope of Line 765 is underlain by a large rotated slump block or growth fault block (Figure 31) which is very similar in form and size to that on single channel Line 324 (Figure 19). The back-rotated slump or fault block is covered by about 0.2 sec (about 200 m) of sediments parallel to the sea floor indicating that the block has been inactive recently.

A well defined BSR can be traced on Line 765 from a water depth of 1,200 m to the north end of the line at 1,500 m for a distance of 12 km (Figure 31). The subbottom depth of the BSR increases regularly from 0.34 sec at 1,200 m to 0.42 sec at 1,500 m water depth. Only a slight difference in acoustic transparency is evident across the BSR on Line 765.

In contrast to nearby lines, the BSR on Line 765 is not present beneath water shallower than 1,200 m (Figure 31, Plate 7). The BSR is present only seaward of the major part of the slump block or downthrown block from the possible growth fault at the shelf-slope break.

The same portion of the continental slope north to Harrison Bay surveyed in Lines 765, 766, and 767 (Plate 7) was also covered by selected single channel lines from the 1973 cruise of the *Burton Island* (Plate 6). Single channel Line 331 (Figure 14) intersects the two multichannel dip lines, 767 and 765. Line 331 intersects Line 767 at a water depth of 1,010 m. A BSR is present on both lines at a subbottom depth of 0.28 sec. Line 767 is oriented along the axis of a submarine canyon with 450 m of local relief. In spite of this, the BSR is vividly developed on Line 767 (Figure 29). The view of the same area by Line 331 (Figure 14) illustrates the unusual situation of a BSR in a bathymetric depression which becomes indistinguishable when traced into the adjoining bathymetric highs. The banks of the submarine trough in which Line 767 is oriented shoal to about 500 m depth. The BSR on the cross section of the trough (Line 331) cannot be traced into sediments

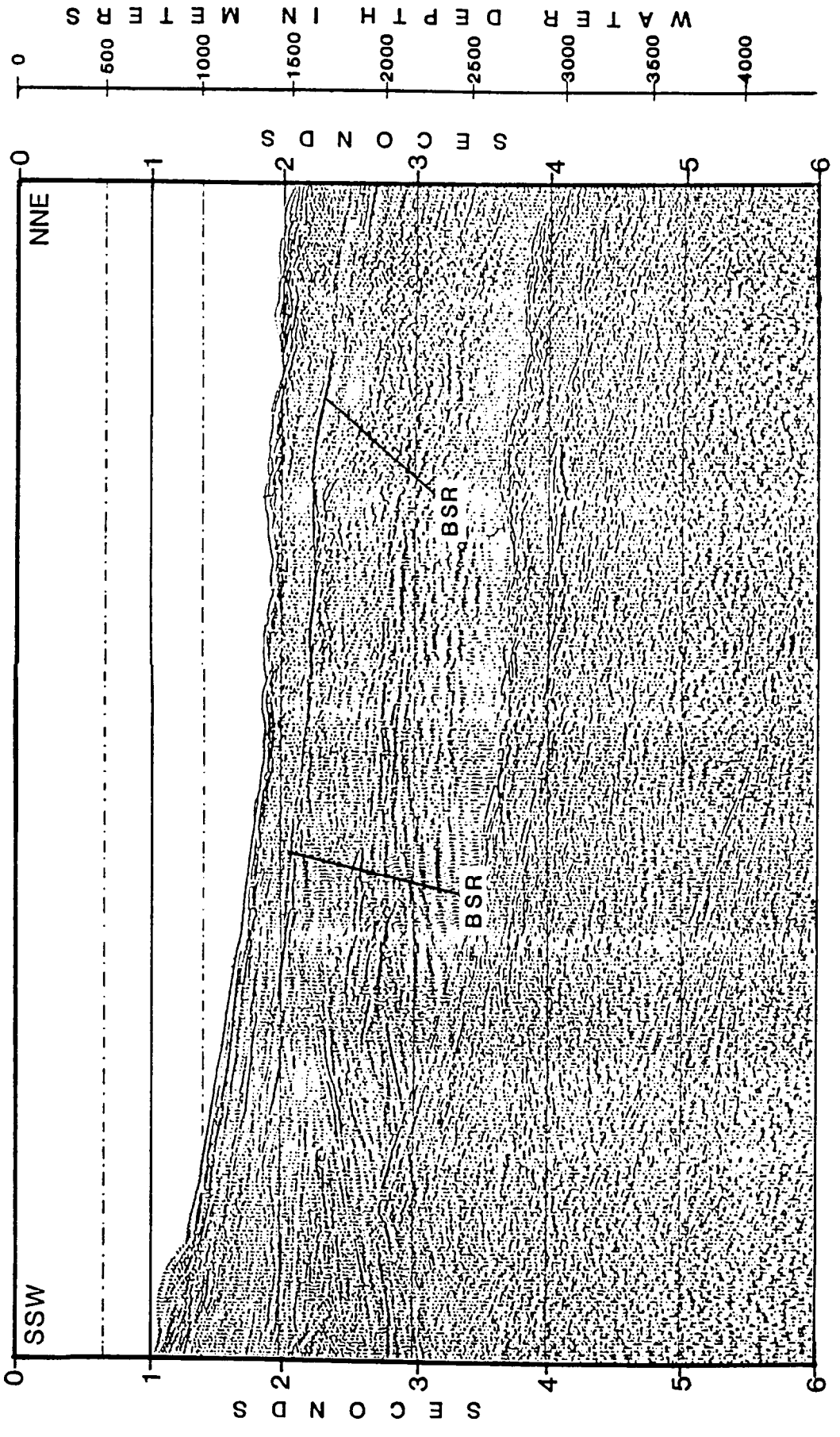

Figure 31. MULTICHANNEL SEISMIC LINE 765

beneath water shallower than 800 m. However, along the floor of the trough as illustrated by Line 767, the BSR is continuous to water depths of about 500 m. It is not clear whether this discrepancy reflects a difference in the BSR resolution of the two lines, or whether the base of the gas hydrate stability zone exists as a distinct horizon beneath shallower water when within the submarine trough. If it is assumed that the water depth at which the BSRs disappear on the two lines represents the minimum pressure - temperature conditions at which gas hydrates are stable, then the temperature of the sea bottom would be expected to be cooler within the canyon than up on the sides. We know of no published reports on possible temperature differences of water within and adjacent to small troughs on the Beaufort continental slope, but Aagaard (1982) did mention that the much larger Barrow Canyon to the west does act as a drain for cold water from Chukchi Sea into the Beaufort Sea. A similar, but smaller scale, drainage system may exist along the slope as suggested by the more extensive BSR on the floor of the trough on Line 767 than on the banks of the trough on Line 331.

Multichannel seismic line 765 (Figure 31) intersects single channel Line 331 (Figure 14) at a water depth of about 1,300 m. Both lines have obvious BSRs at 0.35 sec subbottom at the intersection.

Single channel Line 363 (Figure 21) is oriented obliquely to the strike of the continental slope and intersects both a strike line, 766, and a dip line, 765. Line 363 intersects Line 766 (Figure 30) at a water depth of 1,680 m beneath a bathymetric high on each. The lines both show a BSR at 0.34 to 0.37 sec subbottom. Neither of the lines show much difference in strength of the sediment reflections across the BSR. However, the BSR is better defined on the multichannel line. Line 363 intercepts Line 765 (Figure 31) at about 2,000 m water depth. On both lines, only a suggestion of a BSR is seen in the sediments. Bottom simulating reflectors are very strong within 2 km of the intersection points on each section. However, at the intersection the reflector at the expected subbottom depth obtained by extrapolating from nearby BSRs is approximately the same amplitude as adjacent sediment reflectors. In this condition of a marginally visible BSR, the multichannel line is perhaps slightly better at resolving the faint reflection. Without the presence of distinct BSRs adjacent to the intersection point for comparison, no BSR could be could be confidently identified at the intersection point on either line.

The comparison of BSR characteristics on the multichannel lines (765, 766, and 767) and the intersecting single channel lines (331 and 363) demonstrates that both types of data resolve BSRs at the same subbottom depths. Distinct, high amplitude BSRs are visible to approximately the same degree on both types of lines. Although the multichannel lines resolve the deeper sediment reflections much better than corresponding single channel lines, sediment reflectors within the gas hydrate stability zone and immediately below are much better imaged in the single channel lines. Multichannel seismic lines are optimized during processing to best resolve the sediments of most interest. It is likely that the prints which have been released by Grantz et al. (1982a) were processed so as to bring out deep structural and stratigraphic features of the Beaufort continental shelf and slope. If optimized for the sediment depths and characteristics of the gas hydrate stability zone, it is possible that the resolution of sediment layers and changes of reflection strength across the BSR on the multichannel lines would improve. However in the available data set, the details of sediments and subtle deformation near the BSRs are best

recorded by the analog single channel lines, while the BSRs themselves are recorded equally as well by both single channel and multichannel methods.

Multichannel seismic line 760 is located parallel to and 20 km east of Line 765. Line 760 crosses the continental slope to a depth of about 1,300 m terminating in a well defined submarine canyon (Plate 7). No BSR could be discerned on Line 760, although both Lines 765 and 767 displayed distinct BSRs at the same depth in a similar canyon floor setting.

It is indeed unfortunate that seismic surveying along Line 760 was not continued farther seaward. The submarine canyon in which Line 760 terminates trends to the east-northeast, while Line 760 is oriented north-northeast (Plate 7). Line 760 terminates in the floor of the canyon, but if continued seaward on its course would have transected the seaward wall of the canyon and continued downslope. The seaward wall of the oblique canyon on the trend of Line 760 is of interest because single channel line from the feature collected in 1973 displayed a BSR with the highest reflectivity observed in any lines from the *Burton Island* cruise. The submarine canyon in which Line 760 terminates corresponds with the canyon located 5 km from the right end of the section of single channel Line 331 displayed in Figure 14. The canyon floor on Line 331 (Figure 14) is under 1,600 m of water and is about 6 km down slope from the termination of Line 760 (Plates 6 and 7). The pair of bathymetric highs on Line 331 (Figure 14) which are underlain by the bold BSR would have been surveyed by multichannel seismic methods had Line 760 been continued seaward. Such an extension would have permitted comparison of multichannel and single channel methods for delineation of a major BSR with obvious velocity push down features.

Multichannel seismic line 756 is a dip line crossing the continental slope to a water depth of 1,600 m 35 km east of Line 760 (Plate 7). The continental slope on Line 756 shows evidence of mass wasting or faulting in recent times (Figure 32). Grantz et al. (1983) mapped a fault scarp on Line 756 between water depths of 600 and 1,100 m with a probable separation of 680 m. The scarp is covered by only a thin veneer of sediment indicating late Pleistocene or possibly Holocene deformation. A BSR can be confidently traced for 4 km beneath a slight bathymetric high between 1,320 and 1,500 m water depth (Figure 32). A subtle BSR with a reflection amplitude similar to sediment reflector extends for another 2 km seaward (Figure 32).

Line 756 is located a mere 5 km east of single channel Line 361 (Plates 6 and 7) which displayed a recent fault or slide scarp which appeared to be aligned with the trend of a BSR farther downslope. The BSR on Line 361 (Figure 16) extends shoreward to a water depth of less than 800 m. The BSR on Line 756 dissipates well beneath the fault scarp: the orientation of the fault scarp and BSR on Line 756 do not appear to be related as was proposed for Line 361 (Figure 16).

Multichannel seismic line 755 extends due east from the seaward end of Line 756 obliquely to the strike of the continental slope (Plate 7). Two bathymetric highs are recorded on Line 755, each with about 200 to 300 m of local relief at the

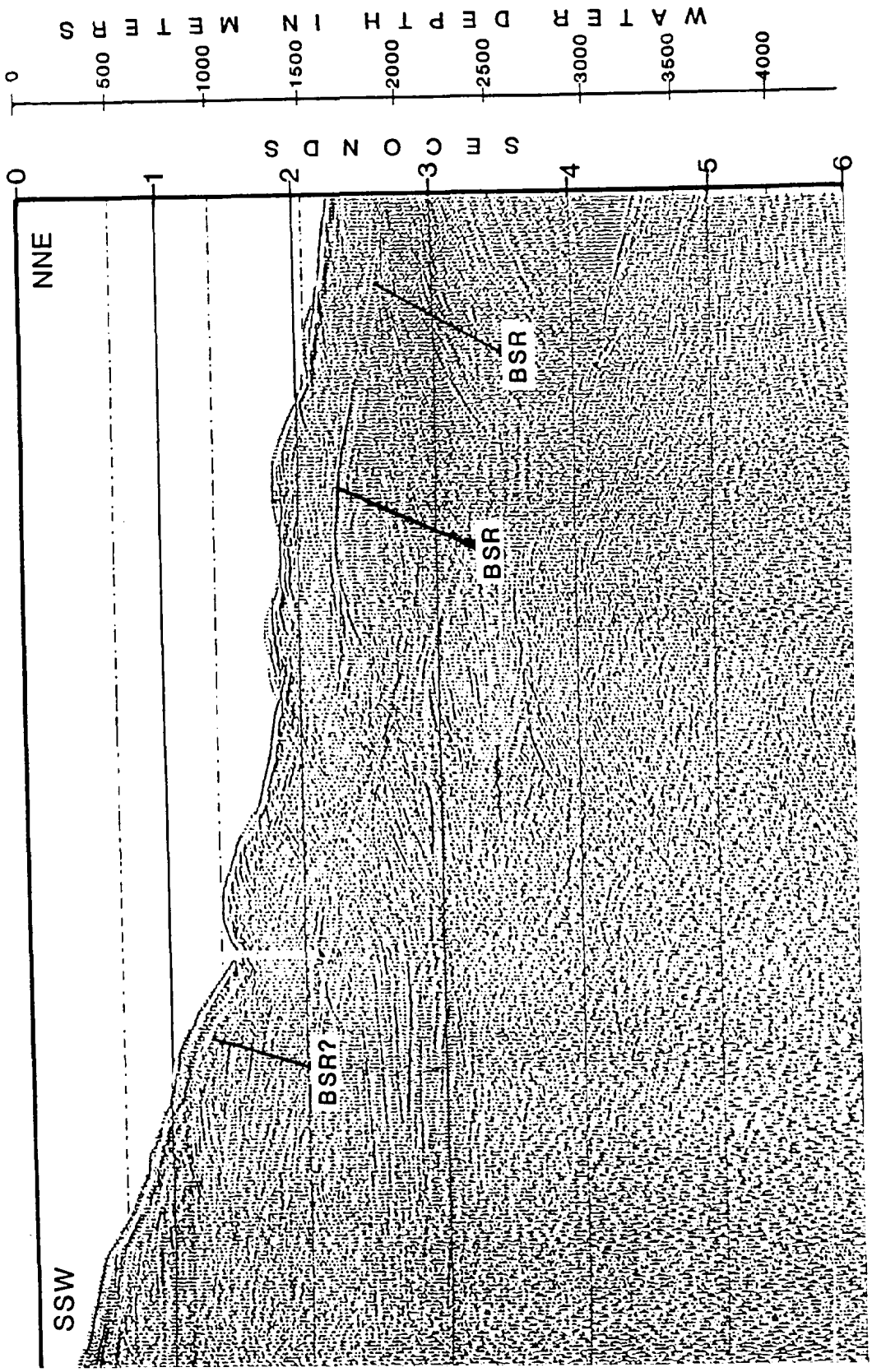

Figure 32. MULTICHANNEL SEISMIC LINE 756

seafloor. Each bathymetric high on Line 755 is underlain by a BSR (Figure 33). The western bathymetric high is underlain by a BSR which extends for 6 km; the BSR beneath the eastern bathymetric high extends for 4 km. The 4 km trough separating the bathymetric highs is devoid of BSRs

The western bathymetric high on Line 755 was also surveyed on a single channel line, 333 (Figure 15). The two lines are parallel for about 7 km (Plates 6 and 7). The depth of the ocean floor on the crest of the bathymetric high is identical on each line indicating that the tracklines of the two surveys coincide. The morphology of the sea floor is also identical on the two lines, although the vertical exaggeration of the single channel line is about double that of the multichannel line. The BSR underlying the bathymetric high is likewise evident beneath both the single channel and the multichannel line. The subbottom depths to the BSR on both lines range from 0.52 sec on the west flank and crest to 0.40 sec where the BSR disappears beneath 1,925 m of water. The sediment layers within and immediately beneath the gas hydrate stability zone are better imaged in the single channel analog record (Figure 15), while sedimentary reflectors deeper than 0.6 sec subbottom are visible only on the multichannel line (Figure 33). The BSR is well imaged on both lines; it is perhaps more obvious on the multichannel line because it is the only strong reflector in the subbottom depth range. The BSR on the single channel line has about the same reflectivity relative to the sea floor reflector as the multichannel line (755) but sedimentary reflectors of near the same magnitude obscure the BSR in the single channel line (333). Neither line displays obvious velocity push down effects or amplitude changes in the sediment reflectors on either side of the BSR.

The BSR beneath the eastern bathymetric high on Line 755 is located at the same subbottom depth range (0.40 to 0.57 sec) as that beneath the western bathymetric high (Figure 33). However, sediment reflectors beneath the BSR of the eastern bathymetric high are better defined than reflectors above the BSR. The reflectors beneath the BSR appear to be bowed downward giving the appearance of a gentle syncline. Whether this is a velocity feature due to possible free gas trapping beneath the base of the gas hydrate stability zone is not clear because no distinct sediment reflectors above the BSR are distinguishable for comparison. One curious aspect of Line 755 is the absence of the BSR in the water bottom multiple reflection. Typically, BSRs are well recorded in not only the primary seismic reflection, but also in the first water bottom multiple. Often the multiple is useful in confirming the possible presence of a BSR; the increased vertical exaggeration of the reflectors can facilitate detection of discordance between a possible BSR and sediment reflectors. On Line 755 sediment layers can be detected in the multiple, but the BSR is invisible.

Multichannel seismic line 753 is oriented parallel to the regional dip of the continental margin north of Simpson Lagoon and 16 km east of Line 756 (Plate 7). Line 753 is the westernmost line from the 1977 cruise of the *S.P. Lee* to survey the lower continental rise of the Alaskan margin (Plate 7). Annotated examples of Line 753 (Figure 34) at a greater vertical exaggeration than the lines available to us have been used to illustrate the structure and seismic stratigraphy of the Alaskan continental margin in many regional geologic studies (Grantz et al., 1979; Grantz and Dinter, 1980; Grantz et al., 1980; Grantz et al., 1981; Grantz and May, 1982;

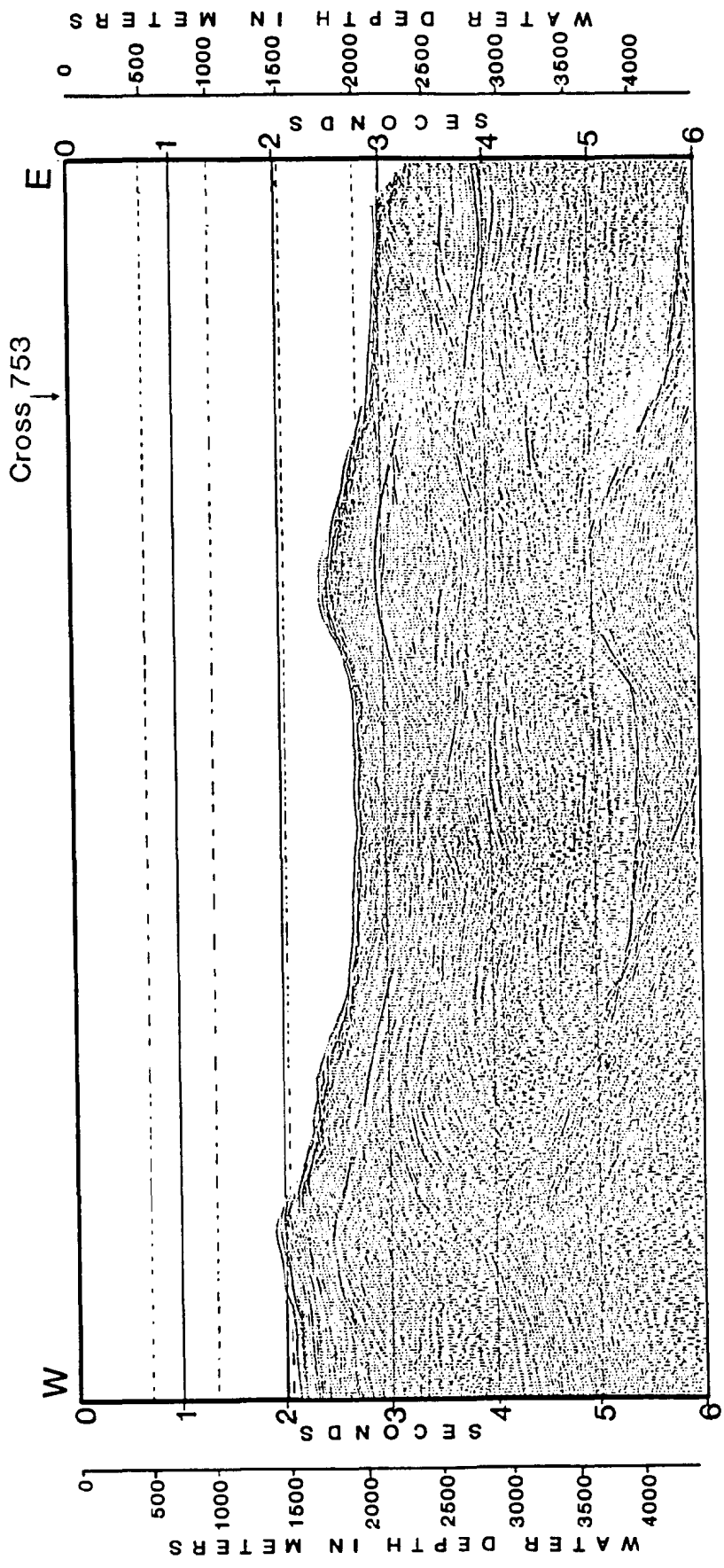

Figure 33. MULTICHANNEL SEISMIC LINE 755

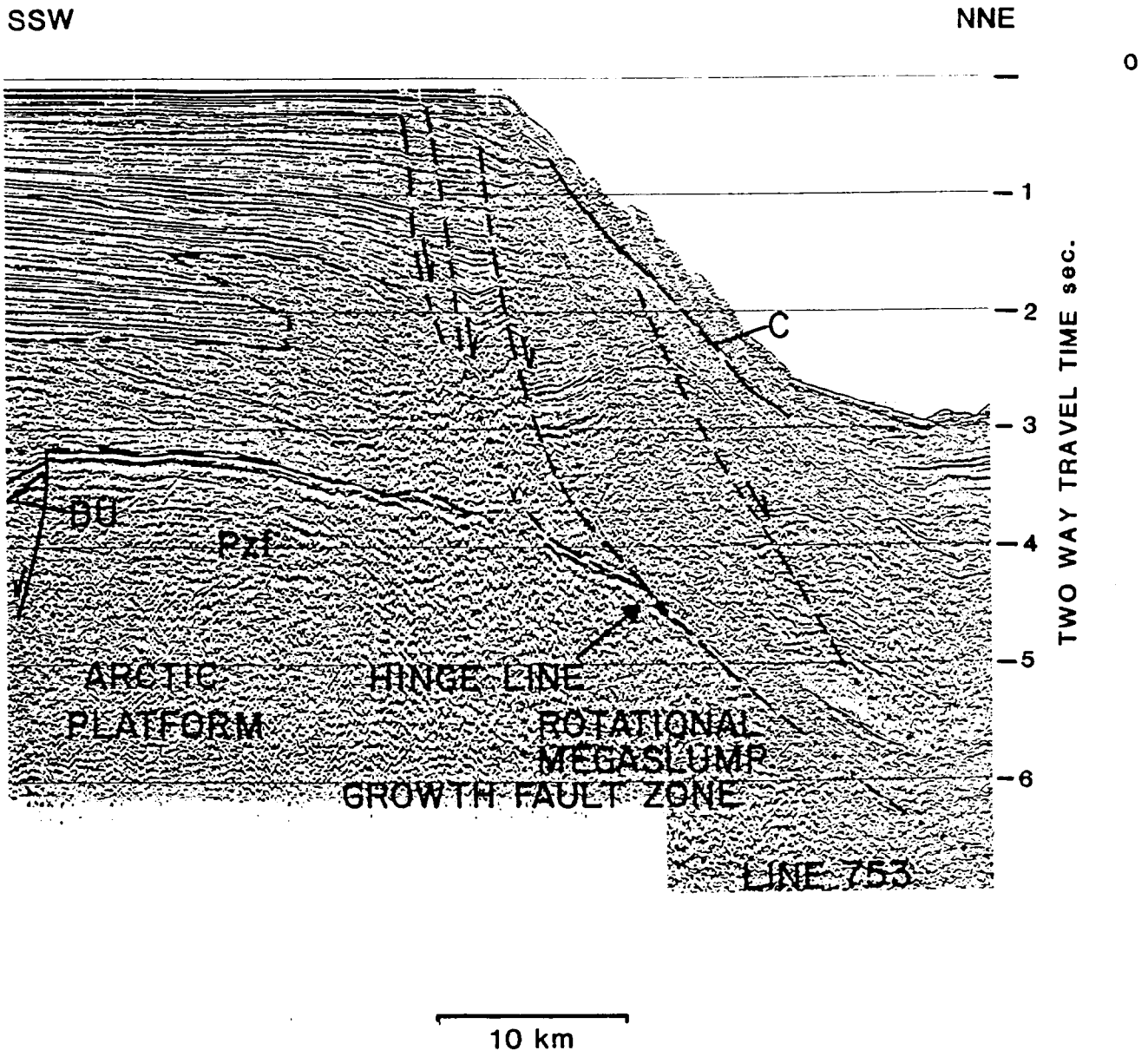

Figure 34. ANNOTATED SECTION OF SEISMIC LINE 753, NORTH OF PRUDHOE BAY

After Grantz and May, 1982

Grantz et al., 1982a). Deep stratal reflectors on Line 753 clearly record the location and configuration of the metamorphic Franklinian sequence basement and faulting at the hinge line (Figure 34). The continental slope and the shelf - slope break on Line 753 is underlain by four well defined listric normal faults or slump failure surfaces. In their many papers, Grantz and his coworkers term the deformed sedimentary prism beneath the continental slope on Line 753 a "rotational megaslump growth-fault zone".

A very strong BSR is present beneath the upper continental slope on Line 753. The BSR was marked as a "clathrate boundary" in the published examples of Line 753 (Grantz et al., 1979; Grantz and Dinter, 1980; Grantz et al., 1980; Grantz and May, 1982; Grantz et al., 1982a). Although the BSR was obscured by heavy annotation, its appearance is unusual compared to others from the Beaufort Sea study region in that the BSR does not closely mimic the seafloor topography in form (Figure 34). In the set of seismic lines released to the public (Grantz et al., 1982b) the anomalous character of the BSR beneath the upper continental slope on Line 753 is even more apparent (Figure 35). The BSR is first visible beneath water 500 m deep and can be traced downslope for 10 km until it dies out beneath water 1,680 m deep. The BSR generally increases in subbottom depth from 0.32 sec at 500 m water depth to 0.46 sec at its termination beneath deeper water. The BSR maintains a very consistent, smooth slope over its entire length (Figure 35). In contrast, the seafloor overlying the BSR is very rough with a hummocky topography consisting of bathymetric highs with over 150 m relief spaced at one or two per kilometer. The reflectivity of the BSR is far greater than that of the sea floor. The poor reflectivity of the seafloor over the BSR on Line 753 suggests that the seafloor is composed of resedimented material which has not been resident long enough to have acquired a reflective sequence of sediments stratified parallel to the sea floor.

Sediment reflectors differ in amplitude across the BSR, but in a manner opposite of that documented in BSRs due to hydrates. The acoustic transparency of the sediments on either side of the BSR is slightly greater than that of adjacent and subjacent sediments (Figure 35). Bottom simulating reflectors attributed to gas hydrates often are characterized by acoustically transparent sediments above the BSR (Shipley et al., 1979). Lower reflector amplitude in sediments above BSRs characterizes the probable gas hydrate reflectors in single channel profiles from the Beaufort Sea study region. However, on multichannel Line 753, the reflectors beneath the BSR are of lower amplitude than those above, i.e. the sediments beneath the BSR are more acoustically transparent. The acoustic transparency of sediments beneath the BSR on Line 753 resembles a seismic bright spot (Figure 35). This apparent seismic bright spot may signify gas accumulation beneath the BSR. However, no velocity push down features are seen in the sediment reflectors underlying the possible bright spot as would be expected if free gas were present.

The BSR beneath the upper slope of Line 753 is thus anomalous in many ways. The reflector does not mimic the seafloor topography to the extent seen in BSRs from nearby sections. The reflectivity of the BSR is much greater than that of the overlying seafloor. Such high reflectivity of the BSR implies that free gas beneath the base of the gas hydrate stability zone may be present; the enormous contrast in seismic impedance needed to produce such a strong BSR would most likely require the presence of a low velocity gas-saturated zone beneath the BSR.

Figure 35 is in a pocket located inside the back cover.

However, the amplitude of sediment reflectors on either side of the BSR does not follow the pattern seen in hydrate BSRs worldwide (Shipley et al., 1979) or elsewhere in the Beaufort Sea study region (e.g. Figures 13 - 20). In spite of these anomalous features, the BSR on Line 753 would appear to be hydrate related because its subbottom depth (0.32 to 0.49 sec) is similar to that of nearby BSRs with more typical features. Although the subbottom depth of the BSR fluctuates locally by 0.05 sec due to seafloor irregularities which are not mimicked by the BSR, its mean depth increases from 0.33 sec beneath 500 m of water to 0.48 sec beneath 1,630 m of water as expected for the base of the gas hydrate stability zone.

We interpret the anomalies of the BSR beneath the upper continental slope on Line 753 to be due to mass wasting along a failure surface coincident with the base of the gas hydrate stability zone. Grantz et al. (1979), Grantz and Dinter (1980), Grantz et al. (1980), Grantz and May (1982), and Grantz et al. (1982a) did not elucidate the deformation of the shallower sediments when they presented the annotated version of Line 753 reproduced here as Figure 34. However in a paper more concerned with the physiographic development of the Alaskan continental margin, Grantz et al. (1981) presented a line drawing of Line 753 with normal faults and gravitational failure surfaces represented. In their drawing, presented in simplified form as Figure 36, they interpreted the hummocky surface of the continental slope to be composed of individual fault blocks separated by listric normal faults dipping seaward. A sole detachment surface approximately parallel to the seafloor was interpreted by Grantz et al. (1981) to underlie the individual fault blocks at about 0.3 to 0.5 sec subbottom. Grantz et al. (1981) also indicated the presence of the base of the gas hydrate stability zone at about 0.10 sec beneath the sole detachment surface. Grantz et al. (1981) did not suggest any connection between the base of the gas hydrate stability zone and the parallel sole detachment surface. On the sections of Line 753 available to us (Figure 35), we find no evidence of separate reflectors corresponding to the sole detachment surface and the base of the gas hydrate stability zone. We interpret the downslope movement of the smaller individual fault blocks above the BSR to have taken place along the gas hydrate phase boundary. That is, we interpret the sole detachment surface and the base of the gas hydrate stability zone diagrammed by Grantz et al. (1981) to be the same surface.

Our interpretation of the mode of failure of the continental slope on Line 753 could help to explain some of the discrepancies noted above. The lack of parallelism of the sea floor and the BSR could be due to the interaction of factors. McIver (1977, 1982) proposed that possible free gas and overpressuring at the base of the gas hydrate stability zone would promote slope failure along the gas hydrate phase boundary surface. By this reasoning, the surface defining the base of the gas hydrate stability zone would necessarily be formed prior to displacement of overlying sediments along it. The linearity of the BSR on Line 753 suggests that the ocean bottom was of similarly low relief when the hydrate boundary surface developed. The present hummocky ocean bottom surface was formed by the movement along the listric normal faults between the individual blocks and along the sole detachment surface. Rotation of the individual fault blocks and reverse drag folding of the headwall portion of the blocks due to the geometrical relationships inherent in listric normal faults would tend to produce uneven sea floor topography, even is the

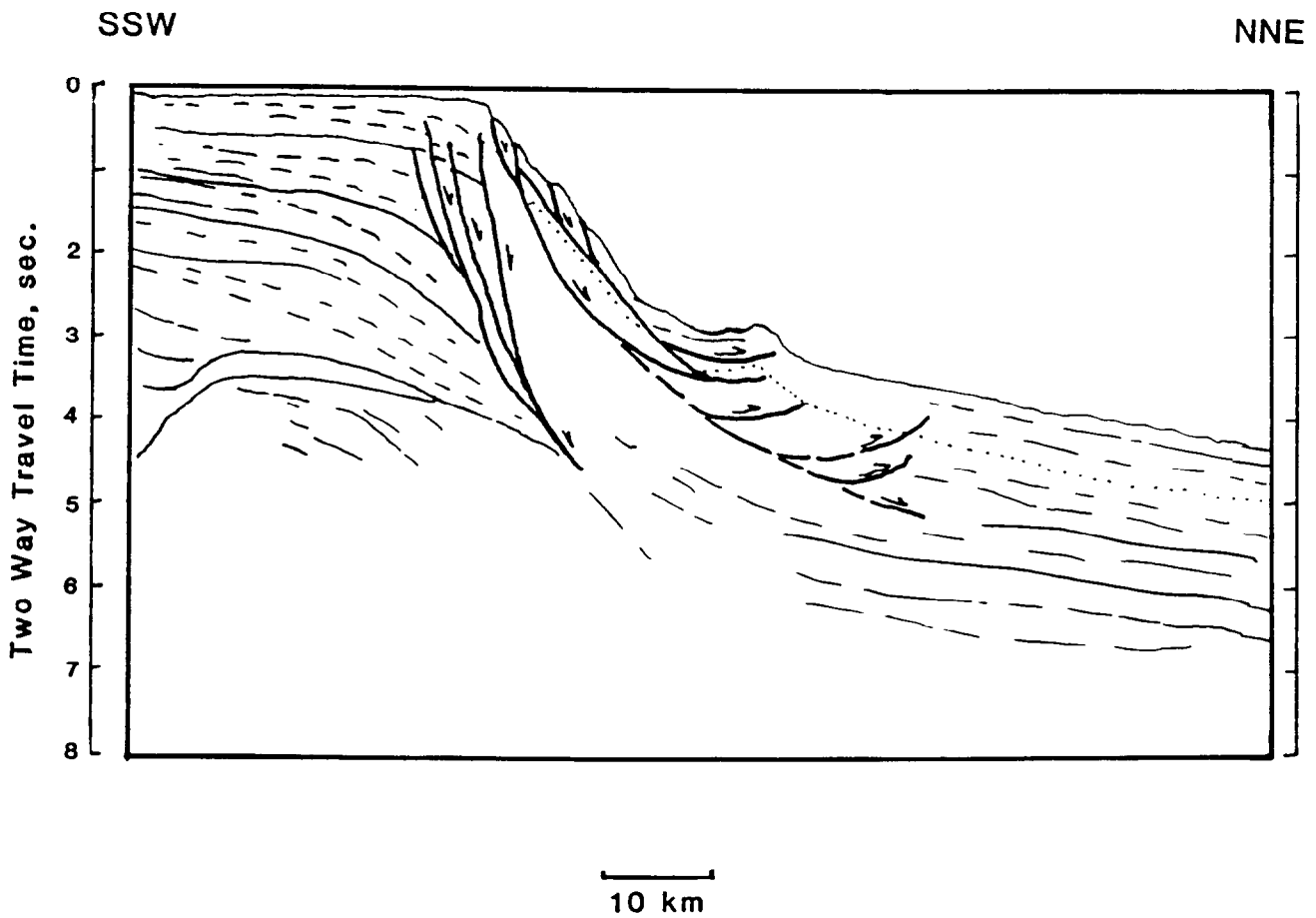

Figure 36. INTERPRETIVE CROSS-SECTION OF ALASKAN CONTINENTAL MARGIN ALONG MULTICHANNEL SEISMIC LINE 753

After Grantz et al., 1981

Base of Gas Hydrate Stability Zone shown by dots.

seafloor had been planar prior to faulting. The present sea floor topography above the BSR is thus a relatively recent surface in comparison to the BSR. If the gravity induced movement of the shallow sediments overlying the BSR were to stop for a substantial period of time, it is to be expected that the continental slope would thermally reequilibrate and the BSR would migrate to a position which parallels the configuration of the contemporary seafloor. However, impending cessation of the downslope movement of the upper 300 to 600 m of sediment is not necessarily indicated.

The continental slope on Line 753 may be in the process of assuming the profile seen on single channel Line 361 (Figure 16). We interpreted the topography of Line 361 to suggest that a large slide lock had moved along a failure plane coincident with a BSR depositing a large slide downslope from the exposed scarp. The apparent youth of the sea floor surface over the BSR on Line 753 is indicated by the lack of laminated sediments draping the individual fault blocks, and the lack of ponded sediments in the depressions at the sea floor exposures of the faults. The sea floor surface upslope and downslope from the hummocky surfaced section of the continental slope appears to be more mature by these criteria. If the proposed movement along the BSR on Line 753 is as recent as suggested, the movement may still be active, and may not cease until sufficient material has accumulated at the base of the slide to "anchor" the motion. A large deposit of material could apply sufficient gravitational stress to the mass slide surface to overcome the potentially elevated pore pressure at the hydrate boundary and increase effective stress to a value in excess of the failure criterion (Hubbert and Rubey, 1959) thereby stabilizing the downslope movement.

The lower continental slope on Line 753 consists of a broad bathymetric high at 2,000 m water depth followed by a uniform, gradually sloping rise to the seaward end of the line at 3,300 m. A distinct BSR is present beneath the bathymetric high (Figures 34 - 36). The BSR extends northward for 12 km from the crest of the bathymetric high before disappearing in the well stratified sediments beneath the continental rise. A high-amplitude reflector periodically appears in the sediments beneath the lower continental rise. The reflector is most likely a sediment layer, but it does occur at a subbottom depth expected for a BSR based on extrapolation of the BSR depths beneath shallower water.

The BSR beneath the bathymetric high at about 2,000 m water depth resembles those described on other seismic lines from the Beaufort Sea study region. The BSR ranges in subbottom depth from 0.42 sec on the shoreward flank to 0.48 sec beneath the crest, and averages over 0.5 sec subbottom beneath the deeper water of the seaward flank before disappearing beneath the continental rise sediments. In accordance with the expected pattern, few sediment reflectors can be discerned in the gas hydrate stability zone of the bathymetric high. Reflectors beneath the BSR are enhanced in amplitude and wavelength, suggesting possible velocity effects. Lines 753 and 755 (Figures 33 and 35) intersect at a water depth of 2,050 m. The bathymetric highs on Line 753 and the east end of Line 755 appear to correspond to the same feature although the lines do not meet on the structure itself. The BSRs at the points of intersection of both lines correspond in both subbottom depth and appearance. The BSRs beneath the correlated bathymetric highs on the two lines

also display probable velocity push down features on each, suggesting that free gas may be trapped beneath the high.

Multichannel seismic line 751 is oriented along the dip of the continental slope due north of Prudhoe Bay (Figure 37). Line 751 is located roughly parallel to and 21 km east of Line 735 (Plate 7). The portion of the continental slope north of Alaska surveyed on Line 751 is characterized by a sea floor with only minor irregularities between 500 and 1,000 m water depth. An annotated copy of Line 751 was presented by Grantz and May (1982). They demonstrated that extensive growth faulting beneath the outer continental shelf has generated the present configuration of the continental margin. Grantz and May (1982) indicated that on Line 751, as on most sections across the Alaskan continental margin, the upper continental slope is underlain by large blocks of Tertiary sediments which slid down northward dipping listric normal faults. The sediments beneath the upper continental slope on Line 751 are rotated in a manner analogous to a conventional slump block to produce stratal reflectors which dip to the south. These sub-slope structures are termed "large slumps" by Grantz et al. (1983) and "rotational megaslumps" by Grantz and May (1982). The deep structure on Line 751 is similar to that on Line 753, but Line 751 displays much less shallow deformation and mass wasting.

Distinct BSRs can be traced over much of the length of Line 751. The annotated version of Line 751 (Grantz and May, 1982) shows a BSR extending about 20 km from beneath a water depth of 1,280 m to the northward end of the section illustrated at 2,380 m water depth. The heavy annotation on the section presented by Grantz and May (1982) precludes assessment of the reflectivity of the BSR. Line 751 was released to the public in Grantz et al. (1982b) in a format with much less vertical exaggeration (Figure 37). Additionally the version of Line 751 released in Grantz et al. (1982b) extended seaward an additional 15 km to a water depth of 2,800 on the lower continental slope. The BSR obscured by the annotation in Grantz and May (1982) is well imaged on Line 751 from Grantz et al. (1982b). The reflectivity of the BSR varies markedly along the 18 km distance indicated by Grantz and May (1982). The BSR is most apparent from a water depth of 2,340 to 2,560 for a distance of about 12 km. The additional 16 km from 1,280 to 2,300 indicated by Grantz and May (1982) to be underlain by a "basal zone of gas hydrate" is underlain by a very faint reflector which attains the high reflectivity typically associated with the base of the gas hydrate stability zone for only 1 km beneath about 1,975 m of water. It is probable that the BSR is much more visible on the original lines available to Grantz and May (1982).

The faint reflector between 1,280 and 2,300 m water depth marked as a BSR by Grantz and May (1982) is seen on the example of Line 751 from Grantz et al. (1982b) to extend farther landward (Figure 37). The very faint BSR annotated on Line 751 as a base gas hydrate reflector can barely be discerned from stratal reflectors at 1,280 m water depth. At 950 m water depth a reflector at about 0.30 sec subbottom appears and continues landward for 3 km before dissipating beneath 370 m of water. The reflector maintains a depth of about 0.30 sec subbottom over the distance and generally follows the bathymetric profile of the seafloor. The poor resolution of near-surface strata beneath the upper continental slope on Line 751 does not preclude the possibility that the BSR beneath the shallow water near the

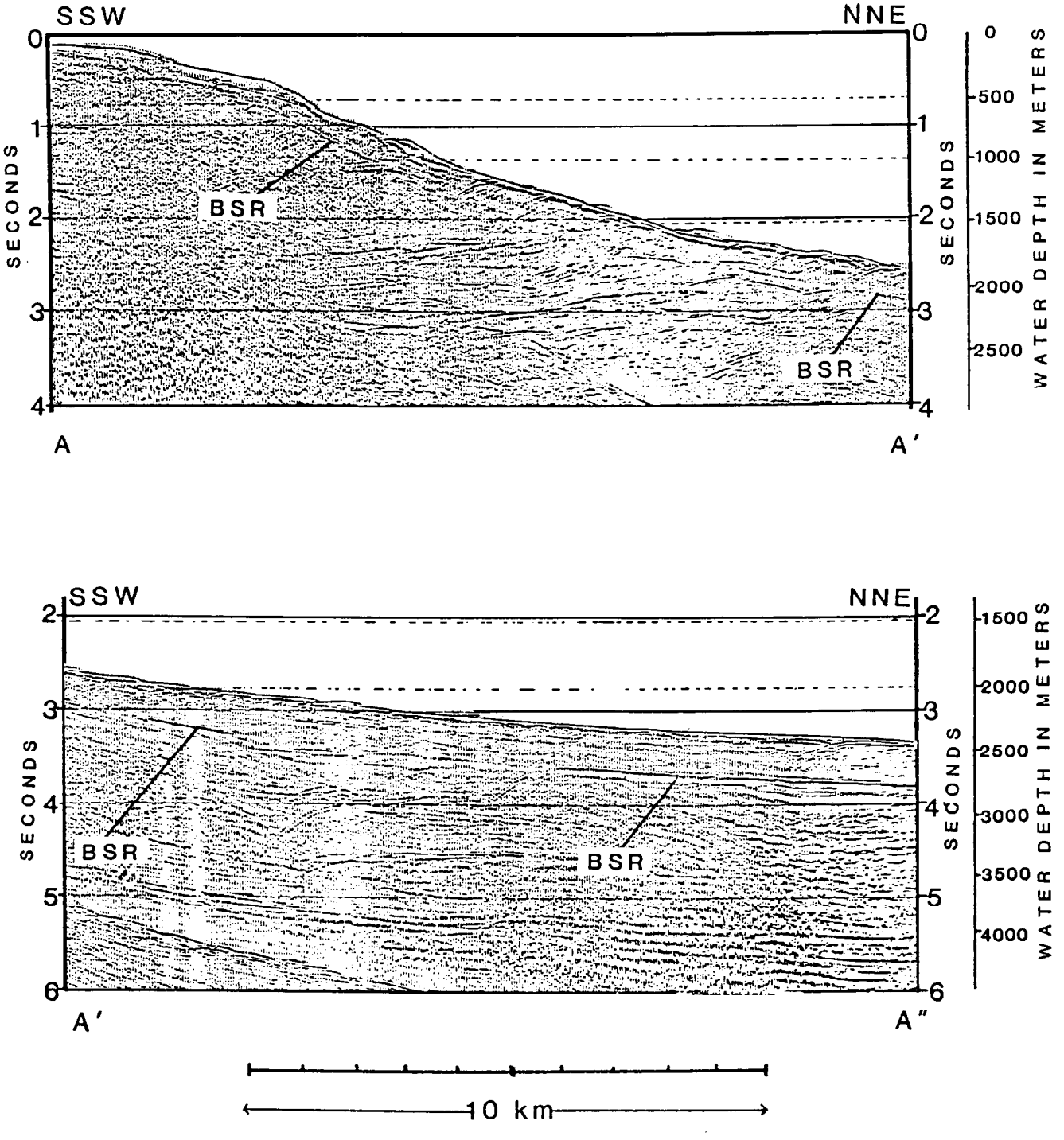

Figure 37. MULTICHANNEL SEISMIC LINE 751

shelf-slope break is sedimentary in origin. However, at a water depth of 850 m the possible BSR intersects a strong reflector at an angle. This discordance suggests a hydrate origin for the reflector. The amplitude of the reflector between 370 and 950 m water depth is on an average greater than that of the similar reflector between 1,280 and 2,300 m identified as a gas hydrate BSR by Grantz and May (1982). Based on these factors we interpret the reflector between 370 and 950 m water depth on Line 751 to mark the base of the gas hydrate stability zone beneath the outer continental shelf and upper continental slope north of Prudhoe Bay.

Beneath the central part of the most reflective section of the BSR on Line 751 (1,600 to 2,575 m water depth) the sediments are bowed downward into an apparent syncline. Similar apparent synclines beneath BSRs have been interpreted by us to indicate possible free gas accumulation beneath bathymetric highs on lines from elsewhere in the Beaufort Sea study region. From the marginal-quality prints of Line 751 available to us, it is not possible to determine if the syncline is a velocity push down effect, or a representation of the true structural orientation of the sediments. However, increased amplitude is noted in the sediment reflectors beneath the BSR compared to the sediment reflectors above the BSR. The effect is most apparent across the part of the BSR which overlies the axis of the syncline. Velocity push down effects beneath bathymetric highs elsewhere on the Beaufort continental margin are associated with the same velocity contrast, suggesting that the syncline beneath the BSR at 1,600 to 2,300 m water depth may be caused by trapped free gas.

Subtle indications of the BSR continue beneath water deeper than 2,370 m on Line 751. Extrapolating the subbottom depth trend of the BSR from its termination as a strong reflector at 2,375 m water depth reveals a faint reflection at the probable depth for the gas hydrate phase boundary. Since the possible seaward extension of the BSR could not be identified without a priori knowledge, we have not included it as a BSR in our areal estimates.

Multichannel Seismic Lines East of Prudhoe Bay

The far northward retreat of the Arctic ice pack during the summer of 1977 permitted the *S.P. Lee* to extensively survey the continental slope north of Alaska to the east of Prudhoe Bay. The 1973 single channel seismic survey aboard the *Burton Island* covered areas of the lower continental slope north of Smith Bay and Harrison Bay, and portions of the upper continental slope as far east as Prudhoe Bay (Plate 6). Ice cover over the eastern portion of the Alaskan continental margin in 1973 limited the *Burton Island* survey to the continental shelf east of Prudhoe Bay. However, ice had withdrawn from the eastern portion of the Beaufort Sea study region permitting multichannel seismic surveying aboard the *S.P. Lee* to extend 300 km north of the Alaskan coast to the abyssal plain and lower continental slope beneath water as deep as 3,400 m (Plate 7).

Multichannel seismic lines 744 through 750 define a 60 km segment of the Alaskan continental margin which is effectively devoid of readily identified bottom simulating reflectors (Plate 7). The continental slope along this interval is characterized by a generally rough topography indicating extensive mass wasting.

One line (749) records a fairly even sea floor, but subsurface sediment reflectors indicate considerable deformation. Evidence for mass wasting and growth faulting abounds on lines from this stretch of the continental slope; however, well defined BSRs were identified on multichannel seismic lines to the west with comparable degrees of structural deformation and recent mass wasting.

Multichannel seismic line 745 is located 15 km east of Line 751 (Plate 7). The continental slope on Line 745 shows evidence of recent large-scale faulting. Grantz et al. (1983) mapped a fault scarp with 580 m displacement on the upper continental slope of Line 745. Grantz et al. (1983) used an annotated line drawing of Line 745 as an example of the style of Quaternary deformation common to the upper continental slope north of Alaska. Their illustration shows a network of faults which have produced the present configuration seen on Line 745. Their figure caption summarizes the structure of the continental slope on Line 745 and by extension that of most of the rest of the continental slope north of Alaska:

> Complex of slump masses as thick as 950 m, and slope-facies sedimentary units overlying a listric normal fault that reaches sea bed at head of continental slope. Uppermost large slump mass dropped about 580 m and moved seaward about 3.5 km. Downslope, beyond end of profile, listric faults presumably die out in a network of small faults or in a buckled zone. Because of their depth, it is less likely that they break a present or former position of the sea bed.

On the line drawing of the structure of Line 745 Grantz et al. (1983) did not annotate a gas hydrate BSR. Other multichannel seismic lines used as examples in the publication had BSRs clearly marked where they were present (e.g. Lines 726 and 732). Our examination of the example of Line 745 released by Grantz et al. (1982b) agrees with the drawing by Grantz et al. (1983) that no gas hydrate reflectors can be conclusively identified on the line.

Multichannel seismic line 749 is located 20 km east of Line 745 and extends northward to a water depth of 3,200 (Plate 7). Although a few minor bathymetric highs with relief similar to those which host BSRs elsewhere on the margin are found on Line 749, no BSRs can be identified on the line.

Multichannel seismic lines 750 and 746 are oriented along the strike of the lower and upper slope respectively. Bathymetric highs are seen on both lines, but no BSRs or hydrate-related amplitude anomalies can be identified.

Multichannel seismic line 747 is located 17 km east of Line 749 (Plate 7). The sea floor and underlying sediments on Line 747 are thoroughly deformed with abundant normal, reverse, and growth faults. Displaced sediments have deformed formed into anticlines with bathymetric expression. In spite of the abundant migrational pathways and potential traps for gas produced by this deformation, no BSRs could be identified on Line 747.

Multichannel seismic line 744 is located 20 km east of Line 747 north of the Canning River delta (Plate 7). Abundant evidence of Quaternary faulting and mass wasting exists in the upper continental slope of Line 744. However, BSRs are not well defined beneath the abundant bathymetric highs on the upper continental

slope. Two reflectors were provisionally identified as BSRs beneath isolated bathymetric highs, but a lack of discordance with nearby sediment reflectors indicates that they may be of sedimentary rather that gas hydrate origin.

Multichannel seismic lines over diapirs. The seismic lines of Alaskan continental slope from Camden Bay east to the seaward projection of the U.S.-Canadian border all display BSRs (Plate 7). The resumption of BSRs on multichannel seismic lines from the continental slope north of Camden Bay following the lack of BSRs between Prudhoe Bay and the Canning river delta corresponds with a change in structural style of the continental margin. From Camden Bay eastward the continental slope and rise is underlain by large shale diapirs (Eittreim and Grantz, 1979; Grantz et al., 1979; Grantz and Dinter, 1980; Grantz et al., 1980; Grantz et al., 1981; Grantz and May, 1982; Grantz et al., 1982a). Seismic velocity of the diapiric material was substantially less than that of the intruded sediments, leading Eittreim and Grantz (1979) to conclude that shale rather than salt cored the diapirs. Spacing of the multichannel seismic line from the *S.P. Lee* was insufficient to determine the morphology of the diapiric bodies, but the bathymetry of the seafloor overlying the diapirs suggests that they are elliptical in plan view with elongation parallel to the strike of the continental slope.

The western limit of the extensive diapir field is well imaged by a series of colinear north-south multichannel seismic lines: 724, 1710, 2710, and 3710 (Plate 7); and by a three lines striking northeast or north-northeast: 743, 2742, and 1725 (Plate 7). The north end of Line 724 displays the outer continental shelf and the first part of the shelf-slope break. Line 724 illustrates the geomorphology common to the outer continental shelf and upper continental slope offshore of the eastern section of the Alaskan continental margin. The flat-laying sediments of the continental shelf extend far seaward of the 100 to 200 m water depth conventionally considered the limit of the continental shelf. The gently sloping continental shelf offshore of northeastern Alaska typically continues to depths of 400 to 700 m before encountering a rapid increase in gradient at the shelf-slope break. Grantz et al. (1981) termed the unusually deep outer continental shelf along this portion of the Alaskan continental margin the Beaufort Ramp.

Multichannel seismic line 724. A possible BSR is located near the north end of Line 724 at the slope break (Figure 38). A reflector 0.40 sec subbottom can be traced from the north end of the line at 690 m water depth landward about 3.5 km until it becomes indistinguishable from concordant stratal reflectors and the 1 sec depth reference line superimposed on the seismic line. The possible hydrate horizon clearly intersects stratal reflectors where the seafloor is increasing in depth rapidly while the sediments retain their very gentle seaward dip.

Multichannel seismic line 1710 is a very short seismic line segment (5 km) which is only slightly offset from Line 724 and overlaps the northernmost 1.5 km of Line 724. The BSR can be traced father down the upper continental slope on Line 1710 (Figure 38). The shelf break is immediately underlain by small slumps or fault blocks which have been displaced downslope along well defined north dipping listric

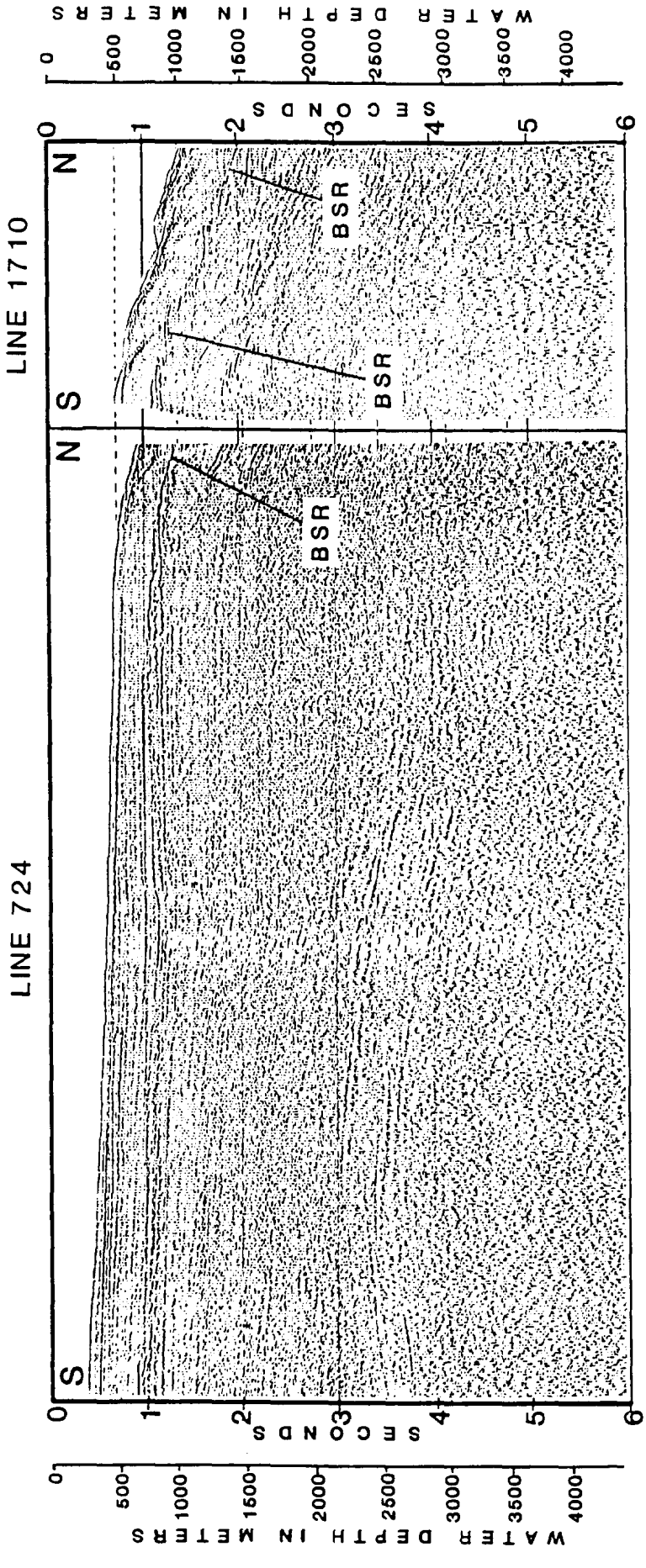

Figure 38. MULTICHANNEL SEISMIC LINES 724 AND 1710

normal faults. The BSR is increased in amplitude near the faults and intersects the faults at an angle. The increased BSR amplitude over the fault suggests that gas hydrate formation, or at least the impedance change associated with BSR reflectivity, was locally enhanced, possibly by deformation and fracturing of the sediments near the fault or by increased hydrocarbon supply by migration along the fault.

Multichannel seismic line 1725. The landward end of the oblique multichannel seismic Line 1725 illustrates the outer continental shelf and upper continental slope near the location of Lines 724 and 1710 (Plate 7). Line 1725 extends about 14 km from a water depth of 500 m to 1,320 m. A very vivid BSR can be traced for the entire length of Line 1725 (Figure 39). The BSR is located 0.40 sec subbottom at the south end of Line 1725 where it intersects Line 724, and increases to 0.45 sec beneath the outer continental shelf where the sediments are approximately horizontally laminated. The zone of active faulting and slumping which constitutes the upper continental slope and the shelf break coincides with a deeper BSR; the reflector attains a subbottom depth of over 0.5 sec beneath the faulted terrane. At the northeast end of Line 1725 the BSR once again is located 0.4 sec subbottom. Although the BSR is very robust at the northeast end of Line 1725, it is absent beneath the southwest end of Line 2725 which begins just 1 km from the end of Line 1725.

Just below the shelf edge on Line 1725, sediment reflectors on either side of the BSR exhibit seismic amplitude and wavelength anomalies which may be caused by trapped free gas. From a water depth of 550 m to about 900 m the sediment reflectors are much better defined beneath the BSR than above (Figure 39). Additionally, the sediment reflectors beneath the BSR are more widely spaced than those above the BSR. As previously seen on single channel lines from offshore of Point Barrow (Figures 16 - 18), this wider spacing of sediment reflectors or velocity push down effect is most apparent when the BSR and sediment reflectors meet at a slight angle. In that instance, the velocity push down causes a much larger angle of incidence of sediment reflectors and BSR beneath the base of the gas hydrate stability zone than above. The poor resolution of stratal reflectors with in the BSR limits the instances when the change in incidence angles is observed. The effect is particularly difficult to observe in the series of multichannel lines from the 1977 cruise of the *S.P. Lee* do to the generally poor resolution of shallower sediments compared to deeper reflectors on this set of data. A strong suggestion of the change in angle of incidence of the sediment reflectors and BSR can be noted beneath the outer shelf of Line 1725 in two locations, immediately below the extreme end of the undeformed shelf sediments, and beneath the subtle monocline seen on the seafloor about 4 km southwest of the shelf-slope break. Poor resolution of strata in the hydrate-filled sediment do not permit numerical estimates of the velocity contrast as was earlier attempted for single channel lines from offshore of Point Barrow.

Multichannel seismic line 2710 continues northward from the north end of Line 1710 following a gap of 2 km with no data. Line 2710 covers the upper continental slope from a water depth of 1,249 m to the lower continental slope and rise at 3,300 m (Plate 7). The portion of the continental slope crossed by Line 2710 is underlain by three diapirs.

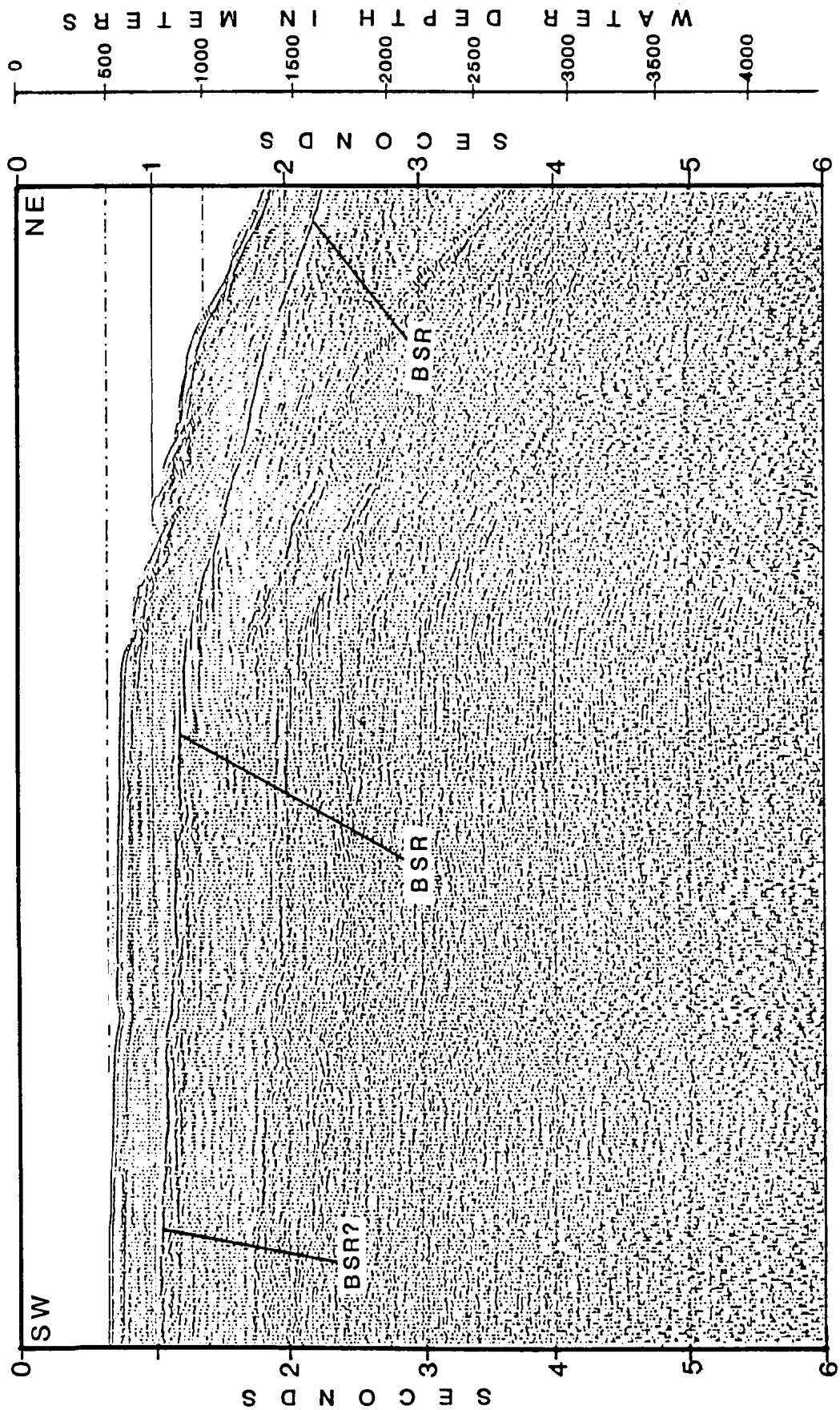

Figure 39. MULTICHANNEL SEISMIC LINE 1725

Bottom simulating reflectors occur over each of the diapirs and beneath the lower continental slope and continental rise shoreward of the diapirs (Figure 40). The northernmost extent of Line 1710 (Figure 38) displayed a BSR at 0.50 sec subbottom. That BSR disappears somewhere in the 2 km gap between Lines 1710 and 2710. On Line 2710 the BSR first appears at a water depth of 1,500 m beneath a small bathymetric high which appears to be a small slump block which slid downslope for a distance of less than 1 km. The BSR becomes much more subtle for about 1.5 km beneath a small trough before regaining high reflectivity beneath a bathymetric high with slightly more relief under 1,600 m of water. The BSR increases in subbottom depth from 0.42 sec beneath the to 0.60 beneath the bathymetric high and shoals to 0.44 sec before disappearing at a water depth of 2,200 m. The bathymetric high beneath which the BSR attains its greatest subbottom depth is a block of material deposited from somewhere upstream and buttressed somewhat by a the upward flexure of a rising diapir.

About 12 km from the disappearance of the BSR in sediments of a syncline another diapir with a BSR can be discerned. The BSR is located at 0.44 sec subbottom beneath the BSR, and 0.48 sec immediately on either side of the apex of the diapir. The BSR is of much lower reflectivity than BSRs elsewhere on Line 2710. It can be resolved over the diapir because of a total absence of sedimentary reflectors over the diapir. The acoustically turbid character of the sediments over the core of the diapir may indicate that the diapir has breached the surface and that the BSR occurs in mobilized material. It is more likely that the lack of distinct sediment reflectors above the diapir is due to the intensity of the deformation above the diapir homogenizing the depositional features of the caprocks. Reflectors approximately continuous with the BSR over the diapir continue into the sediments within the adjacent intraslope basins. Due to the general concordance of the sea floor and sediments within the intraslope basins, it is not clear whether these reflectors are extensions of the BSR over the diapir or are reflective sediment layers.

The BSR beneath the second diapir on Line 2710 could conceivably be a sedimentary reflector rather than the base of the gas hydrate stability zone. The reflector appears to be discordant with sediment reflections on the flank of the diapir. However since diapirism occurred syndepositionally, all sediment reflectors converge. Thus the apparent discordance between the potential BSR and the sediment reflectors may be illusionary. The subbottom depth of the potential BSR over the core of the diapir suggests strongly that it is indeed the base of the gas hydrate stability zone.

No distinct BSR can be traced in the flat laying sediments of the intraslope basin between the second diapir and a third located about 22 km seaward. However, a change in the amplitude of the sediment reflectors is noted within the intraslope basin separating the two lower slope diapirs between 0.7 and 0.8 sec subbottom. The sediment reflectors below 0.7 to 0.8 sec subbottom are much better defined than those above. Again it is possible that the amplitude change, which is commonly associated with gas hydrate presence, is due to a change in character of the sediments. However the subbottom depth of the change and its colinearity with an obvious BSR over the diapir suggest that it may represent the base of the gas hydrate stability zone in the absence of a typical BSR.

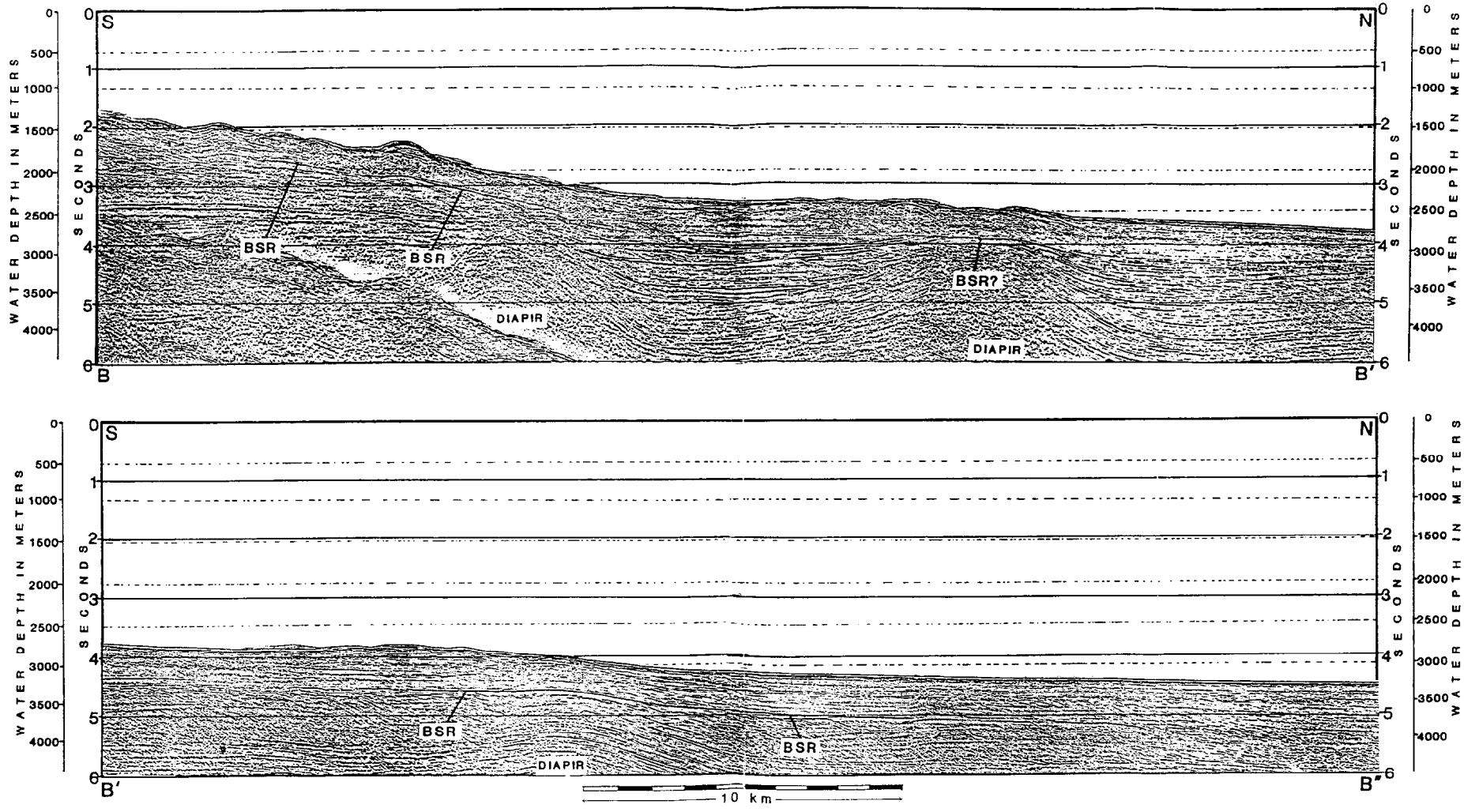

Figure 40. MULTICHANNEL SEISMIC LINE 2710

Multichannel seismic line 2742 is oriented approximately N30°E with its nearshore end about 20 km west of Line 2710. The two lines cross beneath a water depth of 2,650 m (Plate 7). Although no definite correlation of structures beneath the landward portions of the two lines is possible without more closely spaced sections, a diapir beneath a sea floor depth of 1,830 m on Line 2742 (Figure 41) is similar in form to the diapir beneath a sea floor depth of 1,975 on Line 2710. A lower slope diapir beneath the sea floor at 2,200 m water depth on Line 2742 is probably the same as the diapir at 2,420 m water depth on Line 2710.

Unlike the case 16 km to the east as seen in Lines 724, 1710, and 1725, no BSR can be discerned at the shelf-slope break on Line 2742 (Figure 41). The first indication of a BSR on Line 2742 is landward of the crest of the first continental slope diapir beneath 1,600 m water depth. The BSR extends for 6 km under the bathymetric high overlaying the diapiric uplift. The BSR depth ranges from 0.48 sec to 0.58 sec subbottom with a mean depth of 0.52 sec. Beneath the second diapir a very reflective horizon at about 0.7 sec subbottom can be traced for 8 km. Although this reflector beneath a major bathymetric high could conceivably represent the base of the gas hydrate stability zone over the diapir, its concordance with sediment reflectors and the presence of similarly reflective sediment horizons deeper in the sedimentary section preclude our inclusion of it as a hydrate BSR.

Multichannel seismic line 2722 is a north to south dip line located about 15 km east of Lines 724, 1710, and 2710 (Plate 7). At least three diapirs can be discerned beneath the continental slope of Line 2722 (Figure 42). Very minor surface expression of the diapirs on Line 2722 in comparison to nearby seismic lines suggests that the diapirs are intruding more slowly along Line 2722 or perhaps are presently inactive.

A strong BSR is located beneath the upper slope of Line 2722 and appears sporadically for short distances beneath the lower continental slope. The principal BSR on Line 2722 can be traced for about 15 km between water depths of 1,000 m and 1,900 m. The BSR is continuous across faulted areas of the upper continental slope, an intraslope basin of ponded sediments, and a diapir.

The southern limit of the BSR is within a slump or fault block about 1.5 km across bounded on either side by listric normal faults (Figure 42). A moderately distinct portion of the BSR crosses deformed sediment reflectors at a subbottom depth of 0.50 sec. No velocity features are apparent across the BSR within the fault or slump block. The BSR can be traced further downslope through another allochthonous block. This fault block or slump block has apparently experienced greater displacement than that immediately above. It is different from the previously discussed block immediately upslope and those typically encountered on the Alaskan continental slope in that it is bounded on its downslope side by a southward dipping thrust or reverse fault rather than a northward dipping listric normal fault. The block defines a distinct bathymetric high. The BSR is present in the block at greater subbottom depths than in the other allochthonous block immediately upslope. The BSR ranges in depth from 0.56 sec on the south (upslope) flank to 0.60 sec beneath the apex of the bathymetric high, and gradually shoals to 0.54 sec subbottom on the north (downslope) flank of the bathymetric high.

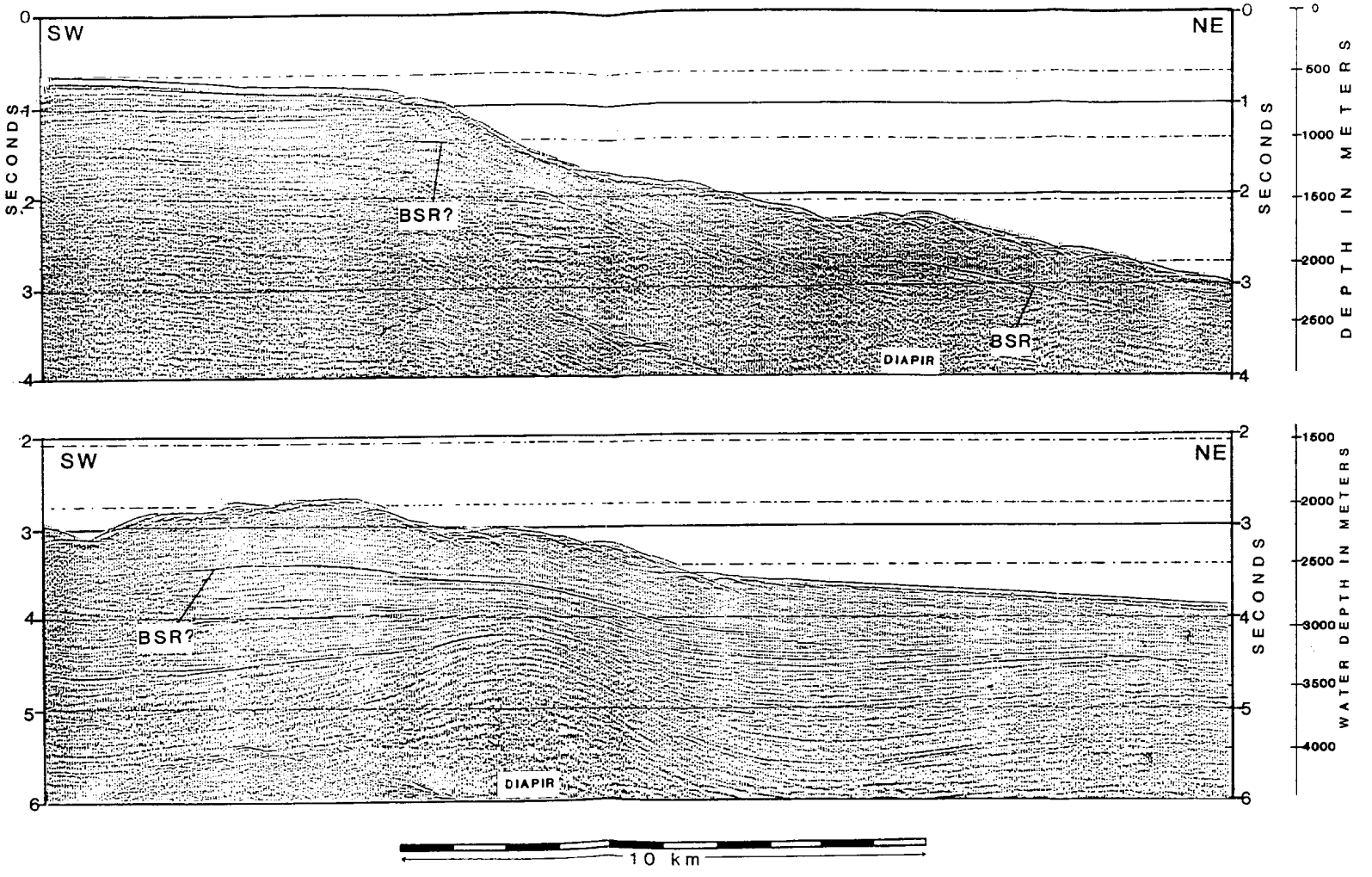

Figure 41. MULTICHANNEL SEISMIC LINE 2742

Figure 42 is in a pocket located inside the back cover.

The BSR continues unabated from the bathymetric high beneath 1,350 m of water through the undeformed sediments of an intraslope basin at 0.52 to 0.54 sec subbottom depth. The BSR is also readily identified over the diapir which served as a dam for the formation of the intraslope basin. Over the diapir at 1,900 m water depth, the BSR is found at a relatively shallow 0.50 sec subbottom. Downslope from the diapir the BSR disappears in the sediments of an intraslope basin before reappearing immediately over another diapir at 2,150 m water depth. The BSR decreases in subbottom depth from 0.48 sec over the southern flank of the diapir to 0.44 sec subbottom beneath the crest of the diapir to 0.49 sec on the north (downslope) flank of the diapir before disappearing into the sedimentary reflectors of a third intraslope basin. The BSR again appears beneath 2,900 m of water on the flanks of a third diapir. The BSR ranges from 0.69 sec subbottom over the seaward flank of the diapir to 0.60 sec over the diapir core.

The section of the BSR on Line 2722 with the highest reflectivity may be underlain by free gas. The most reflective section of the BSR extends from a water depth of 1,390 m to a depth of 1,900 m. This stretch of Line 2722 displays diminished amplitude of sediment reflectors above and enhanced amplitude of reflectors beneath the BSR. Additionally, apparent velocity push down features of sub-BSR reflectors are evident along the 5 km portion of the line with the maximum reflectivity. Reflectors approximately parallel with the overlying BSR are unusually widely spaced. Near the upslope end of the high reflectivity section of the BSR, sedimentary reflectors intersect the BSR at an angle. The relative acoustic transparency of the sediments above the base of the gas hydrate stability zone impedes tracing of the oblique sediment reflectors across the BSR. However, comparison of the orientation of the reflectors below the BSRs with nearby reflectors not masked by amplitude changes suggests that the angle of incidence of parallel reflectors is greater beneath than above the BSR. These velocity push down features suggest the presence of free gas beneath the most reflective portion of the BSR on Line 2722.

The potential of free gas beneath the BSR on Line 2722 is intriguing because the geometry of the BSR does appear to define an effective gas trap. The bold BSR disappears upslope beneath the flank of a bathymetric high. The BSR is most distinct in the sediments of an intraslope basin over which the seafloor is concave upward. If free gas is present beneath the BSR in the intraslope basin it would be expected to migrate upslope along the base of the gas hydrate stability zone to the structurally highest point of the gas hydrate phase boundary due to the buoyancy of the gas bubbles. The gas should thus have pooled beneath the BSR which underlies the bathymetric high immediately upslope from the intraslope basin. A faint BSR can be traced through the bathymetric high, but the highly reflective segment of the BSR with velocity artifacts clearly stops beneath the north flank of the bathymetric high. Close inspection of the point at which the BSR loses its definition beneath the north flank reveals that it coincides with a fault surface. The BSR loses its high reflectivity at its intersection with a southward dipping thrust fault. The fault block of which the bathymetric high is composed has begun to override the autochthonous sediments of the intraslope basin. If the thrust fault can be assumed to have presented a barrier to lateral gas migration beneath the base of the gas hydrate stability zone an explanation of the anomalous location of the highly reflective BSR can be proposed. A combination of a permeability barrier to vertical migration at the base of the gas hydrate stability zone and structural closure by the thrust fault

could have created a trap in which gas could have accumulated sufficiently to have produced the BSR and velocity effects without leakage of gas farther upslope to the anticlinal trap formed by the base of the gas hydrate stability zone, where the accumulation would be expected.

Even if the above suggested trapping mechanism is valid, the possible sub-BSR gas pool may require either unusually effective microbial methanogenesis within the intraslope basin or migration of additional gas from a deeper source. The downslope end of the BSR terminates just downslope of the crest of the first slope diapir. Farther downslope on Line 2722, the only other BSR occurrences are over the flanks or crests of diapirs. Except for the intraslope basin in which the highly reflective BSR is located, the sediments of the continental slope on Line 2722 do not appear to generate sufficient methane for formation of a distinctive BSR except in the immediate proximity of diapirs. The likely accumulation of free gas in a possible trap just upslope of the first slope diapir but not downslope from it is consistent with increased supply of methane to the slope sediments by the diapir.

An underlying diapir could conceivably enhance gas concentrations at the gas hydrate stability zone by at least two separate mechanisms (Finley and Krason, 1986; Krason et al., 1985). Diapirism results in tensional stresses in overlying sediments as evidenced by normal faults commonly identified in seismic sections over diapirs (e.g. Bally, 1983). The extensional faults and fractures over diapirs may increase the permeability of sediments to methane. Thus, in the area of a diapir, methane generated from a thicker section of sediments could be effectively transferred to the gas hydrate stability zone via the fault and fracture system. Additionally, the material in the core of the diapir has been mobilized from depths at which higher geothermal temperatures prevail. It is thus possible that the material coring a diapir may have attained thermal maturity with respect to methane generation even though the intruded country rocks may be immature. The original burial depth of the sediments composing the diapir which appears to have influenced BSR formation on Line 2722 cannot be determined with certainty, but it appears to have been at least 3 sec two-way travel time or about 3,600 m. The depth to thermal maturity on the Beaufort continental shelf ranges from about 3,000 m to 5,000 m (Craig et al., 1985; Dixon et al., 1985; Grantz et al., 1982a). It is possible that the pore fluids of the diapiric core material from the continental slope of Beaufort Sea study region may introduce thermogenic hydrocarbons to shallower immature sediments.

Multichannel seismic line 2725 crosses the Alaskan continental slope obliquely and intersects Line 2722 at an angle of about 45° (Plate 7). Line 2725 and Line 2722 intersect at a water depth of 1,850 m, about 1 km upslope from a diapir (Figure 43). Another diapir is evident on Line 2725 about 10 km downslope from the intersection of the two seismic sections.

A bottom simulating reflector can be traced on Line 2725 for 24 km between water depths of 1,460 and 2,300 m. The BSR begins at the south end of Line 2725 within a bathymetric high which is apparently a slide block displaced from upslope. The BSR is of low reflectivity from the first bathymetric high on Line 2725 through

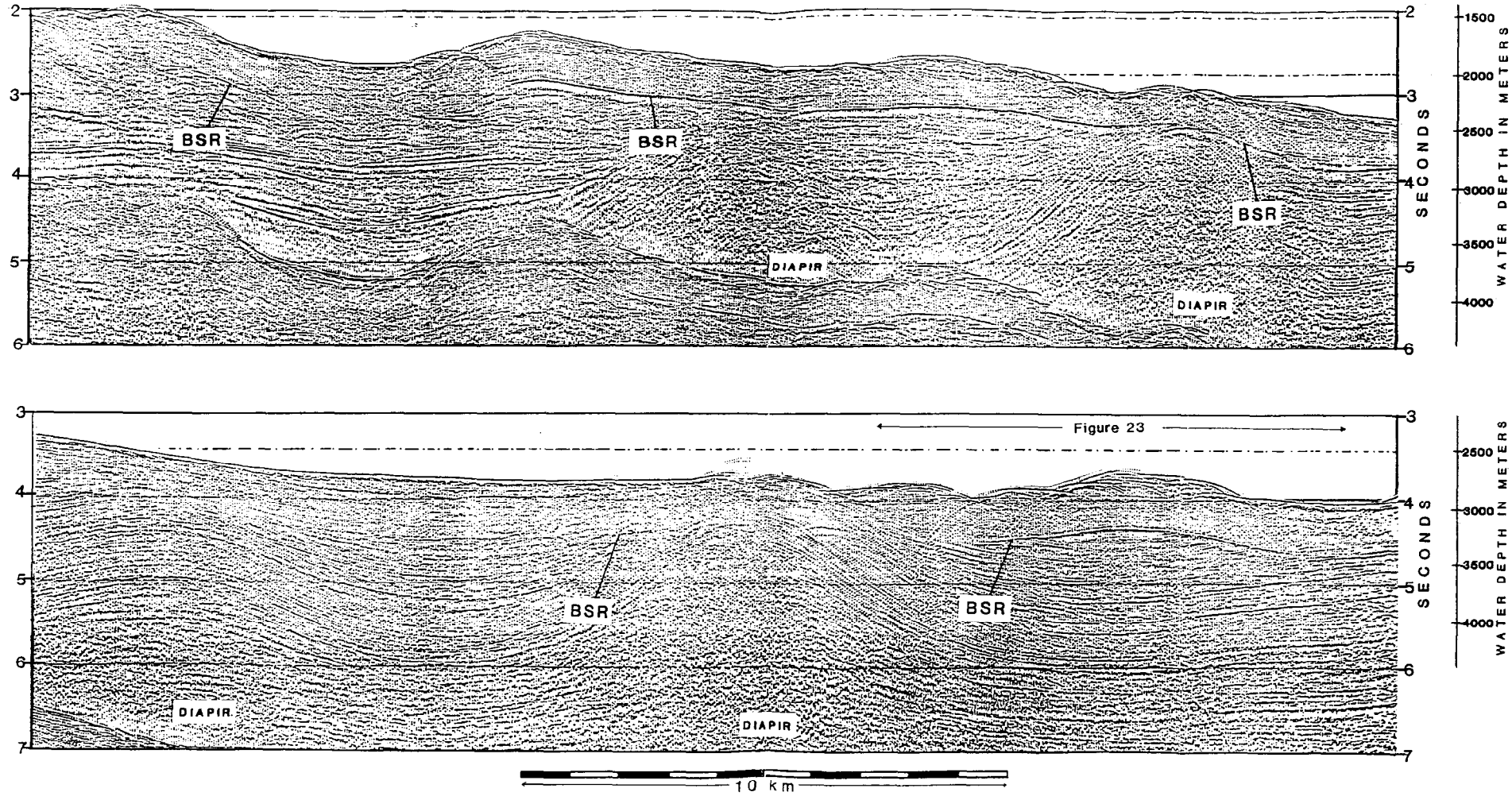

Figure 43. MULTICHANNEL SEISMIC LINE 2725

a small depression on the upper slope. No amplitude or velocity anomalies can be attributed to the BSRs beneath the southernmost bathymetric high on Line 2725

A very highly reflective BSR extends for 16 km from beneath the second bathymetric high from the south end of Line 2725 through a third and a fourth bathymetric high. The particularly bold BSR on Line 2725 overlies two diapirs near the intersection with Line 2722 which can be correlated with some confidence with the BSR-hosting diapirs on Line 2722. As noted on previous lines the diapirs do not always correspond directly with bathymetric highs; low-relief depressions generally directly overlie diapirs on Line 2725. Bathymetric highs are located near the diapirs on Line 2725, but are situated over nearby intraslope basins rather than the cores of the diapirs. The BSRs are most distinct beneath these bathymetric highs adjacent to the diapirs; the BSRs directly over the cores of the diapirs are typically of relatively low reflectivity.

The section of Line 2725 with the particularly bold BSR exhibits amplitude and velocity anomalies, and well defined bright spots (Figure 43). Sediment reflectors are better defined below the BSR than above the BSR. Sediment reflectors beneath the bathymetric highs over the intraslope basins between the diapirs are very widely spaced vertically and show exaggerated dip angles. These features indicate a lower velocity beneath the BSR on Line 2725. An interval 0.10 sec thick below the BSR is completely devoid of any reflection. This bright spot appears to be a manifestation of low seismic velocity, as it consistently occurs in conjunction with the distorted sub-BSR reflectors caused by the velocity push down effects. Notably, the velocity and amplitude features characteristic of the BSR continue about 1 km upslope and downslope of the point at which the BSR itself can no longer be resolved as a distinct reflector.

The BSR occurs at lesser subbottom depths over the diapirs than in the intraslope basins separating the diapirs. On Line 2725 the BSR averages 0.63 m subbottom depth in the intraslope basins, but shoals to subbottom depths of 0.48 over the first diapir and 0.40 over the second (downslope) diapir. These data suggest higher heat flow immediately over the diapirs on Line 2725 than on adjacent areas of the continental slope.

A comparison of Lines 2725 and 2722 near their intersection reinforces the model of BSR development proposed for Line 2722. The BSR upslope of the first diapir on Line 2725 is continuous into the adjoining bathymetric high and is best defined beneath the crest of the bathymetric high (Figure 43). On Line 2722 the BSR continues upslope from the same diapir through the sediments of the intraslope basin but is terminated where it abuts a southward dipping thrust fault. No similar thrust fault exists on Line 2725.

The northeastern terminus of Line 2725 abuts Line 726 about 2 km from the north end of Line 726 (Plate 7). Both lines show a moderately distinct BSR at 0.65 sec subbottom at the intersection. The intersection occurs on a very broad anticlinal fold, possibly cored by a diapir deeper than the limit of seismic resolution. Between the gentle anticline and a diapir 10 km upslope on Line 726, only typical intraslope basin sediments crossed by a very subtle diapir can be identified. However in an analogous position on the lower continental slope on a very close section of Line 2725, one of the best defined BSRs from this part of the Alaskan continental margin is found within the intraslope basin sediments. The BSR is located beneath a

bathymetric high with a sea floor relief of about 150 m. The BSR was used by Grantz et al. (1982b) to exemplify the BSRs of the Beaufort Sea study region. That BSR (Figure 23) shows a distinct contrast between the seismic returns from sediments on either side of the BSR. While it is true that the bathymetric high could have produced a structural trap for gas beneath the hydrate, it is puzzling as to why the BSR should be so well developed locally, Bathymetric highs over adjacent diapirs have only faint BSRs. The bathymetric high with the bold BSR on Line 2725 (Figure 23) is situated over a syncline. Thus, the area from which hydrocarbons collected for trapping beneath the BSR is essentially limited to the area of closure of the trap. Another crossing of this particular unusual bathymetric high would be helpful in assessing the possible migration routes for gases to have become incorporated into gas hydrate within the stability zone and possibly trapped as free gas beneath. If no viable migration pathways exist, the BSR situated directly over an apparently undeformed syncline would suggest that extremely efficient microbial methanogenesis is occurring over a very small area that happens to correspond with this particular bathymetric high.

Multichannel seismic line 3720 is oriented north to south about 17 km east of Line 2722 (Plate 7). Line 3720 depicts the continental slope, continental rise, and abyssal plain north of Barter Island from a water depth of 1,600 m to 3,200 m (Figure 44). The track line map for the 1977 cruise of the *S.P. Lee* (Plate 7) shows that the south end of Line 3720 crosses the western part of a very large bathymetric high on the Alaskan continental slope. The bathymetric high is elongated parallel to the continental slope. It measures about 35 km along the slope and has a sea floor relief of over 300 m. The topography of the continental slope immediately upslope from the large bathymetric high shows evidence of a landward migration of the shelf-slope break. The indentation in the continental slope upslope from the bathymetric high matches the shape of the bathymetric high (Plate 7), suggesting that the bathymetric high consists of a large block of the continental slope or outer continental shelf which has become detached from the continental margin and slid downslope. The slide block on Line 3720 consists of a broad bathymetric high with very poor resolution of sediment layers within and beneath the block. North of the bathymetric high, two diapirs separated by about 10 km and associated intraslope basins are very well resolved. The continental rise and abyssal plain of the Beaufort Sea on Line 3720 are composed of a horizontal, featureless sedimentary section.

A BSR can be traced on Line 3720 for 20 km from the first bathymetric high to the first diapir (Figure 44). The BSR disappears in the intraslope basin separating the two diapirs, but reappears on the south flank of the northern diapir. The BSR continues down the north flank of the deeper diapir into the horizontal sediments of the continental rise. The concordance of the seafloor and the strata beneath 3,000 m water depth precludes detection of BSRs, but amplitude anomalies which may indicate the base of the gas hydrate stability zone appear sporadically beneath the continental slope and abyssal plain to the deepest water surveyed on Line 3720.

The BSR on Line 3720 is most reflective beneath and 8 km downslope from the crest of the bathymetric high on the possible slide block (Figure 44). The

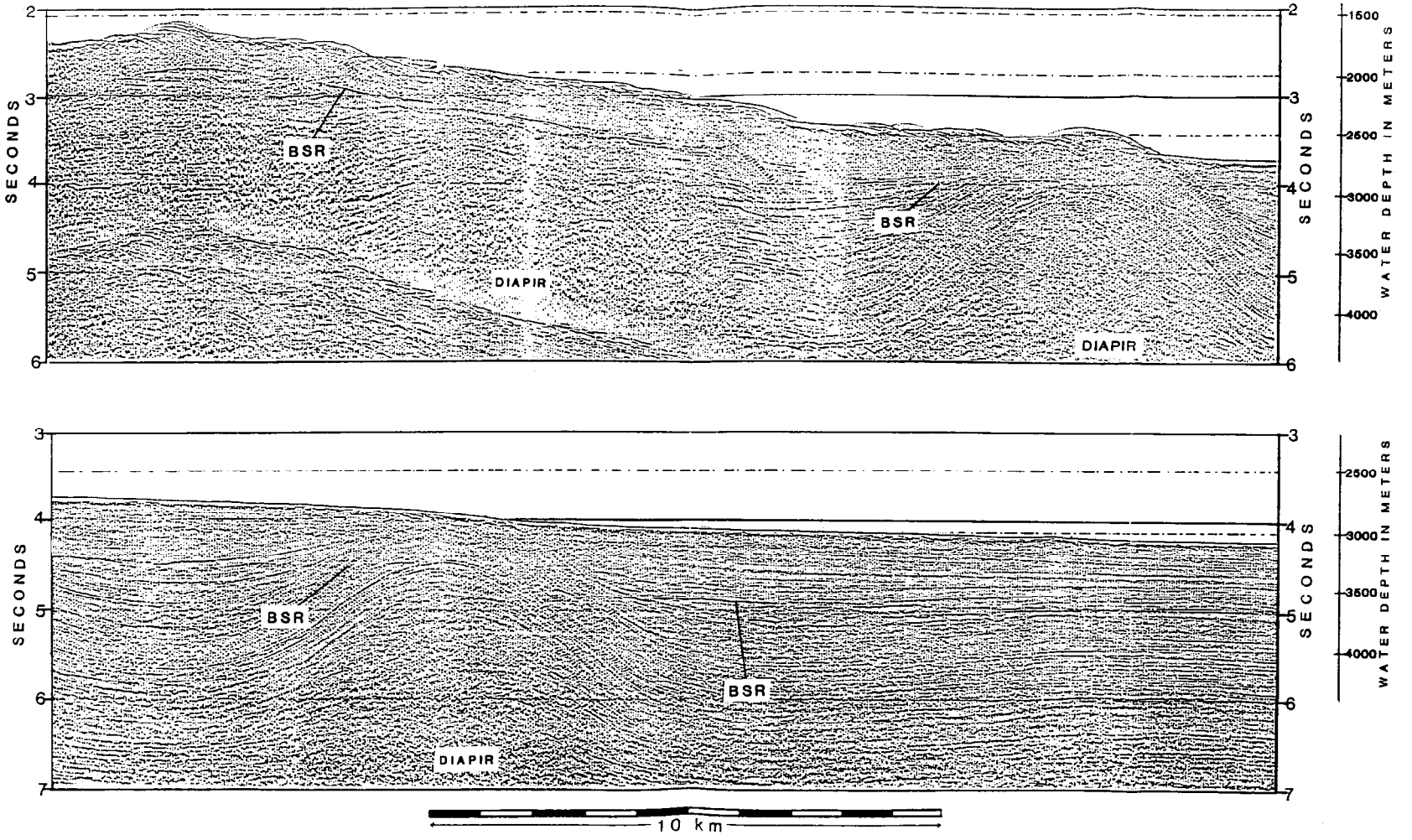

Figure 44. MULTICHANNEL SEISMIC LINE 3720

subbottom depth of the BSR increases from 0.44 sec on the north flank of the bathymetric high to 0.50 sec immediately below the crest before decreasing to 0.40 sec 2 km north of the crest. From there, the BSR increases in subbottom depth to 0.60 sec at the downslope edge of the allochthonous block at 2,250 m water depth. In the autochthonous sediment section upslope from the first diapir, the BSR maintains an average depth of 0.6 sec, but shoals to 0.50 sec over the core of the diapir, before deepening rapidly along the north flank of the diapir to a depth of 0.66 sec in the intraslope basin between diapirs. The subbottom depth of the BSR again diminishes on approaching the second diapir to 0.52 sec over the core of the diapir at a water depth of 2,900 m. On the north flank of the second diapir on Line 3720 the BSR deepens dramatically from 0.52 sec to 0.82 sec in only 3.5 km.

Amplitude anomalies across the BSR are more apparent on Line 3720 than are velocity push down effects. The sedimentary section above the BSR is markedly more acoustically transparent than the underlying section all across the seismic line. The effect is most obvious where the reflectivity of the BSR is the greatest. Minor velocity push down in the form of slightly increased apparent stratal thickness below the BSR can be detected on a few scattered segments of the BSR on Line 3720.

Multichannel seismic line 2725 crosses Line 3720 at a water depth of about 2,780 m (Plate 7). The lines intersect at the intraslope basin separating the two diapirs on Line 3720. Only a faint BSR at 0.66 sec can be resolved on each line at the point of intersection. The diapir downslope from the intersection is well depicted in both lines. The subbottom depth of the BSR over the core of the diapir is slightly greater on Line 3720 (0.52 vs. 0.50 sec). However, the rapid plunge in subbottom depth downslope from the diapir on Line 3720 is not apparent on Line 2725, where the BSR attains a depth of only 0.63 sec about 10 km from where a 0.80 sec subbottom depth was recorded on Line 3720.

Multichannel seismic line 726 is oriented north to south about 20 km east of Line 3720. The outer continental shelf on Line 726 is very flat, sloping gradually to a water depth of 650 m. A very sharp gradient change marks a very recent fault scarp defining the shelf-slope break (Figure 45). Grantz et al. (1983) estimated that about 500 m of vertical movement and 1,000 m of downslope displacement occurred along the northward dipping listric normal fault whose scarp is exposed at the shelf-slope break on Line 726. The depositional stratigraphy of the outer continental shelf is very well preserved within and beneath the down-dropped fault block. The normal fault can be traced clearly through the undisturbed sediment sections and disappears beneath the more chaotic section underlying the major bathymetric high previously discussed in conjunction with Line 3720. Downslope from the bathymetric high, the stratigraphy is again well imaged. Downslope to the end of the line the sediments are composed of simple sequences of diapirs and intraslope basins as on previous lines from this area. The 1 km of horizontal movement along the fault exposed at the shelf-slope break indicates the need for either continued downslope movement of material, or compressional deformation somewhere along the continental slope to balance the space problem. The diapirs beneath the continental slope appear to have buttressed the continental slope from substantial downslope movement. We suggest that the large bathymetric high crossed by Line 726 is a product of the faulting described by Grantz et al. (1983). The contorted stratigraphy

Figure 45 is in a pocket located inside the back cover.

in the bathymetric high compared to the adjacent areas with can be resolved if the bathymetric high is cut by a series of imbricate thrust faults. The elevation of the bathymetric high and its relatively rough topography are consistent with some of the documented movement along the listric normal fault being taken up by thrust sheets ramped along south dipping faults. It is also possible that some of the downslope motion of the fault block dropped from the scarp at the shelf-slope break was also absorbed by deformation of the first slope diapir on Line 726. The first diapir visible on Line 726 beneath a water depth of 2,120 is distinctly asymmetrical, with a more steeply dipping north flank. The other three diapirs on Line 726 and indeed all other previously discussed diapirs from the Beaufort Sea study region are consistently symmetrical in dip of the north and south limbs of the intruded country rock.

A BSR can be traced along parts of the outer continental shelf and below widely separated segments of the continental slope (Figure 45). A reflector with enhanced amplitude can be traced for 6 km landward of the shelf-slope break. The possible gas hydrate BSR maintains a subbottom depth of 0.40 to 0.42 sec beneath water 580 to 650 m deep. The BSR cannot be detected in the relatively undisturbed portion of the down-dropped block seaward of the shelf-slope break. The BSR reappears in the sediments of the bathymetric high which we have interpreted as a thrust-faulted terrane or the toe of a large slump-slide complex. The BSR over the bathymetric high ranges in subbottom depth from 0.42 sec to 0.50 sec over its 12 km extent. Bright spots about 0.10 sec thick are found beneath the BSR under the bathymetric high at 1,460 m water depth. Some velocity push down of sediment reflectors beneath the BSR is indicated, but the complex stratigraphic relationships within the possibly thrust faulted terrane makes the assignment of changes in reflector dips and spacing to velocity differences across the BSR tentative at best. The BSR becomes indistinct seaward of the thrust faulted bathymetric high and reappears about 24 km downslope. On crossing a lower slope diapir a BSR can be traced for about 4 km under water from 2,400 to 2,850 m deep. The the diapir causes a rapid decrease in the subbottom depth of the BSR from 0.60 sec subbottom at 1 km on either side of the axis of the diapiric uplift to 0.40 sec over the core.

Multichannel seismic line 718 crosses the Alaskan continental margin parallel to and 20 km east of Line 726 (Plate 7). The margin depicted in Line 718 differs from the previously described examples in that diapirs can be identified beneath the continental shelf and upper continental slope rather than just beneath the lower continental slope or continental rise (Figure 46).

Bottom simulating reflector can be traced on Line 718 for 30 km between 580 m and 1,900 m water depth and for another 30 km between water depths of 2,500 m and 2,900 m (Figure 46). A very strong reflector parallel to the very gently sloping outer continental shelf (termed the "Beaufort Ramp" by Grantz et al., 1981) is visible from water depth of about 580 m to the shelf-slope break marked by an exposed fault scarp at 800 m. The reflector is concordant with the shelf sediments and thus is not readily identified as the base of the gas hydrate stability zone. However, at the shelf-slope break, the rapid change in slope gradient at the exposed scarp is mimicked by the BSR which clearly cuts across the bedding planes it had paralleled farther upslope. The landward limit of the strong reflector is not well defined; The same reflector could conceivably be interpreted to continue to the

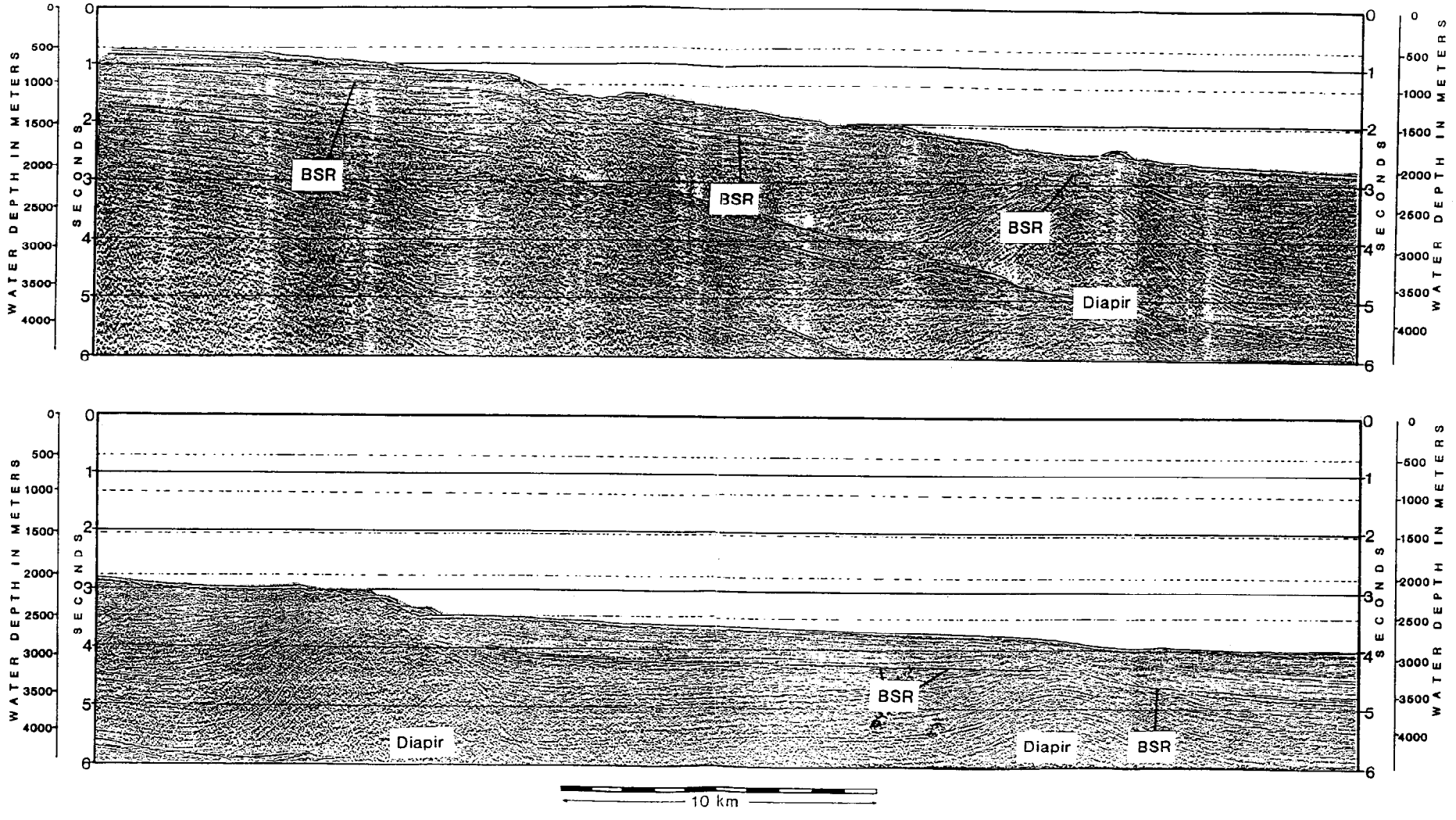

Figure 46. MULTICHANNEL SEISMIC LINE 718

south an additional 10 km to water as shallow as 300 m. However we prefer the more conservative interpretation of continuing the BSR shoreward only as far as continuity with the discordant reflector at the shelf-slope break can be conclusively demonstrated. The BSR maintains a subbottom depth of 0.31 to 0.39 sec between 580 and 1,000 m water depth

The BSR shoals somewhat in the disturbed sediments near the shelf-slope break then deepens downslope in the sediments of intraslope basin (Figure 46). The hummocky topography of the seafloor and the lack of a laminated veneer of sediments over a 2 km interval immediately downslope from the shelf-slope break indicates relatively recent movement. In spite of its probable youth this interval is underlain by a distinct BSR. The BSR is identified at a substantially lesser subbottom depth than that beneath adjacent undisturbed sections. The subbottom depth decreases from 0.39 sec at the shelf-slope break to 0.30 in the disrupted sediments before increasing rapidly in depth to 0.46 sec downslope. The BSR becomes indistinct in the sediments of the intraslope basin before reappearing as an upper slope diapir is approached. The BSR again decreases in subbottom depth in proximity to the diapir at 1680 m water depth. The BSR changes in subbottom depth from 0.41 to 0.46 sec in the intraslope basin upslope from the diapir to 0.36 sec in the upslope flank, to 0.30 sec immediately above the core, and finally deepens to 0.40 sec on the downslope flank of the diapir.

The disappearance of the BSR in the sediments of the north flank of the diapir at 1,900 m water depth initiates a 20 km interval on Line 718 with no obvious BSRs (Figure 46). This hiatus of BSR expression on the continental slope occurs in a geological setting much like that in which vivid BSRs are developed on Line 718 and along many adjacent lines of the Alaskan continental margin east of Prudhoe Bay. A diapir with adjacent intraslope basins is recorded on Line 718 between water depths of 1,980 m and 2,700 m. The diapir appears to be more recently mobile and to have intruded closer to the sea floor than the other diapirs on Line 718. The diapir at 2,200 m water depth also has a topographic expression at the sea floor with an apparent north dipping normal fault coincident with intrusive contact of the diapir and the country rock along the north flank of the diapir. The scarp of this probable fault exhibits over 300 m of relief and is exposed at the sea floor directly over the core of the diapir. Only one reflector could possibly be interpreted as a gas hydrate horizon in this 20 km stretch of the continental slope around the diapir. That reflector crosses the trace of the normal fault on the north flank of the diapir at a subbottom depth of 0.42 sec. The possible BSR can be traced for less than 0.5 km making its assignment as a gas hydrate reflector problematic. Except for this one possible exception, the lack of BSRs in this setting which based on adjacent seismic lines would seem to be an ideal setting for a BSR is puzzling. This example suggests that simple models of BSR formation over diapirs and in nearby intraslope basins have only limited applicability.

The next diapir encountered downslope on Line 718 under water 200 m deep shows little surface expression (Figure 46). The sediments over the diapir are gently arched over the core. Well defined sediment horizons indicate that the depth of the core of the diapir is at least 3 sec subbottom, much greater than the other diapirs on Line 718. A highly reflective BSR can be traced for over 20 km through the sediments arched over the deep diapiric core and into the sediments of the adjoining intraslope basins. The BSR is a very short wavelength, high amplitude reflector

which produces a very sharp and well defined horizon which is clearly discordant with bedding planes, even when the angles of intersection of the sediment and hydrate boundary are small. The sediment reflectors beneath the extensive BSR are substantially enhanced in amplitude relative to reflectors above the base of the gas hydrate stability zone. Some degree of velocity push down is evident beneath the BSR. However, no appreciable difference in the angles on incidence of sediment reflectors across the BSR due to velocity change is seen. Although the core of the diapir is very deep, the subbottom depth of the hydrate diminishes over the diapir in a manner similar to that seen over shallower diapirs. The diapir decreases in subbottom depth from 0.60 sec in the intraslope basin to the south (upslope) of the diapir to 0.50 sec immediately over the diapir. Downslope from the diapir the BSR deepens quickly to 0.64 sec 1.5 km from the core, to 0.73 sec within 5 km. The seaward limit of the BSR on Line 718 is somewhat arbitrary. The parallel strata and sea floor beneath the continental rise preclude picking a distinct hydrate horizon, but minor amplitude changes at 0.74 to 0.80 sec subbottom persists to the north end of the section.

Multichannel seismic line 730 was shot about 15 km east of and parallel to Line 718 (Plate 7). Line 730 covers only the continental shelf and upper continental slope; the line ends at a water depth of 1,460 m. The structure and stratigraphy of the continental margin on Line 730 is similar that on Line 718. The shelf-slope break on Line 730 is characterized by downslope movement on many separate faults, rather than along one principal fault as in Line 718. No diapirs are visible on Line 730.

A BSR exists on Line 730 beneath water depths greater than 500 m. The BSR maintains a subbottom depth of 0.32 sec to a water depth of 950 m. The BSR is only 0.23 sec beneath the sea floor for about 4 km downslope from a small fault scarp. At a water depth of 1,320 m the BSR quickly deepens in the sediment to 0.42 sec at the maximum water depth surveyed of 1,460 m.

Multichannel seismic lines 1716, 2716, and 3716 strike due north and are located 16 km east of line 730 and 27 km east of Line 718. The full continental margin is surveyed by Lines 1716, 2716, 3716, and 4716 to a water depth of about 2,800 m. Five continental slope and rise diapirs are depicted on these lines (Figure 47).

Bottom simulating reflectors are present for at least 44 km on Line 1716 and the entire 22 km of Line 2716 (Figure 47). A strong reflector which appears to cut across sediment reflectors can be traced for 5 km on Line 3716 (Figure 47). Although BSRs were visible in outer continental shelf sediments south of the shelf-slope break on Lines 718 and 730, none are evident on Line 1716 beneath water shallower than 1,280 m. The BSR on Line 1716 begins abruptly within the down-thrown block north of the fault scarp defining the shelf-slope break at 0.35 sec subbottom. The BSR continues to the north within sediments of a small basin of ponded sediments dammed against a diapir beneath 1,600 m of water. The BSR maintain a subbottom depth of 0.40 to 0.50 within the small basin with the greater depths occurring beneath a small bathymetric high. Over the diapir, the BSR

Figure 47 is in a pocket located inside the back cover.

becomes much shallower (0.30 sec) before rapidly increasing to 0.48 sec in the intraslope basin bordering the diapir to the north. Additional diapirs on Line 1716 have a similar effect on BSR depth. Two diapirs at water depths of 1,980 m and 2,100 m are underlain by BSRs at 0.42 sec subbottom, but the BSR is found at depths of as much as 0.54 sec in the intervening basin. The BSR on Line 1716 is very distinct between water depths of 1,320 and 1,680 m. Along this interval, minor velocity push down features are evident beneath the BSR. The highest reflectivity of the BSR occurs beneath the broad bathymetric high at 1,430 m water depth.

The BSR visible for the full length of Line 2716 crosses two diapiric uplifts separated by just 8 km (Figure 47). The BSR clearly cuts across beading planes on the flanks of the diapirs. The subbottom depth of the BSR changes from 0.48 sec over the diapir at 2,500 m water depth to 0.70 sec in a small basin just 3.2 km downslope from the crest of the diapiric upwarp. From that point the BSR shoals to 0.42 sec over the second diapir just 4.8 km from the center of the small intraslope basin. Within 5 km downslope of the second diapir the BSR has increased in depth to 0.82 sec.

Multichannel seismic line 732 covers the outer continental shelf and 7 km of the upper continental slope 18 km east of Line 1716 (Plate 7, Figure 48). The shelf-slope break on Line 732 is marked by a 150 m high fault scarp. Hummocky topography characterizes the sea floor of the upper continental slope from the shelf-slope break at 720 m to the north end of the line at 1,500 m.

A very strong BSR occurs on Line 732 water depths of 560 m to 1,500m (Figure 48). The particularly distinct BSR averages 0.42 sec beneath the sea floor within the horizontally stratified sediments south of the shelf-slope break. The BSR continues to be easily distinguished among the chaotic reflectors of the upper continental slope on Line 732. Just north of he seafloor exposure of the principal fault marking the shelf-slope break the BSR is only 0.24 sec beneath the seafloor. The subbottom depth of the BSR increases regularly to 0.38 sec at the north end of Line 732.

Multichannel seismic line 714 is the easternmost line of the 1977 survey aboard the *S.P. Lee* (Plate 7). Line 714 is located along the seaward extension of the US-Canadian border. Up to 10 separate diapirs are crossed by Line 714.

A distinct BSR occurs for 30 km on Line 714 from a water depth of 900 m to 2,000 m. The BSR becomes visible beneath a bathymetric high composed of a probable fault block bounded to the north and south by north-dipping listric normal faults. Velocity push-down of sediment reflectors beneath the BSR in the bathymetric high suggests the presence of free gas. Downslope from the bathymetric high the BSR diminished in reflectivity for a 5 km interval. The BSR becomes much more prominent for about 4 km directly over a diapir whose core remains at least 1.3 sec beneath the BSR The BSR diminishes in amplitude downslope of the diapir, but can be picked from sediment reflectors in the intraslope basin between diapirs. The BSR shoals about 0.10 subbottom and becomes much more distinct upon approaching another, larger diapir beneath 1,900 m of water. Beneath water deeper than 2,000 m on Line 714, BSR occurrence is sporadic. Distinct BSRs can be resolved only for 2 to 4 km over the crests of the lower slope diapirs. The BSR

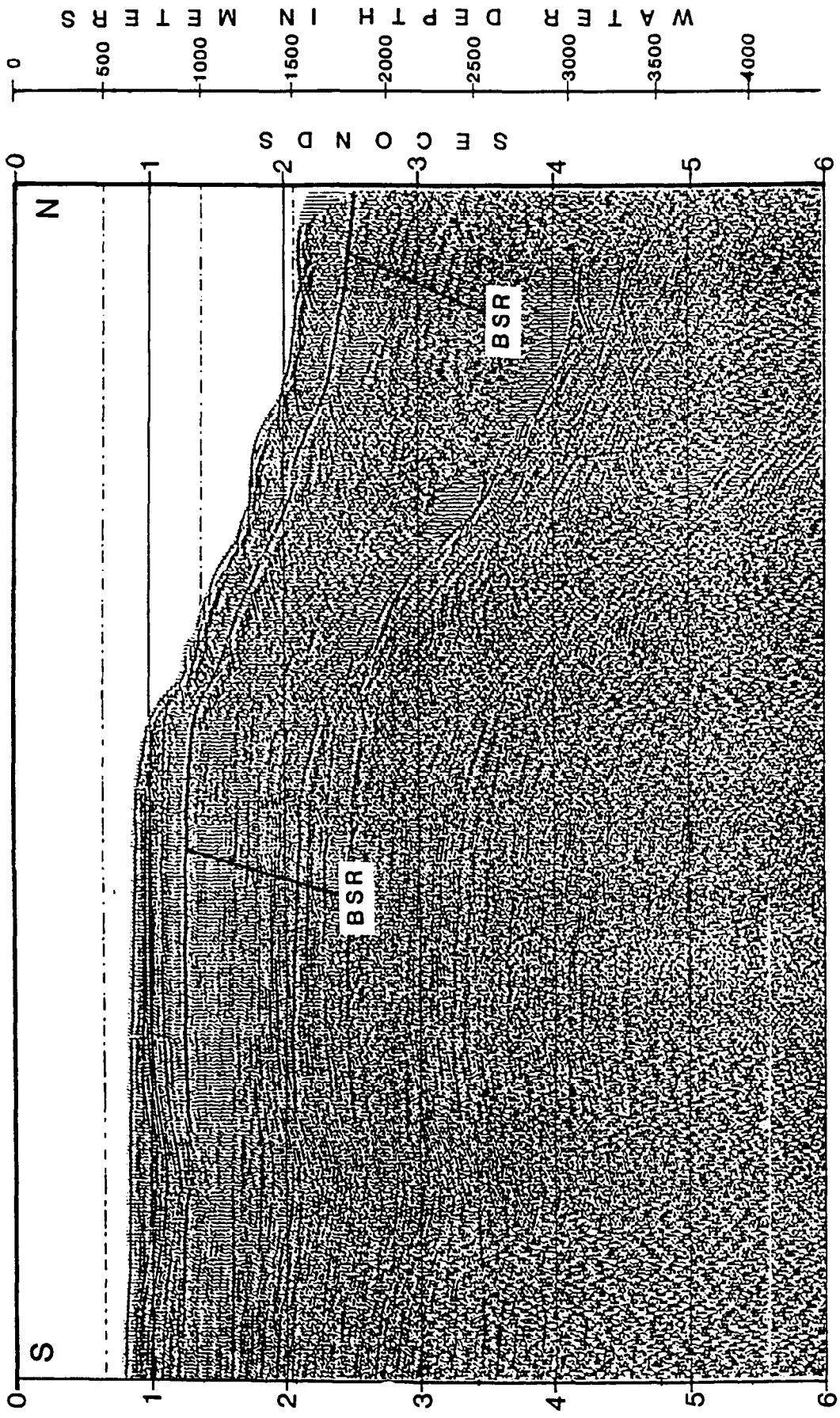

Figure 48. MULTICHANNEL SEISMIC LINE 732

cannot be resolved in the sediments of the small basins separating the five lower slope diapirs.

Gas Hydrate Stability Model

We have modeled the gas hydrate stability zone of the Beaufort Sea study region using empirical pressure and temperature relationships from published laboratory studies. A series of computer programs has been developed by us to calculate the thickness and depth of the gas hydrate stability zone is sediments for different combinations of water depth, water temperature, geothermal gradients, pressure gradients, and pore water salinity. Previous versions of the gas hydrate stability model have been applied to determining the possible areal and vertical extent of gas hydrate occurrences in other gas hydrate study regions (Ciesnik and Krason, 1987; Finley and Krason, 1986a, Finley and Krason, 1986b; Finley et al., 1987; Krason and Rudloff, 1986; Krason et al., 1985, 1986). The model has since been thoroughly revised. The abundance of seismic evidence of gas hydrates makes the Beaufort Sea study region an ideal location to apply the model to test its validity and to further examine gas hydrate formation and stability factors.

Model Design

The model of gas hydrate stability model calculates in situ conditions of pressure and temperature. These calculated values are then compared with gas hydrate stability relationships derived from laboratory data. Equations of gas hydrate stability were derived from dissociation data published by Holder and Johns in Kuuskraa et al. (1983) for methane hydrate and hydrates of various representative thermogenic gas mixtures. The gas hydrate stability at the calculated in-situ pressures and temperatures determined using the logarithmic relationship suggested by Holder:

$$\ln(P) = a + b/K$$

where P represents dissociation pressure, K is formation temperature in Kelvin, and a and b are empirically derived constants. The constants were obtained by least squares curve fitting methods applied to the reported laboratory data. The derived equations were modified using the data provided by Deaton and Frost (1949). The form of the equation quoted above was found to be inadequate to describe the more complex behavior of thermogenic gas hydrates; a method of numerically approximating thermogenic gas hydrate stability was developed to more accurately duplicate laboratory findings.

The model functions by calculating the in situ pressure and temperature for each one meter interval sediment depth. The calculated parameters are compared with the stability fields defined by the empirical equations. The comparison of calculated values and predicted stability conditions indicates whether the one meter sediment interval is above, within, or beneath the gas hydrate stability zone. Once the determination of whether the sediment is within the hydrate stability field is made, the sediment depth is incremented and the procedure is repeated. This primary routine is nested within loops which vary the water depth, geothermal

gradients, and other physical and geological parameters which effect the depth of the gas hydrate stability zone in the sediments.

This exhaustive algorithm for determining the gas hydrate stability conditions of offshore sediments makes inefficient use of computational resources, but may approximate the actual in situ conditions better than more conventional approaches. A very straightforward method of determining the subbottom depth of the base of the gas hydrate stability zone in sediment is to calculate the pressure and temperature at the sea floor, and then to calculate the subbottom depth at which the hydrate dissociates by dividing the temperature rise needed to cause dissociation by the geothermal gradient. One obvious pitfall of this approach is caused by higher confining pressure deep in the sediments tending to stabilize gas hydrates while the increasing temperature is destabilizing hydrates. Calculations on the subbottom depth of the gas hydrate phase boundary performed using sea floor pressure and temperature conditions are inadequate because the greater stability afforded by pressure increasing with depth is not accounted for.

Another problem with the simpler method of determining gas hydrate stability is that it precludes the possibility that gas hydrates may be unstable at the seafloor but become stable deeper in the sediment section. Under conditions of shallow ocean depths and low geothermal gradients, the proportional increase in pressure with each meter of increased sediment depth is greater than the proportional increase in temperature. Thus the stabilizing effect of increasing pressure may overwhelm the destabilizing effect of increasing temperature, and gas hydrates could conceivably become stable at greater depth. The model used in these studies allows for such a possibility. Initial findings that the gas hydrate stability zone may exist at depth in the sediment even though hydrates are not stable at the sea floor were previously presented for the offshore Labrador study region (Krason et al., 1986) and the Colombia Basin study region (Finley et al., 1987).

A graphical method for estimating the thickness and subbottom depth of the gas hydrate stability zone was presented by Kvenvolden and McMenamin (1980), among others. Their method involved replotting the standard pressure and temperature gas hydrate phase diagram by converting the pressure axis to water and sediment depth assuming hydrostatic conditions. The depth and temperature of the sea floor is plotted on the diagram. A line describing subbottom conditions is drawn from the point representing sea floor conditions in the direction of greater temperature and depth. The slope of the line is determined by the geothermal gradient of the area. The depth of the point at which the line indicating subbottom pressure and temperature conditions intersects the gas hydrate phase boundary represents the depth of the base of the gas hydrate stability zone. The thickness of the gas hydrate stability zone can be obtained by subtracting the seafloor depth from the total depth value obtained from the diagram. This method does produce a good first order estimation of gas hydrate stability conditions. However, it is rather inflexible; modifications to account for variations in pressure gradients, bottom temperature, salinity, etc. are not easily accomplished.

The currently used model was first developed and tested in 1985. The model was written in BASIC2 language on a DEC PDP-11/44 computer. The program was translated to Microsoft BASIC for use with MS-DOS microcomputers in 1986. The stability model was rewritten and optimized in 1987 using the Borland International

TurboBASIC compiler. Modifications incorporated into the latest version of the model permit the effect of different combinations of geological parameters to be easily investigated.

A potential weakness of the current version of the gas hydrate stability model may be its direct application of laboratory-derived gas hydrate stability data. The experiments from which the stability data were obtained involved formation and dissociation of gas hydrates produced under conditions of great excess of gas. The formation of usable quantities of gas hydrates in reasonable amounts of time dictates using excess quantities of hydrocarbon gas in laboratory studies. However, a review of the gas hydrate literature by Finley and Krason (1986b) indicated that gas hydrates could form in sediments at much lower concentrations of methane than those used in laboratory studies. The formation of gas hydrates from relatively dilute solutions of hydrocarbon gas in pore water may occur at higher pressures and/or lower temperatures than the often cited empirical data derived in conditions of great excesses of free hydrocarbon gas. Thus, models using the accepted values of gas hydrate stability derived from laboratory studies (e.g. Deaton and Frost, 1949; Holder in Kuuskraa et al., 1983) may overestimate the thickness of the gas hydrate stability zone in sediments where the concentration of hydrocarbon gases in the pore water is sufficient for gas hydrate formation, but not in excess. However, dissociation conditions of samples of the massive gas hydrate recovered from DSDP Site 570 offshore of Guatemala closely matched those predicted by the laboratory studies of Deaton and Frost (1949) indicating that these empirical laboratory data may be appropriate for estimating stability of at least massive gas hydrates in geological settings (Kvenvolden et al., 1984). However, Finley and Krason (1986b, 1988b) and Mathews and von Huene (1985) have reported that the massive gas hydrate at Site 570 was probably formed from locally high concentrations of methane migrating along a fault zone, suggesting that the data from the massive gas hydrates may not be representative of interstitial gas hydrates.

Another possible inadequacy in the computer model of gas hydrate stability results from the uncertainties as to whether the empirical equations used to estimate gas hydrate stability are applicable to hydrates formed in contact with sediments. Some hydrate workers (e.g. Makogon, 1974; Weaver and Stewart, 1982) have indicated that the presence of a porous medium such as typical continental margin sediments destabilizes gas hydrates. Based on these observations, the use of laboratory data to derive in situ gas hydrate stability parameters may produce erroneous results. The work of Kvenvolden et al. (1984) does not directly bear on this concern, since the gas hydrate samples tested were not in direct contact with the mineral matrix due to their massive habit. Work by Makogon (1974) appears to indicate that gas hydrate forms in sediments at pressure and temperatures conditions identical to those in laboratory simulations until the pore spaces become clogged by the hydrates sufficiently to block access of methane to the loci of gas hydrate formation. The work of Makogon (1974) is not sufficiently quantitative or well documented to apply in our model. While a number of workers (e.g. Hunter et al, 1983) indicate that fine grained matrix inhibits gas hydrate formation, the presence of clay minerals derived from volcanic ash deposits was projected by Krason et al., (1985) and Finley and Krason (1986b) to possibly have catalytically enhanced formation of gas hydrate in the Gulf of Mexico and the Middle American Trench study regions. In the absence of any definitive data on the possible stabilizing or destabilizing effects of

the mineral matrix on gas hydrate stability, the laboratory data of Holder (in Kuuskraa et al., 1983) and Deaton and Frost (1949) provides the closest reliable approximation of stability factors in situ conditions.

Predicted Stability Conditions

Assigning reasonable values for water temperature and geothermal gradient give initial estimates for the thickness of the gas hydrate stability zone in the Beaufort Sea study region. Typical water temperatures of the Beaufort Sea vary with season and depth (Coachman and Aagaard, 1974). A baseline bottom water temperature of 0°C was selected for preliminary modeling of gas hydrate stability in the study region. The few exploratory drill holes on the Beaufort continental shelf for which thermal information has been made public indicate that geothermal gradients range from 2.7 to 3.2°C/100 m (Craig et al., 1985; Weaver and Stewart, 1982). A geothermal gradient of 3°C/100 m was selected for initial modeling.

Results for initial modeling of the subbottom depth of the base of the gas hydrate stability zone are illustrated in Figure 49. With a geothermal gradient of 3°C/100 m and bottom water at 0°C, methane hydrate is stable beneath water 210 m deep. The model predicts that the gas hydrate stability zone increases regularly with thickness from 2 m at 210 m of water depth to 650 m beneath 200 m of water.

Gas Composition

Modeling the expected subbottom depth of the base of the gas hydrate stability zone for thermogenic gas hydrates is problematic because the stability field of the hydrate depends on the composition of the thermogenic gas. Increasing concentrations of ethane and heavier hydrocarbons in the gas stabilizes the resultant hydrate (Deaton and Frost, 1949). Very few data on the composition of thermogenic gas from the Beaufort Sea study region are available. In all probability thermogenic gas composition varies widely throughout the study area due to local conditions of source type and maturity, migration distances, and subsequent alteration. Thus it is difficult to project what the "typical" Beaufort Sea thermogenic gas mixture might contain. In the absence of reliable data on gas composition, we have selected a standard gas mixture which may approximate thermogenic gases which have migrated to the gas hydrate stability zone of the Beaufort Sea. Holder and Johns (in Kuuskraa, et al., 1983) presented detailed dissociation data on the hydrate of a hydrocarbon gas mixture which is a reasonable approximation of a thermogenic natural gas. The composition of the gas is: 90.6% methane, 6.6% ethane, 1.8% propane, 0.5% isobutane, and 0.5% n-butane. Although we do not claim that the dissociation properties of this mixture duplicates the behavior of thermogenic gas hydrates in the Beaufort Sea study region, differences between the hydrate stability of the modeled thermogenic mixture and that of methane indicate qualitatively the variability in the thickness and extent of the gas hydrate stability zone in the region due to gas composition.

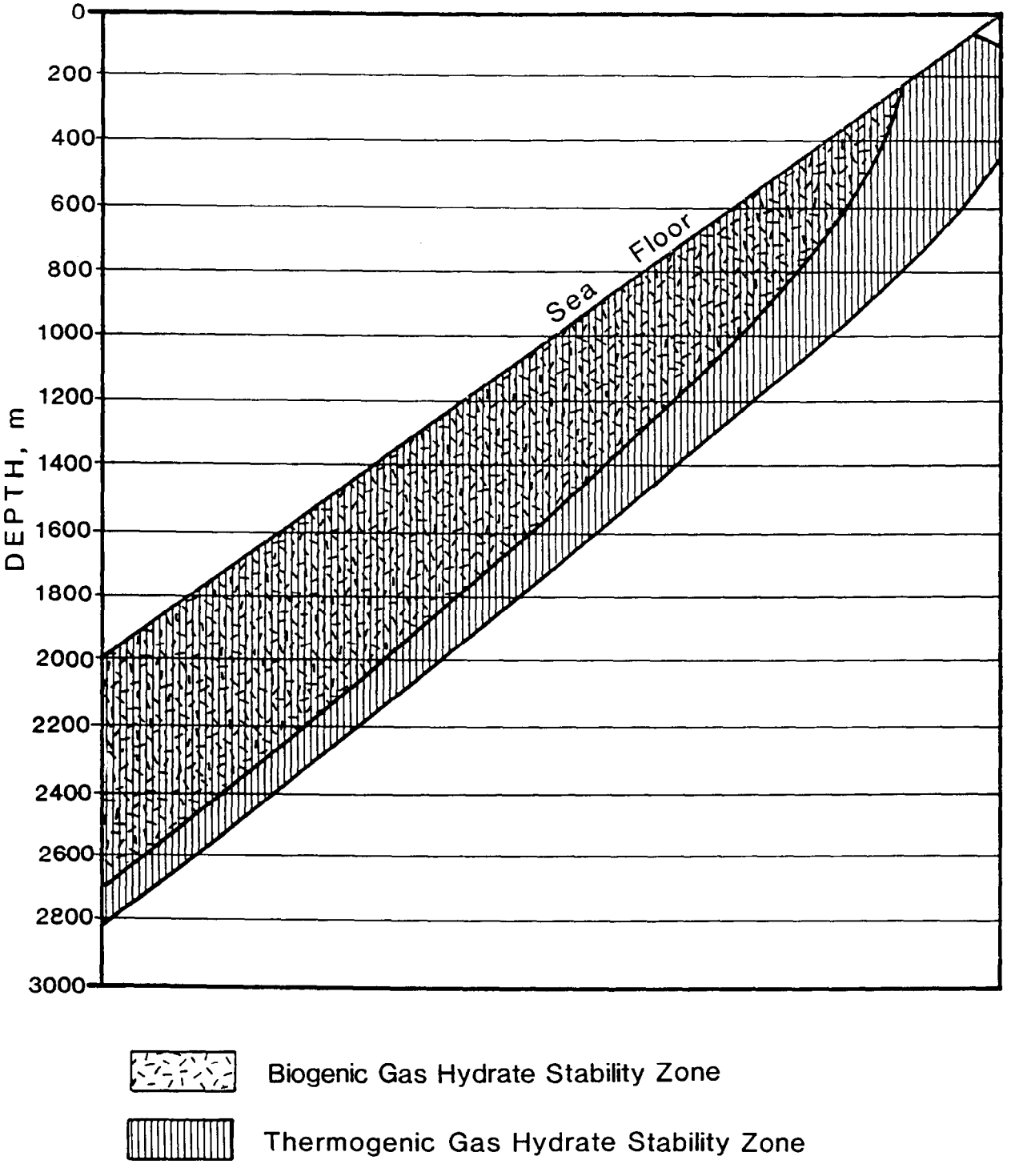

HYDROSTATIC PRESSURE GRADIENT, BOTTOM WATER TEMPERATURE- 0°C

Figure 49. CALCULATED GAS HYDRATE STABILITY ZONE THICKNESS

The thermogenic gas hydrate stability zone is thicker and extends much further landward than the methane hydrate stability zone under identical conditions of bottom water temperature, geothermal gradient, and geostatic gradient (Figure 49). The difference in the thickness of the methane hydrate and thermogenic hydrate stability zones is greater at shallower water depths. Whereas at a water depth of 2,000 m the thermogenic gas hydrate stability zone is only 120 m, or 16% thicker than the methane hydrate stability zone, at a water depth of 400 m the thermogenic stability zone is 300 m or 100% thicker than that for the methane hydrate. Methane hydrate is unstable in sediments beneath water less than 215 m deep. However, at a water depth of 100 m the thermogenic gas hydrate stability zone is 550 m thick. According to the model output illustrated in Figure 49, the thermogenic gas hydrate stability zone continues landward to at least the shore assuming 0°C sea floor and land surface temperatures and 3°C/100 m geothermal gradient.

The thermogenic stability diagram depicted in Figure 49 illustrates the situation discussed in previous paragraphs of gas hydrates not being stable at the sea floor surface, but being stable at depth in the sediment. According to the model output, thermogenic gas of the stated composition can form a hydrate at the sea floor surface beneath water depths of greater than 60 m. However at the shoreline, gas hydrates are unstable at the sea floor surface due to insufficient confining pressure, but are stable at subsurface depths of 70 m to 420 m.

The reason for the smaller difference in thickness of the gas hydrate stability zones for biogenic gas and the representative thermogenic gas at greater water depths becomes apparent upon inspection of the gas hydrate phase diagram (Figure 50). When plotted on a linear temperature axis and a logarithmic pressure axis as in Figure 50, the line separating the methane hydrate and free gas fields is very nearly linear. Least squares fitting of the experimental data for methane hydrate formation gives a Pearsons rho value (r) of 0.9987 indicating a very close approximation to a straight line. However the phase diagram of the selected thermogenic gas is decidedly non-linear and does not parallel the phase boundary of methane hydrate. Figure 50 shows that at low temperatures (e.g. 5°C) the difference in the dissociation pressures of methane hydrate and thermogenic hydrate is large. However, at higher temperatures (e.g. 25°C) the difference in dissociation pressure is much less. This non linearity and lack of parallelism between the phase boundaries of methane hydrate and thermogenic hydrate is manifested in the modeled depths to the base of the gas hydrate stability zone. The pressure at the base of the gas hydrate stability zone increases with the depth of the overlying water column (Figure 51). Beneath shallow water the low confining pressure of the water column requires that the base of the gas hydrate stability zone occur at relatively low temperatures. The difference in the depth to the base of the gas hydrate stability zone beneath shallow water is thus large because the low-temperature portion of the gas hydrate phase boundary applies. Conversely, beneath deep water the much higher confining pressures can stabilize gas hydrates at higher temperatures. Beneath the deeper waters the thickness of the gas hydrate stability zones for methane hydrate and thermogenic hydrate are much closer because the higher temperatures at the base of the gas hydrate stability zone correspond to the high-temperature region on the gas hydrate phase diagram where the stabilities of methane hydrate and thermogenic hydrate are similar.

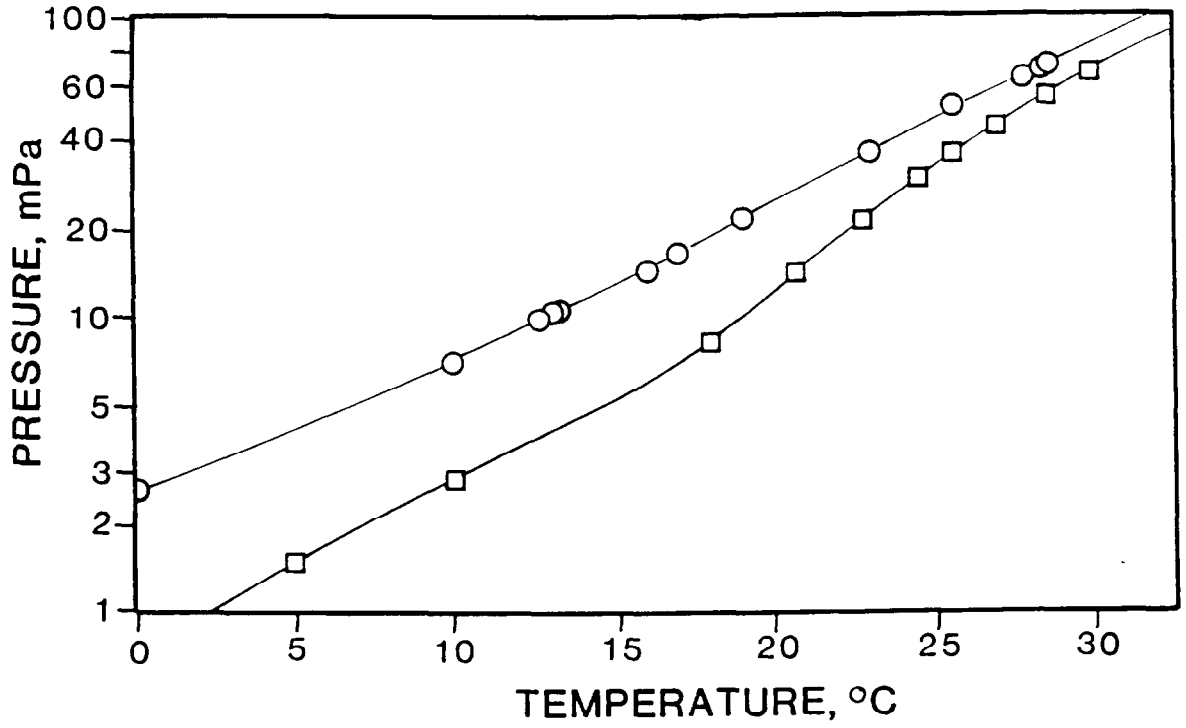

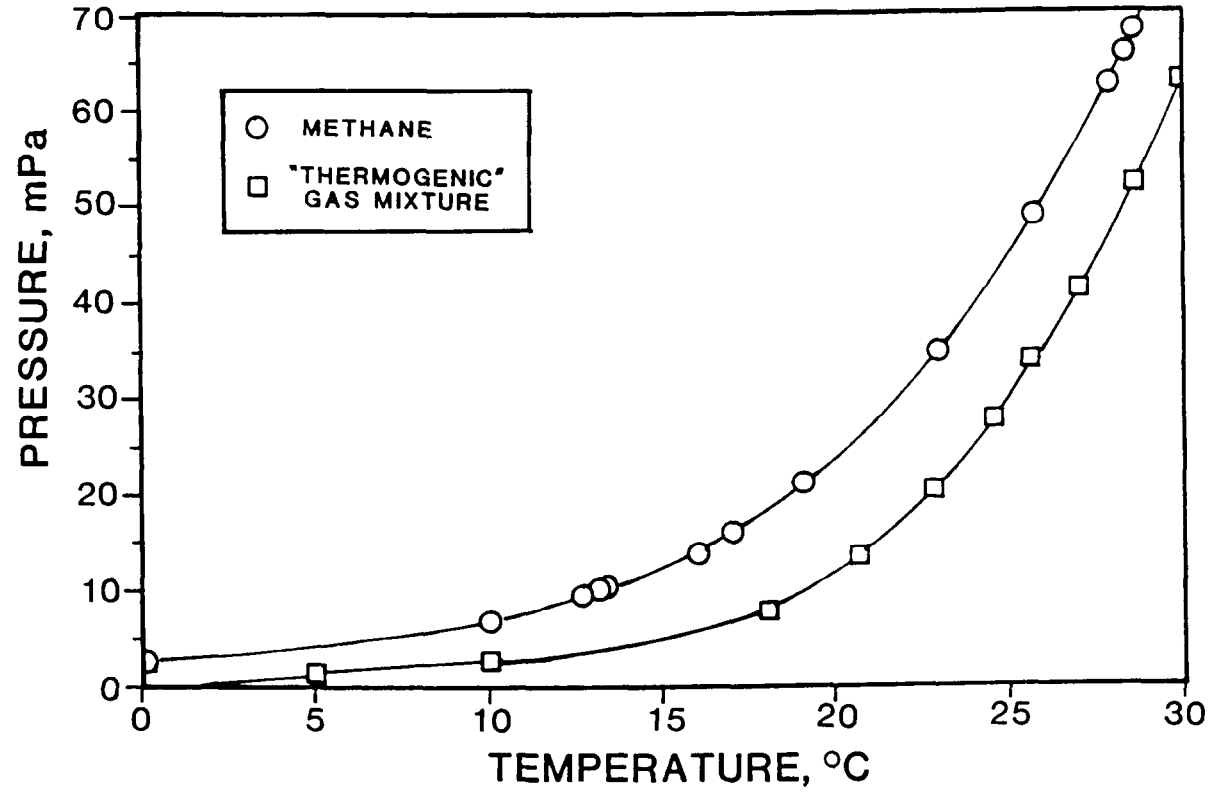

Figure 50. GAS HYDRATE DISSOCIATION CONDITIONS

Data from Kuuskraa et al, 1983

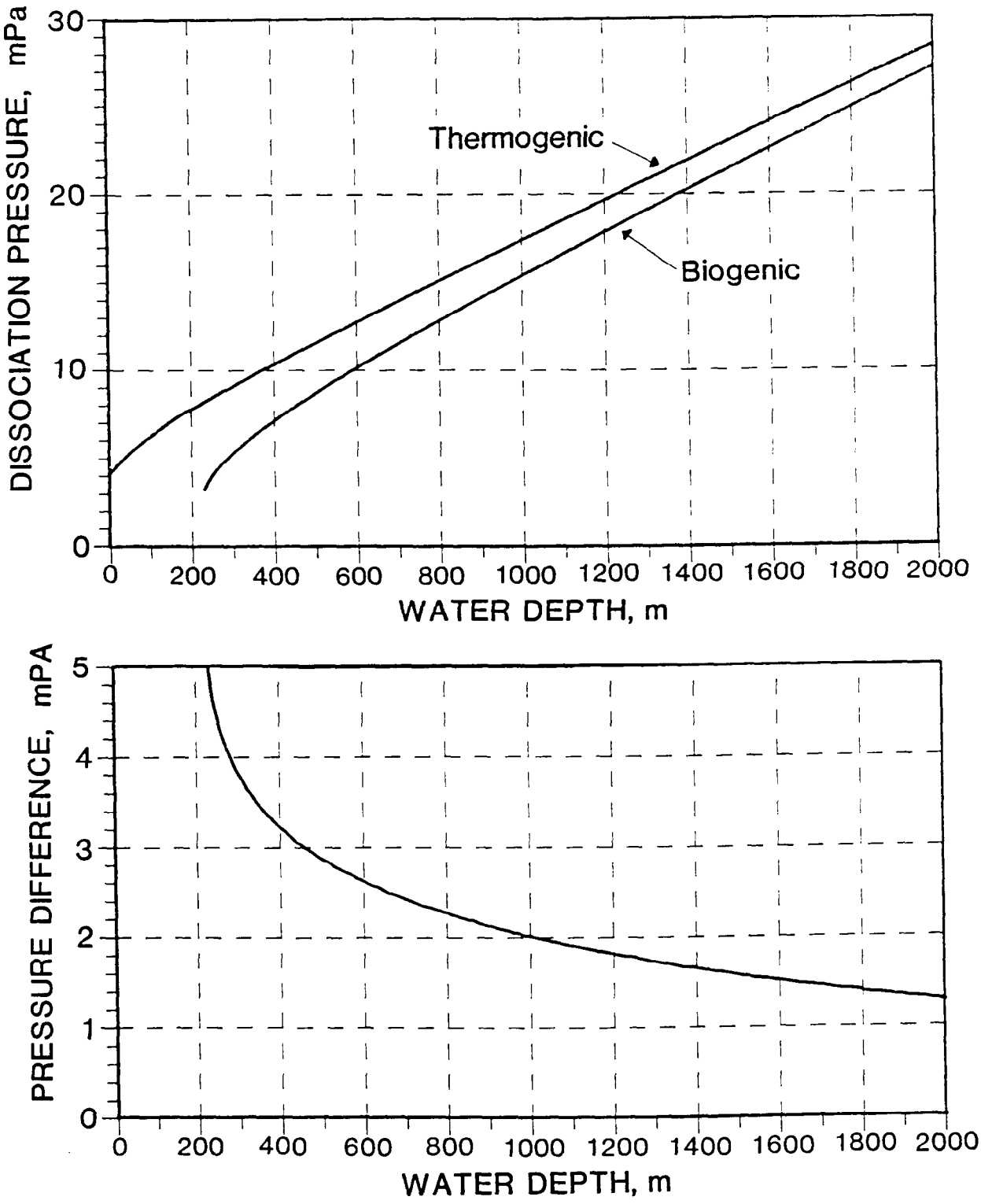

Figure 51. CALCULATED DISSOCIATION PRESSURES OF BIOGENIC AND THERMOGENIC GAS HYDRATES

Hydrostatic Pressure Gradients, Bottom Water Temperature =0°C

Water Temperature

The design of the gas hydrate stability model permits the investigation of the effect of different bottom water temperatures on gas hydrate formation and stability. Figure 52 shows the result of modeling gas hydrate stability conditions using the water temperature data for the Beaufort Sea (Figure 53) presented by Aagard (1974). The results are generally similar to those obtained using a constant bottom water temperature of 0°C, differing only at depths where the measured temperatures diverge significantly from 0°C.

At water depths of less than 350 m the thickness of the gas hydrate stability zone is greater for the actual temperature model than for the fixed temperature model. The temperature data of Coachman and Aagaard (1974) for depths of less than 350 m is below 0°C. The colder bottom water temperatures in this depth range increases gas hydrate stability at depth and at the sea floor. The minimum amount of water required to stabilize gas hydrates at the sea floor is diminished from 230 m to 180 m for methane hydrates and from 80 m to 60 m for thermogenic hydrates (Figures 49 and 52). Increased stability at depth results in an increase of the thickness of the thermogenic gas hydrate stability zone from 630 m to 740 m at a water depth of 100 m.

Between water depths of 350 and 950 m the temperatures measured by Coachman and Aagaard (1974) range from 0° to 0.75°C (Figure 53). The modeled thickness of the gas hydrate stability zone is less in this depth interval using the measured temperatures (Figure 52) than that obtained by assuming a constant bottom water temperature of 0°C (Figure 49). At 600 m water depth the gas hydrate stability zone for methane hydrate decreases from 410 to 390 m. The thermogenic gas hydrate stability zone decreases from 670 to 640 m at 600 m water depth due to application of measured temperatures.

At water depths of greater than about 950 m the water temperatures reported by Coachman and Aagaard (1974) increase from 0°C to about 0.4°C (Figure 53). The corresponding change in the thickness of the gas hydrate stability zone is small. At 2,000 m water depth, the biogenic gas hydrate stability zone increases in thickness about 15 m while the thermogenic gas hydrate stability zone increases about 20 m relative to the thickness predicted for a bottom water temperature of 0°C (Figure 52).

In summary, the effect of using the measured bottom water temperatures from the Beaufort Sea when modeling the thickness of the gas hydrate stability zone is most noticeable at water depths of less than 350 m. Lesser divergence of the measured temperatures from 0°C limits the change in gas hydrate stability zone thickness in sediments beneath water deeper than 350 m. The assumptions used in deriving the gas hydrate stability zone thickness values may be violated beneath water depths of less than about 100 m. Subaerial exposure of the Beaufort continental shelf during the Pleistocene due to a eustatic sea level drop of at least 100 m created periglacial conditions on the present continental shelf resulting in the formation of permafrost. Thermal calculations by Lachenbruch et al. (1982) demonstrated that the thermal perturbations caused by the permafrost beneath the shelf should still be evident. Thus, the actual geothermal gradient of the previously

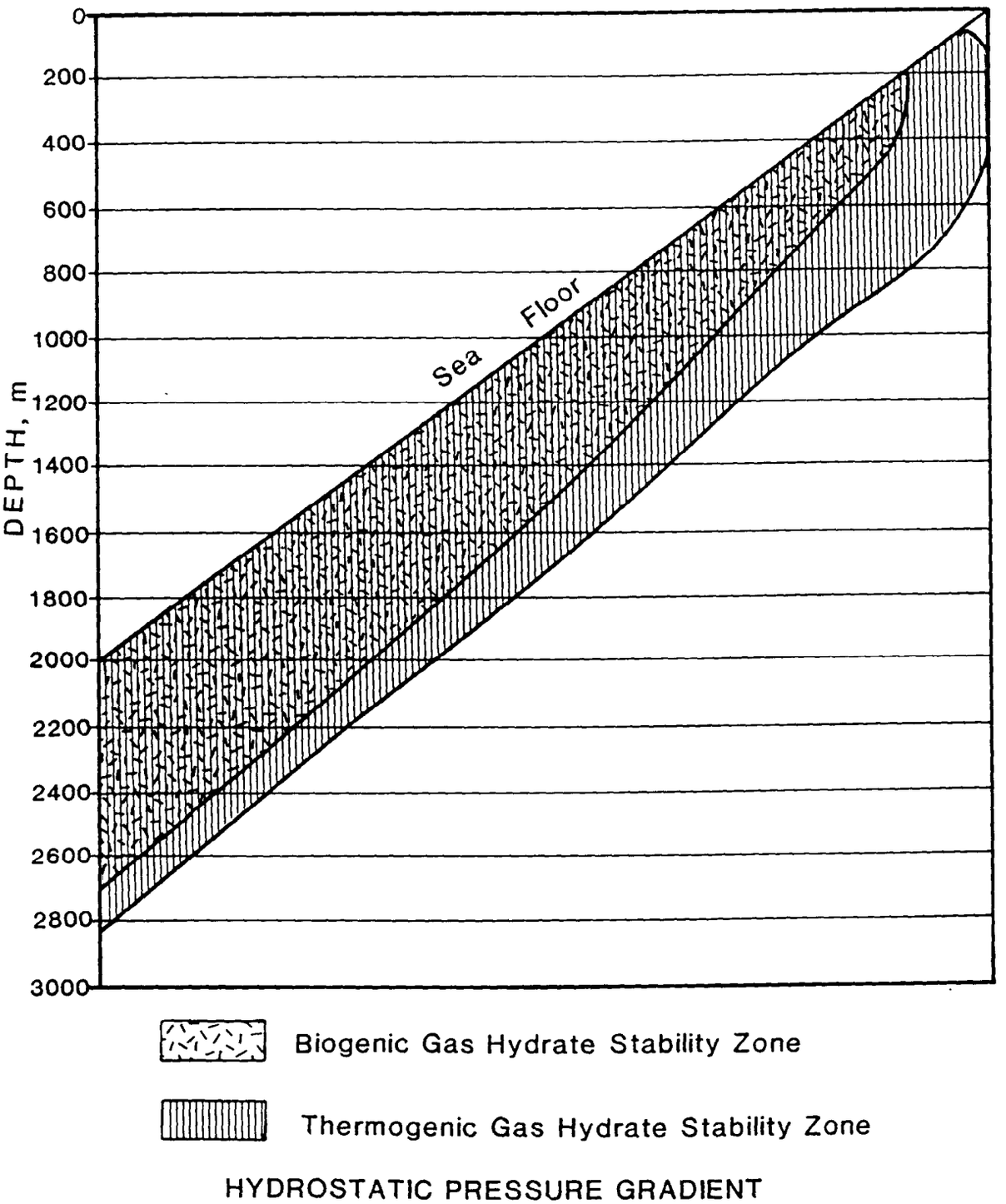

Figure 52. GAS HYDRATE STABILITY ZONE THICKNESS CALCULATED FROM MEASURED BOTTOM WATER TEMPERATURES

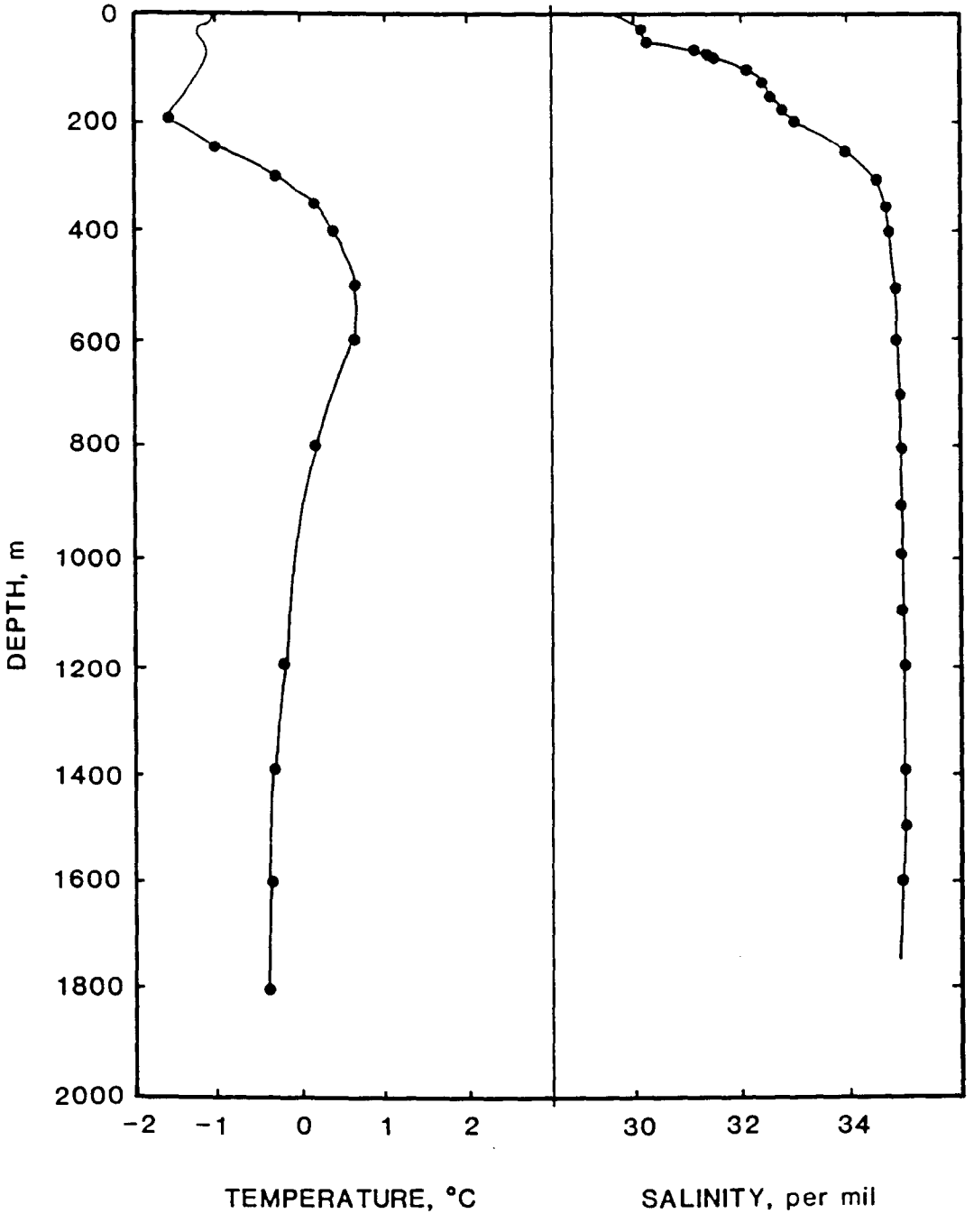

Figure 53. TEMPERATURE AND SALINITY PROFILES OF THE BEAUFORT SEA

After Aagaard, 1982

exposed shelf is projected to be nearly 0°C/100 m to a sediment depth of 300 to 800 m. If the projections of Lachenbruch et al. (1982) are correct the thickness of the gas hydrate stability zone and the subbottom depth to the base of the zone in the sediments of the inner continental shelf of the Beaufort Sea study region would be much greater than derived from the present model which assumed a constant geothermal gradient of 3°C/100 m for the entire sediment section. The effects of possible relict permafrost on the gas hydrate stability zone is discussed explicitly in a later section of this report.

Geothermal Gradients

The effect of different geothermal gradients on the thickness and depth of the gas hydrate stability zone is illustrated in Figure 54. Higher geothermal gradients destabilize gas hydrates and thus result in a thinner gas hydrate stability zone. The magnitude of the thinning of the gas hydrate stability zone for a given increase in the geothermal gradient is less at higher geothermal gradients (Figure 54). The change from 2°C/100 m to 3°C/100 m reduces the methane hydrate stability zone from 700 m to 390 m thickness at a water depth of 600 m assuming the bottom water temperatures reported by Coachman and Aagaard (1974). A geothermal gradient of 4°C/100 m yields a gas hydrate stability zone thickness of 250 m beneath 600 m of water. The diminution of the gas hydrate stability zone upon going from a geothermal gradient of 3°C/100 m to 4°C/100 m is only 45% of that between 2°C/100 m and 3°C/100 m.

The minimum water depth at which gas hydrates are stabilized at the seafloor is not affected by varying geothermal gradients (Figure 54). The stability of gas hydrate at the seafloor is dependent only on the depth of the seafloor, which determines the pressure, and the bottom water temperature. Variations in geothermal gradients effect only temperatures of the sediments beneath the seafloor and thus can affect the stability of gas hydrates only at depth within the sediment column

Lower geothermal gradients increase the likelihood that gas hydrates exist at depth in the sediments at water depths that are too shallow to stabilize hydrates at the seafloor. As reported previously for the Offshore Labrador and Newfoundland study region (Krason et al., 1986) the methane hydrate stability zone in sediments can extend landward of the water depth at which hydrates become unstable at the seafloor under conditions of low geothermal gradients and low bottom water temperatures. Figure 54 demonstrates that under measured Beaufort Sea temperature conditions (Coachman and Aagaard, 1974) the minimum water depth for methane hydrate stability is 185 m for geothermal gradients of 3°C/100 m or more. At 2°C/100 m, however, hydrates are stable at a sediment depth of 280 m beneath water depths of about 120 m, even though hydrates are not stable at the seafloor at water depths of less than 185 m.

Pressure Gradients

Different pressure gradients, expressed as a fraction or multiple of hydrostatic, can be input to the gas hydrate stability model. In the absence of direct

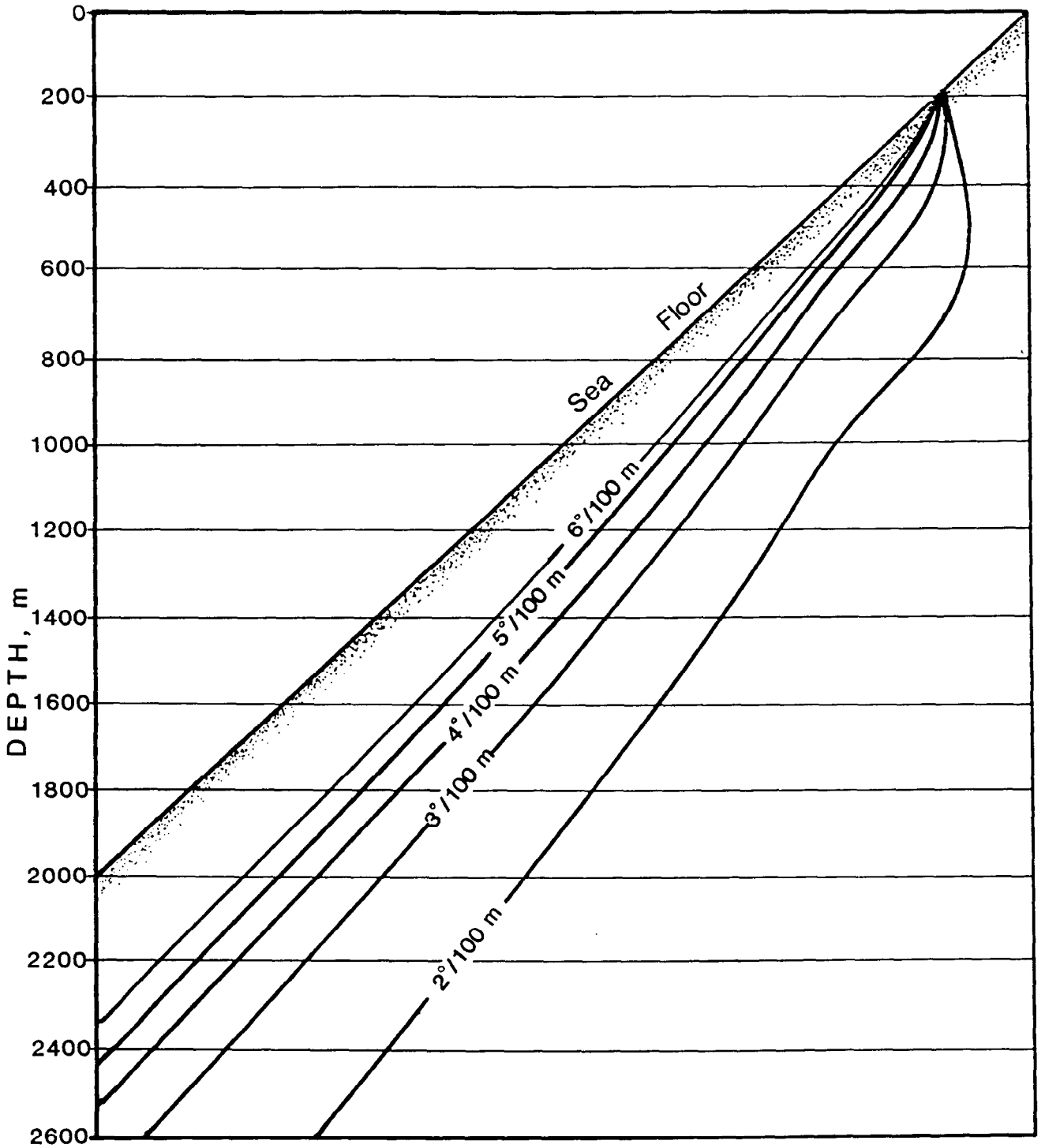

Figure 54. EFFECT OF GEOTHERMAL GRADIENT ON BASE OF GAS HYDRATE STABILITY ZONE

evidence to the contrary, gas hydrate stability in sediments is calculated assuming a hydrostatic pressure gradient. The default hydrostatic gradient used in our program is 10.045 kPa/m which approximates the gradient due to water with salinity approximating that of sea water at 0°C. Provisions exist in the gas hydrate stability model for determining the hydrostatic pressure at the seafloor using measured values of ocean water temperature and salinity when such data are available. The model can also incorporate pressure values measured from drill holes. Since reliable information on water temperature and salinity and on subsurface pressure gradients are rarely available for the deep water frontier regions being studied for gas hydrate potential, the program permits assigning of reasonable pressure gradients to the water column of the sediment section.

Weaver and Stewart (1982) documented overpressured zones in sediments of the Beaufort continental shelf in the Mackenzie Delta. Weaver and Stewart (1982) presented formation pore pressure gradient data for four exploratory wells each with a substantial thickness of subsea permafrost. In three of the wells, the permafrost section was under hydrostatic pressure. Overpressure began at the base of the permafrost zone and increased with depth. On two of the wells, the pressure gradient stabilized at 600 to 800 m at 130% to 140% of hydrostatic. On a third well the gradients had increased to 140% of hydrostatic at 800 m beneath the base of the permafrost, but had not stabilized at the greatest reported depth. The fourth well described by Weaver and Stewart (1982) had pressures of up to 155% of hydrostatic within the permafrost zone. The overpressured zone extended 400 m beneath the base of the permafrost zone whereupon the pressure returned to approximately hydrostatic.

No comparable data are available on the pressure gradients in sediments of the Beaufort continental slope, continental rise, or the Alaskan continental shelf. The abundance of mass wasting on the continental slope and rise of the western portion of the Beaufort Sea study region suggests elevated pore pressures in the sediments near the failure surfaces (Hubbert and Rubey, 1959). The abundance of shale diapirs beneath the continental slope and rise of the eastern part of the Beaufort Sea study region similarly indicate possible overpressured zones according to the mechanisms of shale diapirism proposed by Hedberg (1980).

In the absence of data on possible overpressure in the areas of the study region with the most seismic evidence of gas hydrates, the gas hydrate stability model can be applied to determine the effect of possible pressure variations beneath the continental slope and rise. To limit the interference of other factors which could affect the thickness of the has hydrate stability zone, simulations made for various pressure gradients assumed conditions of biogenic gas, non-saline pore water, and a constant geothermal gradient of 3°C/100 m. The results of the simulation are summarized in Figure 55.

Increasing the pressure gradient in sediments above hydrostatic increases the in-situ pressure at any given depth. At higher pressures gas hydrates are stable at higher temperatures (Figure 50). Thus, gas hydrates are stable at greater subbottom depths at pressure gradients higher than hydrostatic at a fixed geothermal gradient (Figure 55).

The change in the thickness of the gas hydrate stability zone due to varying the pressure gradient is greatest at shallow water depths (Figure 55). At water

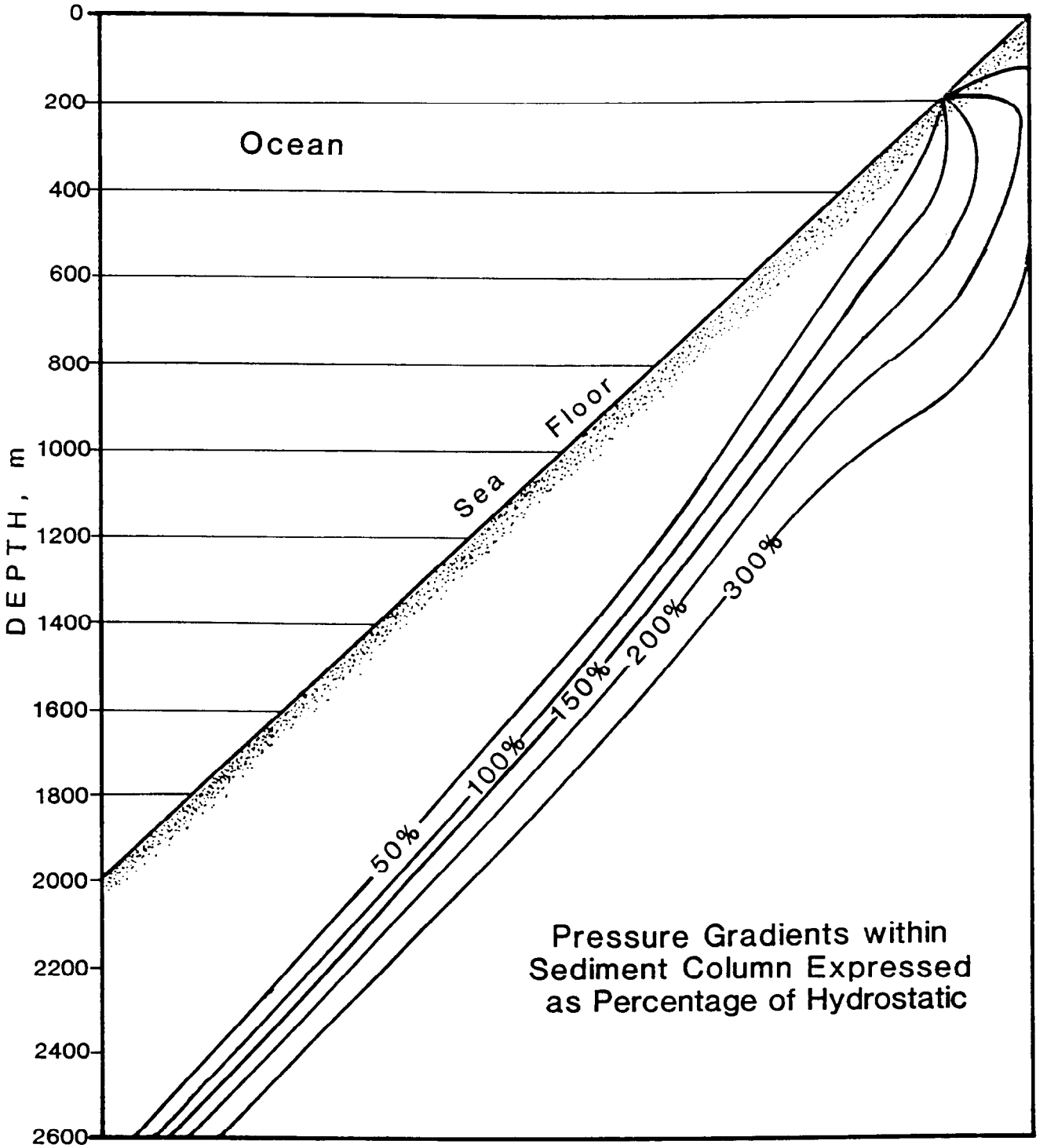

MEASURED BEAUFORT SEA BOTTOM WATER TEMPERATURES (Figure 53)
GEOTHERMAL GRADIENT= 3° C/100 m

Figure 55. EFFECT OF PRESSURE GRADIENT ON BASE OF GAS HYDRATE STABILITY ZONE

depths of 300 m, doubling the pressure gradient effectively doubles the thickness of the gas hydrate stability zone from 250 m to 500 m. At a water depth of 1,500 m, however, the thickness of the gas hydrate stability zone increases by only 15% from 670 m to 770 m in response to doubling the pressure gradient. Comparison of the diagrams illustrating the effect on the gas hydrate stability zone of geothermal gradients (Figure 54) and pressure gradients (Figure 55) shows that while the effects of varying pressure gradients is most obvious at shallow water depths, changes in geothermal gradients is most pronounced beneath deeper water

Pore Water Salinity

Higher pressures or lower temperatures are required to form and stabilize gas hydrates when dissolved electrolytes are present (Deaton and Frost, 1949). The destabilization of gas hydrates by dissolved electrolytes is analogous to freezing-point depression water due to the presence of ionic constituents. Salinity of pore water affects the thickness of the gas hydrate stability zone; the higher pressure and lower temperatures conditions required for saline pore waters indicate that the gas hydrate stability zone will be thinner than that for fresh pore water. The program that we have used to calculate gas hydrate stability conditions can be used to estimate the amount of change in the gas hydrate stability zone caused by pore water salinity.

Published investigations differ in the quantitative effect of salts on gas hydrate stability. A graph showing the depression of gas hydrate formation temperature as a function of salt concentration was constructed by Scott and reported by Kuuskraa et al. (1983). The graph indicates a temperature depression of 0.4°C for hydrate formation from water with NaCl concentrations approximating the total salinity of sea water. Conversely, a graph by the Gas research Institute, also reproduced by Kuuskraa et al. (1983) indicates that the gas hydrate formation temperature is depressed by about 1.0°C by a similar salt concentration.

We have modeled the effects of pore water salinity on the thickness of gas hydrate stability zone of the Beaufort Sea study region. Results for water with salinity approximating that of sea water are presented in Figure 56. Computations were performed assuming both the 0.4°C dissociation temperature change proposed by Scott and the 1.0°C change suggested by the Gas Research Institute. The results of the model computations for the 1.0° C dissociation temperature change scenario are diagrammed in Figure 56. While the effect of differing salinities can be substantial beneath shallow water, little change in the expected gas hydrate stability zone thickness is found at greater water depths.

Application of the Gas Hydrate Stability Model

The gas hydrate stability model which we have developed provides a powerful and flexible tool to investigate local and regional conditions under which gas hydrates may be expected. The stability of gas hydrates in deep sea sediments, and thus the thickness of the gas hydrate stability zone, is dependent on the combination of ocean water temperature and salinity, pore water salinity, geothermal gradients, and pressure gradients existing at a particular location. With the exception of a

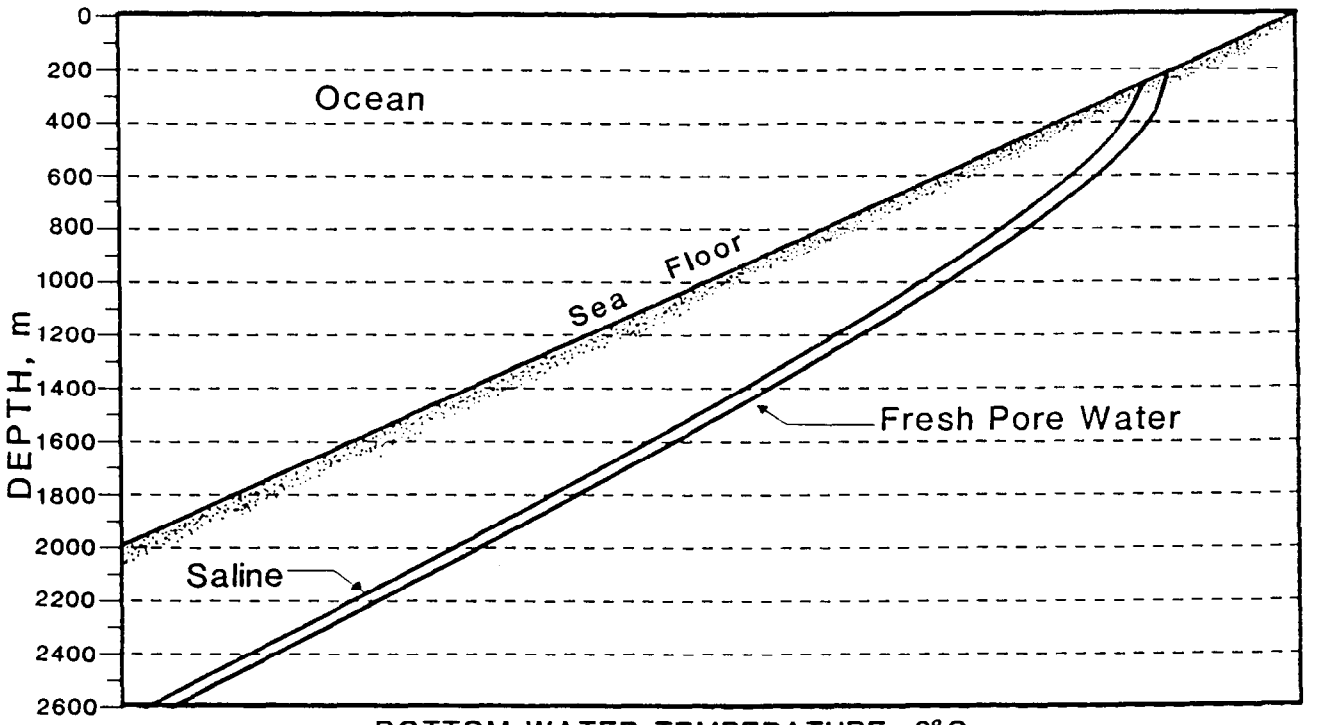

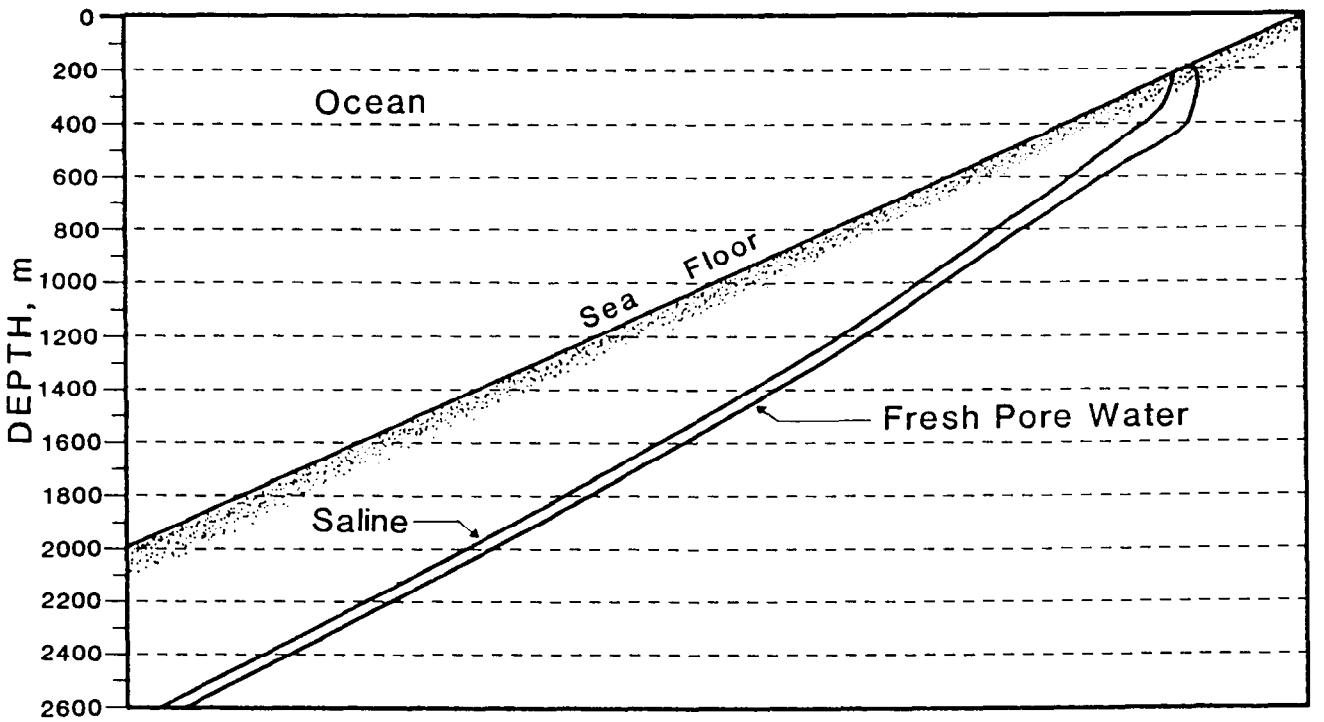

Figure 56. EFFECT OF PORE WATER SALINITY ON BASE OF GAS HYDRATE STABILITY ZONE

limited number of exploratory wells from the Canadian Beaufort continental shelf, data on these subsurface conditions for the Beaufort Sea study region are lacking. For the vast majority of the study region the only evidence for gas hydrate presence is bottom simulating reflectors on seismic lines from the continental slope and continental rise offshore of Alaska.

While data on the physical parameters needed to model gas hydrate stability exactly in the Beaufort Sea study region are lacking, comparison of the depth of BSRs measured from seismic lines and the predictions from the model can provide approximations of those parameters. Relationships of water depth and subbottom BSR depth have been used to estimate geothermal gradients (Yamano et al., 1982) and to verify a gas-hydrate origin of BSRs (Shipley et al., 1979).

Data Base

We have established a data base of the subbottom depth and water depth of BSRs on seismic lines from the continental margin of the Beaufort Sea study region. The data were collected at regular intervals along the single channel seismic lines shot from the *Burton Island* (Plate 6) and the multichannel seismic lines from the 1977 cruise of the *S.P. Lee* (Plate 7). In addition to the depth information, prevailing structural and bathymetric conditions of the seafloor and subjacent strata were noted for each measurement point.

A plot of subbottom depth and water depth of BSRs from the Beaufort Sea shows the expected trend of greater subbottom depth with increasing water depth (Figure 57). In Figure 57 the data set has been divided into three groups. The solid squares on Figure 57 represent BSR measurements located beneath significant bathymetric highs. The stars on Figure 57 represent measurements on BSRs passing over or through diapirs. The open circles on Figure 57 represent BSRs from locations away from bathymetric highs or diapirs. Although a great deal of scatter of the data points is seen in Figure 57, least-squares correlation of water depth and BSR depth gives a moderately good correlation with a correlation coefficient value (r) of 0.73. The data points distant from either bathymetric high or diapirs show the greatest correlation of water depth and subbottom BSR depth with $r = 0.76$. Bottom simulating reflector over diapirs show a distinct but lesser correlation with $r = 0.64$. The BSRs beneath bathymetric highs show a much less pronounced correlation of water depth and BSR depth with $r = 0.36$.

Bottom simulating reflectors passing through or over diapirs occur at shallower subbottom depths than BSRs at similar water depths but distant from the diapirs. The line of best fit displayed on Figure 57 for diapir-associated BSRs is almost exactly parallel to that for other BSRs suggesting that both are due to hydrates. The lines of best fit demonstrate quite convincingly that diapir-associated BSRs occur at subbottom depths averaging 100 m shallower than for other BSRs at the same water depth.

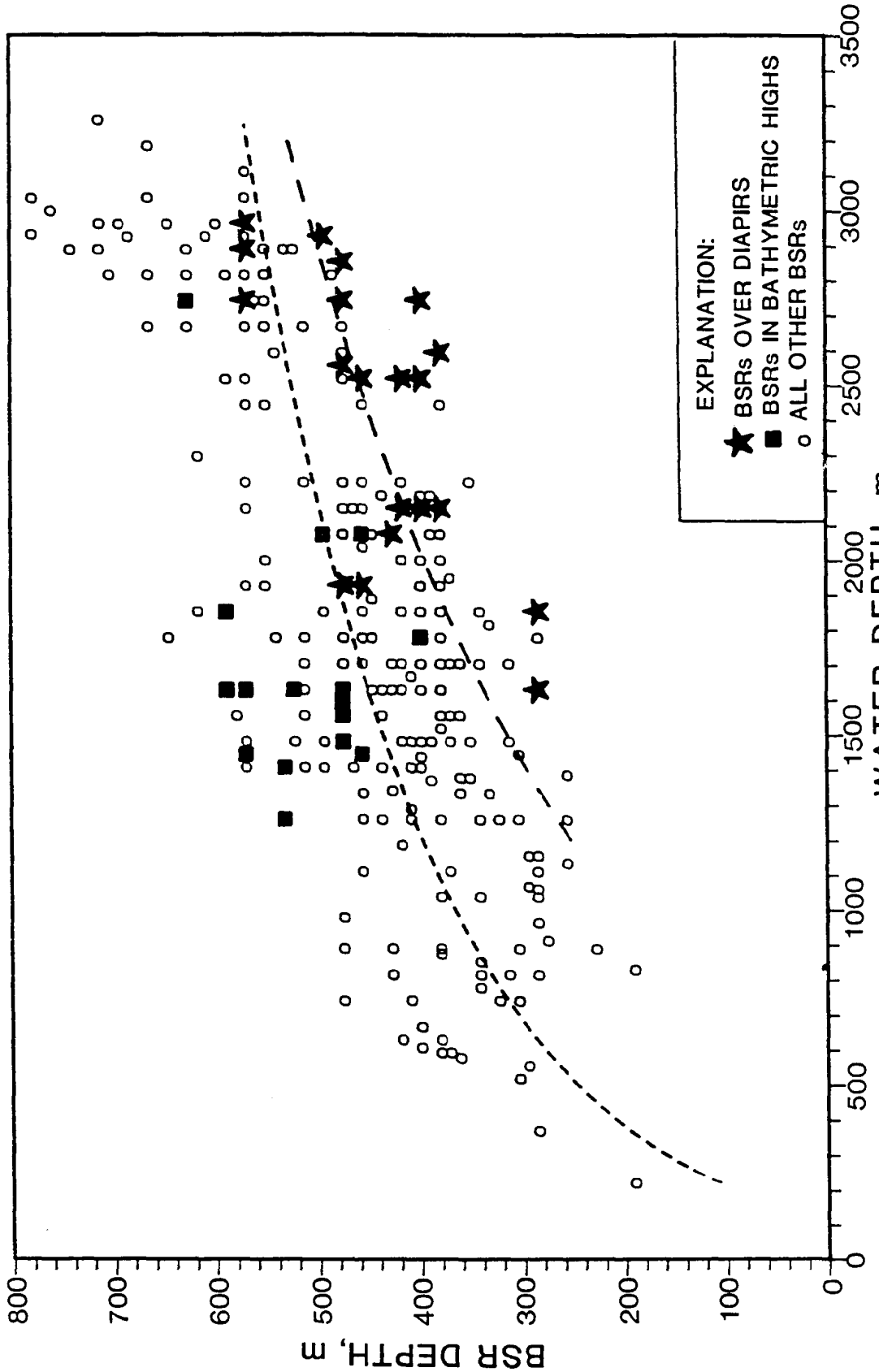

Figure 57. SUBBOTTOM DEPTH OF BOTTOM SIMULATING REFLECTORS, BEAUFORT SEA STUDY REGION

Gas Hydrate Reflector Depth Anomalies

Local variations in geothermal gradients is a readily apparent possible cause of the anomalously shallow BSRs over diapirs. The gas hydrate stability model can be used to evaluate that possibility. Lines representing the water depth to BSR depth relationships predicted for the Beaufort Sea study region by the gas hydrate stability model are superimposed on depths measured from seismic sections in Figure 58. The depth relationships predicted by the model assume hydrostatic pressure gradients, pure methane, and fresh pore water. Actual bottom water temperatures for the Beaufort Sea reported by Coachman and Aagaard (1974) were used to predict the BSR depths in Figure 58. Lines on Figure 58 depict the results of modeling expected water depth to BSR depth relationships using geothermal gradients of 2°C/100 m to 7°C/100 m. All but five of the measured BSR depths occur a water depths corresponding to geothermal gradients between 3°C/100 m and 7°C/100 m. Bottom simulating reflectors located away from bathymetric highs and diapirs, represented by open circles in Figure 58, indicate a full range of possible geothermal gradients from 3°C/100 m to 7°C/100 m. However, the diapir-associated BSRs (represented by stars in Figure 58) correspond to substantially higher geothermal gradients. Comparison of the geothermal isograds on Figure 58 with the lines of best fit for the measured BSR depths on Figure 57 shows that the best-fit line for the nonassociated BSRs is generally congruent with the line representing BSR depths predicted for geothermal gradient of 4°C/100 m at shallow depths and increasing to about 4.2°C/100 m in deeper water. In contrast, the diapir-associated BSRs correspond to geothermal gradients of 4°C/100 m to 7°C/100 with the apparent geothermal gradient decreasing with increasing water depth.

The indications of higher geothermal gradients over diapirs from the Beaufort Sea study region agrees with evidence from salt diapirs of the Blake Outer Ridge. Dillon and Paull (1983) documented BSRs decreasing in subbottom depth over salt diapirs. The relationship was explained as the effect of the high thermal conductivity of salt. The greater heat flow through the diapiric core material results in a convergence of isotherms in the sediments overlying the diapir. Since the base of the gas hydrate stability zone closely mimics isotherms, the BSRs over the salt diapirs at Blake Outer Ridge shallow noticeably.

Shoaling of BSRs over the shale diapirs in the Beaufort Sea study region contradicts the relationships projected by McLeod (1982). Because of the low thermal conductivity of shale, McLeod (1982) projected that BSRs over shale diapirs should occur deeper in the sediment section than BSRs distant from the diapirs and the concomitant thermal perturbation. McLeod (1982) projected that the relative deflection in BSR depth over a diapir may be useful in differentiating the material composing the core; a shallow BSR over a diapir indicates a salt core, a deep BSR over a diapirs indicates a shale core. The diapirs beneath the continental slope and rise of the Beaufort Sea study region are reported to be composed of shale. Eittreim and Grantz (1979) analyzed the seismic velocity of Beaufort Sea diapirs. Seismic velocity values of 1.5 to 2.0 km/sec strongly suggest shale composition; salt diapirs typically range in velocity from 3 to 4.5 km/sec. Canadian authors also concur that the diapirs beneath the Mackenzie Delta are composed of shale.

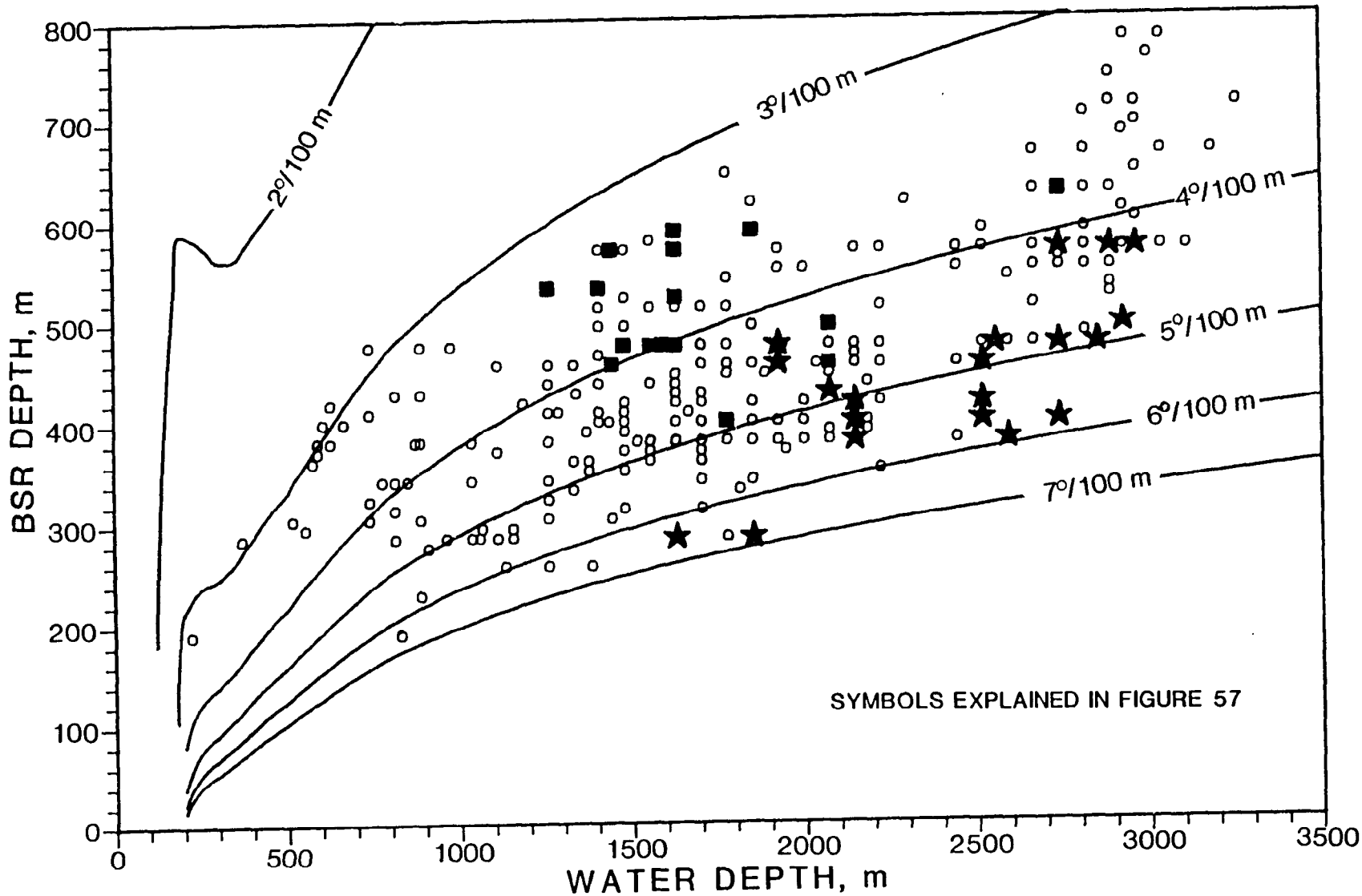

Figure 58. COMPARISON OF MEASURED AND PREDICTED BOTTOM SIMULATING REFLECTOR DEPTHS

Factors other than geothermal gradient could presumably affect the depth of BSRs over diapirs. Anomalous low pressure in sediments over diapirs and /or relatively high pressure in the sediments away from the diapirs could duplicate the BSR depth relationships noted in the Beaufort Sea. The core material of shale diapirs is typically overpressured (Hedberg, 1980). Pressures greater than hydrostatic should cause BSRs passing over or though cores of shale diapirs to be deeper subbottom than BSRs in nearby sediments not affected by the overpressure effects. However, pervasive overpressuring of ocean floor sediments away from the diapirs coupled with underpressured, normally pressured, or less overpressured sediments over diapirs could produce the observed BSR depth relationships. Pressures over diapirs which are consistently less than those elsewhere in the sediments could possibly result if the faulting and fracturing associated with diapiric intrusion vents ubiquitous overpressure to the sea resulting in hydrostatic pressure over the diapir while maintaining overpressure in distal sediments.

A change in salinity of pore water could ostensibly account for shallower BSRs over diapirs. Abnormally saline pore water injected into overlying strata during emplacement of the diapir could potentially cause local destabilization of gas hydrates. However, modeling of the effect of salinity on gas hydrate stability has shown that the change in thickness of the gas hydrate stability zone is minimal within the salinity range expected for marine sediment pore water. Bottom simulating reflectors over diapirs average 100 m shallower than BSRs elsewhere in the Beaufort Sea study region. The work of Scott summarized in Kuuskraa et al. (1983) indicates that the 3°C to 4°C change in gas hydrate equilibrium temperature represented by the 100 m change in BSR depth could be accomplished by increasing pore water salinity over the diapir to 11% to 13%, assuming nonsaline pore water away from the diapir. If the pore water of the sediments away from the diapirs have a salinity comparable to sea water (3.6%), then salinities of 13% to 15% would be necessary to achieve the 100 m change in the depth of the base of the gas hydrate stability zone. This degree of salinity increase seem unlikely to occur over a shale diapir. Although similar salinity signatures have been measured over salt diapirs at DSDP Sites 2, 88, and 92 (Manheim et al., 1973).

Different composition of the hydrocarbon gas from which the hydrates are formed could affect the subbottom depth of the BSRs over the diapirs. Addition of hydrocarbons heavier than methane would stabilize the resulting hydrate and cause the base of the gas hydrate stability zone to be located deeper in the sediments than that for methane hydrate. Hydrocarbons heavier than methane are generated by thermal degradation of organic matter and also by relatively low temperature diagenetic reactions. Since the material constituting the core of diapirs was originally located at a deeper stratigraphic position, gas generated from the core material would be expected to have been generated at higher temperatures than gas in sediments away from diapirs. Gases generated at higher temperatures are characterized by an increase in the content of hydrocarbons heavier than methane. Biogenic gases formed at shallow depths are composed almost entirely of methane (Claypool and Kaplan, 1974). At temperatures less than those required for thermal degradation of kerogen (about 90°C) the concentration of heavier diagenetic gases increases logarithmically with depth (Claypool et al., 1973; Hunt et al., 1980; Kvenvolden and Claypool, 1983). Gases generated during the main phase of hydrocarbon generation contain large amounts of heavier hydrocarbons. Late stages of

thermal hydrocarbon generation produce methane with only minor heavier components (Tissot and Welte, 1984).

The gases dissolved in sediment interstices directly over the shale diapirs of the Beaufort Sea continental slope would in all probability be composed of greater quantities of heavier hydrocarbons than the biogenic gases in sediments away from the diapirs. Whether the source of the gases in the sediments over the diapirs is the core of the diapir or the sediments themselves, the source rocks have been buried more deeply and for a longer period of time than have sediments at comparable subbottom depths away from the diapirs. We stress that a compositional difference, although possibly slight, should exist between gases in the two locations even if the thermal maturity of the source rocks is insufficient to have generated thermogenic gas. The addition of heavier diagenetic gases to the biogenic methane pool of the uplifted rocks should produce a heavier hydrocarbon mixture in sediments that have not attained the threshold of thermogenic hydrocarbon generation. Presence of potential hydrocarbon migration pathways above and around the diapirs increases the likelihood that gases constituting hydrates near would contain appreciable amounts of heavy hydrocarbons.

The presumed addition of heavy hydrocarbons to the gas mixture in sediments over diapirs should cause BSRs over diapirs to be located deeper in the sediments than away from diapirs. Addition of other hydrocarbons to methane increases the stability of the resultant hydrate and thus increases the subbottom depth of the base of the gas hydrate stability zone. Thus, if all other factors were held constant, BSRs over diapirs should be located deeper in sediments than the BSRs at the same water depths away from the diapirs. This prediction is opposite of the relationship observed in seismic lines from the Beaufort Sea study region. The discrepancy suggests that the stabilizing effects of gas composition on gas hydrate have been overwhelmed by larger destabilizing effect due to another factor.

A consistent difference in the topography of the seafloor over diapirs on the continental slope could conceivably be called upon to explain the observed difference in subbottom depths of BSRs over diapirs. Diapirs on the Alaskan Continental margin generally produce distinct bathymetric highs on the overlying seafloor. Depths of BSRs beneath bathymetric highs not underlain by diapirs were recorded to determine whether the unexpectedly shallow BSRs over diapirs are the result of seafloor topography. As seen on Figure 57, BSRs from bathymetric highs without diapirs typically occur deeper subbottom for a given water depth than diapir-related BSRs. The BSRs from bathymetric highs away from diapirs tend to be deeper in sediments than BSRs from areas away from both bathymetric highs and diapirs. Thus, it would appear that the anomalously shallow subbottom depth BSRs overlying diapirs occurs in spite of, rather than due to the bathymetric highs which typically occur above the diapirs.

Analysis of the potential effects of seafloor topography, pressure gradients, salinity, and gas composition anomalies expected from a diapiric intrusion indicate that none of them caused the decrease in subbottom depth of BSRs over diapirs that is seen in Beaufort Sea seismic lines. The only remaining factor which could account for the observed pattern is different geothermal gradients proximal and distal to the diapir. Although Mcleod (1982) professed that geothermal gradients are decreased over shale diapirs, BSRs from the Beaufort Sea demonstrate that the

opposite is more likely. Data summarized on Figure 58 indicate that geothermal gradients over diapirs average about 1°C/100 m greater than those elsewhere.

While the low thermal conductivity of shale claimed by Macleod (1982) to control the thermal regime around diapirs is certainly a factor, other properties of the diapirs appear to be more important in the Beaufort Sea study region. The principal factor which could increase geothermal gradients over diapirs is convection. The diapiric material is intruded from deeper horizons and is thus much hotter than the country rock. If the diapir has not been in place for too great of a period of time, the emanation of heat from the core material to the country rock would increase the geothermal gradient over the diapir. Fluids injected from the diapir into fractures in the country rock would be expected to transfer residual heat from the overheated diapir core to the country rock. Geothermal gradient change due to fluid injection should be especially prevalent based on the findings of Hedberg (1980) that shale diapirs are typically overpressured and undercompacted.

The discrepancy between the predicted and observed thermal condition of shale diapirs in the Beaufort Sea suggests another role for gas hydrate BSRs. The thermal regime of a diapir should be time-dependent. Increases in sensible heat produced by intrusion of hot shale and the expulsion of hot fluids should produce high geothermal gradients over diapirs. Subsequently, when the excess heat from the mobilized core is dissipated, the geothermal gradient over diapirs should return to baseline values in effect prior to the intrusion. After the diapir has been inactive for a long period of time, the low thermal conductivity of the shale core should come into play and depress the geothermal gradients over the diapir as envisaged by Macleod (1982). This change of geothermal gradients during the course of diapir development can be traced by measuring the depth of hydrate BSRs on seismic sections. Thus a coordinated study of seismic stratigraphy and BSR depth measurements could be used to determine the rate at which the diapirs cool. With the thermal model of diapirs so calibrated, the age of a diapir and the relative activity of its intrusion could be assessed with some accuracy by comparing the BSR depths over diapirs with BSR depths away from the thermal influence of diapirs.

Depth Ratios

The depth relationships of BSRs in the three contrasting geologic settings (over diapirs, beneath bathymetric highs, and away from either diapirs or bathymetric highs) can perhaps be easier visualized by examining the ratio of water depth to BSR depth for each. The water depth to BSR depth ratios for all measured points on each seismic line are diagrammed on Figure 59. The depth data for each seismic line is displayed vertically on Figure 59. Ratios from the 23 seismic lines included in the BSR depth data base are displayed on Figure 59 in approximate relative geographic position; Figure 59 can be interpreted as representing depth ratios from seismic lines of the Alaskan continental margin viewed to the north with Point Barrow at the left side of the diagram, Prudhoe Bay at about the center, and the Alaska - Canada border on the right side of the diagram. In this format, it is clear that the water depth to BSR depth ratios of locations far away from either diapirs or bathymetric highs (open circles on Figure 58) vary widely from 1.2 to 6.4 with no

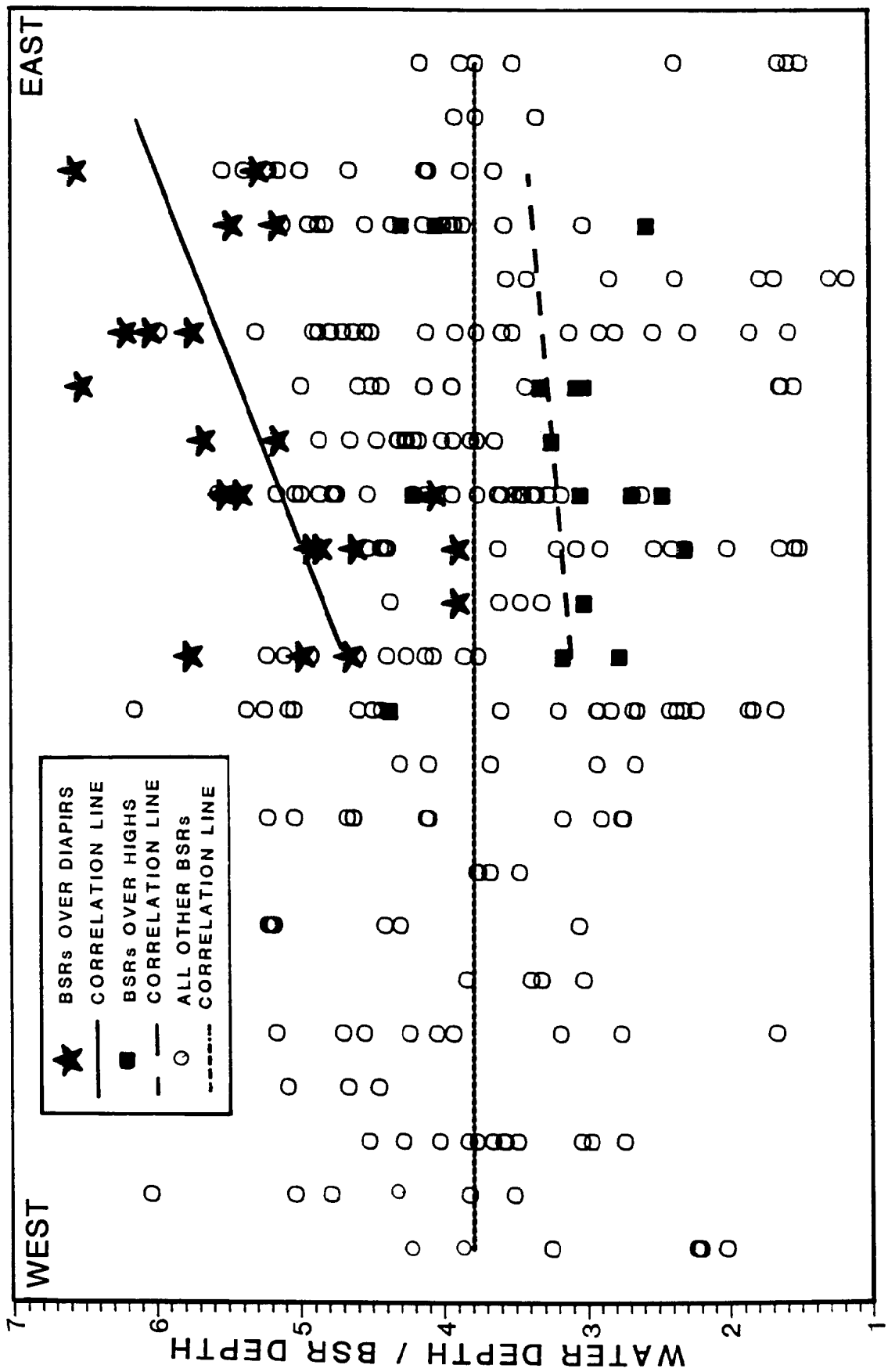

Figure 59. VARIATION OF RELATIVE DEPTH OF BOTTOM SIMULATING REFLECTORS ALONG THE ALASKA CONTINENTAL MARGIN

apparent spatial control. Bottom simulating reflectors beneath simple bathymetric highs have water depth to BSR depth ratios of 2.4 to 4.4, well within the range of non-associated BSRs, but on the low side of the range. Diapir-associated BSRs from the Beaufort Sea study region have water depth to BSR depth ratios of 4.0 to 6.9 which are clearly higher than ratios for bathymetric high settings or non-associated settings.

Ratios of water depth to BSR depth for diapir-associated BSRs appear to increase to the east (Figure 59). Lines of best fit from least-squares correlation the water depth to BSR depth ratio and position of the seismic line for each of the three geologic settings are drawn on Figure 59. The horizontal correlation line for the non-associated BSRs (open circles) suggests no correlation of depth ratio to position. A correlation coefficient (r) of close to 0 confirms the lack of correlation. The best fit line for diapirs beneath bathymetric highs (squares) suggests a slight increase in the depth ratio from east to west. However, a correlation coefficient of less than 0.03 indicates essentially no correlation of depth ratio and position of the seismic line for BSRs beneath simple bathymetric highs. The solid line on Figure 59 represents the best fit line for BSRs over or through diapirs (stars). The line depicts a trend toward higher water depth to BSR depth ratios in seismic lines shot near the Alaskan-Canadian border. Unlike the apparent correlations for the other geologic settings, the trend for BSRs over diapirs appears to be more likely as indicated by a correlation coefficient of 0.54.

Geothermal Gradients

The water depth to BSR depth ratios for seismic lines from the Beaufort Sea study region diagrammed in Figure 59 qualitatively indicate geothermal gradients. High geothermal gradients result in shallow BSRs, which in turn produce high water depth to BSR depth ratios. However the ratios graphed in Figure 59 are not directly correlative with geothermal gradients. As seen in Figure 58, the relationship between BSR depth and geothermal gradient predicted from the gas hydrate stability model is complex. While the trends of greater water depth-to-BSR depth ratios for BSRs over diapirs and higher ratios to the east for BSRs over diapirs seen in Figure 59 may indicate parallel trends for geothermal gradients, directly ascribing the same trends to geothermal gradient may not be justified.

Geothermal gradients could conceivably be obtained directly for specific values of water depth and subbottom BSR depths recorded from seismic lines by solving the equation of gas hydrate stability pressure and temperature for geothermal gradient. However, the gas hydrate stability model which solves for the expected BSR depth based on input geothermal gradients and other site-specific parameters is much more flexible. The gas hydrate stability model allows all parameters to reflect measured or reasonably assumed values. Based on the potential to eventually model the effects of these other parameters on geothermal gradients derived from seismic lines, geothermal gradients from Beaufort Sea seismic lines were determined from the existing gas hydrate stability model rather than by directly calculating the geothermal gradient from the BSR depth. The design of the program to determine the geothermal gradient represented by a BSR is relatively efficient. Rather than model the stability conditions that would produce

the observed BSR depth, the geothermal gradient program merely accesses data files created during one batch run of the gas hydrate stability model.

Through the gas hydrate stability model, the BSR depths measured from seismic lines of the Beaufort Sea were converted to geothermal gradients. The gas hydrate stability model was run using default values of biogenic gas and hydrostatic subbottom pressures. Thickness of the gas hydrate stability zone was calculated for each water depth between 0 and 4,000 m. At each water depth, gas hydrate stability zone thickness was calculated for each geothermal gradient between 2.4°C/100 m and 7.5°C/100 m in 0.1°C/100 m increments. The output file from the model run was organized so that each record contained all BSR depths attainable for each modeled water depth. Geothermal gradients for the Beaufort Sea study region were obtained by another program which accessed this file output from the gas hydrate stability model. The program retrieves the file record corresponding with the measured water depth. The measured BSR depth is then compared with the BSR depths predicted by the model for that water depth and various geothermal gradients. The observed BSR depth seldom matches the depths predicted by the model exactly. Therefore, a routine in the geothermal gradient program determines the geothermal gradient which would produce the unique water depth-BSR depth pair by interpolating between the two predicted BSR depth values which bracket the observed value.

Using these procedures, geothermal gradients were derived for 281 locations in the Beaufort Sea study region at which the water depths and subbottom depths of BSRs had been measured. A mean geothermal gradient value of 4.21°C/100 m with a standard deviation of 0.71 was thus obtained for the outer continental shelf, the continental slope, and continental rise of the Beaufort Sea study region. The geologic setting of the BSR affected the resulting geothermal gradient. Bottom simulating reflectors located in simple geologic and bathymetric settings averaged 4.19°C/100 m. Geothermal gradients from BSRs beneath bathymetric highs average 3.64°C/100 m. As previously speculated, geothermal gradients over diapirs are higher than those elsewhere on the Beaufort continental margin with a mean of 4.86°C/100 m.

Statistical Tests of Geothermal Gradients

Geothermal gradients of the Beaufort Sea study region derived from BSR depths are more amenable to statistical determination of apparent trends than are the directly measured BSR depths. Since BSR depth is the result of the complex interaction of many different factors, analysis of the BSR depth is of limited value. In a previous section, several relationships of the ratio of water depth to BSR depth were noted. However, attempting to correlate the ratio with, for example, water depth is fruitless. Least squares fitting of a regression line to the data would show a correlation even where none was present, because the independent variable (water depth) is a component in the dependent variable (the ratio). The design of our gas hydrate stability model results in an independence of the derived gradient from directly measured values such as water depth. As such, statistical measures of significance or correlations should be valid for derived geothermal gradients.

The apparent difference in the mean geothermal gradient values for different geological settings on the Beaufort continental margin can be tested statistically. The significance of progressively higher geothermal gradients derived from BSRs in bathymetric highs, featureless seafloor settings, and over diapirs can be determined using the analysis of variance method. Application of the method to the Beaufort Sea data set results in an F-statistic of 18.44. Comparison of that statistic with published tables (Davis, 1986) shows that a statistically significant difference exists among the three mean geothermal gradient values (3.65°C/100 m, 4.19°C/100 m, and 4.82°C/100 m) at a 99% confidence level. The analysis of variance method determines if a significant difference exists among group means but does not determine which of the group means is different from the others.

The method of multiple comparisons indicates that each of the three mean geothermal gradient values are significantly different from the others. Two types of multiple comparison tests were performed on the Beaufort Sea data set, the Duncan method and the Student-Neuman-Kuhls method. Each of the methods indicated that the mean geothermal gradients calculated for each of the geological settings were distinct from each of the others at a confidence level of greater than 95%.

While comparing the geothermal gradients derived from all BSRs in the three different settings indicates a distinct difference, it is worthwhile to analyze the variation in geothermal gradients for particular seismic lines. From the suite of seismic lines available from the Beaufort Sea study region, seven lines exhibit BSRs on each of the three analyzed settings.

Lines 2710, 2742, 2722, 2725, 3720, 726, and 1716 each show well developed BSRs over diapirs, through isolated bathymetric highs, and along relatively undisturbed stretches of the continental slope. Table 4 shows the mean geothermal gradient for each seismic line in each of the settings. On each of the seven seismic lines the BSR-derived geothermal gradient is lower beneath isolated bathymetric highs than for other settings. Additionally the geothermal gradients above diapirs are substantially greater than those in other settings for each of the seven lines. This pattern in the individual lines is also depicted in the mean geothermal gradients calculated for each setting; diapirs average 4.7°C/100 m, bathymetric highs average 3.6°C/100 m, and other settings average 4.0°C/100 m.

Multiple comparisons analysis on the seven seismic lines which display BSRs in each of the three settings indicates that the difference in the mean geothermal gradients is significant at confidence levels much greater than 95%.

Geothermal Gradients and Water Depth

Plotting BSR-derived geothermal gradients as a function of water depth suggests that geothermal gradients increase from the outer continental shelf to the continental slope and decrease systematically to the outer continental slope and rise.

The relationship between geothermal gradients and water depth for the Beaufort continental margin is illustrated in Figure 60. The filled diamond symbols on the graph indicate the mean geothermal gradient obtained from BSRs in simple geological settings for each 1,100 m of water depth. The vertical error bars adjoining the diamond symbols indicate the standard deviation from the mean for the

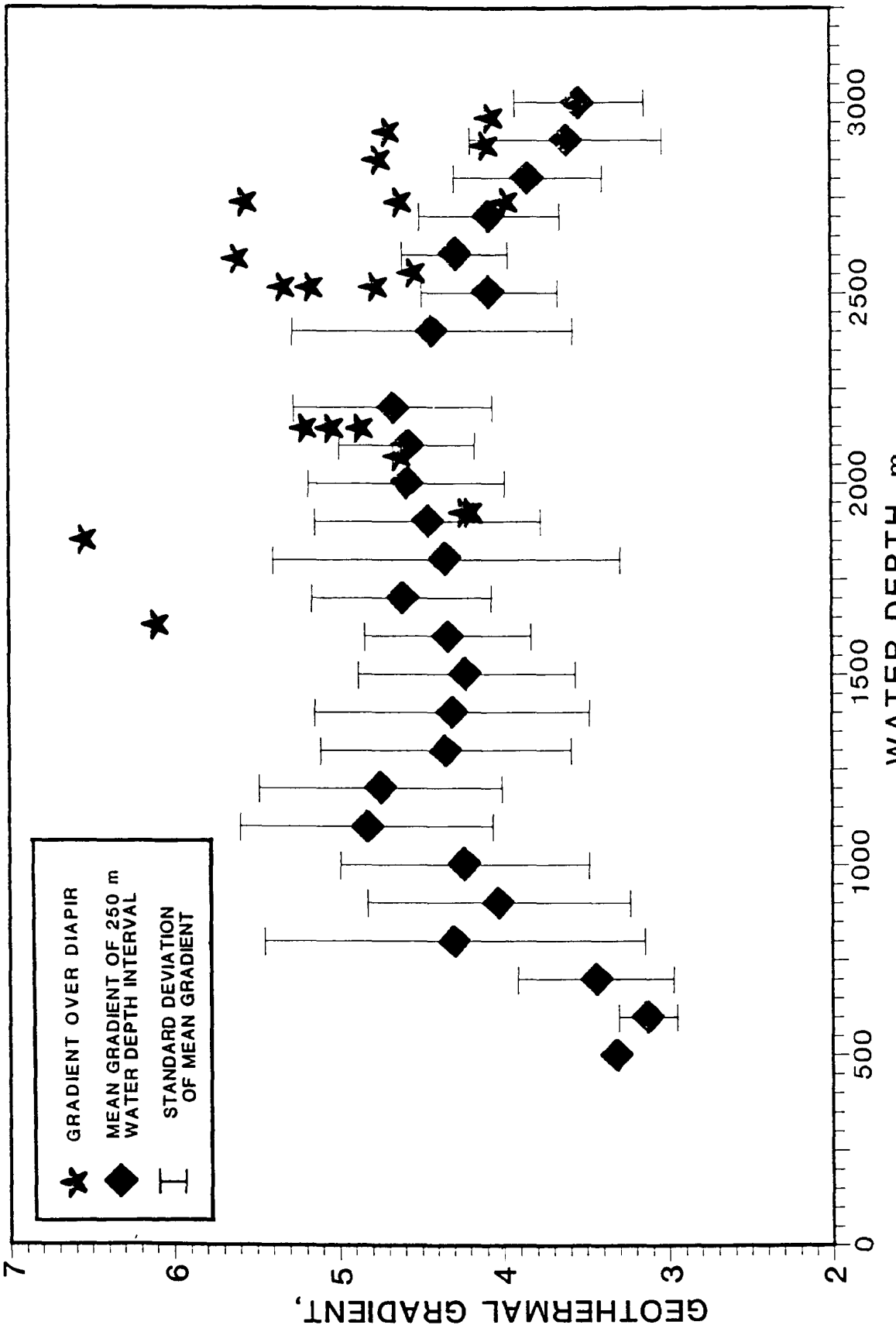

Figure 60. RELATIONSHIP OF GEOTHERMAL GRADIENTS TO WATER DEPTH, ALASKAN CONTINENTAL MARGIN

Table 4.

MEAN DERIVED GEOTHERMAL GRADIENTS FOR DIFFERENT GEOLOGICAL SETTINGS

Seismic Line Number	Geological Setting		
	Diapir	Bathymetric High	Others
726	5.61°C/100 m	3.83°C/100 m	4.05°C/100 m
1716	5.57°C/100 m	3.94°C/100 m	4.70°C/100 m
2710	4.62°C/100 m	3.47°C/100 m	4.08°C/100 m
2722	4.28°C/100 m	3.14°C/100 m	3.42°C/100 m
2725	4.68°C/100 m	3.29°C/100 m	3.96°C/100 m
2742	4.19°C/100 m	3.56°C/100 m	4.01°C/100 m
3720	4.61°C/100 m	3.87°C/100 m	3.96°C/100 m
Average	*4.70°C/100 m*	*3.60°C/100 m*	*4.00°C/100 m*

BSRs in simple settings. The stars in Figure 60 indicate the geothermal gradients obtained from BSRs over diapirs.

A negative correlation (r = -0.40) between geothermal gradients from over diapirs and water depth suggests that upper continental slope diapirs may have higher heat flow than diapirs on the lower continental slope and the continental rise. The small number of diapir data points and their wide scatter makes any such relationship tentative at best.

Geothermal gradients exclusive of those near diapirs increase from the outer continental shelf to the upper continental slope. Mean geothermal gradients from Beaufort Sea BSRs increase from 3.3°C/100 m at 400 m water depth to 4.8°C/100 m at 1,100 m water depth. Least squares correlation of geothermal gradients and water depth from water depths of 200 m to 1,100 m produces a correlation coefficient (r) of 0.65. The resulting linear best fit equation (geothermal gradient = 0.00275 x (water depth) + 1.67) indicates that beneath the upper slope of the Beaufort Sea study region geothermal gradients are increasing at a very rapid rate of 2.75°C/100 m per 1,000 m of water depth increase.

The geothermal gradient to water depth plot (Figure 60) levels out at about 1,100 m water depth. Geothermal gradients average 4.2 to 4.7°C/100 m between 1,100 and 2,300 m. Least squares analysis of the data set of geothermal gradients between 1,100 and 2,300 m water depth gives a correlation coefficient of 0, demonstrating that no consistent linear trend of geothermal gradient and water depths exists between 1,100 and 2,300 m water depth.

Geothermal gradients systematically decrease from water depths of 2,300 m to 3,300 m, the maximum depth recorded for a BSR on the Beaufort Sea continental margin. The mean geothermal gradient indicated by BSRs beneath water from 2,300 to 2,500 is 4.4°C/100 m. At a water depth span of 3,000 to 3,100 m, the mean geothermal gradient has decreased to 3.6°C/100 m. A correlation coefficient of -0.51 indicates that a negative correlation of geothermal gradients with water depths exists on the lower continental slope and the continental rise of the Beaufort Sea. The regression equation (geothermal gradient = -0.0014(water depth) + 7.72) indicates that geothermal gradients decrease at a rate of 1.4°C/100 m per 1,000 m increase in water depth.

The statistically inferred pattern of geothermal gradients rapidly increasing to a water depth of 1,100, staying more or less uniform to water depth of about 2,300 and then decreasing rapidly to the greatest depths surveyed could reflect well documented geological processes on the Beaufort continental margin. The rapid increase to a water depth of 1,100 corresponds with the transition from undeformed outer continental shelf ("Beaufort Ramp" of Grantz et al. (1976)) to the upper continental slope. The highest mean geothermal gradients of 4.9°C/100 m occur between 1,050 m and 1,150 m water depth. This corresponds to the depth range of the well defined scarps resulting from widespread slumping along the continental margin as mapped by Grantz et al. (1983). As discussed by Krason and Ridley (1985), areas of the seafloor from which material has been removed by mass wasting processes are characterized by high geothermal gradients. The remainder of the continental slope from about 1,200 m to 2,300 m water depth is marked by lower but still elevated mean geothermal gradients ranging from 4.2 to 4.8°C/100 m. These values can be interpreted to indicate sliding and slumping, but to a lesser degree than in the 1,100 m water depth zone. The depression of geothermal gradients from their maximum at 1,100 m could be a reflection of the less intensive mass wasting occurring away from the structural shelf-slope break; seismic sections show that wasting is prevalent at all water depths along the continental slope, but fresh slumping scarps are most common around the 1,100 m water depth. Additionally, mass wasting processes on the slope involve both removal of material by sliding and slumping and deposition of some of the material lower on the slope. Thus the slight decrease in geothermal gradient from a maximum at 1,100 m water depth may be due to a combination of diminished removal of material and some minor redeposition on the slope. The dip of the seafloor at depths greater than 2,300 m is less than higher up on the continental slope. Thus, mass wasting processes and their concomitant increases in geothermal gradients are less intensive. These deeper settings are also the principal loci of turbidite deposition from upslope wasting, which should considerably lower the observed geothermal gradient.

Some of the apparent change in geothermal gradient in the sediments of the continental slope and rise may be influenced by the kinetics of gas hydrate formation. The high mean geothermal gradients at water depths near 1,100 m were inferred from unusually shallow BSRs. Since this water depth is characterized by abundant scarps from recent slumping and sliding, geothermal gradients would be expected to be higher than elsewhere on the continental slope. Slow hydrate formation processes may have contributed to the shallow subbottom depths of BSRs and thus the apparently elevated geothermal gradients. Methane and water mixtures have been shown in laboratory studies to require supercooling to form hydrates

rapidly (Makogon, 1974; Berecz and Ballas Achs, 1982). The temperature at the base of the gas hydrate stability zone beneath the recent slump scarps may not correspond to the equilibrium temperatures assigned by the gas hydrate stability model due to a kinetically induced lag in the formation processes.

Variation of Geothermal Gradients along the Beaufort Continental Margin

Calculated geothermal gradients are plotted as a function of approximate relative location of the seismic lines from which the were obtained in Figure 61. As in previous graphs in this section, solid squares represent data points obtained from BSRs beneath bathymetric highs. Stars in Figure 61 represent geothermal gradients from BSRs overlying diapirs. Open circles on Figure 61 indicate geothermal gradients from BSRs in all other geologic or bathymetric settings. The line composed of very short dashes is the linear best fit regression line for BSRs from simple geological settings. The line composed of longer dashes is the linear regression line for gradients obtained from BSRs beneath bathymetric highs. The solid line on Figure 61 is the best fit line for gradients from BSRs over diapirs. The X-axis values on Figure 61 range from the westernmost multichannel seismic line to display BSRs (Line 771) (Plate 7) to the easternmost (Line 732) (Plate 7). The X-axis can thus be roughly interpreted as relative distance from west to east along the Beaufort continental margin offshore of Alaska. The distance between each value on Figure 61 thus equals about 20 km, the approximate spacing of the parallel lines from the 1977 survey aboard the *S.P. Lee*.

Mean geothermal gradients obtained from BSR depths via the gas hydrate stability model show an slight overall decrease from west to east from offshore of Point Barrow to offshore of the Canadian border (Figure 61). This apparent overall decrease from west to east is composed of two constituent trends, a decrease followed by a rapid increase. Mean geothermal gradients decrease rapidly from offshore of Point Barrow to offshore of Prudhoe Bay. However, geothermal gradients increase from west to east from a minimum offshore of Camden Bay to the Canadian border. The increase in mean geothermal gradients from offshore of Prudhoe Bay to offshore of the Canadian border is consistently seen not only in BSRs from simple geological settings, but also for BSRs over diapirs and beneath bathymetric highs.

A wide range of gradients is seen on each of the lines displayed in Figure 61. The six values obtained for Line 771, for example, range from 3.2°C/100 m to 6.4°C/100 m. A smaller range of values is seen on some of the lines , e.g. 4.7°C/100 to 5.2°C/100 m for Line 765. Least-squares curve fitting procedures generates a line of best fit with only a minimal correlation ($r = -0.22$). The correlation line, composed of very short dashes on Figure 61, predicts that typical geothermal gradients decrease from about 4.7°C/100 m on the west to about 3.8°C/100 m at the eastern limit of the data.

Geothermal gradients from BSRs overlying diapirs increase from west to east (Figure 61). The increase in geothermal gradients to the east on the Beaufort continental margin is both more rapid and more statistically verifiable. The correla

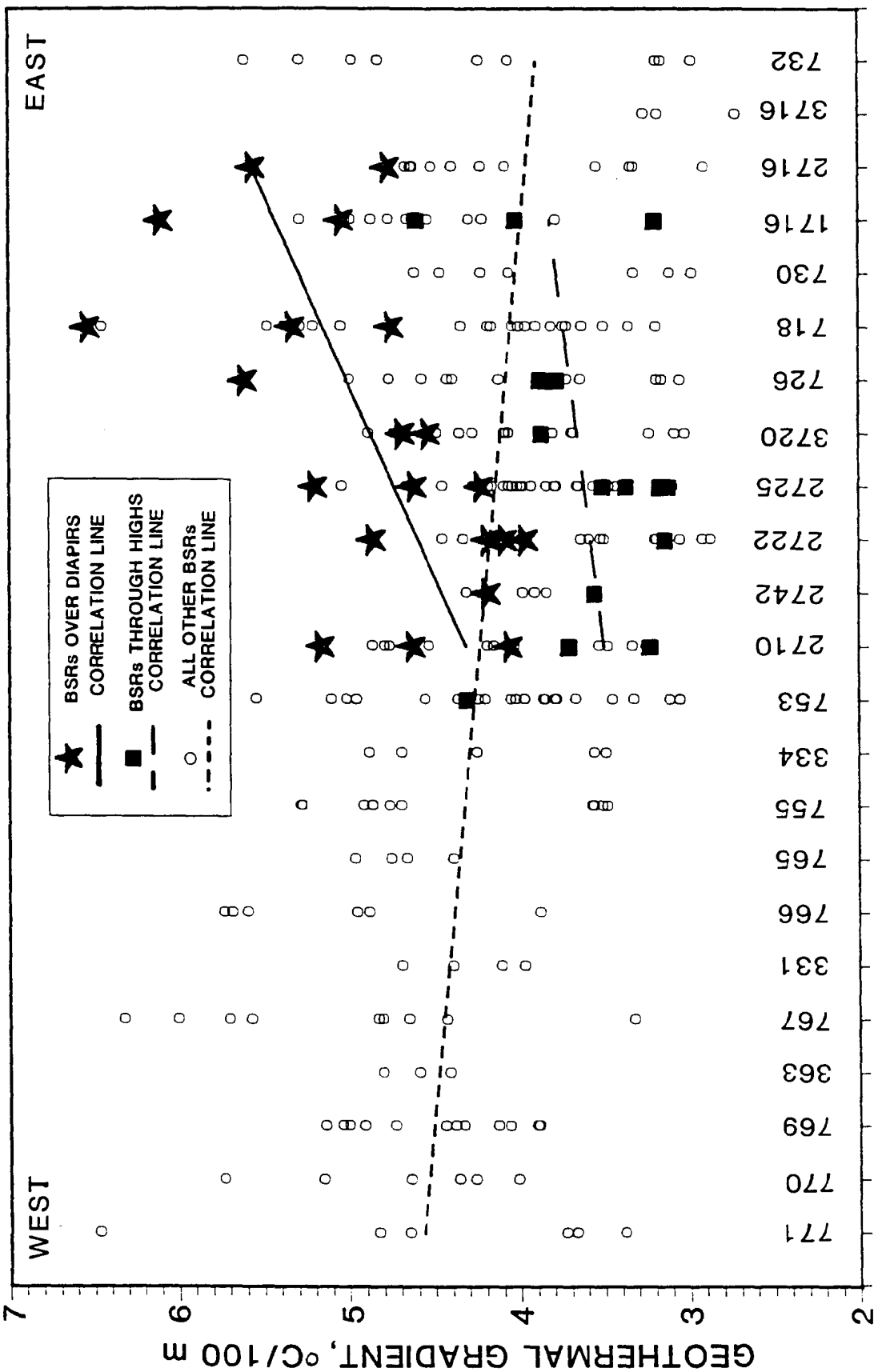

Figure 61. GEOTHERMAL GRADIENTS FROM GAS HYDRATE REFLECTORS

tion equation derived by least-squares methods indicates that gradients increase at a rate of about 0.8°C/100 m per 100 km distance eastward along the continental margin. A correlation coefficient (r) of 0.61 indicates a more confident assignment of an actual trend than the possible trend cited above for gradients not associated with diapirs.

Geothermal gradients derived from BSRs beneath bathymetric highs increase to the east (Figure 61). The correlation coefficient for the bathymetric high associated geothermal gradients of 0.51 indicates a less direct relationship than for gradients over diapirs (r = 0.61), and a more direct relationship than for gradients not associated with diapirs or bathymetric highs (r = 0.27). Some of the apparent rise of geothermal gradients from west to east beneath bathymetric highs may be due to variation in the relief of the highs, which was not quantified in this analysis.

The range of geothermal gradient values for each of the measured seismic lines obscures trends and makes confirmation of the relationships between geothermal gradient and location predicted by least-squares correlation difficult to confirm. An alternative type of presentation of the same data is shown in Figure 62. In Figure 62 the mean geothermal gradient value for each line is plotted as an open diamond. Vertical bars on Figure 62 indicate the standard deviation of data set from the mean. The two dashed lines on Figure 62 are linear correlation lines of best fit obtained from the least-squares method. The lines were obtained by considering gradients obtained from seismic lines west of about 147°W longitude separately from those to the east. The break point for dividing the data set into two groups was selected to be consistent with lateral changes in the geology and BSR distribution of the Alaskan continental margin. Between Lines 753 and 2710 on Figure 62 a 50 km stretch of the continental margin is devoid of detectable BSRs in the available seismic lines. This hiatus in BSR presence, occurring just northwest of Prudhoe Bay, also separates lines with distinct diapirs to the east from lines to the west with no obvious diapiric structures.

Figure 62 illustrates that geothermal gradients generally decrease from west to east to the break point in the data set at Line 2742. Conversely, geothermal gradients appear to increase from west to east between the data break point (approximately Prudhoe Bay) and the Canadian border. Once again, the wide scatter of the data indicate that these trends should be approached with caution. Correlation coefficients (r) of -0.27 and 0.38 for the western and eastern data sets respectively suggest that a significant lateral change in geothermal gradient occurs, but the change is not unequivocal.

One inconsistency in the interpretation of Figure 62 is readily apparent. The correlation lines suggest a lateral change of geothermal gradients along the continental margin. However, as seen in Figure 60 BSR-derived geothermal gradients show a distinctive relationship to water depth. It is conceivable that the variation in geothermal gradients which we propose to exist along the Beaufort continental margin offshore of Alaska may be merely the result of variation of water depth at the points measured. We attempted to use unbiased, methodical sampling of the BSR depths to develop our data base. However, a variation of an old adage applies here, BSRs are where you find them. That is, if a particular seismic line had well developed BSRs beneath shallow water, the BSRs were measured and included into the data base without concern that their inclusion would bias the sample suite to

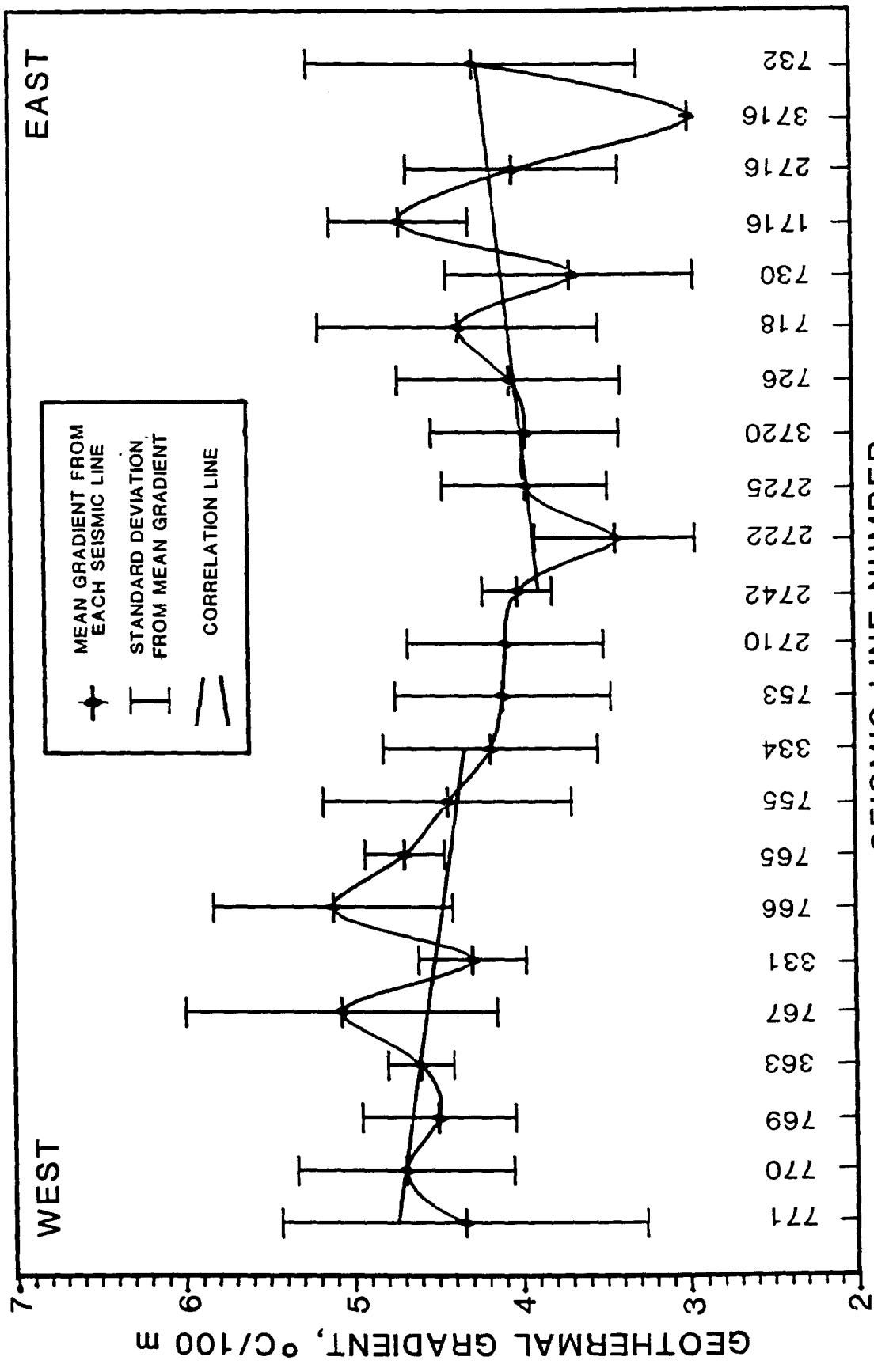

Figure 62. VARIATION OF GEOTHERMAL GRADIENTS ALONG THE ALASKAN CONTINENTAL MARGIN

shallow water observations. Thus it remains possible that the locations which we project to have very high geothermal gradients, i.e. near Point Barrow and the Canadian border, are overloaded with BSR measurements from depths which from Figure 60 are seen to characteristically exhibit high geothermal gradients.

The potential effects of this possible sample bias can be addressed by normalizing the geothermal gradient data to a consistent depth range. In the discussion on the relationship of geothermal gradients and water depth, a strong positive correlation was noted at water depths of less than 1,200 m (Figure 60). Between 1,200 and 2,300 m, no relationship of water depth and geothermal gradients was apparent (Figure 60). However, at water depths greater than 2,300 m a distinct inverse relationship was noted with geothermal gradients decreasing beneath deeper water (Figure 60). To counter the effect of the variation of geothermal gradients with water depth, gradients beneath very shallow water and beneath very deep water were normalized to values correlative to those beneath intermediate waters.

The procedure for normalizing derived gradient values involves quantifying the agreement of each sample point with the correlation line prevailing for that particular water depth segment. For water depths of less than 1,150 m and greater than 2,300 m each measured geothermal gradient was subtracted from the value predicted for that water depth by the least-squares correlation line. The resulting difference in predicted and measured geothermal gradients was then added to the typical geothermal gradient for the 1,150 to 2,300 m water depth interval, the mean value of 4.435°C/100 m. By this procedure the variation among individual calculated geothermal gradient values for given water depth intervals is maintained while the systematic variation of geothermal gradients is corrected.

The effect of normalizing calculated geothermal gradient values by this procedure is diagrammed in Figure 63. Comparison of the top diagram normalized gradients vs water depth in Figure 63 with a similar representation of non-normalized geothermal gradient values in Figure 60 shows that the systematic pattern of lower mean geothermal gradient values under very shallow and under very deep water has been removed. The standard deviation of the mean gradients is typically increased by 10% by the procedure, suggesting that the normalization procedure may have been somewhat oversimplified.

The lower diagram on Figure 63 demonstrates than the same pattern of geothermal gradient variation along the Alaskan continental margin seen for calculated geothermal gradients (Figure 62) persists when the gradients are normalized to remove possible sample bias. The mean and standard deviation of normalized geothermal gradients graphed on the lower panel of Figure 63 differ somewhat from those seen for the original data (Figure 61). However the correlation lines plotted on both Figures 62 and 63 indicate that the geothermal gradients of the continental margin decrease from line 771 near Point Barrow to line 2722 north of Camden Bay. From Camden bay eastward to near the Canadian Border, both figures show an eastward increase in geothermal gradients. The qualitative agreement in the trends in geothermal gradient data suggest that (1) the data set is not substantially biased by water depth of the sampled points, and (2) the illustrated trends may be accurate indicators of the true variation of geothermal gradient along the Alaskan continental margin.

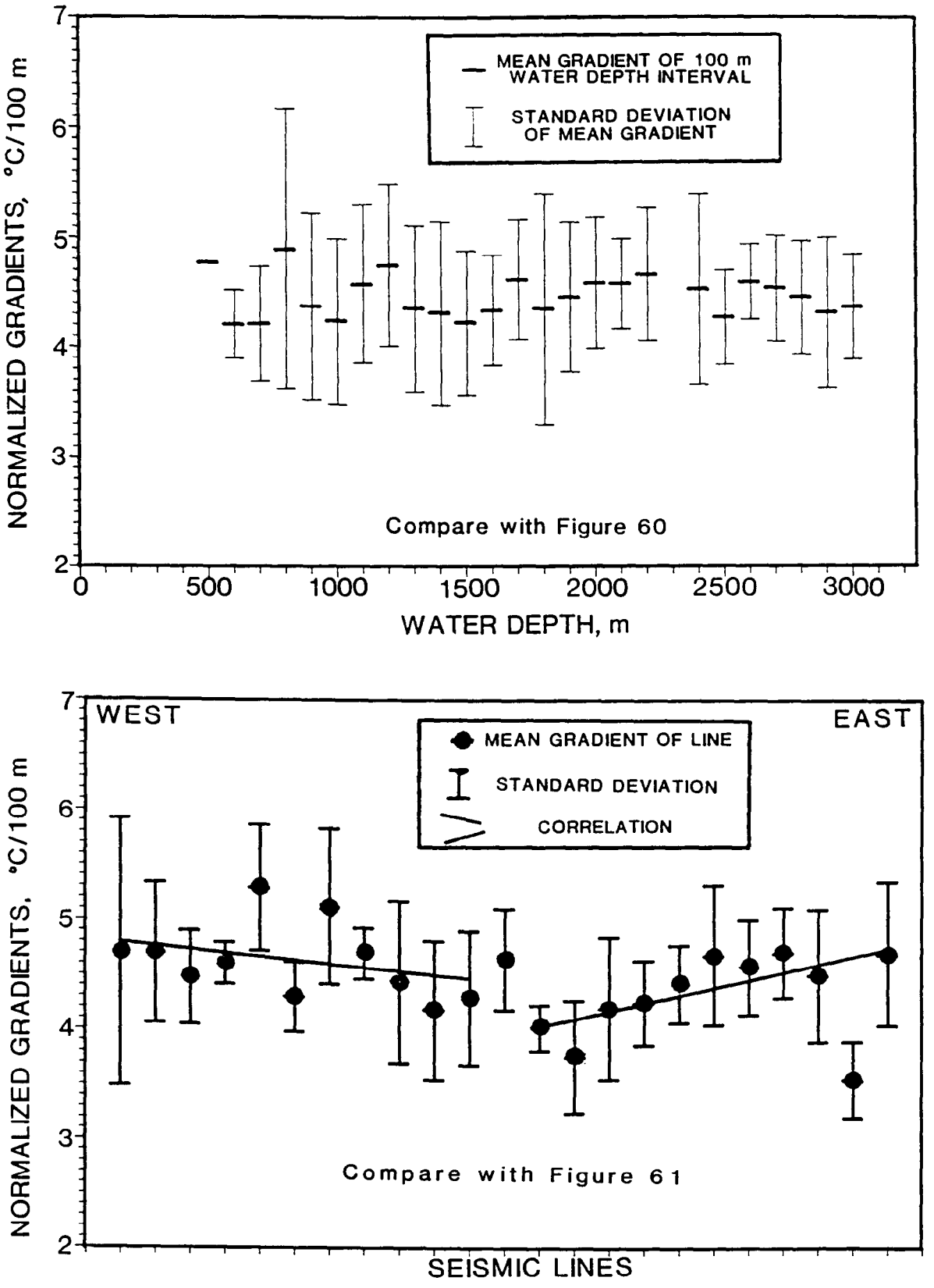

Figure 63. EFFECT OF NORMALIZATION ON GEOTHERMAL GRADIENT VARIATION

The data sets from which Figures 61, 62, and 63 are constructed all show three trends of geothermal gradient variation along the Alaskan continental margin. Just considering the geothermal gradient values calculated from BSRs far removed from either bathymetric high or diapirs, geothermal gradients decrease from west to east (Figure 61). When the suite of seismic lines is broken into two sets, a western set from Lines 771 to 753 (Plate 7), and an eastern set from line 2710 to 732 (Plate 7), two trends are seen (Figures 62 and 63). Geothermal gradients appear to decrease from west to east for the western group of lines, and to increase from west to east for the eastern group of lines. This pattern of decreasing then increasing geothermal gradients is evident in both the original data (Figure 62) and after the data have been normalized (Figure 63) to counteract the systematic variation of geothermal gradients with water depth (Figure 60).

The wide variation of the measured geothermal gradients raises the question of whether the observed correlations of BSRs and position of the seismic line are legitimate. With the wide scatter of data seen in Figure 61, any correlations obtained may spurious representations of local variations in geothermal gradient or any of a number of factors which can alter the depth of a BSR. Statistical tests exists to test whether any correlation obtained from least squares curve fitting is significant. The most common procedure is to convert the correlation coefficient (r) obtained from the data to a "t" score. The t value obtained from the r value can then be used to estimate the significance of the proposed correlation. Using the conversion formula and tabulated values for t from Davis (1986) the correlations diagrammed in Figures 61, 62, and 63 were tested for significance. The results of significance testing are displayed in Table 5

Table 5.

SIGNIFICANCE ESTIMATES OF DERIVED GEOTHERMAL GRADIENTS

Seismic Lines	Measured Geothermal Gradients		Normalized Geothermal Gradients	
	r	Confidence Level	r	Confidence Level
All	-0.24	99%	-0.12	90%
West	-0.27	99%	-0.19	95%
East	0.20	98%	0.34	99%

The results of t-tests for significance shown in Table 5 indicate that each of the noted correlations is valid at 90% confidence level or greater. The pattern of decreasing geothermal gradient values from west to east for the entire suite of lines as well for the western group only as indicated by the negative correlation coefficient in Table 5 is verified. The correlation coefficient (r), and thus the significance

for trends in the western and entire suite of lines is greater for the actual measured geothermal gradients than for the normalized data set. This implies that some of the relationship of geothermal gradients and position seen in the western group and the entire suite of lines was probably not due to water depth biasing of the sample, or that the normalizing procedure was not adequate to remove the bias.

The the eastern group of lines increases in geothermal gradient to the east (Figures 62 and 63, Table 5). The correlation coefficient and the confidence level of the significance of the correlation are substantially greater in the normalized data set. Thus correlations of the eastern group of seismic lines are much better when the variation of geothermal gradients with water depth (Figure 60) are compensated for by the normalization procedure (Figure 63).

It could be argued that the use of correlation coefficients and particularly t-tests to determine their significance are not appropriate for the Beaufort Sea seismic data set. The position variable in the is not continuously variable; each seismic line was assigned a simple ordinal number for relative position, rather than using actual separation between the lines. Also, the procedures assume normal distribution of the correlated variables, which cannot be demonstrated for the position variable. It is perhaps more appropriate to use the less restrictive methods of nonparametric statistical analysis to verify the apparent trends seen in the data. Of the many nonparametric methods for assessing correlations, the Spearman Rank Correlation is the most directly comparable to the conventional least squares parametric method (Koch and Link, 1980; Davis, 1986) The results of Spearman Rank testing of the data sets illustrated in Figures 61, 62, and 63 are summarized in Table 6

Table 6.

NONPARAMETRIC SIGNIFICANCE ESTIMATES OF DERIVED GEOTHERMAL GRADIENTS

Seismic Lines	Measured Geothermal Gradients		Normalized Geothermal Gradients	
	rho	Confidence Level	rho	Confidence Level
All	-0.18	not signif.	-0.03	not signif.
West	-0.26	80%	-0.13	not signif.
East	0.24	80%	0.37	95%

In Table 6 the non-parametric measure of correlation, rho, is listed along with significance estimates from published tables (Koch and Link, 1980; Davis, 1986). The rho values in Table 6 are analogous with the r values listed in Table 5,

with 0 indicating no correlation, 1 indicating a perfect direct correlation, and -1 indicating a perfect negative correlation.

Comparison of Tables 6 and 7 shows much lower significance of all postulated correlation, when the less restrictive, and perhaps more appropriate, nonparametric statistical methods are used to test the correlations. Table 6 shows that the general decrease in geothermal gradient to the east in the entire sample suite ("All" in Table 5) is not significant and could be attributed to random variation. The decrease in geothermal gradients postulated for the western set of lines from Point Barrow to near Camden Bay is assessed to be significant at a much lower confidence level in the nonparametric case (80% vs. 99%). When the normalized version of the western seismic suite is tested, nonparametric methods do not detect a significant correlation.

The only correlation which is significant for both the measured and normalized data suites is for the eastern group of lines (Table 6). The rho value of 0.24 for the calculated geothermal gradient values from these lines indicates a correlation that is significant at about an 80% confidence level (Figure 62). The significance of the correlation in the normalized data set is considerably greater, 95%.

Seismic Velocity Anomalies

Gas hydrate presence in marine sediments may be detected by anomalously high seismic velocities. Stoll (1974) and Paull and Dillon (1981) reported that the interval above the base of the gas hydrate stability zone showed measurably greater seismic velocities than underlying sediments on seismic lines from the Blake Outer Ridge. Shipley et al. (1979), however, reported no measurable high-velocity zone above the BSRs on a large number of multichannel seismic lines from around Atlantic, Gulf of Mexico, Caribbean, and Pacific margins. De Boer et al. (1985) similarly reported no measurable velocity anomaly above the base of the gas hydrate stability zone on proprietary seismic lines from around the word which exhibited distinct BSRs.

We have examined all available seismic velocity data from the 1977 cruise of the *S.P. Lee* (NOAA, 1983) to determine if visible BSRs display seismic velocity anomalies like those illustrated by Paull and Dillon (1983). Analysis of the interval seismic velocity at each of the 756 shot points for which data were released indicates no instance in which interval velocity decreased with depth. The situation described by Paull and Dillon (1983) of a high velocity hydrate-filled layer overlying a low velocity layer was thus not duplicated in the data from the Beaufort Sea study region. The vertical resolution of the stacking velocity intervals from the Beaufort Sea data set was apparently not sufficiently fine to differentiate any velocity anomalies from gas hydrates.

Eittreim and Grantz (1979) discussed the seismic velocity data from multichannel seismic lines collected in 1977 aboard the *S.P. Lee*. They used the anomalously low velocity of material coring one of the many diapirs on the Alaska continental margin to infer that the diapirs are cored by mobile shale rather than higher velocity salt. They also displayed a short segment of seismic line 3710 which showed velocity changes coincident with distinct sediment reflectors. The velocity

change seen at the about 5.8 seconds on the line segment (Figure 64) is similar in form to that reported by Paull and Dillon (1981) for gas hydrate filled sediments from the Blake Outer Ridge. A strong reflector at about 1.1 sec subbottom coincides with the velocity inversion. While the reflector is more than likely a sediment reflector, it may represent the base of the gas hydrate stability zone which is not marked by a distinct BSR due to the concordant relationship of the sediment layers and the sea floor in the abyssal plain of the Beaufort Sea.

The velocity data released from the 1977 cruise of the *S.P. Lee* (NOAA, 1983) do not agree with the interval velocities for representative lines from the Beaufort Sea study region published by Eittreim and Grantz (1979). They showed two velocity profiles, one on Line 714, the other on Line 3710 (Figure 64) where seismic velocity of an interval is less than that of an overlying interval. Publicly released velocity profiles for the two sections indicates that interval velocities increase regularly with depth. We assume that Eittreim and Grantz (1979) used a set of interval velocities more detailed than that available to the public in their work.

Subsea Permafrost

The gas hydrate stability zone in the Beaufort Sea study region is controlled by the thermal conditions of the offshore sediments. Other gas hydrate study regions have been shown to have simple thermal conditions which produce gas hydrate stability zones that increase regularly in thickness with water depth, e.g. offshore of Mexico (Finley and Krason, 1986b). The thermal structure of the continental margin of the Beaufort Sea is complicated by formation of permafrost in the sediments of the continental shelf during the Pleistocene.

Permafrost formed while the present continental shelf was subaerially exposed during the Wisconsin stage of glaciation affects the present thermal conditions of the shelf sediments. The 100 to 150 m drop in sea level during the most recent glaciation exposed the Beaufort continental shelf to very low temperature periglacial conditions. Of the very large area of the shelf exposed by the eustatic sea level change, it is probable that only the Mackenzie Trough may have been glaciated (Plate 2) (Hopkins, 1985). The low surface temperatures elsewhere on the shelf resulted in widespread formation of permafrost. Subsequent inundation of the Beaufort continental shelf by relatively warm ocean water has greatly increased the surface temperature of the continental shelf making permafrost presently unstable. However, the slow warming of the continental shelf sediments of the Beaufort Sea has permitted isolated patches of subsea permafrost to exist to the present. Patches of relict subsea permafrost beneath the Beaufort Sea continental shelf have been detected from seismic data (Morack et al., 1983; Neave and Sellmann, 1983), from electromagnetic soundings (Ehrenbard et al., 1983), and by drilling (Sellmann and Chamberlain, 1979: Weaver and Stewart, 1982).

The possible presence of gas hydrates beneath the base of the relict subsea permafrost is supported by analogy with onland occurrences and by well-logging data. Gas hydrates have been recovered from beneath permafrost on the North Slope of Alaska (Osterkamp and Payne, 1981). The presence of gas hydrates

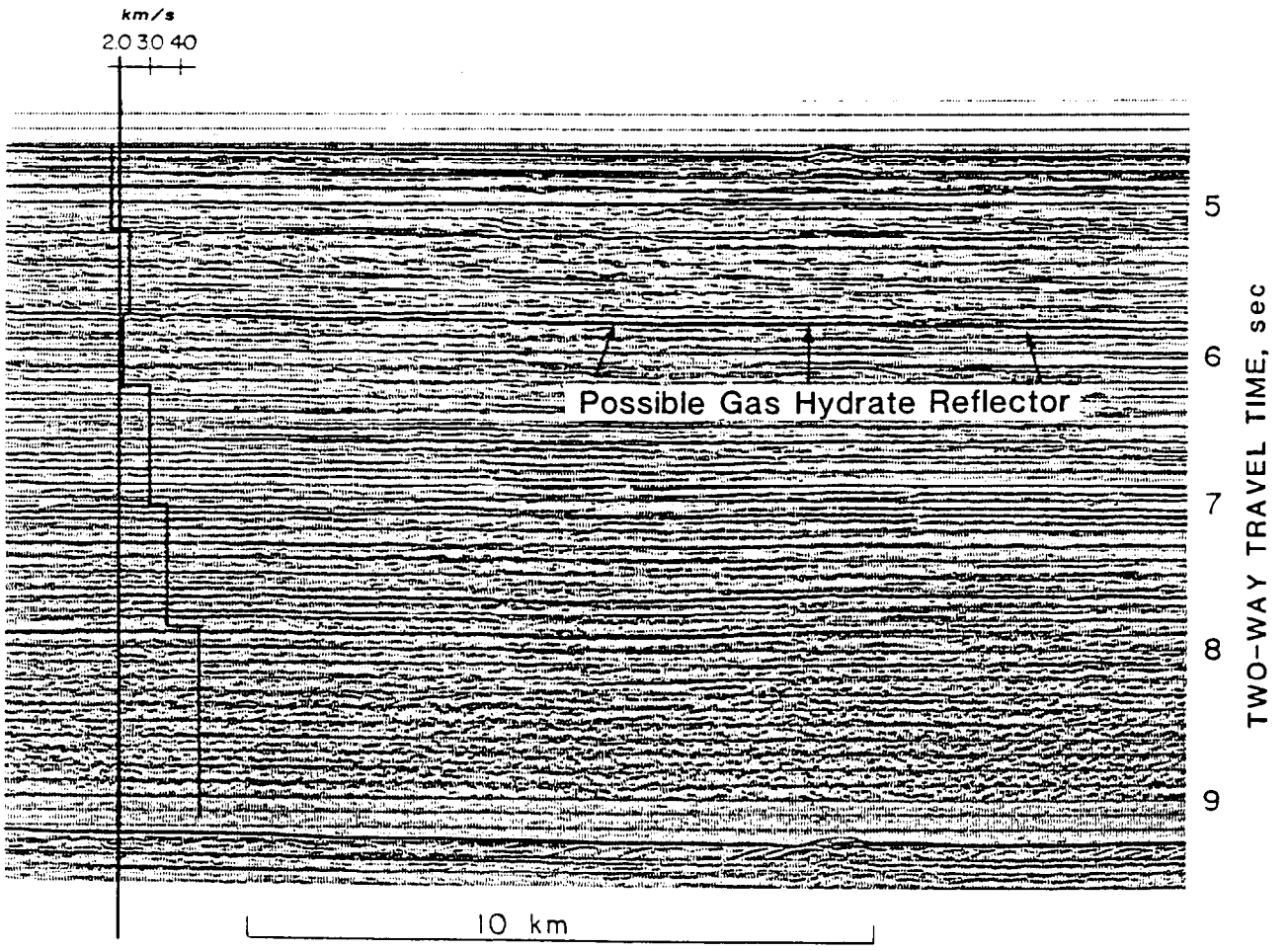

Figure 64. SECTION OF MULTICHANNEL SEISMIC LINE 3710 OFFSHORE OF CAMDEN BAY, ALASKA SHOWING POSSIBLE GAS HYDRATE VELOCITY ANOMALY

After Eittreim and Grantz, 1979

beneath permafrost has been inferred from well log data from the North Slope of Alaska (Osterkamp and Payne, 1981), the Mackenzie Delta of Canada (Bily and Dick, 1974), and the Canadian Beaufort shelf (Weaver and Stewart, 1982).

The presence of permafrost can greatly extend the range of environments where gas hydrates are stable. The net effect of subsea permafrost layer is to depress the sediment temperature far below typical for a given subbottom depth. In typical deep sea sediment, the temperature is at a minimum at the seafloor and increases with depth at a rate of 2° to 4° per 100 m. A subsea permafrost layer results in a reversal of this situation; the sediment temperature decreases from the seafloor to the permafrost, and increases with depth only beneath the permafrost. Increased sediment temperature due to geothermal heating typical limits the gas hydrate stability zone to the upper 300 to 800 m of deep sea sediments. Likewise, low confining pressures beneath shallow water columns also typically limits the gas hydrate stability zone to sediments beneath water 400 to 700 m deep. Since subsea permafrost indicates very low temperatures deep in the sediment column, the gas hydrate stability conditions of low temperature and high pressure can be achieved in shelf sediments beneath water much shallower than the generally accepted minimum for gas hydrate stabilization.

The gas hydrate stability model discussed in a previous section can be used to estimate the degree of gas hydrate stabilization to be expected from subsea permafrost presence. Data from exploratory drill holes on the Beaufort shelf indicate significant overpressuring (Weaver and Stewart, 1982). The temperature at the base of ice-bound permafrost is typically -1 to -2°C (Sellmann et al, 1977). Either higher pressures or lower temperatures at the base of the subsea permafrost would tend to enhance gas hydrate stability. However, assumptions of hydrostatic pressure gradients through and beneath the permafrost layer, and a 0°C temperature at the base of the permafrost layer were applied in the modeling to obtain a conservative estimate of the effect of subsea permafrost on gas hydrate stability.

Modeling results indicate that gas hydrates can exist beneath subsea permafrost at shallow sea water depths (Figure 65). The lines on Figure 65 represent the thickness of the gas hydrate stability zone at various water depths for different depths to the base of the subsea permafrost. Figure 65 indicates that gas hydrates are stable to a minimum water depth of about 200 m beneath subsea permafrost whose base occurs at 50 m subbottom. Subsea permafrost to a subbottom depth of about 150 m is sufficient to stabilize underlying gas hydrates to the shallowest water depth modeled. Thus, the model indicates that when the depth of the base of the subsea permafrost zone is at least 150 m subbottom gas hydrate can exist beneath the subsea permafrost shoreward to the coastline.

Theoretical Studies

Mackay (1972) speculated that large areas of the Canadian Beaufort shelf may be underlain by subsea permafrost. Mackay (1972) used climatic and oceanographic data to support his contention that relict permafrost exists beneath the continental shelf of the Mackenzie Delta. He further suggested that the relatively warm water from the Mackenzie River would make subsea permafrost unlikely near the Mackenzie Trough. He proposed that nearshore areas east of the Trough may

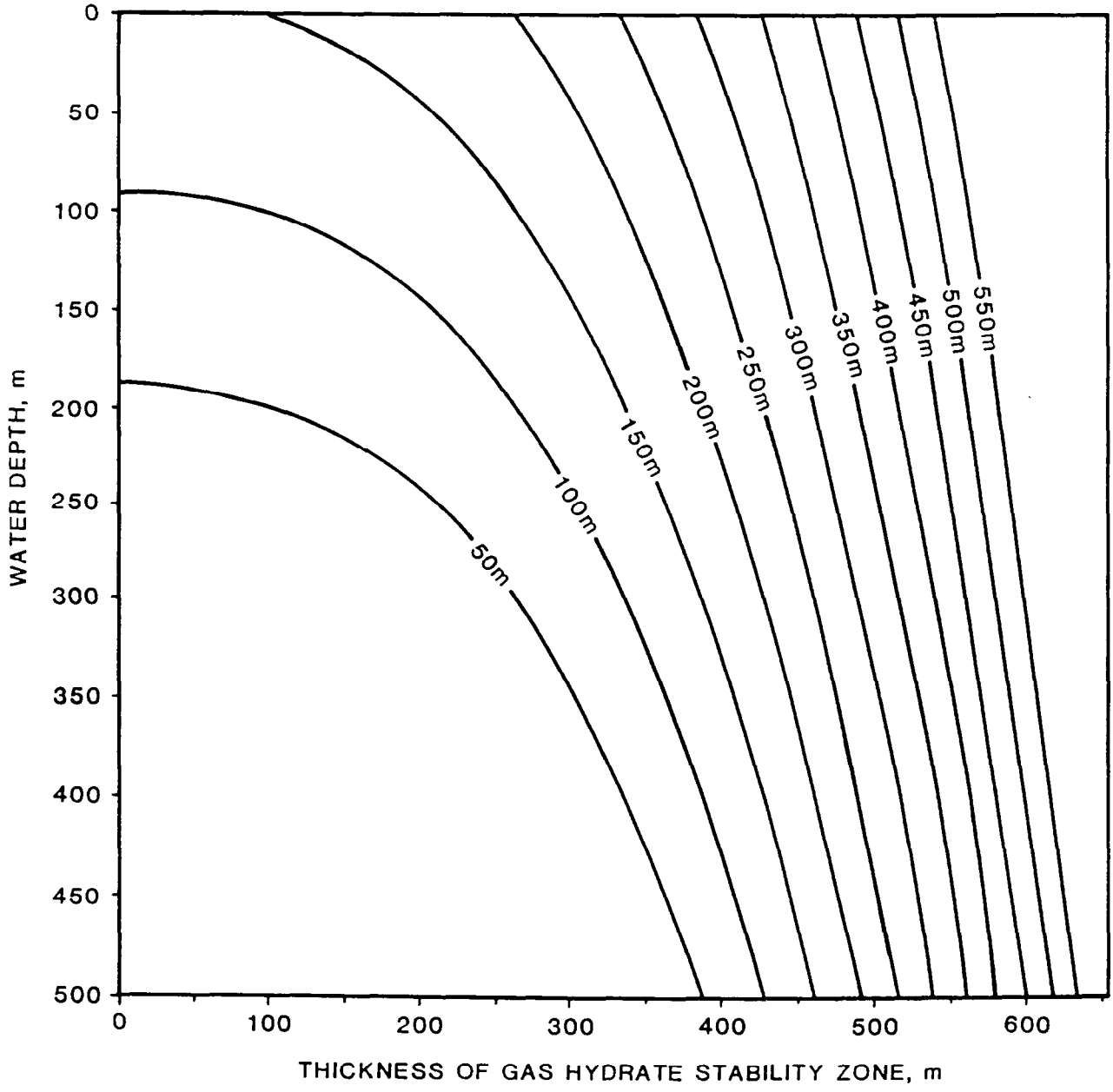

Figure 65. THICKNESS OF THE GAS HYDRATE STABILITY ZONE FOR DIFFERENT SUBBOTTOM DEPTHS OF THE BASE OF SUBSEA PERMAFROST

be underlain with seaward extensions of onland permafrost with expected thicknesses of 300 to 600 m.

Vigdorchik (1980) determined the potential for subsea permafrost on the Beaufort shelf offshore of Alaska by computer modeling. Vigdorchik (1980) combined measurements of water temperature, water salinity, seafloor sediment type, and isostatic, tectonic, and eustatic uplift to derive the likelihood for permafrost conditions. Using weighting factors to account for data reliability and relative importance of each factor, Vigdorchik (1980) produced a map showing high potential for permafrost at shallow subbottom depths at 5 locations on the Beaufort shelf. While these findings hold possible importance for engineering purposes, their direct relevance to hydrate stability is minimal, since as Figure 65 shows that the base of the permafrost must be in the 120 to 150 m subbottom depth range for substantial formation of methane hydrate to occur beneath the shallow waters overlying the shelf.

Based on his work on near-surface subsea permafrost, Vigdorchik (1980) did speculate on deep, relict permafrost beneath the Alaskan Beaufort shelf. Vigdorchik (1980) divided the Alaskan Beaufort shelf into three regions with respect to relict permafrost potential based principally on evidence of Quaternary subsidence, and hence potential for having been subaerially exposed to periglacial conditions during the Pleistocene.

The westernmost area defined by Vigdorchik (1980) extends from Point Barrow to just east of Prudhoe Bay. Vigdorchik (1980) projected that region to be "suitable" for relict permafrost. He speculated that relict subsea permafrost would exist from the shore to the 60 m isobath which occurs 60 to 80 km from the shoreline. The top of the permafrost was postulated to probably occur at 50 to 100 m subbottom with an average thickness of 100 to 120 m.

The central area of subsea permafrost potential between Prudhoe Bay and just west of Demarcation Bay (148°W to 142°W) has subsided much less and thus is less likely to have extensive relict subsea permafrost (Vigdorchik, 1980). Subsea permafrost in this region is projected to be limited to 18 to 22 km from the present coastline. Vigdorchik (1980) estimated that relict subsea permafrost within this zone would average 150 to 200 m tapering seaward to 30 to 50 m at the seaward limit.

The third area listed by Vigdorchik (1980) extends eastward from about Demarcation Bay (142°W). Because of low subsidence rates projected for the eastern area near the international boundary, relict subsea permafrost was estimated to extend no farther than 2 to 5 km offshore.

Seismic Surveys

The extent of subsea permafrost on the Beaufort shelf has been investigated by seismic refraction methods. Hunter (1973) mapped selected areas of the Canadian Beaufort shelf displaying unusually high seismic velocities. Since frozen sediments have much higher seismic velocities than do typical sediments, Hunter inferred that the high-velocity refractor was the top of a layer of ice-bonded permafrost.

Further work by Hunter et al. (1978, 1983) refined the seismic refraction methods for detecting the top of subsea permafrost and reported some success in determining the lower boundary. Coarse and fine-grained materials differ in their seismic responses at low temperatures. Ice forms more rapidly and to a greater degree in coarse sediment interstices (Hunter, 1973). Coarse sediments at very low temperatures display higher acoustic velocities than do silts and clays. The seismic velocity contrast between frozen and unfrozen material used in refraction studies to map permafrost thus depends not only on the temperature of the sediment, but also on its composition. Areas mapped as having high-velocity refractors indicative of ice-bonded subsea permafrost in the Canadian sector of the Beaufort Sea study region correspond to areas of the delta dominated by coarser grained material.

Hunter (1973) and Hunter et al.(1978, 1983) demonstrated that no seismic evidence of ice bonded subsea permafrost existed on the Canadian Beaufort shelf west of about 135°W (Plate 2) No high velocity refractors were found beneath water deeper than 90 m. Except for the difference in probable grain size of the sediments, no correlation of frozen and non-frozen areas of the shelf and documented structural or stratigraphic features was noted. Additionally, Hunter et al. (1978) reported that the top of the permafrost could be detected at depths of greater than 250 m. Two permafrost layers were detected over much of the Canadian Beaufort Sea (Figure 66). A shallow, thin layer at about 70 m subbottom was the more extensive. Over large areas of the shelf, the deeper layer with a top at between 120 and 250 , subbottom was estimated to have a thickness of greater than 30 m.

Hunter et al.(1983) mapped an area west of the principal permafrost occurrence which displayed seismic velocities which were anomalously high (>1,800 m/sec) but less than the threshold value they applied permafrost (2,500 m/sec). They suggested that the intermediate-velocity area was caused by partially frozen fine grained sediments or gas hydrates.

Rogers and Morack (1978) studied permafrost by seismic reflection and refraction immediately offshore of Prudhoe Bay. They were able to tie their geophysical data to drill holes nearshore to estimate the top of the permafrost to about 16 km offshore. The seismic methods and sources used produced different estimates of the depth to the top of the subsea permafrost layer. Generally the top of the ice-bonded permafrost zone dips seaward at about 1° reaching a subbottom depth of 100 to 150 m at 16 km from shore.

Neave and Sellmann (1978, 1984) reported on seismic evidence of permafrost beneath the Beaufort continental shelf offshore of Alaska. Their work relied on velocity determined from refraction analysis of lines from Harrison Bay and Prudhoe Bay. Neave and Sellmann (1978, 1984) demonstrated that a shallow high velocity layer exists beneath the seafloor from the shoreline to about 30 km north of Prudhoe Bay. The shallow high-velocity zone extended about 40 km to the east and west of Prudhoe Bay (Figure 67). Additionally, a shallow high velocity zone was mapped along the extreme western part of Harrison Bay averaging 10 km from the shoreline to its seaward limit.

A deep high velocity zone was mapped by Neave and Sellmann (1978, 1984) beneath the eastern half of Harrison Bay (Figure 67). the refractor dipped about 3°

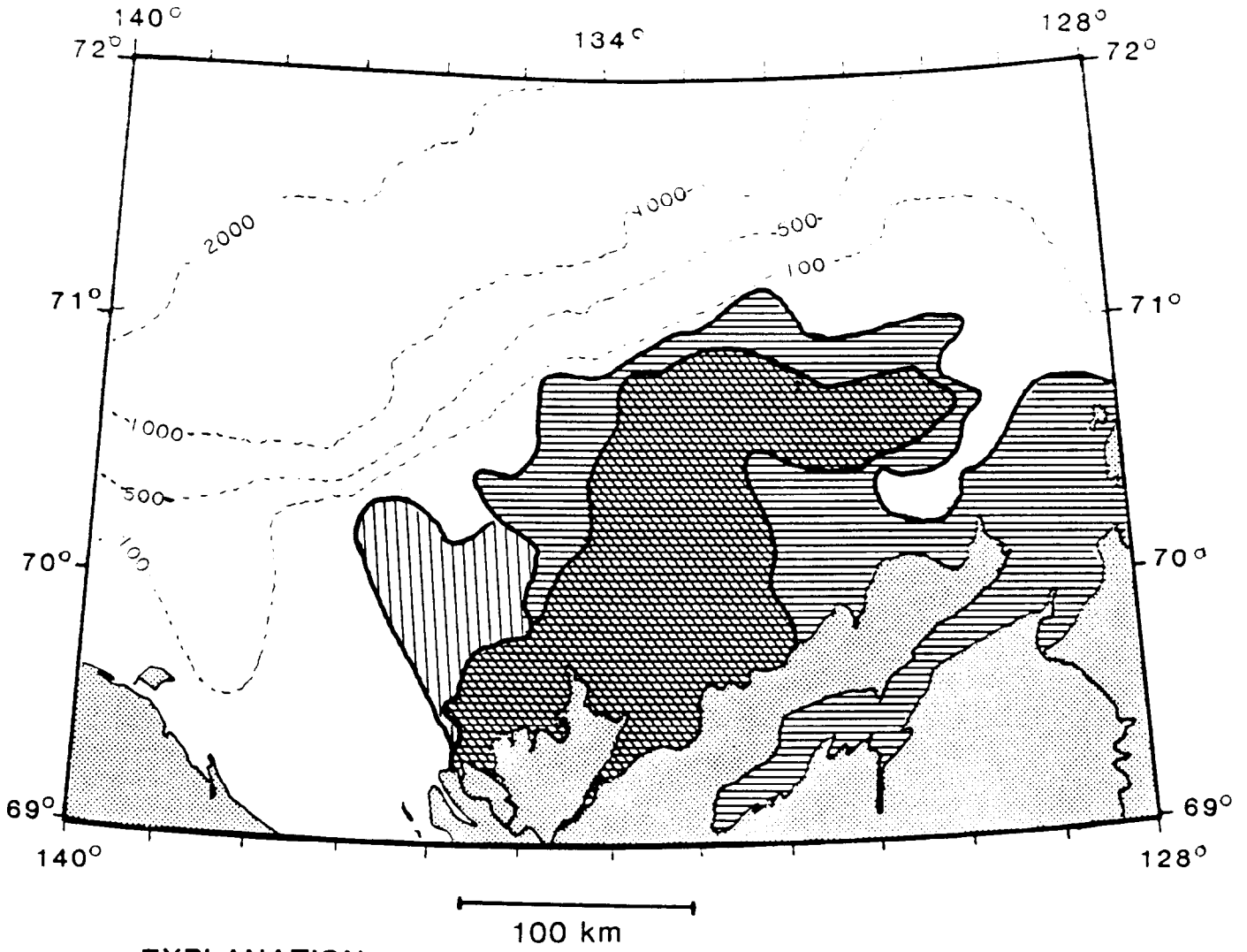

Figure 66. **DISTRIBUTION OF SEISMIC VELOCITY ANOMALIES, CANADIAN BEAUFORT SHELF**

After Hunter et al, 1978, 1983

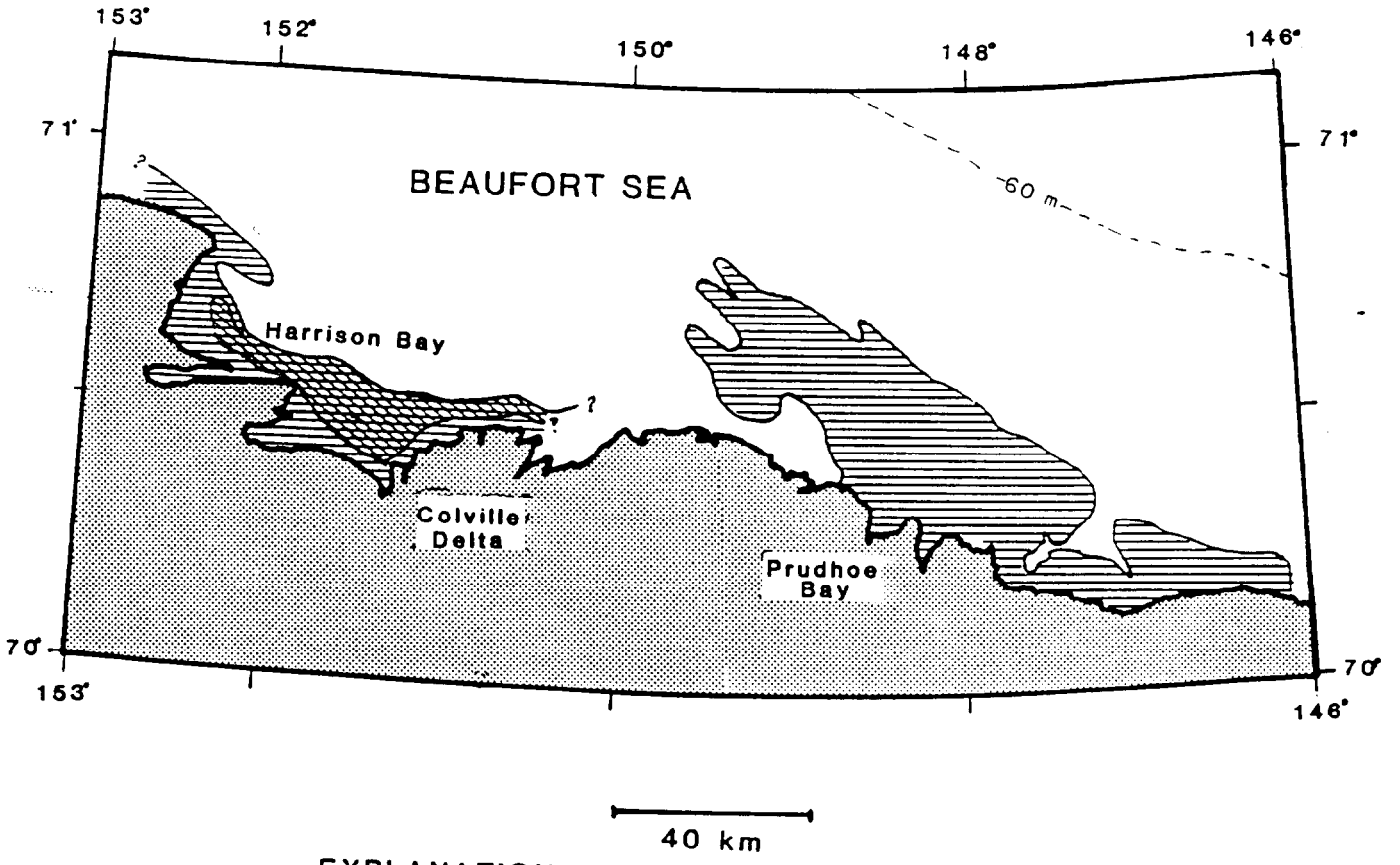

Figure 67.

DISTRIBUTION OF SEISMIC VELOCITY ANOMALIES, ALASKAN BEAUFORT SHELF

Adapted from Neave and Sellmann, 1984

seaward to a maximum depth of 200-300 m and disappeared about 15 km from the shoreline.

Neave and Sellmann (1984) used reflection seismic data from farther out on Beaufort shelf to augment their nearshore refraction work. They noted three persistent reflectors in seismic lines from north of Harrison Bay and Prudhoe Bay. Reflectors at 200, 450 m, and 750 m sub-sea level corresponding to 0.3, 0.6, and 1.0 sec two-way travel time using their assumed sediment velocity of 1,500 m/sec, could be traced for up to 60 km across the continental shelf beneath water as deep as 100 m. Neave and Sellmann (1983, 1984) interpreted these reflectors as boundaries between frozen and unfrozen sediment. they projected that the reflector at 200 m coincides with the nearshore high-velocity layer at about the same depth which was mapped as the top of the frozen sediments by refraction. They further postulated that the 450 m reflector corresponded to the base of the permafrost zone. They offered no explanation for the 750 m reflector but inferred that it was somehow permafrost related. Neave and Sellmann (1983, 1984) assumed that the reflections were caused by permafrost but did mention that they could alternatively been persistent sediment reflectors.

Electromagnetic Surveys

The top of the subsea permafrost zone can often be mapped using seismic methods. However the depth of the base of the permafrost layer is not reported in published results of seismic surveys. The depth of the base of the subsea permafrost zone is the of importance for assessing the extent of gas hydrates. If the base of the subsea permafrost layer is more than about 140 m, methane hydrate could exist beneath the permafrost beneath very shallow ocean depths (Figure 65).

Mapping of subsea permafrost from seismic data relies on increases in seismic velocity in frozen sediments. In addition to seismic velocity, resistivity of sediments increase exponentially with interstitial ice content (Houkstra, 1975). Concurrently high values of sonic velocity and resistivity are used to delineate intervals containing permafrost from well logs (e.g. Osterkamp and Payne, 1981).

Recent developments in the methodology of electrical surveying produce data on subsurface resistivity with good vertical and lateral resolution. Transient electromagnetic sounding methods are capable of resolving resistivity changes at both the top and the bottom of subsea permafrost layers (Ehrenbard et al., 1983; Rozenberg et al., 1985). A cross-section of a transient electromagnetic survey from near Prudhoe Bay extending 8 km beneath the Beaufort Sea shows the interpreted thickness and depth of the permafrost zone (Figure 68).

Drilling Results

Weaver and Stewart (1982) reported data on subsea permafrost obtained from exploratory drilling on the Canadian Beaufort shelf. Depths to the base of permafrost were presented for 10 wells: Tarsiut, Orvilruk, Nektoralik, Kopanoar, Koakoak, Kenalooak, Nerlerk, Ukalerk, Kagluik, and Kilannak. The depths to base of permafrost reported by Weaver and Stewart (1982) for the 10 wells are plotted on

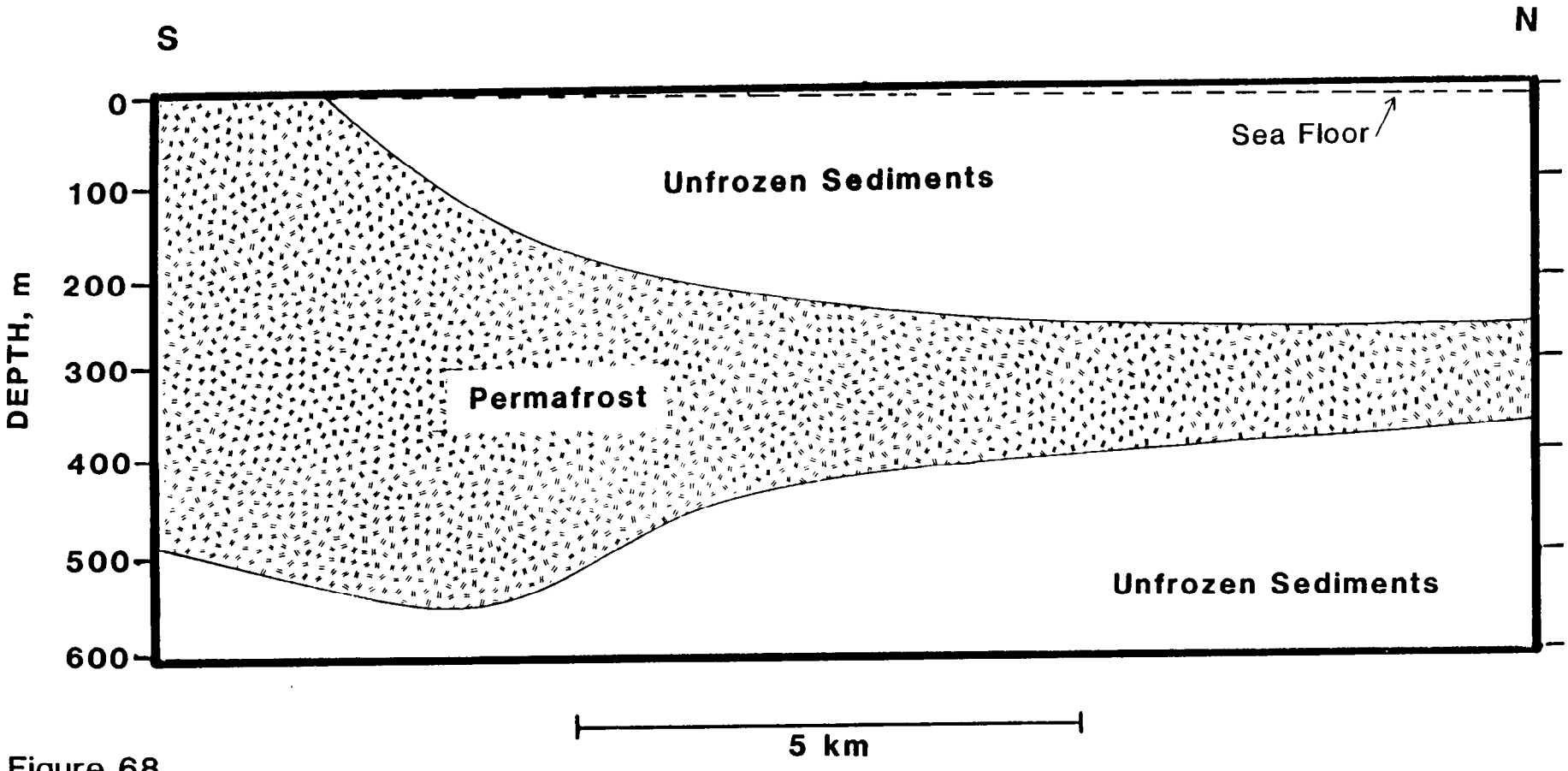

Figure 68.

THICKNESS OF PERMAFROST BENEATH THE CONTINENTAL SHELF NEAR PRUDHOE BAY FROM TRANSIENT ELECTROMAGNETIC SURVEY

After Ehrenbard et al., 1983

Figure 69 along with provisional contours suggested by the data. The map shows a zone with thick permafrost (680 to 780 m) due north of Kugmallit Bay. To the east and west permafrost depths shoal to 400 m.

Formation temperature and pressure data were combined by Weaver and Stewart (1982) to yield estimates of the gas hydrate stability field at each well. Pressure, temperature, and calculated hydrate stability fields are shown for four representative wells (Nerlerk, Koakoak, Ukalerk, and Kopanoar) are shown in Figures 70 and 71. Each well has pressure gradients substantially greater than hydrostatic (approximate 10 kPa/m) beneath the permafrost. These overpressured zones beneath the permafrost stabilize gas hydrates, allowing hydrates to exist at higher temperatures than is the sediments were under hydrostatic pressure conditions. Thus, the pervasive overpressuring of sub-permafrost sediments results in the zone of hydrate stability being substantially thickened beneath the permafrost on the Canadian Beaufort shelf. Neither formation temperature nor geopressure gradients were explicitly reported for all 11 wells. Data reported on the depth to the base of the gas hydrate stability zone (Table 7) can be used to generate of the calculated thickness of the gas hydrate zone (Figure 72). The map of the thickness of the gas hydrate stability zone (Figure 72) is similar to that for the depth to the base of the permafrost (Figure 69). Thicker permafrost indicates that low temperatures exist at greater depths with concomitant high pressures; the greater pressures at a given temperatures beneath the thicker permafrost zones enhances gas hydrate stability producing a thicker gas hydrate stability zone.

Weaver and Stewart (1982) published portions of the well logs from the four holes for which hydrate stability depths were calculated. In addition, Weaver and Stewart (1982) presented the depth intervals at which permafrost and hydrates were actually observed, and the calculated zone of gas hydrate stability.

Figure 73 shows the well log records from the Nerlerk well. The resistivity log show a sharp decrease at about 670 m depth. At the same depth the caliper log assumes a relatively constant value in contrast to the washouts encountered up hole. Both of these indicators suggest the base of a frozen zone, either hydrates or permafrost, occurs at 680 m depth. the sonic log, shows a distinct increase in velocity (decrease in sonic travel time) at the same general depth. The sonic log from Nerlerk contradicts the initial conclusions of frozen material above 680 m; both permafrost and gas hydrates typically cause increases in sonic velocity (Mathews, 1983). The drilling fluid was devoid of hydrocarbon gases to a depth of about 510 m where it began to increase regularly with depth, reaching a maximum of 6,000 units at 680 m.

Weaver and Stewart (1982) apparently did not recover any hydrates from the Beaufort shelf wells. They instead relied on well logs to establish hydrate presence. Their approach was that an interval that was within the gas hydrate stability zone calculated from temperature and pressure with geophysical log properties similar to permafrost, but with abundant drilling gas indicated hydrate presence. Except for scattered peaks, the sonic log from Nerlerk was not consistent with frozen material above 680 m depth. But temperature measurements, caliper logs, and resistivity values indicate that some of the pore water is present in the solid phase. The column on the far right of Figure 73 indicate the interpretations of Weaver and

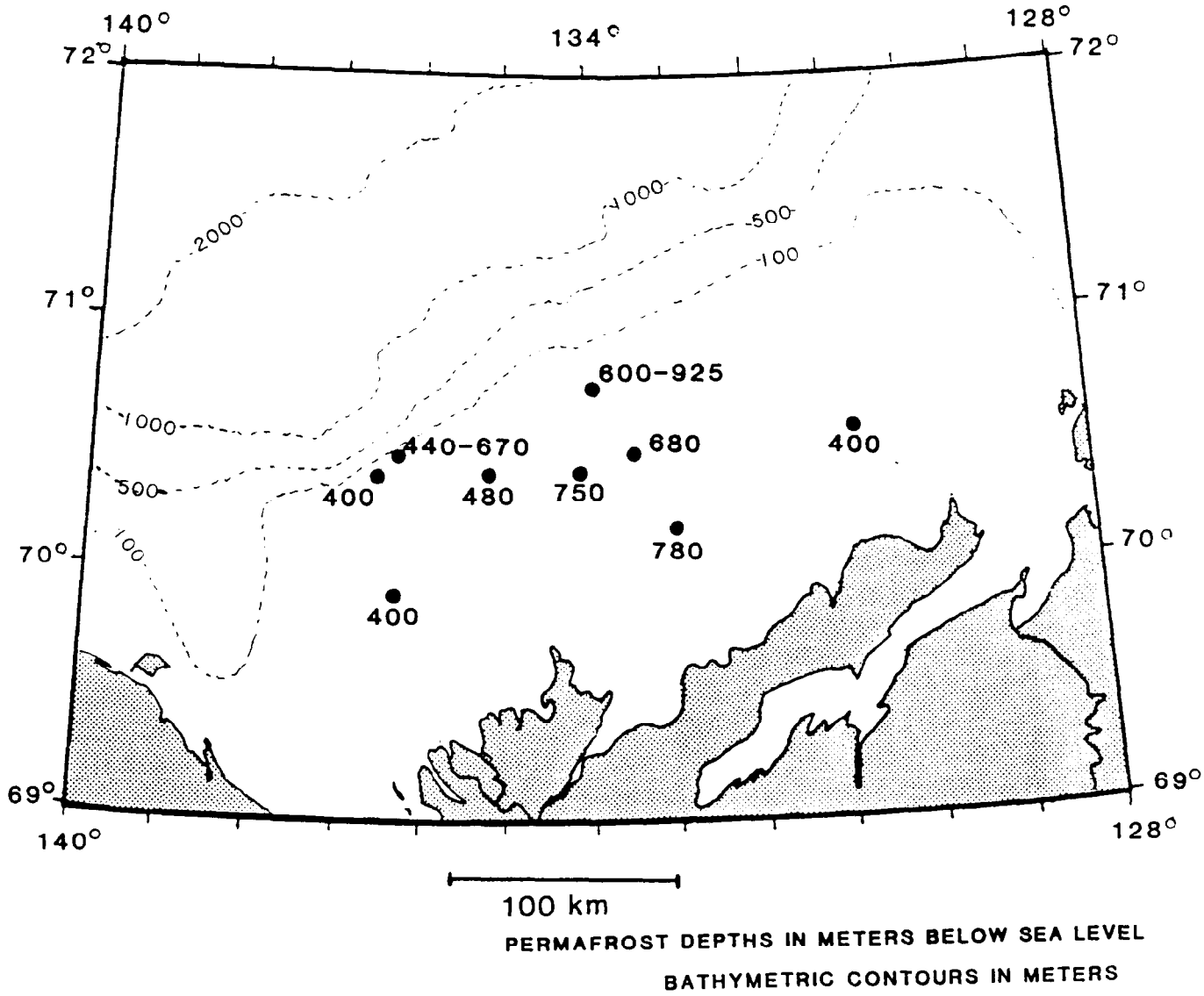

Figure 69. **DEPTH TO BASE OF PERMAFROST FROM EXPLORATORY DRILLING, CANADIAN BEAUFORT SHELF**

Data from Weaver and Stewart, 1982

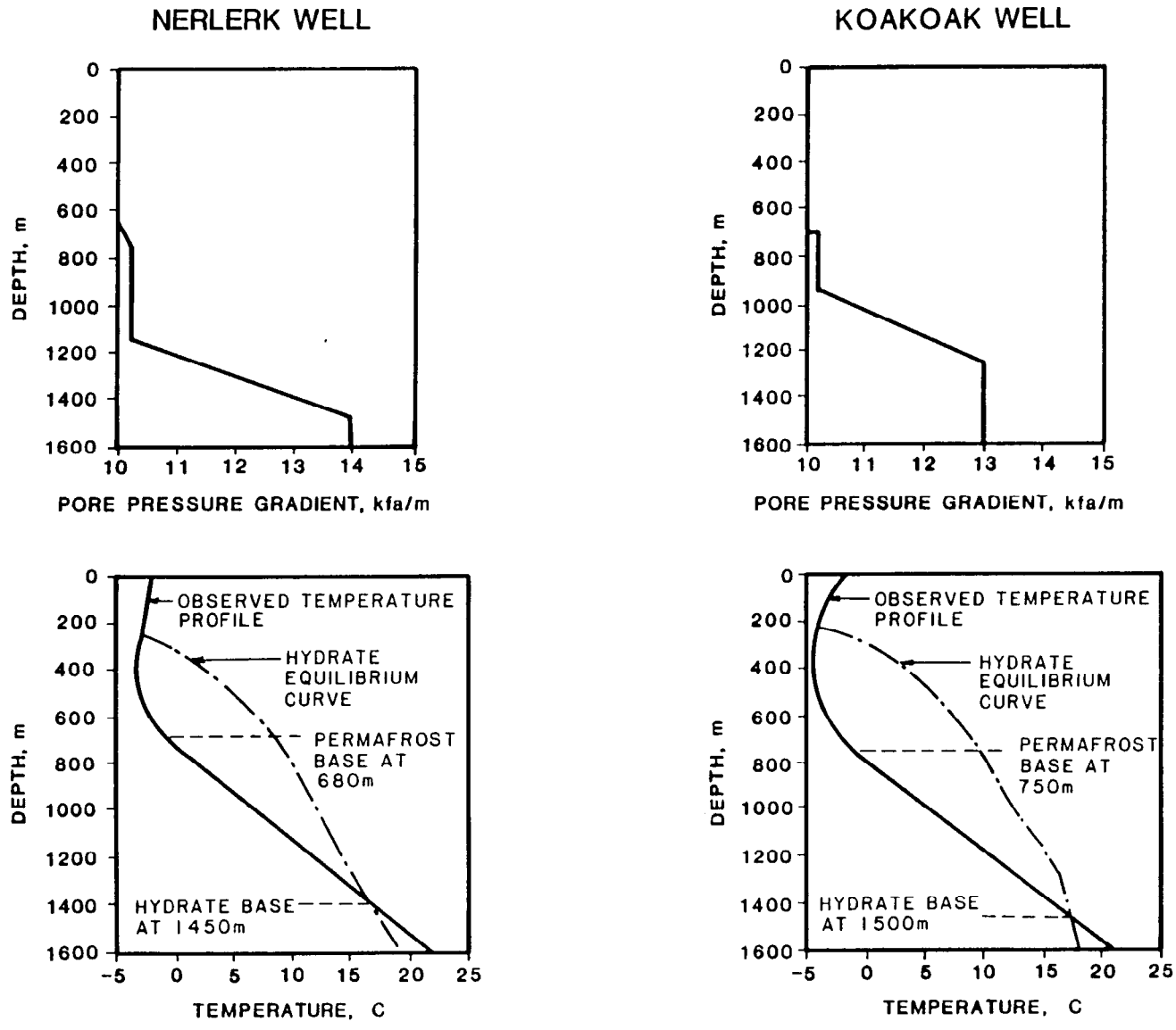

Figure 70. PORE PRESSURE, TEMPERATURE, AND CALCULATED GAS HYDRATE STABILITY CONDITIONS, NERLERK AND KOAKOAK WELLS, BEAUFORT SEA OFFSHORE OF CANADA

After Weaver and Stewart, 1982

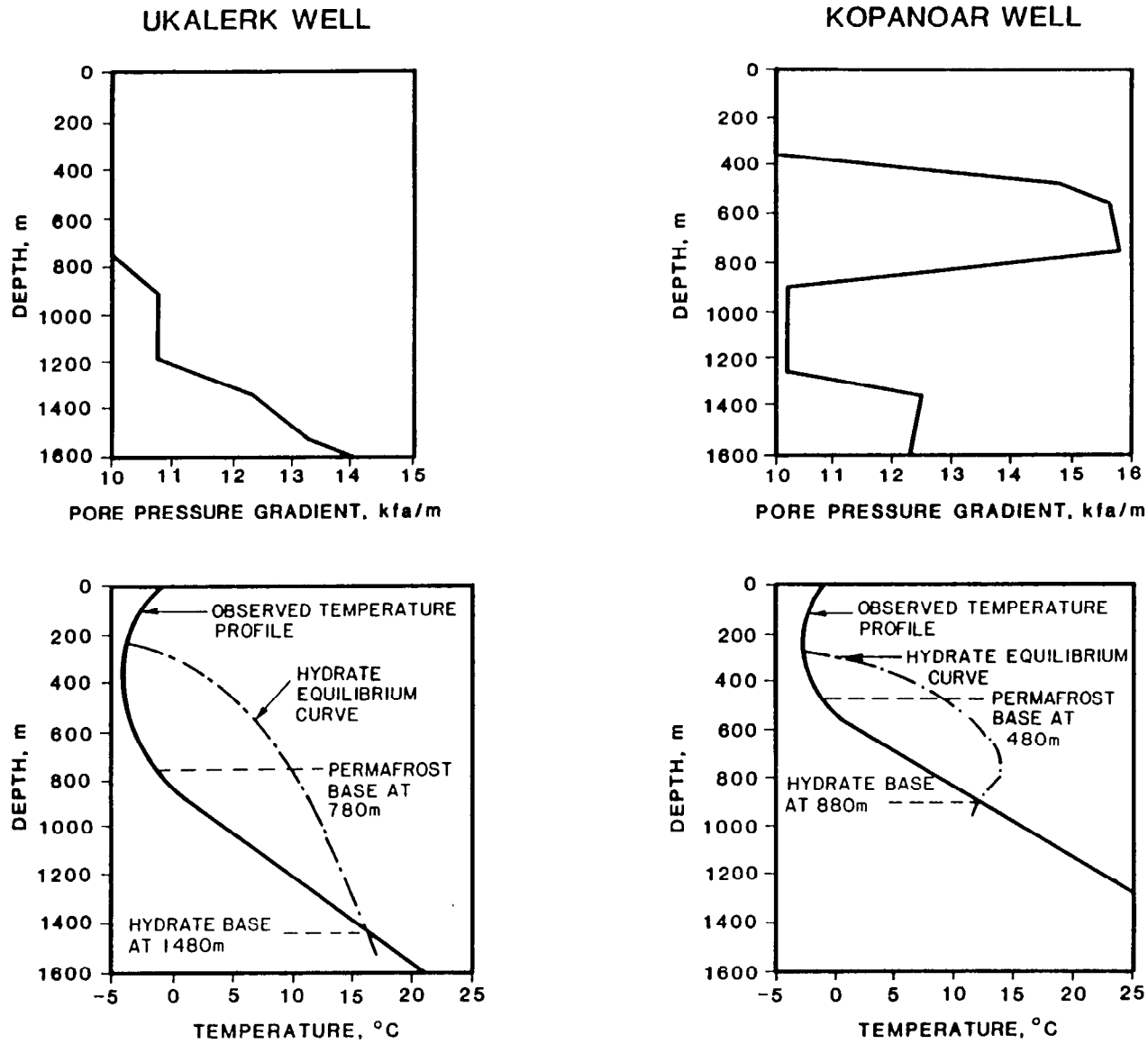

Figure 71. PORE PRESSURE, TEMPERATURE, AND CALCULATED GAS HYDRATE STABILITY CONDITIONS, UKALERK AND KOPANOAR WELLS, BEAUFORT SEA OFFSHORE OF CANADA

After Weaver and Stewart, 1982

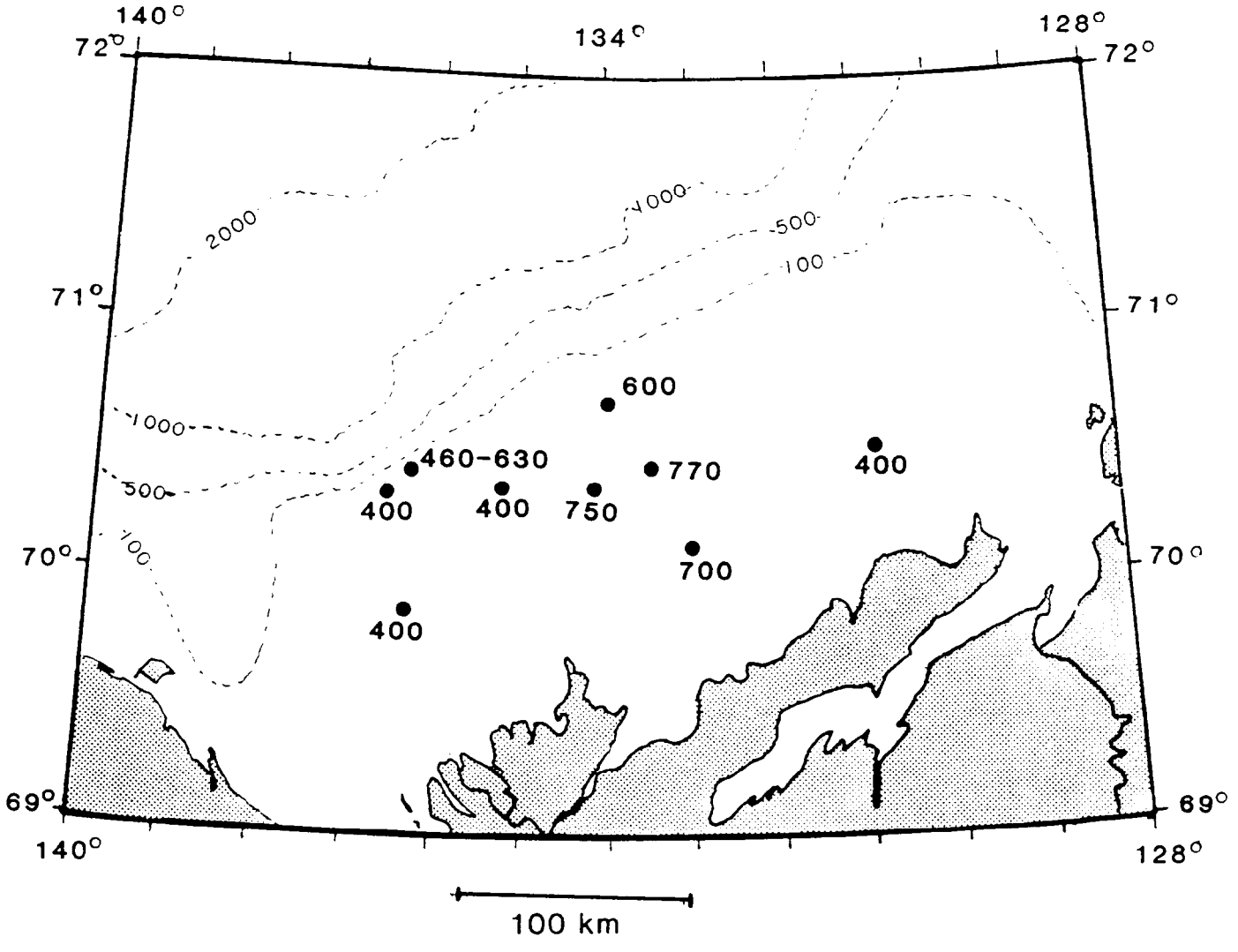

BATHYMETRIC CONTOURS AND GAS HYDRATE ZONE THICKNESS IN METERS

Figure 72. CALCULATED GAS HYDRATE STABILITY ZONE THICKNESS CANADIAN BEAUFORT SHELF

Data from Weaver and Stewart, 1982

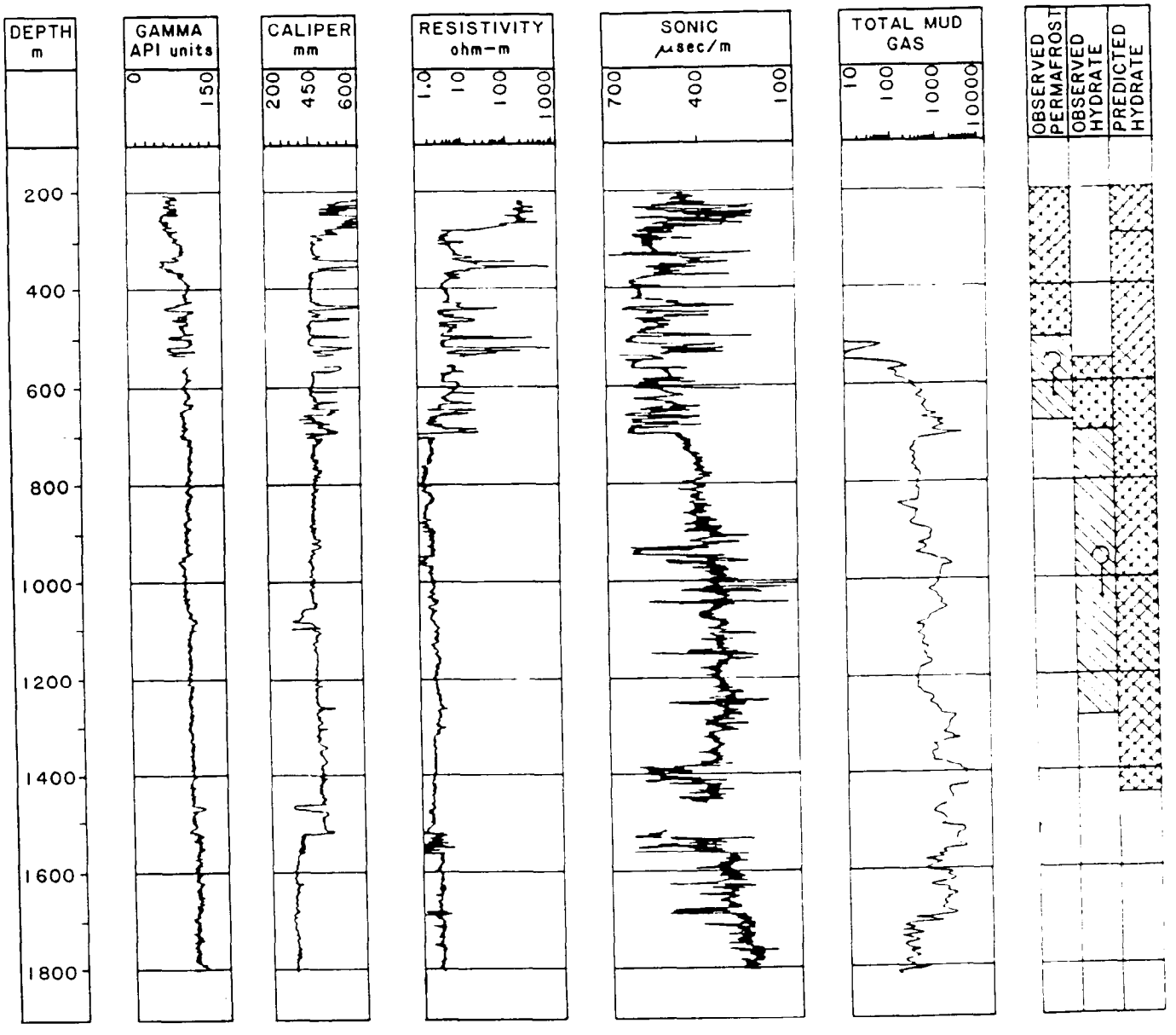

Figure 73. WELL LOGS AND PERMAFROST AND GAS HYDRATE OCCURRENCES, NERLERK WELL, BEAUFORT SEA OFFSHORE CANADA

After Weaver and Stewart, 1982

Stewart (1982) that the interval with high resistivity and abundant gas between about 530 m and 680 m depth contained hydrates.

Table 7.

DEPTH OF PERMAFROST BASE AND PREDICTED DEPTH AND THICKNESS OF GAS HYDRATE STABILITY ZONE BENEATH CANADIAN BEAUFORT SHELF

Adapted from Weaver and Stewart (1982)

Well	Base of Permafrost (m below s.l.)	Predicted Base of Hydrate Zone (m below s.l.)	Predicted Thickness of Hydrate Zone (m)
Tarsiut	400	800	400
Orvilruk	400	800	400
Nektoralik	440-670	900-1300	460-630
Kopanoar	480	880	400
Koakoak	750	1500	750
Kenalooak	600-925	1200-1560	600-630
Nerlerk	680	1450	770
Ukalerk	780	1480	700
Kagluik	400+	800+	400
Kilannak (not located)	300	700	400

Logs from the Koakoak well are more equivocal with regard to gas hydrate presence. Caliper and resistivity logs indicate some permafrost at depths of less than about 750 m (Figure 74). The lack of a sharp break at the base of the apparent permafrost, and abundant low resistivity material suggest that the permafrost occurs in lenses which become less abundant at depth. The lack of a sonic log through the interval of interest complicates interpretation of the possible presence of permafrost. Some low levels of gas (less than 100 units) occur between 200 and 500 m depth, but higher levels do not occur until depths of 800 m and more are reached. Weaver and Stewart (1982) project a permafrost zone to 750 m. The isolated gas-bearing units within the permafrost zone between 250 and 500 m are suggested to be caused by isolated hydrate zones. Beneath the permafrost base at 750 m, the geophysical logs do not indicate high velocity, high resistivity material that suggest extensive hydrate development. However, the zone does transfer gas to the drilling mud and is within the calculated gas hydrate stability zone to a depth of about 1450

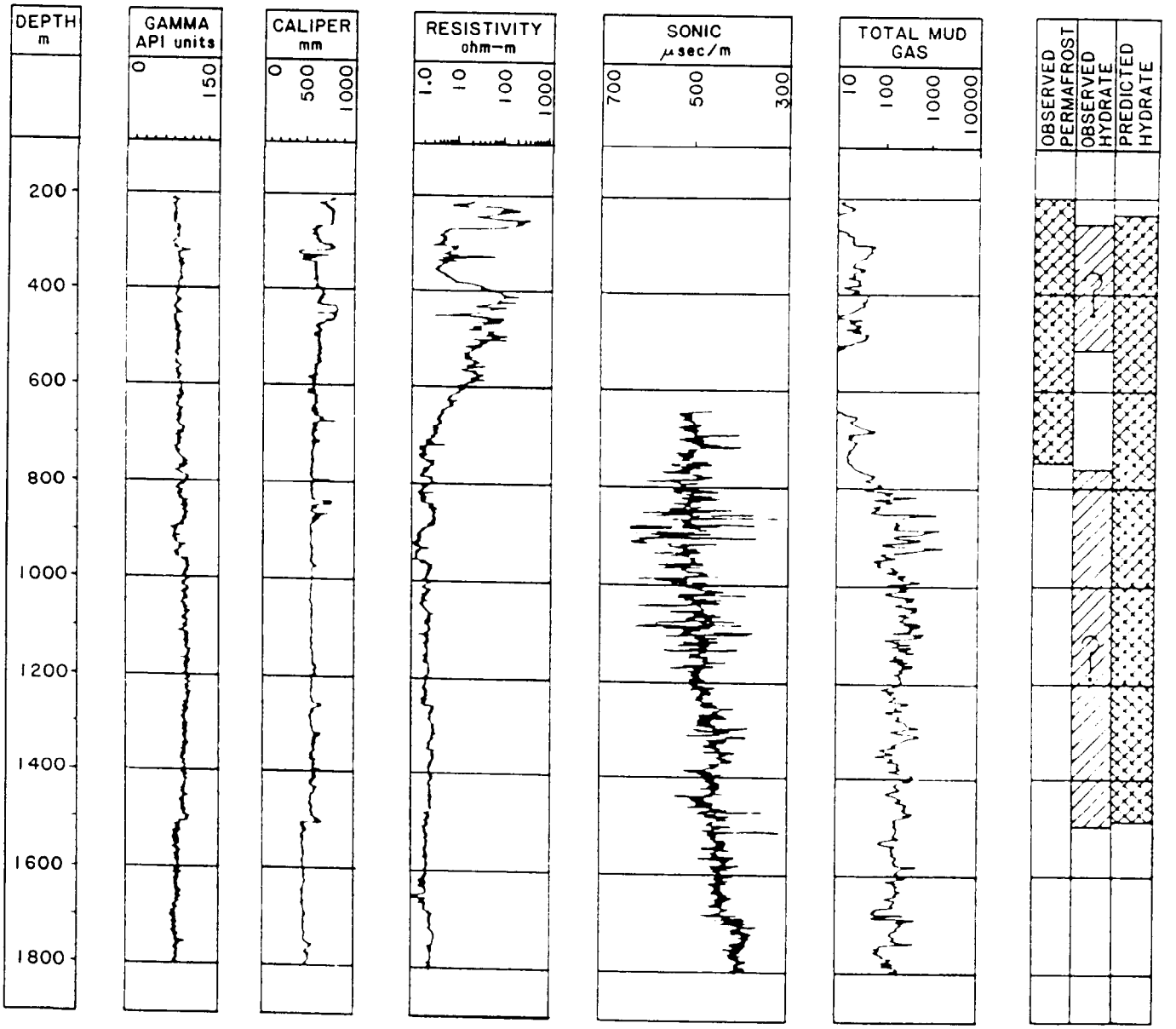

Figure 74. **WELL LOGS AND PERMAFROST AND GAS HYDRATE OCCURRENCES, KOAKOAK WELL, BEAUFORT SEA OFFSHORE CANADA**

After Weaver and Stewart, 1982

m leading Weaver and Stewart (1982) to project that some isolated gas hydrate may exist in the zone. No change in any of the logs from Koakoak are seen at the calculated base of the stability zone.

Logs from the Ukalerk well show the concurrently high resistivity and sonic log values expected for ice-bonded permafrost above about 710 m (Figure 75). Somewhat elevated values of resistivity and sonic velocity are recorded between about 710 and 780 m suggesting that permafrost may also occupy this interval. Gas content increases from 0 at about 650 m and ranges from about 50 units to 100 units throughout the hole. Once again the gas-rich zones beneath the base of the permafrost at the Ukalerk do not generally have the geophysical signatures which would suggest hydrates; only the correspondence of elevated gas content within the calculated gas hydrate stability zone suggest their presence.

One interval between about 1,170 and 1,200 m depth at Ukalerk does show geophysical and mud gas signature expected of a zone with extensive gas hydrate pore occupancy (Figure 75). Concurrently elevated caliper, resistivity, sonic, and mud gas strongly suggest an isolated zone of gas hydrates in the sediments.

Well logs and the interpretations of Weaver and Stewart (1982) are shown in Figure 76 for the Kopanoar well. The lack of any well logs from depths of less than 700 m complicate interpretations of possible permafrost or gas hydrate presence. Weaver and Stewart (1982) have interpreted the base of the permafrost zone to occur at about 480 m. It is assumed that they had access to the missing logs or that temperature readings from the well located the permafrost base. Well logs show a washout zone between 700 and 740 m with very high resistivity and sonic velocity values and a moderate gas content. Weaver and Stewart (1982) interpret this zone as a hydrate zone. The resistivity log from Kopanoar drops to a consistent low value at about 750 m suggesting that frozen material (hydrates according to the interpretation of Weaver and Stewart) does not occur at greater depths. However the high-velocity spikes on the sonic log continue to nearly 1,000 m depth, implying that hydrates may occur in the low-resistivity interval between 750 m and 1,000 m depth. Mud gas content through the high-velocity interval is elevated, and most of the interval is within the calculated gas hydrate stability zone. Weaver and Stewart (1982) interpreted the high-velocity, gassy zone between 750 and 1,000 m depth as possibly containing hydrates (Figure 76).

Data presented by Weaver and Stewart (1982) showed a rough correspondence of overpressured zones and intervals in which hydrates are either inferred from logs or calculated from temperature and pressure data. Pore pressure gradients from Nerlerk show a slight increase at about 640 m and a constant gradient to about 1,150 m. The gradient then rapidly increases to about 140% of hydrostatic at about 1,500 m depth. The initial increase does occur close to the base of the possible hydrate zone delineated by resistivity and caliper measurements at about 680 m. The rapid increase in pore pressure at 1,150 m is reasonably close to the calculated base of the gas hydrate stability zone. The argument could be made that the overpressure is a result of methane produced by dissociating hydrates. In the example of Nerlerk some increases in pore pressure were found to approximately align with both the base of gas hydrates seen on logs and the base of the calculated hydrate zone.

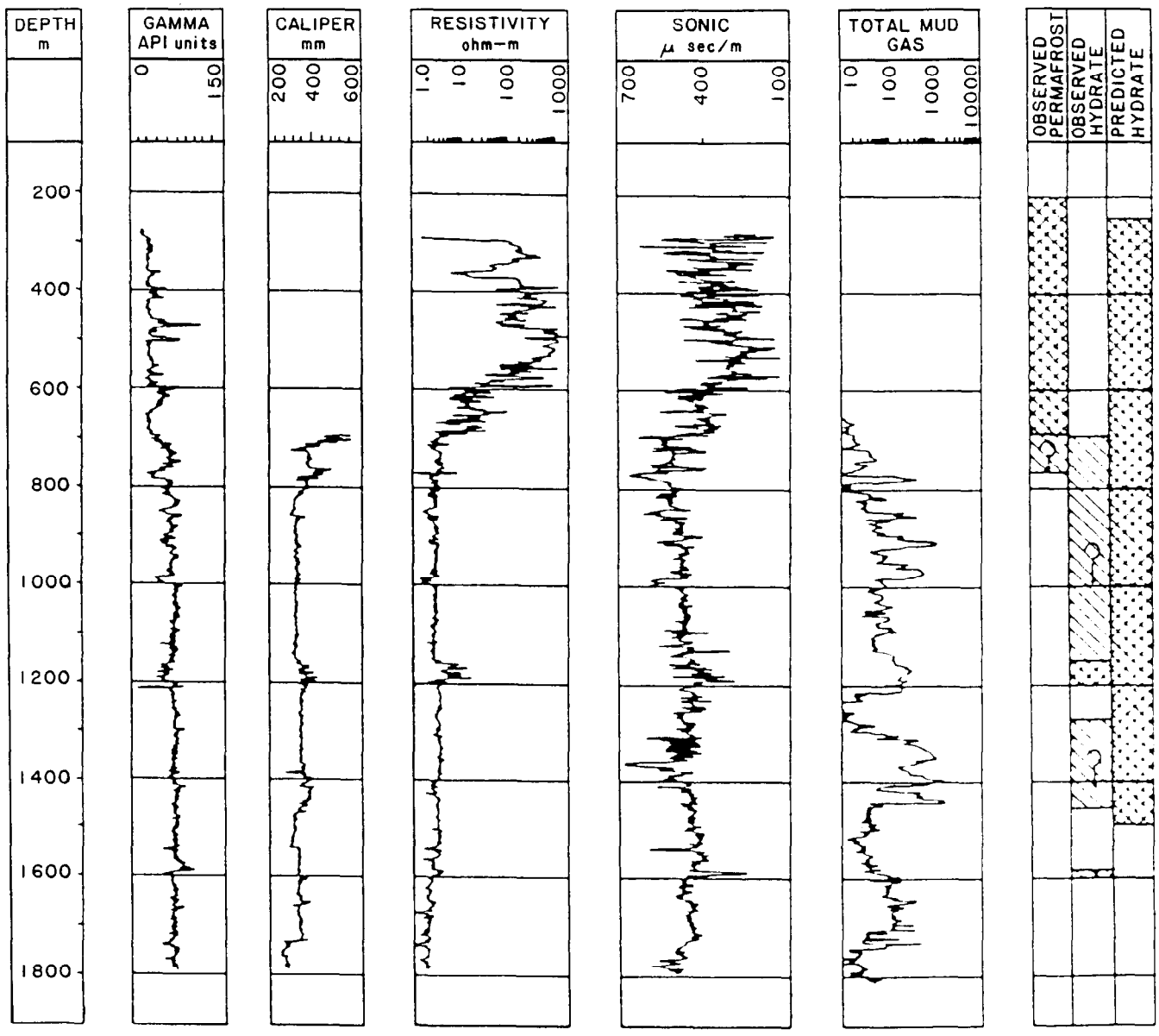

Figure 75. WELL LOGS AND PERMAFROST AND GAS HYDRATE OCCURRENCES, UKALERK WELL, BEAUFORT SEA OFFSHORE CANADA

After Weaver and Stewart, 1982

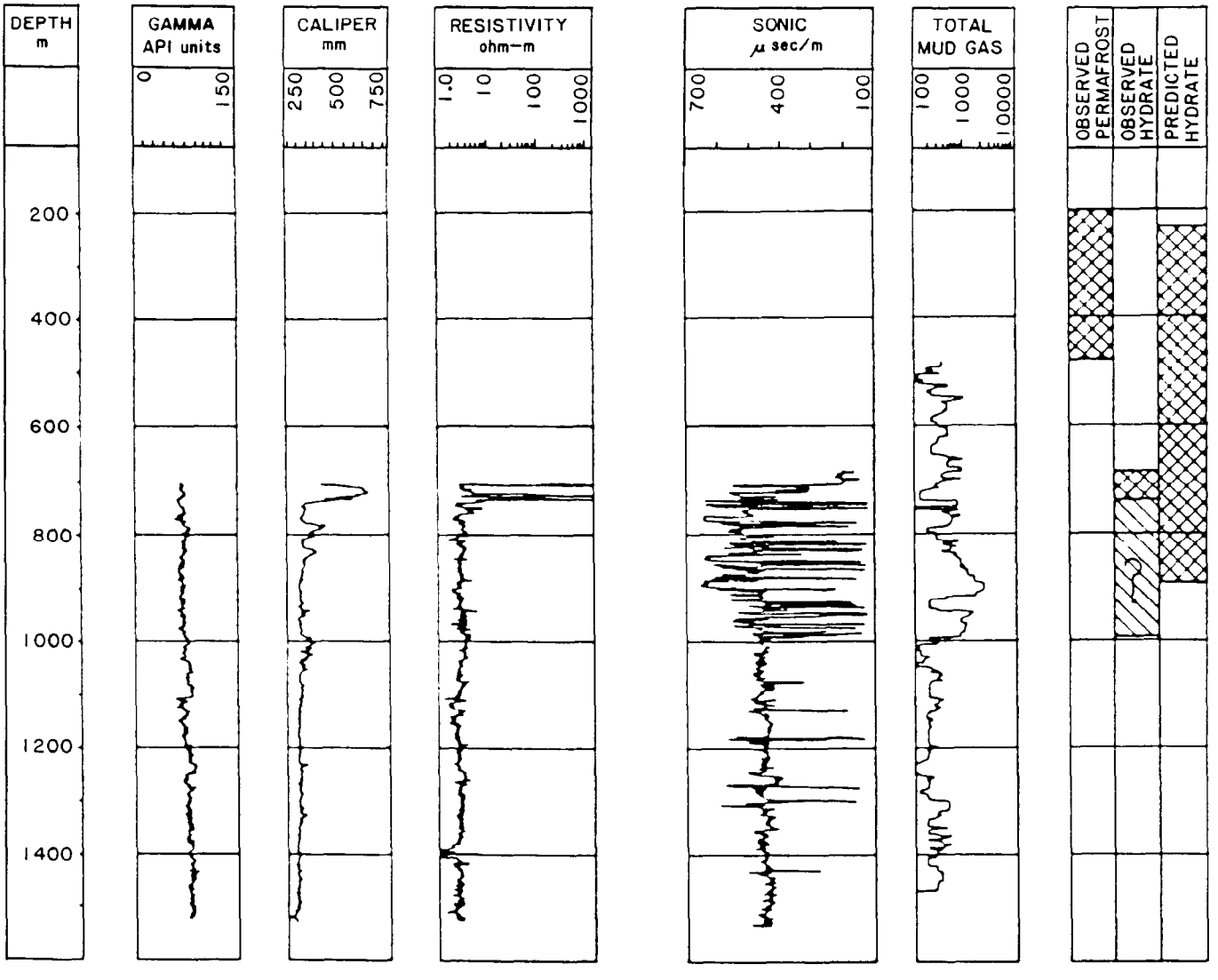

Figure 76. WELL LOGS AND PERMAFROST AND GAS HYDRATE OCCURRENCES, KOPANOAR WELL, BEAUFORT SEA OFFSHORE CANADA

After Weaver and Stewart, 1982

The pore pressure gradient diagram of Koakoak (Figure 70) is qualitatively similar to that of Nerlerk. The initial deviation from hydrostatic occurs at about 700 m depth and continues at perhaps 3% greater than hydrostatic to about 950 m. The pore pressure gradient then increases rapidly to about 30% greater than hydrostatic at about 1280 m depth. The shallower increase in pore pressure is in the same region as the base of the hydrate layer. The sharp increase in pore pressure at 950 m and the leveling off at 1,280 m occur within the calculated gas hydrate stability zone with no particular well-log expression.

The pore pressure gradient diagram of Ukalerk (Figure 71) also displays a pattern of progressive increases marked by steps. The initial deviation from hydrostatic occurs at about 770 m depth, close to the depth of the base of the permafrost layer. An inflection point in the pore pressure graph occurs at about 1,190 m depth where the pore pressure gradient begins to rapidly increase from a consistent pressure of 10% in excess of hydrostatic (11 kPa/m) to 30% greater than hydrostatic (13 kPa/m). The depth of that inflection does agree with the approximate depth of a 50 m thick high-resistivity, high-velocity washout zone with abundant mud gas which is very likely a gas hydrate interval. Another inflection of much lesser magnitude occurs at about 1,500 m near the calculated depth of the base of the gas hydrate stability zone.

A much more complex pore pressure gradient to depth relationship is represented for the Kopanoar well (Figure 71). The pore pressure gradient increase from hydrostatic at about 380 m to about 50% over hydrostatic at 500 m to about 156% of hydrostatic at 800 m. In contrast to the previous examples, the pore pressure gradient drops dramatically at 800 m to only 3% over hydrostatic at 900 m depth. Well logs are not presented for the shallow depths at which the pore pressure gradient begins its rapid increase (Figure 71). However, Weaver and Stewart (1982) show that the base of permafrost occurs at about 480 m from temperature measurements (Figure 71). No hydrates are inferred by Weaver and Stewart (1982) between 480 m and about 700 m, an interval with rapidly increasing pore pressure gradients, possibly due to the lack of logs through the interval. The dramatic drop in pore pressure gradient between 800 and 900 m occurs in an interval where Weaver and Stewart (1982) suggest the presence of hydrates based on sonic and mud gas values (Figure 71). A further curious aspect of the zone of falling pressure at 800 to 900 m depth in the Kopanoar well is that while the pressure is falling with depth, the mud gas content is increasing exponentially from 200 units to 3,000 units. Since increases in pressure gradients at Nerlerk, Koakoak, and Ukalerk wells had provisionally been attributed to increasing amounts of gas from dissociation of relict gas hydrates, the decrease in pressure and increase in hydrocarbon mud gases near the base of the projected gas hydrate stability zone is of note. Pore pressure gradients again increase rapidly at about 1,280 m depth at Kopanoar, far below the base of the gas hydrate stability zone.

The data and interpretations of Weaver and Stewart (1982) provide critical information on the extent of permafrost and hydrates on the Canadian Beaufort shelf. Whereas previous public reports on relict permafrost relied on seismic velocity anomalies (e.g. Neave and Sellmann, 1984; Hunter et al., 1978) Weaver and Stewart (1982) reported direct drilling data. Their statement that both permafrost and hydrates were found in the all the exploratory wells suggests that both are

common beneath the Canadian Beaufort shelf. In contrast, the seismic studies of subsea permafrost distribution from the area predicted much less widespread distribution of subsea permafrost.

Gas Resources Associated with Gas Hydrates

The probable volume of gas contained in hydrates can be estimated from extensive seismic and drilling evidence of hydrates in the Beaufort Sea study region. Seismic data from the continental shelf offshore of alaska permits a fairly confident estimate of hydrate-related gas volumes. Drilling evidence of gas hydrates from the continental shelf offshore of Canada likewise is easily extrapolated to determine probable gas volumes in hydrates in that area. The Alaska continental shelf and the Canadian continental slope have scant evidence of gas hydrates. Gas volume estimates for these regions are obtained by extending the estimates from areas for which assessments are well constrained by either seismic or drilling evidence. Bathymetric highs on the continental slope of the study region suggest that large traps exist for free gas beneath the base of the gas hydrate stability zone.

Continental Slope and Rise Offshore of Alaska

The extensive suite of seismic data available for the Beaufort Sea study region displays abundant evidence for gas hydrates (Plates 6 and 7). We have digitized the sea-floor and hydrate reflections on all available seismic lines from the study region. The weighted average of 27,021 individual shotpoint measurements indicates that visible BSRs are present on about 62% of the multichannel seismic lines (Table 8). It is very likely that hydrates exist in sediments of the continental slope and rise offshore of Alaska where no BSRs are visible. However, the 62% figure provides a conservative baseline estimate of probable areal hydrate distribution.

Bottom simulating reflectors occur between water depths of 275 m and 3,300 m in the Beaufort Sea study region. Detritus from the fan or cone of the Mackenzie delta has covered the lower continental slope in the eastern part of the study region. Due to this more rapid sedimentation, the seafloor is flat and featureless in the eastern part of the study region compared to the west. Detection of BSRs depends on a discordance between the seafloor and underlying sediment reflectors. The flat seafloor and regularly laminated sedimentary layers beneath the deeper water of the eastern part of the study region restrict visible BSRs to water depths of 2,600 m or less compared to the 3,200 m depths at which BSRs are located in the western part of the Alaska continental slope.

The water depth range at which BSRs are visible typically extends about 120 km normal to the trend of the continental margin. The continental slope extends about 600 km from the western border of the study region at the Barrow canyon to the eastern limit of seismic data at 141°W. The areal extent of seismic evidence of gas hydrates in the continental slope of Alaska is thus 62% of 72,000 km^2 or about 4×10^{10} m^2.

Table 8.

PROPORTION OF MULTICHANNEL SEISMIC LINES WITH BOTTOM SIMULATING REFLECTORS

Line Number	Water Depth				
	400 - 1,000 m	1,000 - 2,000 m	2,000 - 3,000 m	3,000 - 3,500 m	400 - 3,500 m
714	53%	74%	38%	n.d.	49%
718	99%	59%	47%	n.d.	58%
724	64%	n.d.	n.d.	n.d.	64%
726	64%	44%	29%	n.d.	39%
730	92%	90%	n.d.	n.d.	91%
732	72%	99%	n.d.	n.d.	78%
750	n.d.	n.d.	49%	54%	50%
751	51%	46%	72%	n.d.	61%
753	81%	51%	64%	n.d.	63%
755	n.d.	94%	21%	n.d.	78%
756	0%	55%	n.d.	n.d.	40%
765	0%	71%	n.d.	n.d.	61%
766	n.d.	76%	n.d.	n.d.	76%
767	92%	62%	n.d.	n.d.	69%
769	9%	87%	88%	n.d.	70%
770	n.d.	41%	63%	n.d.	50%
771	81%	50%	n.d.	n.d.	64%
773	37%	32%	n.d.	n.d.	35%
774	42%	n.d.	n.d.	n.d.	42%
1710	92%	100%	n.d.	n.d.	92%
1716	0%	88%	46%	n.d.	69%
1725	90%	100%	n.d.	n.d.	91%
2710	n.d.	81%	66%	100%	75%
2716	n.d.	n.d.	99%	n.d.	99%
2722	88%	67%	35%	77%	55%
2725	n.d.	71%	58%	n.d.	63%
2742	0%	78%	67%	n.d.	56%
3716	n.d.	n.d.	84%	n.d.	84%
3720	n.d.	83%	62%	33%	61%
All Lines (weighted average)	*62%*	*69%*	*52%*	*72%*	*62%*

n.d. = no data

The vertical distribution of the gas hydrate which causes the BSR in the single channel and multichannel seismic lines is not known with any certainty. The bright spots and distorted reflectors beneath some BSRs suggest that free gas is trapped beneath a hydrate seal. The presence of free gas beneath the BSR in turn suggests that the vertical extent of the hydrate must be significant to account to have the low permeability necessary to trap gas. However, Deboer et al. (1985) demonstrated that a sediment layer 1 m thick which was saturated with hydrate was sufficiently impermeable to trap a 50 m gas column. The low permeability demonstrated by the velocity anomalies beneath BSRs (e.g. Figures 14, 21, 27, 46) could be accomplished by a thin layer of sediment thoroughly cemented by hydrates or by a thicker layer of less imbued with hydrates. Analysis of the seismic gathering velocities collected by Grantz et al. (1982a) and archived at the National Geophysical Data Center did not reveal any consistent velocity anomaly above the Beaufort Sea BSRs which would indicate thickness of the hydrate layer.

We assign a hydrate pore occupancy value of 50% to the sediments producing the bottom simulating reflectors in the continental slope north of Alaska. Assuming 40% porosity for the sediment, the 4×10^{10} m^2 area of the slope underlain by BSRs would contain 8×10^9 m^3 of hydrate per 1 m thickness of the hydrate layer. If a 150:1 gas to hydrate volumetric conversion factor is applied the probable in-place gas volume from hydrates can be calculated for a range of hydrate layer thickness:

1 m thickness: 1.2×10^{12} m^3 (42 tcf)
10 m thickness: 1.2×10^{13} m^3 (420 tcf)
100 m thickness: 1.2×10^{14} m^3 (4,200 tcf)

In the absence of any direct thickness information, we propose that 400 tcf is the most probable estimate of potential gas resources in gas hydrates in the continental slope north of Alaska.

Continental Slope and Rise Offshore of Canada

We have found no seismic evidence of gas hydrate presence in the few scattered seismic lines reviewed from the continental slope and rise offshore of Canada. The slope and rise offshore of Canada constitutes the Mackenzie cone and fan, distal parts of the Mackenzie delta. Parallels can be drawn between the Mackenzie cone and fan and analogous features in the Gulf of Mexico associated with the Mississippi delta. While numerous recoveries of gas hydrates have been reported from the Louisiana continental slope, distinct seismic signature of the hydrates are not evident (Krason et al., 1985)

Recent discoveries of commercial quantities of oil and gas at the Amauligak field in the Mackenzie delta suggest good potential for generation of biogenic and thermogenic gas in slope and rise sediments. Additionally, shale diapirs are reported from the slope and rise offshore of Canada; diapirs appear to enhance gas hydrate formation in sediments of the continental slope north of Alaska. Thus, while no direct seismic evidence of hydrates was documented in this area, gas hydrates are probably formed in sediments of the continental slope and rise offshore of Canada to a similar extent as offshore of Alaska.

About 60,000 km^2 of the continental slope and rise offshore of Canada suitable for hydrate formation is within the Beaufort Sea study region. With no direct evidence of hydrate presence, we conservatively estimate the areal extent of hydrates to be 33% of that mapped north of Alaska or 20%. In accordance with these estimates, hydrates occur in an area of about 1.2×10^{10} m^2.

Using the same default values of 50% hydrate pore occupancy and 40% porosity yields an estimate of 2.4×10^9 m^3 of hydrate per 1 m thickness of the zone. With a volumetric conversion factor of 150, gas volumes for various mean thickness values are calculated:

1 m thickness: 3.6×10^{11} (12 tcf)
10 m thickness: 3.6×10^{12} (120 tcf)
100 m thickness: 3.6×10^{12} (1,200 tcf)

Due to the lack of direct evidence for hydrate presence, we estimate the most probable gas volume in this area to be 50 tcf.

Continental Shelf Offshore of Canada

Abundant drilling evidence exists of gas hydrates in sediments beneath subsea permafrost from the continental shelf offshore of Canada. Weaver and Stewart (1982) documented geophysical and mud-gas log evidence of hydrates from exploratory drill holes. Judge (1988, personal communication) has indicated that gas hydrates are well developed beneath relict permafrost in 2 principal areas of the continental shelf. One irregularly shaped area reportedly extends north of Kugmallit bay between 60 to 130 km offshore. The area of reported hydrate occurrence averages 50 km east to west and covers about 3,500 km^2. In this area some 20 exploration wells have encountered sediments which display the characteristic log responses associated with hydrates. Judge reported that the hydrates were found as deep as 1,800 m subbottom. The hydrates were reported to occupy sand layers.

Another smaller area covering about 200 km^2 was reported to occur due north of the mouth of the Mackenzie river delta. Additional evidence of hydrates occurs in scattered holes in the nearshore areas of the delta where the seafloor is covered by 10 to 20 m of water. In this western area of hydrate occurrence, sand intervals 50 to 60 m containing hydrates have been recorded.

Reports of hydrate presence suggest that hydrates occur in sediments of the continental shelf offshore of Canada over 25% of the total area. With about 50,000 km^2 of continental shelf in this part of the Beaufort Sea study region, the probable areal extent of hydrates is about 1.2×10^{10} m^2. Weaver and Stewart (1982) indicated that "observed hydrate" zone, that is intervals in which log indications of hydrates were very convincing, ranged from 0 m to over 100 m, with typical values of perhaps 30 m. If 30 m thickness of the zone is taken as typical over the areal extent of the hydrates, then about 3.5×10^{11} m^3 of hydrate-containing sediment exists beneath the Canadian portion of the Beaufort continental shelf. Since the sediments within the gas hydrate stability zone beneath the permafrost zone are deeper than the continental slope sediments in the stability zone, a lower sediment porosity value of 30% is assumed. Since no seismic evidence exists that the hydrates

are sufficiently developed to decrease permeability to the point of forming a gas trap, the hydrate pore occupancy is assumed to be 25%. These assigned values yield a probable hydrate volume estimate of 2.5 x 10^{10} m^3. At 150 m^3 methane at STP for each 1 m^3 of hydrate, some 4 x 10^{12} m^3 (140 tcf) of gas exists in hydrate form.

Continental Shelf Offshore of Alaska

The continental shelf north of Alaska is relatively unexplored in comparison to the shelf offshore of Canada. While numerous hydrocarbon discoveries of economic importance have been recorded from the Mackenzie delta, no comparably large finds are publicly known from the Alaskan sector. Based on both the lack of drilling evidence of hydrates and the lower potential for significant hydrocarbon accumulation demonstrated by the lower degree of success in exploring for conventional hydrocarbons, we assign a lower probability of hydrate occurrence to the continental slope offshore of Alaska.

The 37,000 km^2 of continental shelf north of Alaska which is within the Beaufort Sea study region is assigned a probable areal hydrate extent of 8%. Using the same porosity and hydrate pore occupancy estimates as applied for the Canadian shelf area 7 x 10^9 m^3 of hydrate exist north of Alaska beneath water shallower than 400 m. This corresponds to about 1 x 10^{12} m^3 (35 tcf) of natural gas in hydrate form.

Free Gas in Sub-Hydrate Traps

Highly irregular seafloor topography of the continental slope in the Beaufort Sea study region is expressed as corresponding relief in the base of the gas hydrate stability zone. Closed anticlinal gas traps can be formed beneath bathymetric highs by the relief of base of the hydrate zone combined with the low permeability of sediments with interstitial gas hydrates.

Offshore Alaska. The wide spacing of the seismic coverage of the continental slope north of Alaska limits the precision with which these potential gas traps can be mapped. For some particularly large and well defined topographic highs, the approximate surface closure can be obtained directly from the bathymetric map of Greenberg et al. (1982) (Plate 1). The data base used to prepare the map included not only the multichannel and single channel seismic lines which we reviewed for BSR occurrence, but also 25 kHz depth profile data, and depth soundings. The map thus provides data on sea-floor configuration at locations away from the seismic lines reproduced elsewhere in this report.

Two large bathymetric highs were mapped by Greenberg et al. (1981) on the continental slope north of Alaska. The larger high is located at about 143.8°W and 71.1°N beneath water 1,500 to 1,700 m deep (Plate 1). The high is crossed by multichannel seismic line 726 (Plate 7). The bathymetric high mapped by Greenberg et al. (1981) corresponds with the feature that dominates the right half of the upper panel of Line 726 in Figure 45. From Figure 45, the high can be seen to extend for about 8 km. A very prominent BSR is evident in the high. The potential sub-hydrate gas trap on Line 726 has about ut 0.4 sec of closure at the BSR which corresponds to about 350 m. The bathymetric high measures about 15 x 40 km on

the bathymetric map for an approximate areal extent of 400 km^2 or 4 x 10^8 m^2. Assuming that the rest of the potential trap is defined by the domed configuration of the BSR in Figure 45, an approximate enclosed sediment volume of 6 x 10^{10} is calculated. Using a reservoir porosity of 30% and a 50% Sw value yields an maximum gas volume of 9 x 10^9 m^3 at reservoir temperature and pressure. The reservoir pressure can be assumed to be hydrostatic for an average value of 200 atm. A mean reservoir temperature of 30°C can be assumed based on model results indicating a temperature of 25°C and a 4°C/100 m geothermal gradient. Under these reservoir conditions, the a compressibility factor (Z) of 0.83 is appropriate. These assumed and derived values can be applied to the gas state equation to obtain probable reservoir volumes at standard temperature and pressure:

$$V_{stp} = \frac{P_{reservoir} \times V_{reservoir} \times 273}{Z \times T_{reservoir}}$$

A possible gas volume of 2 x 10^{12} m^3 or 70 tcf is thus assigned for the gas trap beneath the hydrate layer on multichannel seismic line 726. A distinct bright spot exists beneath the BSR in the trap in Figure 45, suggesting that some amount of gas may in fact be trapped in the structure. There is no definitive indication of the degree of trap filling, but the bright spot does extend for a considerable distance along the line. An intentionally conservative estimate of 30% porosity was applied to the potential reservoir sediments. The shallow subbottom depth of the reservoir (500 - 800 m) and the prevalence of mass-wasting and resedimentation on the slope suggest that a higher value may be more appropriate. At 50% porosity, the possible gas volume increases to 3.3 x 10^{12} m^3 or 120 tcf.

A much smaller closed bathymetric high exists at about 152.5°W and 72°N at north of Smith Bay at water depths of 1,300 to 1,700 m (Plate 1). The area of closure of the high measures about 5 km x 3 km or about 12 km^2. The enclosed volume of sediment of this high is about 2.4 x 10^9 m^3. Using the same estimates of 30% porosity and 50% Sw yields a figure of 3.6 x 10^8 m^3 of gas at reservoir conditions. Correction to standard conditions by the above equation produces a figure of 8 x 10^{10} m^3 or 3 tcf.

Potentially significant bathymetric highs may exist on the continental slope which would not be immediately evident in Plate 1 at the contour interval of 200 m used by Greenberg et al (1981). The map in Plate 1 was analyzed by computer to detect subtle topographic variations which are not evident on viewing the map directly. The bathymetric contours of Plate 1 were digitized, and a surface corresponding the seafloor bathymetry of the continental slope was generated using the geostatistical method of kriging. The 84,000 km^2 Alaskan continental slope was modeled as 40,401 grid cells measuring 630 m in the dip direction and 2,830 m along the strike of the slope. Each cell was assigned a bathymetric value by analysis of the bathymetry of the 10 nearest digitized values using a quadrant search pattern. The resulting surface was then analyzed numerically to locate and measure any closed bathymetric highs. The procedure identified 34 closed bathymetric highs with the potential to serve as sub-hydrate gas traps.

The two potential gas traps discussed above which were identified visually from Plate 1 were also located by the numerical procedure. This suggests that the numerical procedure is a legitimate means of locating possible bathymetric highs which do not occur at the required depth intervals to be evident on the bathymetric map. Results from the surface modeling were normalized to the area and volume of the large high seen on line 726 (Figure 45). The large high on line 726 contains 17% of the area and 30% of the volume of the sum of the 34 highs identified by analysis of the modeled surface. These estimates suggest that total potential volume of the sub-hydrate gas traps is about 6.6 x 10^{12} m^3 or 230 tcf for the continental slope offshore of Alaska.

The extent of possible sub-hydrate gas traps can also be estimated directly from seismic lines. The location, water depth, and BSR depth was digitized at 50 m intervals for each available seismic line from the continental slope offshore of Alaska. The seafloor depth data for each seismic line from the study region was numerically analyzed to detect, locate, and measure bathymetric highs on the seafloor of the continental slope. Bathymetric highs with a relief of less than 10 m and those at water depths of less than 300 m were ignored. The results of the data base analysis are presented in Table 9. A total of 124 bathymetric highs were detected by this method.

The volumes of the sub-hydrate gas traps potentially present beneath each bathymetric high were calculated by applying a number of reasonable assumptions. The bathymetric highs were usually crossed only once by a seismic line. The very large majority of seismic lines analyzed are dip lines which run from shallow water to deep water. Thus the analysis of the digitized seismic lines generates estimates for the relief and the length of the bathymetric high perpendicular to the trend of the continental margin. Data on the extent of the highs along the strike of the margin are absent. Without a much more extensive grid of seismic data, the shapes of the highs remain unknown. A conservative estimate of the volume of the possible sub-hydrate gas traps beneath each bathymetric high was obtained by assuming that the highs were circular in plan view. With the length and relief data from the lines, a volume estimate for sediments contained in each potential trap was derived by considering the traps to be dome structures with diameters equal to the length of the trap on the seismic line, and height equal to the vertical relief from the line (Table 9). Gas volumes associated with each trap was calculated from the volume estimate using modeled in-situ reservoir pressure and temperature values by applying the estimates of 30% porosity and 50% Sw. These values were applied to the equation:

$$V_{stp} = \frac{P_{reservoir} \times V_{reservoir} \times 273}{Z \times T_{reservoir}}$$

Table 9.

ESTIMATED VOLUME OF POTENTIAL SUB-HYDRATE GAS TRAPS

Seismic Line	Water Depth (m)	Trap Length (km)	Vertical Relief (m)	Sediment Volume (m^3)	Gas Volume (m^3)	Gas Volume (tcf)
774	427	1.4	27	3.05×10^7	4.71×10^8	0.02
771	975	4.95	79	7.92×10^8	1.95×10^{10}	0.69
770	1,864	3.6	223	1.15×10^9	4.54×10^{10}	1.61
770	1,864	3.75	32	2.18×10^8	8.57×10^9	0.30
769	1,044	1.1	37	1.97×10^7	5.07×10^8	0.02
769	1,146	0.55	26	5.24×10^6	1.44×10^8	0.01
769	1,262	4.55	86	5.58×10^8	1.64×10^{10}	0.58
769	1,502	1.6	70	8.56×10^7	2.85×10^9	0.10
769	1,687	2.0	100	1.96×10^8	7.14×10^9	0.25
769	1,972	0.95	31	1.50×10^7	6.17×10^8	0.02
766	1,820	7.0	201	3.92×10^9	1.51×10^{11}	5.36
766	1,820	6.35	401	5.63×10^9	2.17×10^{11}	7.70
765	1,359	0.65	30	7.53×10^6	2.33×10^8	0.01
765	1,401	2.0	39	8.69×10^7	2.75×10^9	0.10
765	1,452	2.0	54	1.05×10^8	3.42×10^9	0.12
756	1,353	1.4	44	5.32×10^7	1.64×10^9	0.06
756	1,102	1.25	71	5.77×10^7	1.54×10^9	0.05
755	1,982	5.4	236	2.39×10^9	9.87×10^{10}	3.49
755	1,541	3.5	175	8.56×10^8	2.91×10^{10}	1.03
753	822	1.25	52	3.66×10^7	8.05×10^8	0.03
753	2,145	2.25	46	1.04×10^8	4.58×10^9	0.16
753	2,143	1.85	93	1.55×10^8	6.82×10^9	0.24
750	2,931	4.65	40	4.68×10^8	2.67×10^{10}	0.95
750	2,902	0.95	20	1.09×10^7	6.19×10^8	0.02
745	1,220	0.75	54	1.91×10^7	5.46×10^8	0.02
745	1,837	4.5	247	2.36×10^9	9.17×10^{10}	3.25
747	1,625	2.0	56	1.10×10^8	3.89×10^9	0.14
747	1,504	1.0	60	2.92×10^7	9.73×10^8	0.03
747	1,460	3.95	100	6.48×10^8	2.12×10^{10}	0.75
747	1,431	0.65	35	8.43×10^6	2.71×10^8	0.01
744	1,976	3.55	205	8.99×10^8	3.71×10^{10}	1.31
744	1,965	6.85	267	4.51×10^9	1.85×10^{11}	6.55
743	2,455	3.75	156	8.50×10^8	4.18×10^{10}	1.48
743	2,442	0.6	18	4.01×10^6	1.96×10^8	0.01
743	2,441	1.25	32	2.53×10^7	1.24×10^9	0.04
2742	1,665	1.8	59	9.34×10^7	3.36×10^9	0.12
2742	2,290	9.5	340	1.27×10^{10}	5.91×10^{11}	20.91
2710	1,429	0.95	48	2.07×10^7	6.66×10^8	0.02
2710	1,525	0.65	31	7.36×10^6	2.48×10^8	0.01
2710	1,680	1.2	84	6.78×10^7	2.46×10^9	0.09
2710	2,353	1.15	25	1.85×10^7	8.81×10^8	0.03
2710	2,357	0.6	23	4.91×10^6	2.33×10^8	0.01
2710	2,357	0.6	27	6.48×10^6	3.08×10^8	0.01

Table 9. (Continued)

ESTIMATED VOLUME OF POTENTIAL SUB-HYDRATE GAS TRAPS

Seismic Line	Water Depth (m)	Trap Length (km)	Vertical Relief (m)	Sediment Volume (m^3)	Gas Volume (m^3)	Gas Volume (tcf)
2710	2,460	0.75	29	9.68×10^6	4.77×10^8	0.02
2710	2,779	7.1	82	2.19×10^9	1.19×10^{11}	4.23
1725	555	1.25	17	1.67×10^7	2.94×10^8	0.01
2725	1,490	0.8	34	1.24×10^7	4.11×10^8	0.01
2725	1,504	1.65	68	9.50×10^7	3.17×10^9	0.11
2725	1,928	8.25	291	6.95×10^9	2.81×10^{11}	9.94
2725	1,924	3.65	85	4.63×10^8	1.87×10^{10}	0.66
2725	2,150	1.95	60	1.17×10^8	5.15×10^9	0.18
2725	2,670	0.6	33	6.77×10^6	3.57×10^8	0.01
2725	2,757	4.55	60	4.63×10^8	2.51×10^{10}	0.89
2725	2,815	1.8	37	6.82×10^7	3.77×10^9	0.13
2725	2,877	5.35	201	2.36×10^9	1.32×10^{11}	4.69
2725	2,857	1.0	39	2.11×10^7	1.18×10^9	0.04
2722	2,472	1.0	19	1.18×10^7	5.83×10^8	0.02
2722	2,314	0.65	26	6.19×10^6	2.90×10^8	0.01
2722	2,145	1.15	39	2.95×10^7	1.30×10^9	0.05
2722	1,331	1.7	81	1.15×10^8	3.51×10^9	0.12
2722	612	1.05	16	1.14×10^7	2.11×10^8	0.01
3720	1,793	6.4	218	3.13×10^9	1.20×10^{11}	4.23
3720	2,522	1.9	76	1.26×10^8	6.32×10^9	0.22
3720	2,954	0.6	41	7.85×10^6	4.51×10^8	0.02
3720	3,012	2.9	19	9.70×10^7	5.67×10^9	0.20
3720	3,035	0.8	17	7.23×10^6	4.25×10^8	0.02
726	2,856	4.3	127	9.96×10^8	5.56×10^{10}	1.97
726	2,680	0.65	19	4.51×10^6	2.39×10^8	0.01
726	2,367	5.75	42	6.01×10^8	2.87×10^{10}	1.02
726	2,071	0.6	20	4.32×10^6	1.85×10^8	0.01
726	1,739	10.35	326	1.55×10^{10}	5.78×10^{11}	20.45
726	621	1.4	22	2.47×10^7	4.60×10^8	0.02
718	2,941	2.9	21	1.13×10^8	6.45×10^9	0.23
718	2,933	1.2	15	1.50×10^7	8.59×10^8	0.03
718	2,886	0.7	18	5.75×10^6	3.24×10^8	0.01
718	2,175	0.6	13	3.53×10^6	1.57×10^8	0.01
718	1,804	1.0	47	2.43×10^7	9.32×10^8	0.03
718	1,143	2.3	82	1.89×10^8	5.18×10^9	0.18
730	1,049	0.7	36	9.87×10^6	2.54×10^8	0.01
730	1,158	1.1	18	1.45×10^7	4.00×10^8	0.01
1716	1,272	1.05	34	2.01×10^7	5.92×10^8	0.02
1716	1,567	4.2	147	9.16×10^8	3.15×10^{10}	1.12
1716	2,121	2.15	25	6.70×10^7	2.92×10^9	0.10
2716	2,356	0.75	16	5.99×10^6	2.85×10^8	0.01
2716	2,604	1.9	23	5.27×10^7	2.72×10^9	0.10
3716	2,841	0.7	22	6.72×10^6	3.74×10^8	0.01

Table 9. (Continued)

ESTIMATED VOLUME OF POTENTIAL SUB-HYDRATE GAS TRAPS

Seismic Line	Water Depth (m)	Trap Length (km)	Vertical Relief (m)	Sediment Volume (m^3)	Gas Volume (m^3)	Gas Volume (tcf)
3716	2,861	3.4	30	1.49×10^8	8.35×10^9	0.30
3716	2,870	3.6	23	1.74×10^8	9.74×10^9	0.34
3716	2,868	6.55	34	8.36×10^8	4.69×10^{10}	1.66
3716	2,869	1.5	34	3.79×10^7	2.12×10^9	0.08
732	1,541	1.0	33	1.92×10^7	6.52×10^8	0.02
732	553	0.6	19	3.87×10^6	6.78×10^7	0.00
714	2,474	0.8	17	7.26×10^6	3.59×10^8	0.01
714	2,478	2.35	38	1.11×10^8	5.52×10^9	0.20
714	2,555	1.55	25	3.88×10^7	1.97×10^9	0.07
714	2,408	0.9	15	8.17×10^6	3.95×10^8	0.01
714	2,320	0.8	19	8.01×10^6	3.76×10^8	0.01
714	2,268	1.8	24	4.50×10^7	2.07×10^9	0.07
714	2,061	2.0	36	7.60×10^7	3.24×10^9	0.11
714	1,047	0.55	52	9.78×10^6	2.52×10^8	0.01
305	2,659	0.55	45	7.53×10^6	3.96×10^8	0.01
305	2,053	0.7	102	2.49×10^7	1.06×10^9	0.04
305	1,866	7.95	294	5.53×10^9	2.18×10^{11}	7.71
323	1,906	0.55	21	4.23×10^6	1.69×10^8	0.01
323	1,582	2.3	99	3.12×10^8	1.08×10^{10}	0.38
363	1,348	5.15	374	2.85×10^9	8.77×10^{10}	3.10
363	1,359	7.05	606	1.06×10^{10}	3.27×10^{11}	11.57
363	1,660	6.95	266	4.83×10^9	1.74×10^{11}	6.14
363	2,427	1.55	113	1.21×10^8	5.90×10^9	0.21
363	2,349	2.8	349	8.68×10^8	4.12×10^{10}	1.46
363	2,174	0.6	18	4.23×10^6	1.88×10^8	0.01
363	1,853	0.55	61	9.61×10^6	3.76×10^8	0.01
363	1,812	1.6	160	1.52×10^8	5.84×10^9	0.21
331	1,022	2.0	242	3.55×10^8	8.99×10^9	0.32
331	1,176	1.55	269	2.30×10^8	6.41×10^9	0.23
331	1,430	2.35	340	7.30×10^8	2.35×10^{10}	0.83
331	1,563	5.1	524	4.46×10^9	1.53×10^{11}	5.42
361	1,067	0.7	175	3.71×10^7	9.67×10^8	0.03
333	1,807	3.3	272	1.08×10^9	4.13×10^{10}	1.46
333	1,837	5.3	434	3.86×10^9	1.50×10^{11}	5.32
334	1,302	1.5	110	9.07×10^7	2.72×10^9	0.10
303	1,086	0.85	42	1.72×10^7	4.54×10^8	0.02
303	1,091	0.9	80	3.36×10^7	8.89×10^8	0.03
303	1,077	3.2	240	1.26×10^9	3.30×10^{10}	1.17
Average:	*1,914*	*2.45*	*100*	*9.11×10^8*	*3.61×10^{11}*	*1.27*
Total					**4.48×10^{13}**	**157.56**

to obtain the gas volume figures listed in Table 9. Summing up the gas volumes of each potential trap gives an estimated free-gas potential of 4.5×10^{12} m^3 or 160 tcf for the continental slope and rise offshore of Alaska.

The large high on line 726 (Figure 45) is the only bathymetric high with an independently derived volume estimate with which to evaluate the methodology used to derive the volume estimates in Table 9. From the bathymetric map (Plate 1) and line 726 (Figure 45), we previously estimated an enclosed sediment volume of 6×10^{10} m^3 and a gas volume of 2×10^{12} m^3 (70 tcf). The estimates from Table 9 for the same feature are 1.6×10^{10} m^3 sediment volume and a gas volume of 5.8×10^{11} m^3 (20 tcf). Thus, direct measurement of the trap gave volume estimates 3.5 times greater than the numerically-derived values. The discrepancy is in part due to the shape of the structure. Plate 1 shows that the feature is elongated parallel to the strike of the continental slope; whereas the figures in Table 9 assumed that the feature was circular in plan view. The measured dimensions of 15 x 40 km are greater than the 10.35 km diameter from the numerical method

It is possible and indeed likely that some of the other structures mapped from the digitized seismic lines (Table 9) are also elongate, and thus the underlying traps are of greater volume than listed in Table 9.

The aggregate volume of potential gas traps is greater than the total listed in Table 9 because of the wide spacing and irregular distribution of the seismic lines which form the basis for the estimates in Table 9. The multichannel seismic lines used for the estimates are concentrated in the eastern part of the Alaskan continental slope. These lines are spaced an average of 20 km apart (Plate 7). Since the average bathymetric high listed in Table 9 extends for 2.5 km, seven of the typical topographic highs could exist between the seismic lines and thus not be represented in the estimates in Table 9. However, the most volumetricly significant traps listed in Table 9 (greater than 1 tcf) range in length from 2.8 to 10.4 km with an average of about 6 km. Thus, the 20 km spacing of the multichannel seismic lines may have permitted an average of two highs, each 6 km in diameter to go undetected, suggesting that the actual volume of gas may be 3 times the 4.5×10^{12} m^3 (160 tcf) cited in Table 9, or 1.3×10^{13} m^3 (480 tcf). The net effect of argument used in this paragraph is similar to the previous treatment proposing that some of the structures are elongated rather than circular; to apply both approaches to the potential volume figures would be redundant.

While the eastern portion of the continental slope offshore of Alaska was regularly surveyed with multichannel seismic lines (Plate 7), The western portion of the margin was only sporadically surveyed by single channel lines (Plate 6). While the precise proportion of the continental margin which was not surveyed is not clear, we propose that the total in Table 9 be increased by 25% to account for the irregular distribution of seismic lines on the Alaskan continental slope and rise. The correction due to irregular distribution and the correction for seismic line spacing are additive in nature, indicating a potential gas volume of 1.6×10^{13} m^3 (560 tcf).

A number of other factors could serve to modify the gas estimates derived above. The relief of the BSRs which occur beneath bathymetric highs is typically less than the relief of the sea floor. This factor would tend to diminish the potential gas volume estimates from those quoted above. The bathymetric highs may not have sufficient hydrates developed in the gas hydrate stability zone to serve as an

effective trap. Similarly, insufficient gas may be available to fill the traps. However, the high heat flow which we have documented over mud diapirs in the eastern part of the Alaskan continental slope results in relief in the isotherms, and thus in the base of the gas hydrate stability zone which is not expressed as relief at the seafloor. Since the methodology by which the estimates in Table 9 were derived depend on seafloor relief, such heat-induced traps near diapirs are not included. We contend that these and other conceivable modifying effects can not be reliably quantified; to apply corrections due to these ancillary factors would only add uncertainty to already tenuous estimates.

To summarize, we estimate that traps beneath the gas hydrate stability zone exist offshore of Alaska which are capable of containing 1.6 x 10^{13} m^3 (560 tcf) of gas. This estimate was derived using conservative assumptions of 30% porosity and 50% water saturation (Sw). Seismic lines from a number of the potential traps display bright spots or velocity anomalies which are evidence of occupancy by gas. However, these anomalies are insufficient to estimate the degree of gas occupancy of the traps. We suggest that 20% of the available trap volume is occupied by gas, for potential resource estimates of 3.2 x 10^{12} m^3 or 110 tcf.

Offshore Canada. Seismic data for the continental slope offshore of Canada are scarce. Rapid progradational sedimentation by the Mackenzie delta tends to produce a seafloor with fewer irregularities than the mass wasting dominated slope offshore of Alaska. Free gas traps at the base of the gas hydrate stability zone depend on seafloor irregularities to generate relief in the controlling isotherms. Based on these factors we estimate that traps capable of containing 4 x 10^{12} m^3 (140 tcf) of gas exist offshore of Canada. Due to the prevalence of mud diapirs which may charge the traps with thermogenic gas or at least promote migration of gas to the traps, we estimate that 30% of the possible traps are occupied, for a potential free-gas resource estimate of 1.2 x 10^{12} m^3 or 42 tcf.

Conclusions

Gas hydrates exist in the Beaufort Sea study region based on evidence from both seismic lines and from logs of exploratory drill holes. Bottom-simulating reflectors (BSRs) exist on 62% of the seismic lines from water depths greater than 400 m offshore of Alaska. The BSRs exhibit characteristics which are generally accepted as characteristic of reflectors at the base of the gas hydrate stability zone (Shipley et al., 1979). Velocity and amplitude anomalies of sediment reflectors beneath some BSRs indicate that free gas is trapped beneath the gas hydrate stability zone. No direct seismic evidence of hydrate presence in the sediments of the continental shelf is documented for the Beaufort Sea study region. However, a deep, high velocity refractor identified in beneath Harrison Bay, Alaska may indicate a hydrate interval beneath subsea permafrost.

Gas hydrates have been identified beneath subsea permafrost offshore of Canada in the Beaufort Sea study region. Gas-bearing intervals with high velocity and resistivity exist at depths greater than the base of subsea permafrost. The anomalous intervals tend to generate well-bore washouts rather than mud-cake

buildups, in spite of their occurring predominantly in sandy sediments. Since these unusual sediment intervals occur only within the gas hydrate stability zone, the unusual geophysical properties are most likely due to gas hydrate presence. Hydrates occur in a large portion of the exploratory wells drilled on the continental slope offshore of Canada.

Seismic lines from the study region indicate that gas hydrate formation may influence mass-wasting processes. Several seismic lines from the study region (e.g. Line 753, Figure 35) show movement along detachment surfaces coincident with the base of the gas hydrate stability zone. Seismic lines from the Beaufort Sea study region present the best evidence to date of competent hydrate-cemented hemipelagic sediments slide downslope along failure surfaces in underlying incompetent, possibly gassy sediments. This suggests that gas hydrate formation and concomitant nearsurface cementation and permeability changes may be a principal factor in the diagenetic and structural development of passive margins worldwide.

The abundant seismic evidence of hydrates in the study region has been compiled into a digital data base for analysis. Using this collection of data we have determined geothermal conditions of the sediments and the variation of these properties with water depth and location. Higher geothermal gradients are associated with sediments beneath intermediate water depth, and at the extreme eastern and western portion of the study region. These trends correspond with rapid mass-wasting at intermediate water depths in the western portion of the study region, and diapiric intrusions in the eastern part of the study region. Convection, and possible hydrothermal systems associated with the diapirs appear to compensate for the low thermal conductivity of the shale which constitute the cores of the diapirs.

The areal extent of bottom simulating reflectors was determined from the data base compiled from the seismic data from the study region. From these areal extent values, estimates of potential gas resources associated with hydrates were determined. The estimates have a wide range due to uncertainties on the vertical extent of hydrates indicated on seismic lines. We determined a most-probable in-place estimate for gas in hydrate form in the continental slope and rise offshore of Alaska of 1.2×10^{13} m^3 or 400 trillion cubic feet (tcf). The continental slope and rise offshore of Canada is estimated to contain 1.4×10^{12} m^3 (50 tcf) of gas in hydrate form; the lower figure due principally to the lack of demonstrated evidence of hydrate presence in the area. The continental shelf offshore of Canada is estimated to contain 4×10^{12} m^3 (140 tcf) of gas in hydrate form. That estimate is based principally on drilling data. The continental shelf offshore of Alaska is estimated to contain 1×10^{12} m^3 of gas in hydrates. We estimate that sub-hydrate traps exist in the study region with sufficient closed volume to contain 2×10^{13} m^3 (700 tcf) of free gas. We estimate that approximately 4.4×10^{12} m^3 (150 tcf) of free gas is present in these sub-hydrate traps.

Gas hydrates are widely distributed in the study region. The very limited geochemical data which is available for the sediments of the study region indicate that the source of the methane in the gas hydrates is terrestrial organic matter. Biogenic processes are probably responsible for most of the methane in continental

slope sediments. Some thermogenic component to the hydrocarbon gases is very likely in the eastern part of the study region. The probability of thermogenic contribution is particularly high over shale diapirs, where the high heat flow and diapiric intrusion decreases the effective depth to thermal maturity and fracture systems promote migration of hydrocarbons to the gas hydrate stability zone. As noted by Finley and Krason (1986b) bottom simulating reflectors at anomalously great subbottom depths may indicate thermogenic gas hydrates. An example of such potential thermogenic gas hydrate reflectors is seen on Line 2742 (Figure 41), among others.

A near total lack of sedimentological and geochemical data from the study region hinders interpretation of geological controls on hydrate formation and stability. This significant data gap could be closed by drilling and analysis of sediments from selected sites in the study region. In the absence of these critical data, this study has concentrated on the available seismic data. With additional data from the sediments of the study region, the preliminary findings from this report could be tested and refined.

REFERENCES

Bally, A.W., 1983, ed., Seismic Expression of Structural Styles: American Association of Petroleum Geologists Studies in Geology Series # 15

Bily, C., and Dick, J.W.L., 1974, Naturally occurring gas hydrates in the Mackenzie Delta, N.W.T.: Bulletin of Canadian Petroleum Geology, v. 32, p. 340-352

Bird, K.J., 1985, The framework geology of the North Slope of Alaska as related to Oil-source rock correlations, *in* Magoon, L.B., and Claypool, G.E., eds., Alaska North Slope Oil/Rock Correlation Study: American Association of Petroleum Geologists Studies in Geology #20, p. 3-30.

Brooks, J.M., and Bryant, W.R., 1985, Geological and geochemical implications of gas hydrates in the Gulf of Mexico--final report: College Station, Texas A&M University, report submitted to U.S. Department of Energy, 131 p.

Buffler, R.T., 1983 Structure of the Mexican Ridges foldbelt, southwest Gulf of Mexico, *in* Bally, A.W., ed., Seismic Expression of Structural Styles: American Association of Petroleum Geologists Studies in Geology Series # 15, v. 2, p. 2.3.3.16 - 2.3.3.21.

Carpenter, G., 1981, coincident sediment slump/clathrate complexes on the U.S. continental slope: Geo-Marine Letters, v. 1, p. 29-32.

Ciesnik, M., and Krason, J., 1987, Basin Analysis, Formation and Stability of Gas Hydrates in the Black Sea, Geological Evolution and Analysis of Confirmed or Suspected Gas Hydrate Localities, Volume 11: U.S. Department of Energy, DOE/MC/21181-1950, Vol. 11, 88 p.

Claypool, G.E., and Kaplan, I.R., The origin and distribution of methane in marine sediments, *in* Kaplan, I.R., ed., Natural Gases in Marine Sediments: New York, Plenum Press, p. 94-129.

Claypool, G.E., and Magoon, L.B., 1985, Comparison of oil-source rock correlation data for Alaskan North Slope: techniques, results, and conclusions, *in* Magoon, L.B., and Claypool, G.E., eds., Alaska North Slope Oil/Rock Correlation Study: American Association of Petroleum Geologists Studies in Geology #20, p. 49-84.

Claypool, G.E., Presley, B.J., and Kaplan, I.R., 1973, Gas analysis of sediment samples from legs 10, 11, 13, 15, 18, and 19, *in* Creager, J.S., Scholl, D.W., et al., Initial Reports of the Deep Sea Drilling Project, v. 19: Washington, D.C., US GPO, p. 879-884.

Coachman, L.K., and Aagaard, K., 1974, Physical oceanography of the Arctic and subarctic seas, *in* Herman, Y., ed., Marine Geology and Oceanography of the Arctic Seas, New York, Springer Verlag, p. 1-72.

Craig, J.D., Sherwood, K.W., and Johnson, P.P., 1985, Geologic report for the Beaufort Sea planning area, Alaska: Minerals Management Service OCS Report MMS 85-0111, 192 p.

de Boer, R.B., Houbold, J.J., and Lagrand, J., 1985, Formation of gas hydrates in a permeable medium: Geologie en Mijnbouw, v. 64, p. 245-249.

Dillon, W.P., Grow, J.A., and Paull, C.K., 1980, Unconventional gas hydrate seals may trap gas off southeast U.S.; Oil and Gas Journal, v. 78., n 12, p. 124-130.

Dinter, D.A., 1982, Holocene marine sediments on the middle and outer continental shelf of the Beaufort Sea north of Alaska: U.S. Geological Survey Miscellaneous Investigations Map I-1182-B, scale 1:500,000.

Dixon, J., 1986, Cretaceous to Pleistocene stratigraphy and paleogeography, northern Yukon and northwestern District of Mackenzie: Bulletin of Canadian Petroleum Geology, V. 34, p. 49-70.

Dow, W.G., 1977, Petroleum source beds on continental slopes and rises, *in* Geology of continental margins: American Association of Petroleum Geologists Continuing Education Notes Series 5, p d1-d37.

Ehrenbard, R.L., Hoekstra, P., and Rozenberg, G., 1983, Transient electromagnetic soundings for permafrost mapping, *in* Proceedings of the 4th International Conference on Permafrost, Fairbanks, Alaska, 1983: Washington, D.C., National Academy Press, p.656-671.

Eittreim, S. and Grantz, A., 1979, CDP seismic sections of the western Beaufort continental margin: Tectonophysics, v. 59, p. 251-262.

Finley, P., and Krason, J., 1986a, Basin Analysis, Formation and Stability of Gas Hydrates in the Colombia Basin; Geological Evolution and Analysis of Confirmed or Suspected Gas Hydrate Localities, Volume 7: U.S. Department of Energy, DOE/MC/21181-1950, Vol. 7 (DE86006637), 134 p.

Finley, P., and Krason, J., 1986b, Basin Analysis, Formation and Stability of Gas Hydrates of the Middle America Trench; Geological Evolution and Analysis of Confirmed or Suspected Gas Hydrate Localities, Volume 9: U.S. Department of Energy, DOE/MC/21181-1950, Vol. 9, 243 p.

Finley, P., and Krason, J., 1988, Review of proposed massive gas hydrate formation processes, Proceedings of the Third Chemical Conference of North America: Am. Chem. Soc. (abs), p 453.

Finley, P., Krason, J., and Dominic, K., 1987, Evidence for Natural Gas Hydrate Occurrences in the Colombia Basin: Am. Assoc. Petroleum Geologists Bull., v. 71, n. 5, p. 555-556.

Grantz, A. and May, S.D., 1982, Rifting history and structural development of the continental margin north of Alaska, *in* Watkins, J.S., and Drake, E., eds., Studies in continental margin geology: American Association of Petroleum Geologists Memoir 34, p. 77-100.

Grantz, A., Barnes, P.W., Dinter, D.A., Lynch, M.B., Reimnitz, E., Scott, E.W., 1980, Geologic framework, hydrocarbon potential, environmental conditions, and anticipated technology for exploration and development of the Beaufort Shelf north of Alaska: U.S. Geological Survey Open-File Report 80-94, 40 p.

Grantz, A., Boucher, G., and Whitney, O.T., 1976, Possible solid gas hydrate and natural gas deposits beneath the continental slope of the Beaufort Sea: U.S. Geological Survey Circular 733, p. 17.

Grantz, A., Dinter, D.A., and Biswas, N.N., 1982c, Map, cross sections, and chart showing late Quaternary faults, folds, and earthquake epicenters on the Alaskan Beaufort shelf: U.S. Geological Survey Miscellaneous Investigations Series Map I-1182-C, scale 1:500,000.

Grantz, A., Dinter, D.A., Hill, E.R., May, S.D., McMullin, R.H., Phillips, R.L., and Reimnits E., 1982a, Geologic framework, hydrocarbon potential, and environmental conditions for exploration and development of proposed oil and gas lease Sale 87 in the Beaufort and northeast Chukchi Seas: U.S. Geological Survey Open-File Report 82-482, 71 p.

Grantz, A., Eittreim, S., and Dinter, D.A., 1979, Geology and tectonic development of the continental margin north of Alaska: Tectonophysics, v. 59, p. 263-291.

Grantz, A., Eittreim. S., and Whitney, O.T., 1981, Geology and physiography of the continental margin north of Alaska and implications for the origin of the Canada Basin, *in* Nairn, A.E.M., Churkin, M., and Stehli, F.G., eds., The Ocean Basins and Margins: New York, Plenum Press, v. 5, p. 439-492.

Grantz, A., Mann, D.M., and May, S.D., 1982b, Tracklines of multichannel seismic-reflection data collected by the U.S. Geological Survey in the Beaufort and Chukchi Sea in 1977 for which profiles and stack tapes and available: U.S. Geological Survey Open-File Report 82-735, 1 map sheet with text, seismic profiles distributed by the National Geophysical Data Center, Boulder, Colorado..

Grantz, A., McHendrie, G.G., Nilsen, T.H., and Yorath, C.J., 1974, Seismic reflection profiles, 1973, on the continental shelf and slope between Bering Strait and Barrow, Alaska, and Mackenzie Bay, Canada: U.S. Geological Survey Open-File Report, 49 sheets seismic reflection profiles, 2 maps.

Greenberg, J., Hart, P.E., and Grantz, A., 1981, Bathymetric map of the continental shelf, slope, and rise of the Beaufort Sea north of Alaska: U.S. Geological Survey Miscellaneous Investigations Map I-1181-A., scale 1:500,000.

Hedberg, H.D., 1980, Methane generation and petroleum migration, *in* Roberts, W.H., and Cordell, R.J., eds., Problems of Petroleum Migration: American Association of Petroleum Geologists, Studies in Geology No. 10, p. 179-206

Hubbert, M.K., and Rubey, W.W., 1959, Role of fluid pressure in mechanics of overthrust faulting: Geological Society of America Bulletin, v.70, p. 115-166.

Hunt, J.M., 1979, Petroleum Geochemistry and Geology: San Francisco, W.H. Freeman and Company, 617 p.

Hunt, J.M., Huc, A.Y., and Whelan, J.K., 1980, Generation of light hydrocarbons in sedimentary rocks: Nature, v. 288, p. 670-688.

Hunter, J.A., Neave, K.G., MacAulay, H.A., and Hobson, G.D., 1978, Interpretation of sub-seabottom permafrost in the Beaufort Sea by seismic methods, *in* Proceedings of the 3rd International Conference on Permafrost: v.1, p. 514-526.

Jones, P.B., Brache, J., and Lentin, J.K., 1980, The geology of the 1977 offshore hydrocarbon discoveries in the Beaufort-Mackenzie basin, N.W.T.: Bulletin of Canadian Petroleum Geology, v. 28, p. 81-102.

Koch, G.S., and Link, R.F., 1980, Statistical analysis of geological data: Dover Publications, New York, 850 p.

Krason, J., and Ridley, W.I., 1985, Basin Analysis, Formation and Stability of Gas Hydrates in the Blake-Bahama Outer Ridge; Geological Evolution and Analysis of Confirmed or Suspected Gas Hydrate Localities, Volume 1: U.S. Department of Energy, DOE/MC/21181-1950, Vol. 1, (DE86001006), 100 p.

Krason, J., and Rudloff, B., 1985, Basin Analysis, Formation and Stability of Gas Hydrates Offshore of Newfoundland and Labrador; Geological Evolution and Analysis of Confirmed or Suspected Gas Hydrate Localities, Volume 4: U.S. Department of Energy, DOE/MC/21181-1950, Vol. 4 (DE86001069), 123 p.

Krason, J., Ciesnik, M., and Finley, P., 1986, Evaluation of the geological relationships to gas hydrate formation and stability, *in* Komar, C.A., ed., Proceedings of the Gas Hydrates, Arctic/Offshore Research, and Deep Source Gas Contractors Review Meeting: U.S. Department of Energy, DOE/METC-86/6037 (DE86006604), p. 23-38.

Krason, J., Ciesnik, M., and Finley, P., 1987, Evaluation of the geological relationships to gas hydrate formation and stability, *in* Komar, C.A., ed., Proceedings of the Unconventional Gas Recovery Contractors Review Meeting: U.S. Department of Energy, DOE/METC-87/6080 (DE87006490), p. 309-324.

Krason, J., Finley, P., and Rudloff, B., 1985, Basin Analysis, Formation and Stability of Gas Hydrates in the Western Gulf of Mexico; Geological Evolution and Analysis of Confirmed or Suspected Gas Hydrate Localities, Volume 3: U.S. Department of Energy, DOE/MC/21181-1950, Vol. 3, (DE86001057), 168 p.

Kuuskraa, V.A., Hammershaimb, E.C., Holder, G.D., Sloan, E.D., 1983, Handbook of Gas Hydrate Properties and Occurrence: U.S. Department of Energy, DOE/MC/19239-1546, 178 p.

Kvenvolden, K.A., and McMenamin, M.A., 1980, Hydrates of natural gas: A review of their geologic occurrence: U.S. Geological Survey Circular 825, 11 p.

Kvenvolden, K.A., Claypool, G.E., Threlkeld, C.N., and Sloan, E.D., 1984, Geochemistry of a naturally occurring massive marine gas hydrate: Organic Geochemistry, v. 6, p. 703-713.

Lachenbruch, A.H., Sass, J.H., Marshall, B.V., and Moses, T.H., 1982, Permafrost, heat flow, and the geothermal regime at Prudhoe Bay, Alaska: Journal of Geophysical Research, v. 87, p. 9301-9316.

Ladd, J.W., Ibrabim, A.K., McMillen, K.J., Latham, G.V., and von Huene, R.E., 1982, Interpretation of seismic reflection data of the Middle America Trench offshore Guatemala, *in* Aubouin, J. et al, Initial Reports of the Deep Sea Drilling Project, v. 67: Washington, D.C., US GPO, p. 675-689.

Lerand, M., 1973, Beaufort Sea, *in* McCrossan, R.G., ed., The future petroleum provinces of Canada--their geology and potential: Canadian Society of Petroleum Geologists Memoir 1, p. 315-386.

MacLeod, M.K., 1982, Gas hydrates in ocean bottom sediments: American Association of Petroleum Geologists Bulletin, v. 66, p. 2649-2662.

Magoon, L.B., and Bird, K.J., 1985, Alaskan North Slope petroleum geochemistry for the Shublik Formation, Kingak Shale, Pebble Shale Unit, and Torok Formation, *in* Magoon, L.B., and Claypool, G.E., eds., Alaska North Slope Oil/Rock Correlation Study: American Association of Petroleum Geologists Studies in Geology #20, p. 31-48.

Magoon, L.B., and Claypool, G.E., 1981, Two oil types on North Slope of Alaska--implications for exploration: American Association of Petroleum Geologists Bulletin, v. 56, p. 644-652.

Magoon, L.B., and Claypool, G.E., 1985, Introduction, *in* Magoon, L.B., and Claypool, G.E., eds., Alaska North Slope Oil/Rock Correlation Study: American Association of Petroleum Geologists Studies in Geology #20, p. xi-xiv.

Makay, J.R., 1972, Offshore permafrost and ground ice, southern Beaufort Sea: Canadian Journal of Earth Science, v. 9, p. 1550-1561.

Makogon, Y.F., 1974, Hydrates of Natural Gas: Geoexplorers Associates, Denver, 178 p.

Manheim, F.T., Sayles, F.L., and Waterman, L.S., 1973, Interstitial water studies on small core samples, Deep Sea Drilling Project Leg 10, *in* Initial Reports of the Deep Sea Drilling Project, v. 10: Washington, D.C., US GPO, p. 615-623.

Mathews, M.A., and von Huene, R., 1985, Site 570 methane hydrate zone, *in* von Heune, R., et al., Initial Reports of the Deep Sea Drilling Project, v. 84: Washington, D.C., US GPO, p. 773-790.

McIver, R.D., 1977, Hydrates of natural gas--important agent in geological processes: Geological Society of America Abstracts with Programs v. 9, p. 1089-1090.

McIver, R.D., 1982, Role of naturally occurring gas hydrates in sediment transport: American Association of Petroleum Geologists Bulletin, v. 66, p. 789-792.

Morack, J.L., MacAulay, H.A., and Hunter, H.A., 1983, Geophysical measurements of subbottom permafrost in the Canadian Beaufort Sea, *in* Proceedings of the 4th International Conference on Permafrost, Fairbanks, Alaska, 1983: Washington, D.C., National Academy Press, p. 866-871.

Neave, K.G., and Sellmann, P.V., 1983, Seismic velocities and subsea permafrost in the Beaufort Sea, Alaska, *in* Proceedings of the 4th International Conference on Permafrost, Fairbanks, Alaska, 1983: Washington, D.C., National Academy Press, p. 894-898.

Neave, K.G., and Sellmann, P.V., 1984, Determining distribution patterns of ice-bonded permafrost in the U.S. Beaufort Sea from seismic data *in* Barnes, P.W., Schell, D.M., and Reimnits, E., eds., The Alaskan Beaufort Sea Ecosystems and Environments: New York, Academic Press, p. 237-257.

Osterkamp, T.E., and Payne, M.W., 1981, Estimates of permafrost thickness from well logs in northern Alaska: Cold Regions Science and Technology, v. 5, p. 13-27.

Paull, C.K., and Dillon, W.P., 1981, Appearance and distribution of the gas hydrate reflection in the Blake Ridge region, offshore southeastern United States: U.S. Geological Survey Miscellaneous Field Studies, Map MF-1252.

Pearson, C., Murphy, J., Halleck, P., Hermes, R., and Mathews, M., 1982, Sonic and resistivity measurements on Berea Sandstone containing tetrahydrofuran hydrates: a possible analog to natural gas hydrate deposits, *in* Proceedings of the 4th International Conference on Permafrost, Fairbanks, Alaska, 1982: Washington, D.C., National Academy Press, p. 973-978.

Rogers, J.C., and Morack, J.L., 1978, Geophysical investigation of offshore permafrost, Prudhoe Bay, Alaska, *in* Proceedings of the 3rd International Conference on Permafrost: v.1, p. 560-566.

Sellmann, P.V., and Chamberlain, E.J., 1979, Permafrost beneath the Beaufort Sea near Prudhoe Bay, Alaska: Offshore Technology Conference, 11th, Houston Texas, 1979, Proceedings, v. 3 OTC paper 3527, p. 1481-1488.

Sellmann, P.V., Chamberlain, E., Ueda, H.T., Blouin, S.E., Garfield, D., and Lewellen, R.I., 1977, CRREL-USGS Subsea permafrost program Beaufort Sea Alaska operational report: Hanover, NH, U.S. Corps of Engineers, Cold Regions Research and Engineering Laboratory, 19 p.

Shipley, T.H., and Didyk, M.B., 1982, Occurrence of methane hydrate offshore of southern Mexico, *in* Watkins, J.S., et al., Initial Reports of the Deep Sea Drilling Project, v. 66: Washington, D.C., US GPO, p. 547-555.

Shipley, T.H., Houston, M.H., Buffler, R.T., Shaub, F.J., McMillen, K.J., Ladd, J.W., and Worzel, J.L., 1979, Seismic reflection evidence for widespread possible gas hydrate horizons on continental slopes and rises: American Association of Petroleum Geologists Bulletin, v. 63, p. 2204-2213.

Snowdon, L.R., 1980, Resinite--a potential petroleum source in the Upper Cretaceous/Tertiary of the Beaufort-Mackenzie Basin, *in* Miall, ed., Facts and Principles of World Petroleum Occurrence: Canadian Society of Petroleum Geologists Memoir 6, p. 509-521.

Snowdon, L.R., and Powell, T.G., 1982, Immature oil and condensate--modification of hydrocarbon generation model for terrestrial organic matter: American Association of Petroleum Geologists bulletin, v. 66, p. 775-788.

Stefanon, A., 1980, The acoustic response of some gas-charged sediments in the northern Adriatic Sea., *in* Mankey, K.L., ed., Seismic Methods for Seafloor Mapping: New York, Plenum Press, p. 73-84.

Stoll, R.D. and Bryan, G.M., 1979, Physical properties of sediments containing gas hydrates: Journal of Geophysical Research, v. 63, p. 1629-1634.

Stoll, R.D., Ewing, J.I., and Bryan, G.M., 1971, Anomalous wave velocities in sediments containing gas hydrates: Journal of Geophysical Research, v. 76, p. 2090-2094.

Stoll, R.D., 1974, Acoustic waves in saturated sediments, *in* Hampton, L., ed., Physics of Sound in Marine Sediments, New York, Plenum Press, p. 19-39.

Summerhayes, C.P., Bornhold, B.D., and Embley, R.W., 1979, Surficial slides and slumps on the continental slopes and rises of Southwest Africa: A reconnaissance study: Marine Geology, v. 31, p. 265-277.

Tissot, B.T., and Welte, D.H., 1984, Petroleum formation and occurrence: New York, Springer-Verlag, 538 p.

Vigdorchik, M.E., 1980, Submarine permafrost on the Alaskan continental shelf: Boulder, CO, Vestview Press, 121 p.

Weaver, J.S., and Stewart, J.M.., 1982, In situ hydrates under the Beaufort Sea Shelf, *in* French, M.H., ed., Proceedings of the Fourth Canadian Permafrost Conference, 1981: National Research Council of Canada, p. 312-319.

Willumsen, P.S., and Cote, R.P., 1982, Tertiary sedimentation in the southern Beaufort Sea, Canada, *in* Watkins, J.S., and Drake, E., eds., Studies in continental margin geology: American Association of Petroleum Geologists Memoir 34, p. 283-294.

Yamano, M., Uyeda, S., Aoki, Y., and Shipley, T.H., 1982, Estimates of heat flow derived from gas hydrates: Geology, v. 10, p. 339-343.